

VARIABLE ANGLE PHOTOELECTRON SPECTROSCOPY

Thesis by
Donald Mills Mintz

In Partial Fulfillment of the Requirements
for the Degree of
Doctor of Philosophy

California Institute of Technology
Pasadena, California
1976

(Submitted September 23, 1975)

Copyright © by
DONALD MILLS MINTZ
1975

To my parents

ACKNOWLEDGMENTS

I wish to express my appreciation to Professor Aron Kuppermann for the advice and encouragement he gave me while I worked with him at Caltech.

I am greatly indebted to Doug Mason, my predecessor on this project. He designed most of the instrument and wrote some PDP8/e software that was crucial to obtaining good experimental results.

I am happy to thank Professor Allan L. Smith for introducing me to the field of photoelectron spectroscopy while I was an undergraduate at Yale.

I have learned much from interacting with other members of the Kuppermann group. Thanks are due especially to Dr. Oren A. Mosher and Dr. Michael J. Coggiola. In addition, Bob Walkup and Jeff Sell are due thanks for assistance in the later stages of the research reported here.

Without the skilled assistance of the members of the Chemistry instrument shop, especially Bill Schuelke and Tony Stark, none of the experimental work reported here could have been possible.

The financial support of the Energy Research and Development Administration, the National Science Foundation, and the Shell Oil Company Foundation is gratefully acknowledged.

ABSTRACT

This thesis describes the design, construction, and performance of a variable angle photoelectron spectrometer. The experiment consists of a stationary resonance line lamp, a sample chamber, and a rotatable electrostatic electron energy analyzer. Experiment operation is extensively automated through several interfaces to a small on-line digital computer.

Results are presented for a variety of atomic, diatomic, and polyatomic sample gases. In the case of Ar, Ne, N₂, and CO, higher order lines in the resonance line lamp produce many peaks which do not overlap extensively with those of the principal vacuum-ultraviolet output. The additional lamp output lines allow for measurement of the variation of the photoelectron angular distribution asymmetry parameter, β , with photoelectron energy. Results for Ar and Ne are in good agreement with previous theoretical calculations.

For N₂, we find a discontinuity in the variation of β near 5 eV photoelectron energy for the $v' = 0$ peak of the $X^2\Sigma_g^+$ ionic state. The result is interpreted in terms of the possible mechanisms: autoionization, variation of the electric dipole transition moment with internuclear distance, and resonance phenomena. For peaks of the $A^2\Pi_u$ ionic state, the variation of β with ionic vibrational level matches the variation with photoelectron energy. For CO, anomalous structure is assigned to higher peaks of the CO $X^2\Sigma^+$ vibrational progression. The dominant mechanism is probably autoionization.

Photoelectron angular distributions were measured for the series of olefins: ethylene, isobutylene, 2-methyl,2-butene, and 2,3-dimethyl,2-butene. The variation of β with electron energy was inferred by a comparison of data for the four structurally similar molecules. In the $\sigma 2p$ orbital ionization region of the spectrum, we find a similar variation of β with electron energy over bands corresponding to widely varying orbital symmetries. In the π orbital ionization region of the spectrum, β increases with increasing electron energy, taken from the variation of β across the vibrational envelopes. Accompanying the drop in β for π ionization with increasing methyl substitution is an anomalous drop in β at the high ionization potential end of the $\sigma 2p$ region which may indicate the presence of σ/π orbital mixing.

Photoelectron angular distributions were measured for a series of di-olefins. In the case of allene, we propose the ordering $2e, 3b_2, 1e$ for the three lowest-lying orbitals on the basis of a deconvolution of the band in the ionization potential range 14-16.5 eV. A re-examination of 1,3-butadiene supports the π, π, σ energy ordering of low-lying molecular orbitals. The variation of β across the $\sigma 2p$ region in the photoelectron spectra of 1,4-pentadiene and 1,5-hexadiene supports an earlier notion that through-space interaction of the π -bonds dominates through-bond interaction. Spectra of the π region suggest that the interaction between π moieties decreases in going from 1,4-pentadiene to 1,5-hexadiene.

In an examination of low-lying structure of 1,4-cyclohexadiene,

the anomalously low β value for the lowest π -ionization band probably arises from σ/π mixing.

In an examination of the two low-lying photoelectron bands of pyridine below 11 eV IP, the sharp rise of β across the 9-10 eV band is interpreted in terms of the orbital ordering n, π, π .

TABLE OF CONTENTS

	<u>Page</u>
Acknowledgments	iii
Abstract	iv
CHAPTER 1 Introduction	1
References	4
CHAPTER 2 Theory	6
2.1 Theoretical Description of Photoionization	6
2.2 Survey of Theoretical Calculations	17
2.2.1 Atomic photoelectron angular distributions	17
2.2.2 Molecular photoelectron angular distributions	20
References	24
CHAPTER 3 Experimental	27
3.1 Introduction	27
3.2 Paper I: A Variable Angle Photoelectron Spectrometer	28
CHAPTER 4 Results and Discussion: Noble Gases	69
4.1 Introduction	69
4.2 Argon	69
4.3 Neon	72
References	74
CHAPTER 5 Results and Discussion: Diatomic Molecules	80
5.1 Paper II: Electron Energy Dependence of the Differential Photoelectron Cross Section of N ₂	80
5.2 Carbon Monoxide	133
References	137

TABLE OF CONTENTS (continued)

	<u>Page</u>
CHAPTER 6 Results and Discussion: Polyatomic Molecules	143
6.1 Paper III: Variable Angle Photoelectron Spectroscopy of Ethylene, Isobutylene, 2-Methyl, 2-butene, and 2, 3-Dimethyl, 2-butene.	143
6.2 Paper IV: Variable Angle Photoelectron Spectroscopy of Allene, 1, 3-Butadiene, 1, 4-Pentadiene, and 1, 5-Hexadiene	196
6.3 1, 4-Cyclohexadiene	233
References	238
6.4 Pyridine	239
References	244
APPENDIX A: Helmholtz Coil Design and Specifications	246
APPENDIX B: Volume Correction	250
APPENDIX C: Data Acquisition Procedures	257
APPENDIX D: Sample Handling	272
APPENDIX E: Statistical Treatment of Data	280
APPENDIX F: π Bands of Methyl-substituted Ethylenes	286
APPENDIX G: List of Vendors	292
Propositions	300

CHAPTER 1 - INTRODUCTION

Since 1961,^{1,2} photoelectron spectroscopy has provided a powerful tool for the understanding of molecular electronic structure. For ionization by monochromatic light of energy $h\nu$, the energy in excess of an ionization potential IE_n appears as kinetic energy of the ejected electron:

$$h\nu = IE_n + E_{kin} \quad (1)$$

When the monochromatic light is chosen to be the strong HeI resonance line at 584 Å, ionization from the range of valence orbitals, labelled n , with binding energies up to 21.21 eV is possible. Unlike absorption spectroscopy or photoionization mass spectrometry, photoelectron spectroscopy is not a threshold technique. Therefore, the difficulties in measuring thresholds inherent in the other techniques do not appear.

The last five years have seen a rapid increase in the number of chemical compounds studied. Much of the research is chemically oriented, in part due to the availability of commercial spectrometers³ of high resolution and good sensitivity. Chemists were able to explicate much of the structure of a wide range of polyatomic molecules based on results of semi-empirical calculations,^{4,5} an analysis of vibrational fine structure,⁶⁻⁸ and a consideration of families of related molecules.⁹⁻¹² They were able to isolate bands due to certain electronic functional groups and later study the interactions of those groups.¹²⁻¹⁴

As long ago as 1927, physicists¹⁵ realized that the angular distribution of atomic photoelectrons ejected by linearly polarized light was not isotropic, but rather of the form $a + b \cos^2 \phi$, where ϕ is the angle between the light polarization axis and the direction of the detected photoelectrons. A derivation of the form of the photoelectron angular distribution for atoms and molecules for non-polarized light is included in Chapter 2.

Most of the angular distribution studies to date have been physical, rather than chemical, in nature. Techniques for the measurement had been developed largely by experimental physicists. Much of the early apparatus yielded artifacts in the angular distribution^{16,17} or permitted the experimentalist only limited flexibility^{18,19} in the type of samples studied or the photon range covered. The use of a stationary lamp and single rotatable electron energy analyzer is a powerful technique which yields the best flexibility in photon range and allows the best opportunity to diagnose and remedy angular distribution artifacts. A description of the present apparatus, based upon the stationary lamp and rotatable electron energy analyzer design, appears in Chapter 3.

Most of the photoelectron angular distribution studies to date have examined atoms and a few diatomics, for which comparisons to accurate theoretical calculations can be made. Even though we call ourselves chemists, several research problems presented themselves and the urge to contribute here was overpowering. Results for argon and neon are presented in Chapter 4 and for molecular nitrogen and

and carbon monoxide in Chapter 5.

Except for the studies of one research group elsewhere, none of the experimental angular distribution work in the literature is chemically oriented. A comprehensive examination of photoelectron angular distributions for a broad collection of molecules by this group²⁰ appeared at a conference in 1971. Since that time only isolated studies of polyatomic molecules have appeared in the literature.^{18, 21, 22}

We present here another step in the chemical direction. From the behavior of the angular distribution asymmetry parameter, β , for benzene¹⁸ and several of the methyl substituted ethylenes,²² we might expect to understand the behavior of β for all simple olefins. However, nature had a few surprises for us as the discussions of four olefins, ethylene, isobutylene, 2-methyl, 2-butene, and 2,3-dimethyl, 2-butene, and four diolefins, allene, 1,3-butadiene, 1,4-pentadiene, and 1,5-hexadiene, can confirm. These hydrocarbons, comprising two papers, form the heart of Chapter 6. In addition, the chapter presents results for pyridine and 1,4-cyclohexadiene, which can be interpreted in the light of trends found in the four olefins and four diolefins.

REFERENCES

1. F. I. Vilesov, B. C. Kurbatov, A. N. Terenin, Dokl. Akad. Nauk SSSR, 138, 1329 (1961).
2. D. W. Turner, M. I. Al-Joboury, J. Chem. Phys. 37, 3007 (1962).
3. Perkin-Elmer Photoelectron Spectrometers, Model Nos. PS-15, PS-16, PS-18, Perkin-Elmer Ltd. (Beaconsfield, England); JASCO Photoelectron Spectrometer, Model Nos. PE-1, PE-1A, Japan Spectroscopic Co., Ltd. (Bozman, MD); Vacuum Generators ESCA2 Spectrometer.
4. S. D. Worley, Chem. Rev. 71, 295 (1971); M. J. S. Dewar, S. D. Worley, J. Chem. Phys. 50, 654 (1969).
5. C. Fridh, L. Åsbrink, E. Lindholm, Chem. Phys. Lett. 15, 282 (1972).
6. E. Haselbach, Chem. Phys. Lett. 7, 428 (1970).
7. W. C. Price in P. Hepple (editor) Molecular Spectroscopy (Institute of Petroleum, London, 1968) p. 221.
8. A. W. Potts, D. G. Streets, J. Chem. Soc. Faraday II 70, 875 (1974).
9. C. R. Brundle, M. B. Robin, N. A. Kuebler, H. Basch, J. Amer. Chem. Soc. 94, 1451 (1972).
10. K. Kimura, S. Katsumata, T. Yamazaki, H. Wakabayashi, J. Electron Spectr. 6, 41 (1975).
11. P. Bischof, E. Heilbronner, Helv. Chim. Acta 53, 1677 (1970).
12. M. Beez, G. Bieri, H. Bock, E. Heilbronner, Helv. Chim. Acta 56, 1028 (1973).

13. J. C. Bünzli, A. J. Burak, D. C. Frost, *Tetrahedron* 29, 3735 (1973).
14. E. Heilbronner, *Israel J. Chem.* 10, 143 (1972).
15. G. Wentzel, *Z. Phys.* 41, 828 (1927).
16. D. A. Vroom, A. R. Comeaux, J. W. McGowan, *Chem. Phys. Lett.* 3, 476 (1969); J. W. McGowan, D. A. Vroom, A. R. Comeaux, *J. Chem. Phys.* 51, 5626 (1969).
17. J. Berkowitz, H. Ehrhardt, *Phys. Lett.* 21, 531 (1966).
18. J. A. Kinsinger, J. W. Taylor, *Int. J. Mass Spectrom Ion Phys.* 10, 445 (1973).
19. P. Mitchell, K. Codling, *Phys. Lett.* 38A, 31 (1972).
20. T. A. Carlson, G. E. McGuire, A. E. Jonas, K. L. Cheng, C. P. Anderson, C. C. Lu, B. P. Pullen, in D. A. Shirley (editor) *Electron Spectroscopy* (North-Holland, Amsterdam, 1972) p. 207.
21. D. L. Ames, J. P. Maier, F. Watt, D. W. Turner, *Faraday Disc. Chem. Soc.* 54, 277 (1972).
22. R. M. White, T. A. Carlson, D. P. Spears, *J. Electron Spectr.* 3, 59 (1974).

CHAPTER 2 - THEORY

$$i\hbar \frac{\partial \Psi}{\partial t} = H \Psi$$

2.1 Theoretical Description of Photoionization

The usual treatment of the interactions of matter with electromagnetic fields proceeds by the semiclassical theory of radiation.¹ This theory treats the light classically, so that the vector potential is assumed known to any degree of accuracy desired. On the other hand, the particles' motion is treated quantum mechanically. In a fully quantum mechanical Quantum Electrodynamical Theory of photoionization, transition probabilities can be expanded to high orders in the interaction of the light and matter. However, for the case of ionization of atoms and molecules by noble gas resonance lamps, the interaction of light and matter is weak. We therefore retain only the terms to first order in the expansion of the Quantum Electrodynamical interactions; "the potential acts only once."²

As a consequence, we expect simple first order time dependent perturbation theory to give an adequate description of our experiment. At time $t=0$, we assume that all of the particles in the system lie in the ground state indexed n . At some time later, after the perturbation is turned on, we can calculate the probability of finding the system in state $f \neq n$.

Choosing the Coulomb gauge and assuming weak light intensity, we can express the Hamiltonian as a sum of a stationary term and the

time dependent perturbation:

$$\begin{aligned} H &= H_0 + H'(t) \\ &= (T_{\text{op}} + V_{\text{op}}) + \frac{ie\hbar}{mc} \underline{\underline{A}} \cdot \underline{\underline{\nabla}} , \end{aligned} \quad (2-1)$$

Here, m is the electron mass, $\underline{\underline{A}}$ is the vector potential of the electromagnetic field, and c and e have their usual meanings. From Maxwell's equations, we obtain a wave equation for the vector potential $\underline{\underline{A}}$ with solutions:

$$\underline{\underline{A}} = 2 |\underline{\underline{A}}_0| \underline{\underline{P}} \exp \{ i (\underline{\underline{k}} \cdot \underline{\underline{r}} - \omega t + \theta) \} . \quad (2-2)$$

Here, $|\underline{\underline{A}}_0|$ is related to the intensity of the radiation in units $\text{ergs} \cdot \text{cm}^{-2} \cdot \text{sec}^{-1}$ by:

$$I = \frac{\omega^2 |\underline{\underline{A}}_0|^2}{2\pi c} . \quad (2-3)$$

$\underline{\underline{P}}$ is the complex unit polarization vector, which points along the polarization direction of the incident radiation. $\underline{\underline{k}}$ and $\underline{\underline{r}}$ are the propagation vector and position coordinate of the electromagnetic radiation. The variable θ is the real quantity defined by:

$$\underline{\underline{P}} \cdot \underline{\underline{P}} = \exp(2i\theta) . \quad (2-4)$$

We next solve the time dependent Schrödinger equation,

$$i\hbar \frac{\partial \Psi(\underline{\underline{r}}, t)}{\partial t} = H \Psi(\underline{\underline{r}}, t) , \quad (2-5)$$

by expanding the time dependent wavefunction, $\Psi(\underline{r}, t)$, in a basis of stationary state solutions to H_0 . Here, we employ time dependent coefficients which describe how the stationary state evolves with time:

$$\Psi(\underline{r}, t) = \sum_f C_f(t) \exp(-iE_f t/\hbar) \phi_f(\underline{r}). \quad (2-6)$$

If we let the system have unit amplitude in state n at time $t=0$, then, after a small increment of time, for $f \neq n$:

$$C_f(t) = \frac{-i}{\hbar} \int_0^t \langle \phi_f | H'(\underline{r}, t') | \phi_n \rangle \exp(-i\omega_{fn} t') dt' \quad (2-7)$$

where $\hbar\omega_{fn} = E_f - E_n$ is the difference in energy of the two stationary states f and n .

We can evaluate the transition probability per unit time for the absorption of radiation, a transition rate, for discrete initial and final states as:

$$W = \frac{|C_f(t)|^2}{t} = \frac{4e^2 |A_0|^2}{m^2 c^2} \left| \langle \phi_f | e^{i\mathbf{k} \cdot \mathbf{r}} \mathbf{p} \cdot \nabla | \phi_n \rangle \right|^2 \frac{\sin^2[\frac{1}{2}(\omega - \omega_{fn})t]}{(\omega - \omega_{fn})^2 t}, \quad (2-8)$$

where we have substituted for H' and performed the integral over t' . For small t , the transition rate will vary linearly with time, which contradicts physical sense for laboratory experiments. The solution to the problem lies in abandoning one of the three motions about the physical system:

- 1) discrete initial state n
- 2) discrete final state f
- 3) monochromatic distribution of light frequencies.

The final state of the system is an ion and a free electron with ultimately continuously variable energy. Therefore, we abandon notion 2 above and introduce a density of final states, $\rho(E) = d\bar{n}/dE$.

To calculate the correct physical transition rate, we integrate the transition rate of Eq. 2-8 over the number of final states contributing to the transition:

$$W_{\text{phys}} = \frac{1}{8} \int W \bar{n}^2 d\bar{n} d\Omega. \quad (2-9)$$

Here, $\bar{n}^2 d\bar{n} d\Omega$ represents the number of photoelectron trajectories ejected into solid angle $d\Omega$ with the principal quantum number lying between \bar{n} and $\bar{n} + d\bar{n}$, where \bar{n} is the principal quantum number of a particle in a three-dimensional box of characteristic dimension L .

The factor of $\frac{1}{8}$ is included to limit our consideration to only positive velocity components v_x, v_y, v_z . The integral over $d\bar{n}$ is converted to an integral over photoelectron energy with the final result:

$$W_{\text{phys}} = \frac{\pi e^2 L^3 \hbar}{(2\pi \hbar c)^2} \cdot \frac{k_f |\hat{A}_0|^2}{m} \left| \langle \phi_f | e^{i\hat{k} \cdot \hat{r}} \hat{p} \cdot \hat{\nabla} | \phi_n \rangle \right|^2 d\Omega \quad (2-10)$$

Here, k_f is the wavenumber of the ejected photoelectron whose energy is $E = \hbar^2 k_f^2 / 2m$.

We can convert the transition rate into a differential photoionization cross section by dividing by the total incident photon current density, the intensity of radiation from Eq. 2-3 divided by the energy per photon, $\hbar\omega$. Furthermore, we assume the validity of the dipole approximation, for which the expansion of the exponential:

$$e^{i\mathbf{k}\cdot\mathbf{r}} = 1 + i\mathbf{k}\cdot\mathbf{r} + \dots \cong 1, \quad (2-11)$$

is truncated after the first term. The photon wavelength, for photoionization by vacuum ultraviolet radiation, is long compared to the characteristic dimensions of a typical molecular photoelectron target. Thus, the $\mathbf{k}\cdot\mathbf{r}$ term and higher order terms can be neglected.

The final result is the dipole velocity form of the differential photoionization cross section:³

$$\frac{d\sigma^v}{d\Omega} = \frac{L^3 k_f}{2\pi m c \omega} \left| \mathbf{P} \cdot \langle \phi_f | e \nabla | \phi_n \rangle \right|^2, \quad (2-12)$$

where we recall that L^3 is the volume of quantization in the determination of the density of final states. Some workers^{4, 5} have adopted a unit normalization, in which case L^3 is replaced by $(2\pi)^3$.

This expression is easily converted into the dipole length form by noting a commutation relation for the quantum mechanical operators \mathbf{v} , \mathbf{r} , and H_0 :

$$\mathbf{v} = \frac{i}{\hbar} [H_0, \mathbf{r}], \quad (2-13)$$

where H_0 is the Hamiltonian of the stationary state. The dipole length form becomes:

$$\frac{d\sigma}{d\Omega} = \frac{L^3 m k_f \omega}{2\pi \hbar^2 c} \left| \underline{\hat{P}} \cdot \langle \phi_f | e \underline{\hat{r}} | \phi_n \rangle \right|^2. \quad (2-14)$$

Only for exact wavefunctions ϕ_f and ϕ_n will the dipole length and velocity expressions be equivalent.

The dipole matrix element, $\langle \phi_f | e \underline{\hat{r}} | \phi_n \rangle$, after the integration over \underline{r} , will still be a vector. This is assured by the form of the final state wavefunction, which depends on the wave vector \underline{k}_f , of the ejected photoelectron. Further, the box normalized final state wavefunction contains a dependence on L^3 , the quantization volume. Thus Eq. 2-14 contains an angular dependence only on the angle between the vectors $\underline{\hat{P}}$ and \underline{k}_f and ultimately is independent of L^3 .

Bethe and Salpeter⁶ have derived a simple analytical expression for Eq. 2-14 from a consideration of the symmetry inherent in the experiment. Their argument is reproduced here because of its importance: The matrix element $\langle \phi_f | e \underline{\hat{r}} | \phi_n \rangle$, and thus the differential cross section, do not depend explicitly on \underline{k} , but only on the angle between the polarization ($\underline{\hat{P}}$) direction of the photon and the propagation direction of the photoelectron. For an initial discrete state ϕ_n , there is a dependence on the quantization direction and orientation (magnetic) quantum numbers. We are experimentally measuring $d\bar{\sigma}/d\Omega$, a differential cross section averaged over the possible orientation

quantum numbers of the initial state. Thus, the final result does not depend on single orientation quantum numbers. Also, even the orientation-averaged cross section depends only on the angle between the light polarization and photoelectron propagation directions.

Bethe and Salpeter asserted that the differential cross section remains unchanged upon inversion of the photoelectron propagation direction from \underline{k}_f to $-\underline{k}_f$, with the polarization axis fixed. To show this, they changed the variable of integration from \underline{r} to $-\underline{r}$ and reversed the quantization direction of ϕ_n . The resulting integrand is unchanged except for a change in sign and $d\bar{\sigma}/d\Omega$ is unchanged. Changing the sign of \underline{k}_f , as shown in Fig. 2-1, thus shows $d\bar{\sigma}/d\Omega$ to be symmetric about a perpendicular to the light polarization axis.

Bethe and Salpeter then show that the ultimate dependence on $\theta' = \angle(\underline{P}, \underline{k}_f)$ is $\alpha + \beta \cos^2 \theta'$: Express the variable \underline{r} in Eq. 2-14 in the coordinate system (r, θ'', ϕ'') with respect to \underline{k}_f . The integrands of Eq. 2-14 will depend on the relative orientations of \underline{r} and \underline{P} . Then, by spherical trigonometry, we can write $\underline{r} \cdot \underline{P}$ in the form:

$$\underline{r} \cdot \underline{P} = r(\cos \theta' \cos \theta'' + \sin \theta' \sin \theta'' \cos \phi''), \quad (2-15)$$

where \underline{P} lies along $\phi' = 0$. The matrix elements of Eq. 2-14 thus depend on θ' only through the $\cos \theta'$ and $\sin \theta'$ in Eq. 2-15. To calculate the averaged cross section, $d\bar{\sigma}/d\Omega$, the dipole integrals are summed over orientations and the squared. Because of the plane of symmetry, the cross terms must vanish, leaving only terms in $\cos^2 \theta'$ and $\sin^2 \theta'$.

Figure Caption

Fig. 2-1 Diagram that illustrates the Bethe-Salpeter⁶ argument for the symmetry of $d\bar{\sigma}/d\Omega$ about a perpendicular to the light polarization axis.

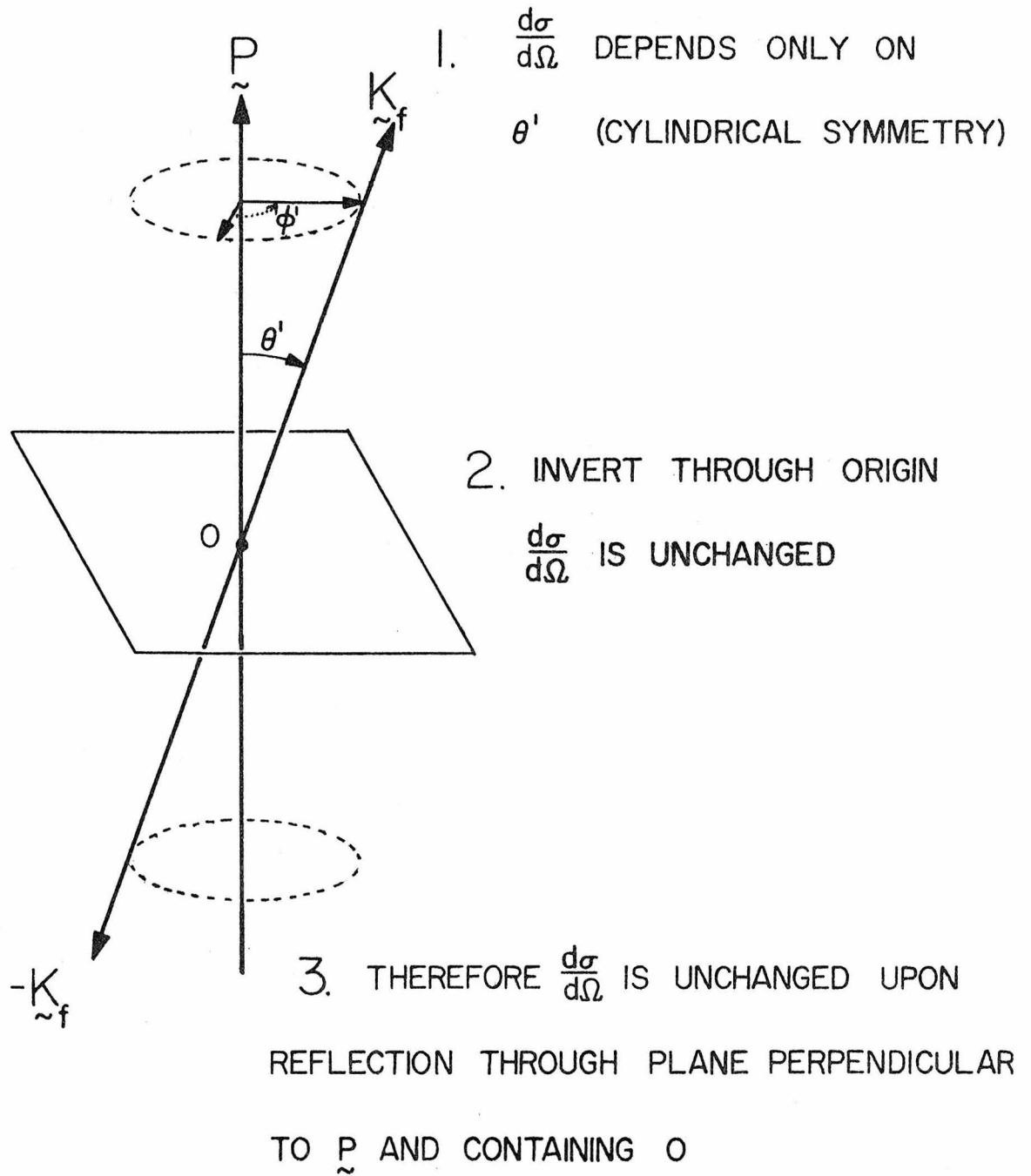


Figure 2-1

Later, Cooper and Zare⁷ forced the form of the angular distribution for photoionization by linearly polarized light into a slightly different form:

$$\frac{d\bar{\sigma}}{d\Omega} = \frac{Q}{4\pi} [1 + \beta P_2(\cos \theta')] . \quad (2-16)$$

Here Q is the integral photoionization cross section, $P_2(x)$ is a Legendre Polynomial $[P_2(x) = \frac{1}{2}(3x^2 - 1)]$, and β is termed the "asymmetry parameter". The asymmetry parameter varies in the range $-1 \leq \beta \leq 2$ for experiments on orientation averaged initial states and thus describes the deviation of the angular distribution from isotropy.

Photoionization of N-electron targets and electron scattering from N-1 electron targets bear fundamental resemblance, as physical intuition might suggest. They are both N electron problems. Furthermore, it would appear that calculations of photoelectron angular distributions would benefit from the voluminous work of electron scattering theorists on the subject. Unfortunately, calculations of photoionization can only benefit partially, largely due to the difference in the mathematical boundary conditions imposed on two physically different experiments.

Still, the link is strong. In both cases, we need wavefunctions of an N-1 electron core with a free electron. A considerable amount of information about the dynamics of the electron-core interaction lies in the wavefunction. Thus, both Q and β of Eq. 2-16 are expected to

incorporate dynamical information; the parameters should depend both on the molecule studied and upon the photoelectron energy.

This point is immediately apparent upon examination of the form of β derived for atoms by Cooper and Zare.⁷ For an atomic electron in a definite state of total angular momentum ℓ , assuming a central field for the electron-core interaction, and assuming L-S coupling is valid,

$$\beta = \frac{\ell(\ell-1)\sigma_{\ell-1}^2 + (\ell+1)(\ell+2)\sigma_{\ell+1}^2 - 6\ell(\ell+1)\sigma_{\ell+1}\sigma_{\ell-1}\cos(\delta_{\ell+1} - \delta_{\ell-1})}{(2\ell+1)[\sigma_{\ell-1}^2 + (\ell+1)\sigma_{\ell+1}^2]} . \quad (2-17)$$

The $\sigma_{\ell-1}$ and $\sigma_{\ell+1}$ are radical dipole integrals for the $\ell-1$ and $\ell+1$ outgoing waves:

$$\sigma_{\ell\pm 1} = \int_0^{\infty} r R_{n\ell}(r) G_{k\ell\pm 1}(r) dr \quad (2-18)$$

where $R_{n\ell}(r)$ and $G_{k\ell\pm 1}(r)$ are radial functions for the initial and final states. Here $\delta_{\ell\pm 1}$ are the corresponding phase shifts.

By averaging over orientations of the polarization vector about the photon propagation direction, Cooper and Manson⁸ obtained the differential photoelectron cross section for the unpolarized light output from noble gas resonance lamps:

$$\frac{d\sigma}{d\Omega} = \frac{Q}{4\pi} [1 - \frac{1}{2}\beta P_2(\cos\theta)] . \quad (2-19)$$

The angle θ is now the angle between the directions of photon propagation and photoelectron ejection. The parameters β and Q have the same meaning as in Eq. 2-16. As a corollary of Eq. 2-19, experiments at a "magic angle" of $\theta = 54.7^\circ$, where $P_2(\cos 54.7^\circ) = 0$, yields a spectrum whose intensities are independent of β .

Experiments at the "magic angle" are necessary in order to equitably compare the spectral intensities at two neighboring bands. Kinsinger and Taylor⁹ have discussed the problems of interpreting band intensities using the 90° spectra generated by fixed angle instruments. In this case, values of -1 and +2 for a given band yield estimates of total cross sections differing by a factor of 2.

2.2 Survey of Theoretical Calculations

2.2.1 Atomic photoelectron angular distributions

In 1927, G. Wentzel¹⁰ first suggested that the angular distribution for electrons photoionized from the hydrogen atom should take the familiar dipole form. He showed that the intensity should have the following angular dependence:

$$I \sim \sin^2 \theta \cos^2 \varphi \quad (2-20)$$

Where θ is the angle between the directions of photon propagation and photoelectron propagation. Here, φ represents the azimuthal angle of photoelectron ejection about the axis of photon propagation. A short time later, Sommerfeld and Schur^{11,12} derived the angular dependence for ionization from K and L shells of hydrogenic atoms. They

indicated that the angular distribution takes the form

$$I \sim a + b \cos^2 \theta', \quad (2-21)$$

where θ' is the angle between the light polarization axis and the photoelectron ejection direction. In 1933, Bethe¹³ generalized these results to photoionization from electron subshells or arbitrary angular momentum quantum number, ℓ . He expressed the final result in terms of integrals between radial continuum functions for the outgoing electron and bound state eigenfunctions for the initial state, but did not evaluate any of the integrals.

After this initial theoretical activity and limited experimental¹⁴ activity, little appeared in print until the Berkowitz and Ehrhardt¹⁵ study in 1966. In 1968, Lin¹⁶ finished the Bethe calculation for atomic hydrogen by performing the radial integrals over Whittaker functions and one-electron hydrogenic functions analytically. He obtained closed forms for the angular distributions for the photoionization of 1s, 2s, 2p, 3p, 3s, and 4d initial states in terms of the energy of the outgoing photoelectron.

Further theoretical developments were coupled to the pioneering experimental studies of photoelectron angular distribution by Hall and Siegel.¹⁷ Cooper and Zare⁷ rederived the early theory of Bethe to cover photoionization from one electron atoms with the electron in an eigenstate of L^2 , assuming L-S coupling was valid. They introduced the asymmetry parameter β of Eq. 2-16. Within the Bethe-Cooper-Zare one-electron formalism, Manson and Kennedy^{18, 19} have

calculated the electron energy dependence of β within the Hartree-Slater and Hartree-Fock models for a wide range of atoms. For noble gas ionization within 10 eV of threshold, this method gives excellent agreement with experiment for ionization from np subshells, as discussed below.

Several groups have suggested improvements on the central field, L-S coupling model for open shell atoms and for atoms where j-j coupling is present. The angular-momentum transfer theory of Dill has been applied to atomic sulfur,^{20,21} selenium and bromine,²² as well as the autoionization of xenon.²³ Walker and Waber²⁴ have calculated the electron energy dependence of β for xenon, cadmium, and mercury in the j-j coupling approximation. Marr²⁵ has independently calculated the electron energy dependence of β for the cesium 6s subshell, for which j-j coupling produces deviations from the $\beta = 2$ expected from the Cooper-Zare formalism.

Several groups have included the effects of electron correlation on the electron energy dependence of β . Amusia's group, applying the random-phase-approximation-with-exchange, has calculated the electron energy dependence of β for a series of noble gases.²⁶ Near ionization threshold for argon, experimental results²⁷⁻²⁹ agree slightly better with the Hartree-Fock calculation of Manson and Kennedy¹⁸ than with that of Amusia, et al.²⁶ However, for energies near the Cooper minimum in the 3p cross section, Houlgate, et al.²⁸ have found better agreement with Amusia's results.²⁶ In this electron energy region, the two calculations differ greatly--by as much as 1.5.

Simplifications in the random-phase-with-exchange theory as discussed by Lin³⁰ may make the method tractable for a larger range of atoms and molecules.

2.2.2 Molecular photoelectron angular distributions

Theory is not as well developed for molecular calculations. The symmetry of molecules is of course lower than that of atoms. Thus, for a single center expansion of the final state of photoelectron plus ion, we expect a large interaction of different outgoing ℓ waves. Although this " ℓ spoiling" is small for the ionization of H_2 ,³¹ it is probably much larger for N_2 . Good agreement between experiment^{32,33} and theory³¹ for H_2 has been one result. Agreement with the results of Schneider and Berry³⁴ for the ionization of N_2 is not as good, as seen in Table II of Chap. 5.

The theory of Schneider and Berry³⁴ and Tully, Berry, and Dalton³¹ averages the photoelectron angular distribution of the target molecule over rotational levels of the initial state. Buckingham, Orr, and Sichel^{35,36} have presented theory for molecules for which resolution of rotational fine structure allows for measurement of β for individual rotational transitions. The authors consider the coupling of molecular angular momenta in Hund's cases a and b, but make no numerical calculation for specific molecules.

Several approximate theories show promise in calculations of the electron energy variation in β for molecules. The mathematical representation of the final electronic state, that of a free electron

moving in the field of a positive ion, is complex, even for the photoionization of hydrogen atoms. The approximate theories simplify mathematical expressions, typically by requiring a particular form for the final state wavefunction.

Several groups have required the final state to be a plane wave orthogonalized to occupied ground state orbitals of the molecule (OPW). Lohr³ has reported the variation of β with photoelectron energy for the vanadium atom and the ethylene molecule. Later, Ellison³⁷ generalized the OPW method of Lohr to molecules of any arbitrary symmetry for which an LCAO-MO description was available. Rabalais^{38,39} then calculated β values for N_2 , Ne, and the series of hydrides isoelectronic to Ne. This method may give the gross variation of β with electron energy for ionization over 100 eV above threshold. However, it cannot be accurate for ionization near threshold, since the plane wave function fails to represent the long range Coulombic potential felt strongly by a slowly moving photoelectron.

Huang and Ellison⁴⁰ have modified the OPW formalism in order to get better agreement with experiment. Their extended OPW method orthogonalizes the continuum plane waves to a minimum number of unoccupied virtual molecular orbitals as well as to all of the occupied orbitals. The method gives good agreement with experiment for H_2 , but results differ only slightly from OPW results for N_2 and CH_4 .³⁸

Several groups have forced the potential felt by the photoelectron to be Coulombic. Although this method is computationally more

expensive than the OPW approach, results should agree better with experiment, in principle.

Ritchie⁴¹ has parameterized initial molecular orbitals via a single-center expansion and calculated a perturbative form for the photoelectron wavefunction. When the wavenumber of the outgoing photoelectron is k , the method is valid to $O(k^{-2})$, which means that the theory is applicable only to X-ray photoionization. Ritchie cautions that numerical calculation of accurate photoelectron wavefunctions for lower energy photoionization must await the direct solution of the appropriate coupled radial equations.

Iwata and Nagakura⁴² have forced the photoelectron wavefunction into a single center hydrogenic form which is then orthogonalized to the occupied molecular orbitals. They quote orbital photoionization cross sections and β values over a 900 eV range of photon energie for Ne, HF, H₂O, NH₃, CH₄, Ar, and H₂S. In principle, the method should not be as accurate as that of Kennedy and Manson,¹⁸ who solve the differential equation for the Hartree-Fock wave function directly. However, the calculation of Iwata and Nagakura and the experimental results of Wuilleumier and Krause⁴³ show a minimum in the 2s photoionization cross section at a photon energy of roughly 100 eV, where the Kennedy and Manson¹⁸ calculation goes through a maximum. For ionization from a particular orbital, there might be N nodes in the appropriate radial wavefunction. Then, there should be N minima (called Cooper-minima) in the variation of the subshell cross section with photoelectron energy. Iwata and Nagakura⁴² suggest that their

orthogonalization procedure brings about the minimum in the 2s cross section. In any case, the angular distribution calculations of Iwata and Nagakura for molecular photoionization may well be fairly accurate.

For ionization from largely p-like orbitals of Ne, Ar, NH_3 , and H_2O , Iwata and Nagakura⁴² find an interesting difference between the variation of β with electron energy for orthogonalized Coulomb (OCW) and OPW photoelectron functions. Within 35-40 eV of ionization threshold, β is generally an increasing function of electron energy. However, β_{OPW} reaches a minimum at roughly 5 eV above threshold near -1. Below 5 eV above threshold, β_{OPW} is a decreasing function of electron energy, in contrast to the monotonic increase of β_{OCW} in this region. Furthermore, in the threshold region where β values in both calculations are monotonically increasing with electron energy, β_{OPW} is approximately 1 unit of β lower than β_{OCW} .

A new method proposed by J. Dehmer and D. Dill probably shows the most promise for angular distribution calculations for molecular photoionization.⁴⁴ This method, called the "multiple-scattering method", has been applied previously to the general theory of particle scattering.⁴⁵ By this method, the potential of a molecule or molecular ion is represented as a cluster of non-overlapping spherical potentials centered on the atomic sites.⁴⁶ Calculations based upon the multiple scattering method are available at present only for the K-shell photoionization of N_2 .⁴⁷

REFERENCES

1. L. I. Schiff, Quantum Mechanics 3rd edition (McGraw-Hill, New York, 1949) p. 397.
2. R. P. Feynman, Quantum Electrodynamics (W. A. Benjamin, New York, 1961).
3. L. L. Lohr, in D. Shirley (editor) Electron Spectroscopy (North-Holland, Amsterdam, 1972) p. 245.
4. I. G. Kaplan, A. P. Markin, Opt. Spectry. 24, 475 (1968); 25, 275 (1968).
5. W. Thiel, A. Schweig, Chem. Phys. Lett. 12, 49 (1971).
6. H. A. Bethe, E. E. Salpeter, Quantum Mechanics of One and Two Electron Systems, (Springer-Verlag, Berlin, 1957) pp. 308-310.
7. J. Cooper, R. N. Zare, in S. Geltman, K. Mahanthappa, N. Brittin (editors) Lectures in Theoretical Physics Vol. XI-C (Gordon and Breach, New York, 1969) p. 317.
8. J. W. Cooper, S. T. Manson, Phys. Rev. 177, 157 (1969).
9. J. A. Kinsinger, J. W. Taylor, Int. J. Mass Spectrom. Ion Phys. 10, 445 (1973).
10. G. Wentzel, Z. Phys. 41, 828 (1927).
11. A. Sommerfeld, G. Schur, Ann. Phys. 4, 409 (1930).
12. G. Schur, Ann. Phys. 4, 433 (1930).
13. H. Bethe, Handbuch der Physik, Zweite Auflage, Quantentheorie (Springer-Verlag, Berlin, 1933) V. 24, p. 482.
14. M. A. Chaffee, Phys. Rev. 37, 1233 (1931).
15. J. Berkowitz, H. Ehrhardt, Phys. Lett. 21, 531 (1966).

16. S. H. Lin, Can. J. Phys. 46, 2719 (1968).
17. J. L. Hall, M. W. Siegel, J. Chem. Phys. 48, 943 (1968).
18. S. T. Manson, D. J. Kennedy, Phys. Rev. A 5, 227 (1972).
19. S. T. Manson, J. Electron Spectr. 1, 413 (1973).
20. D. Dill, S. T. Manson, A. F. Starace, Phys. Rev. Lett. 32, 971 (1974).
21. D. Dill, A. F. Starace, S. T. Manson, Phys. Rev. A 11, 1596 (1975).
22. S. T. Manson, A. F. Starace, D. Dill, in J. S. Risley, R. Geballe (editors) Electronic and Atomic Collisions (U. of Washington, Seattle, 1975).
23. D. Dill, Phys. Rev. A 7, 1976 (1973).
24. T. E. H. Walker, J. T. Waber, Phys. Rev. Lett. 30, 307 (1973); J. Phys. B. 7, 674 (1974).
25. G. V. Marr, J. Phys. B 7, L47 (1974).
26. M. Ya. Amusia, N. A. Cherepkov, L. V. Chernysheva, Phys. Lett. 40A, 15 (1972).
27. See Chap. 4, this work.
28. R. G. Houlgate, J. B. West, K. Codling, G. V. Marr, J. Phys. B 7, L470 (1974).
29. W. S. Watson, D. T. Stewart, J. Phys. B 7, L466 (1974).
30. C. D. Lin, Phys. Rev. A 9, 181 (1974).
31. J. C. Tully, R. S. Berry, B. J. Dalton, Phys. Rev. 176, 95 (1968).
32. R. Morgenstern, A. Niehaus, in L. Branscomb (editor) Electronic and Atomic Collisions (North-Holland, Amsterdam, 1971) p. 167.

33. T. A. Carlson, A. E. Jonas, J. Chem. Phys. 55, 4913 (1971).
34. B. Schneider, R. S. Berry, Phys. Rev. 182, 141 (1969).
35. A. D. Buckingham, B. J. Orr, J. M. Sichel, Phil. Trans. Roy. Soc. Lond. A268, 147 (1970).
36. J. M. Sichel, Mol. Phys. 18, 95 (1970).
37. F. O. Ellison, J. Chem. Phys. 61, 507 (1974); 62, 4587 (1975).
38. J. W. Rabalais, T. P. Debies, J. L. Berkosky, J.-T. J. Huang, F. O. Ellison, J. Chem. Phys. 61, 529 (1974); 62, 4588 (1975).
39. T. P. Debies, J. W. Rabalais, J. Amer. Chem. Soc. 97, 487 (1975).
40. J.-T. J. Huang, F. O. Ellison, Chem. Phys. Lett. 29, 565 (1974).
41. B. Ritchie, J. Chem. Phys. 60, 898 (1974); 61, 3279, 3291 (1974).
42. S. Iwata, S. Nagakura, Mol. Phys. 27, 425 (1974).
43. F. Wuilleumier, M. O. Krause, Phys. Rev. A 10, 242 (1974).
44. S. T. Manson, private communication.
45. K. M. Watson, Phys. Rev. 88, 1163 (1952); 89, 575 (1953); 103, 489 (1956); 105, 1388 (1957); D. Agassi, A. Gal, Ann. Phys. (N.Y.) 75, 561 (1973).
46. D. Dill, J. L. Dehmer, J. Chem. Phys. 61, 692 (1974).
47. J. L. Dehmer, D. Dill, Phys. Rev. Lett. 35, 213 (1975).

CHAPTER 3 - EXPERIMENTAL

$$\underline{\underline{F}} = e [\underline{\underline{E}} + \underline{\underline{v}} \times \underline{\underline{B}}]$$

3.1 Introduction

The present experimental apparatus consists of four basic components, a stationary line source lamp, a sample chamber, a rotatable electron energy analyzer and detection system, and a computer-based data acquisition system. The basic design is given in Paper I, section 3.2, to follow and in the Masters Thesis of Douglas C. Mason. Paper I also motivates the computer automation of data acquisition, reduction, and display features.

Several experimental procedures and calculations had not yet been fully documented, so they are presented in Appendices A-E. Appendix A summarizes the design calculation and specifications of the Helmholtz coils. The results of a calculation of the intersection of two cones is included in Appendix B. Appendix C describes data-taking strategies. Appendix D describes the sample inlet system and methods of sample handling. Statistical theory relating to the weighted least squares calculation of the photoelectron asymmetry parameter and its variance appears in Appendix E.

3.2 Paper I - A Variable Angle Photoelectron Spectrometer

A Variable Angle Photoelectron Spectrometer

D. M. Mintz, D. C. Mason, and A. Kuppermann

Arthur Amos Noyes Laboratory of Chemical Physics,
California Institute of Technology, Pasadena, California 91125

The design, construction, and performance of a spectrometer for measuring the angular and energy distributions of electrons photoejected by rare gas resonance light are described. Results using 584.4 Å photons from a helium lamp are reported. Flexibility of instrumental design allows for the use of other light sources. A 180° hemispherical electrostatic electron energy analyzer is rotatable about the center of an enclosed sample chamber. The instrument is highly automated, with an on-line computer used to control detector angle and the data acquisition and reduction. This is required by the large volume of data produced.

I. INTRODUCTION

Since the early 1960's, photoelectron spectroscopy has found wide acceptance as a tool for studying the electronic structure of molecules.^{1, 2} Monochromatic light sufficiently energetic to ionize atoms or molecules ejects photoelectrons whose energies are given by

$$E_e = h\nu - E_I ,$$

where E_I is the energy needed to ionize the molecule. The resulting ion can be electronically, vibrationally, and rotationally excited. E_I is determined from a knowledge of $h\nu$ and measurement of E_e and furnishes information on the strength of molecular bonds, molecular geometry in ground and ionic states, and intramolecular interaction of functional groups.² In addition, the measurement of photoelectron intensities as a function of photon energy has facilitated the modeling of complex processes in plasmas and in the upper atmosphere.³

Since 1968,^{4, 5} it has been realized that the angular distribution of photoelectrons contained additional information of value in the interpretation of their energy spectra. Briefly, for nonpolarized light, the angular distribution for electric-dipole ionization has the form

$$\frac{d\sigma}{d\Omega} = \frac{Q}{4\pi} \left[1 - \frac{\beta}{4} (3 \cos^2 \theta - 1) \right] , \quad (1)$$

where $d\sigma/d\Omega$ is the differential photoelectron cross section for a given transition, Q is the corresponding total cross section, θ is the angle between the light axis and the velocity vector of the outgoing electron, and β is a single asymmetry parameter in the range -1 to 2 that describes the deviation of the angular distribution from an isotropic one. The

values of β and Q depend on the characteristics of the electron ejected, such as its angular momentum, and on the wavelength of the light employed.

The first modern experimental work in measuring photoelectron angular distributions was carried out by Berkowitz and Ehrhardt,⁶ who employed a moveable electrostatic retarding grid energy analyzer and a fixed lamp. More recent approaches to measuring photoelectron angular distributions using vacuum ultraviolet excitation can be divided into four categories.

Carlson,⁷ following on the success of employing moveable X-ray sources for measuring X-ray photoelectron angular distributions, has rotated the lamp around a fixed ionization region followed by a stationary energy analyzer. Results have been obtained in studies of a wide range of sample vapors.⁸ This method suffers only in that relatively simple lamps can be used; variation of incident wavelength using a rotatable monochromator and continuum light source would be very cumbersome. In a similar spirit, the angular distributions of photodetached electrons have been studied by rotating the polarization direction of a laser light source.⁵

A second group has employed two separate light sources of different degrees of polarization.^{9, 10} Here, both the lamp and detector are fixed and β may be extracted¹¹ from a knowledge of photon polarization and relative intensity in the two experiments. This method suffers from a lack of measurement redundancy and consequently, the presence of experimental artifacts that affect the angular distribution and yield spurious results cannot be detected directly.

Several groups have opted for a multiple detector for measuring photoelectron angular distributions. Ames et al.¹² and Samson¹³ have used a pair of channeltron-type electron multipliers accepting electrons emerging from a single energy analyzer after having been ejected in different directions from a single ionization region. These measurements suffer principally from lack of redundancy and the need to normalize results to β values obtained by other methods. Both experiments assume that relative detector response is constant with time. Early results obtained by McGowan et al.¹⁴ used a sectorized spherical retarding potential analyzer. In order to maximize signal into an electrometer, large sectors subtending a 15° range in θ were employed. Angular resolution is thus 15° and the effect of averaging the angular distribution over β must be considered. The inability to operate the detector in a pulse-counting mode limits experimental sensitivity. Results for low electron energies (NeI ionization of Ar) indicated artifacts due to stray electric or magnetic fields.

A fourth approach, the one originally employed by Berkowitz and Ehrhardt,⁶ uses a stationary line source lamp and a single moveable detector. This has been the method favored subsequently by Morgenstern et al.,¹⁵ Harrison,¹⁶ Dehmer et al.,¹⁷ and the present workers.¹⁸ Flexibility in choice of light source is one consequence of this design approach.

Several recent studies with tunable light sources and moveable electron energy analyzers appear promising. Houlgate et al.¹⁹ and Watson and Stewart²⁰ have measured photoelectron angular distributions for noble gases using synchrotron radiation and a vacuum ultraviolet

monochromator. When the experimental arrangement is fully optimized to permit them to obtain spectra at high resolution²¹ this should be a very powerful technique for the study of molecular photoionization.

II. APPARATUS

A block diagram of the apparatus is given in Fig. 1. It consists of a lamp, a sample chamber, and an energy analyzer, all mounted on an 18 in. diameter stainless steel flange which is bolted to a high vacuum system, and a data acquisition system. The individual components are described below.

A. Lamp

The HeI (584.4 Å) capillary discharge lamp is a variant of the Geissler tube described by Newburgh *et al.*²² A scaled section view is given in Fig. 2. Matheson UHP grade helium flows through a Linde-type 4X molecular sieve-filled trap immersed in liquid nitrogen before entering the rear of the lamp. The discharge is maintained between a low magnetic permeability stainless steel anode at positive high voltage and a grounded tungsten carbide cathode through a quartz capillary of length 19 mm and bore 2mm. Other materials used in fabricating the lamp include aluminum for the main body, boron nitride for insulators, and elastomeric O-ring seals that allow the lamp to be tested outside of the vacuum chamber.

The region between discharge and the main vacuum chamber is pumped by a $\frac{1}{2}$ l/s and a $2\frac{1}{2}$ l/s mechanical pump in a differential pumping arrangement. This reduces the pressure rise in the main vacuum chamber to 10^{-5} Torr during lamp operation. Light passes through a

0.9 mm diameter aluminum capillary before entering the sample chamber. Kerosene lines connected to a recirculating pump and heat exchanger cool the lamp during operation. Lamp power is supplied by a J. Fluke Model 407 power supply through a $1320\ \Omega$, 150 W ballast resistor. The discharge is initiated by striking a tesla coil to a starter electrode located in back of the anode.

The lamp cathode was ground from tungsten carbide in order to maximize resistance to cathodic sputtering. Sputtering over a period of two months of continuous lamp operation constricts the light exit hole in the cathode by 20-30%. Previous designs employing molybdenum cathodes underwent degradation of similar magnitudes in operation periods of only two weeks.

Typical lamp operating parameters are a discharge current of 100 mA and an anode voltage of +365 V. Precise measurements of operating pressure inside the lamp are not made. However, between the molecular sieve trap and the lamp body, a Wallace and Tiernan manometer registers 8 Torr, so that the lamp operating pressure is estimated at 2-4 Torr.

Photon flux is monitored inside the sample chamber by a photodiode similar in design to that of Samson.²³ The anode of the flux-measuring device, at a potential of +12 V, is hidden from the inside of the sample chamber by a strip of 100 lines/in. gold mesh which is maintained at the same potential as the tungsten photocathode. A Victoreen Model VTE-2 electrometer measures the photocathode current to ground. Assuming a 14% quantum efficiency of the undegassed photocathode surface,²⁴ we estimate a photon flux of 1.8×10^{11} photons/sec

passing through the ionization region. The angular width of the light beam, as determined by appropriate apertures, was 1.8° .

The lamp was tested on a vacuum ultraviolet monochromator without Zeolite trapping of the helium. Only one significant vacuum ultraviolet impurity line at 1216 \AA was observed, but its intensity did not exceed 1% of the 584.4 \AA principal line. Subsequent tests on the photoelectron spectrometer run with CS_2 in the sample chamber, as recommended by Turner,² revealed no detectable low electron energy peak arising from 1216 \AA ionization to the \tilde{X} ionic state.

Lamp parameters of helium pressure and discharge current are adjusted to maximize the photocathode current. Under these conditions, photoelectrons arising from ionization by the helium 537 \AA ($1s^2 \leftarrow 1s3p$) and 522 \AA ($1s^2 \leftarrow 1s4p$) lines are observed with respective counting rates of 2% and 0.5% of the corresponding 584.4 \AA peaks.

B. Sample Chamber

The sample chamber was designed to maximize electrostatic shielding, minimize gas leakage, and reduce the photoelectron background counting rate produced by the unabsorbed photon beam. The sample chamber, shown in Fig. 3, consists of three coaxial shells made of gold-plated copper. Gas enters the base through GI into the inner chamber, IS. Electrically, this chamber is insulated from the other chambers and is connected to the rotating energy analyzer. The middle shell, MS, remains fixed with respect to the lamp. The photon beam enters the inner shell by a slot, HS, in the outer shell, OS, a 2 mm aperture, LI, in the middle shell, MS, and a slit in the inner shell. The unabsorbed photon beam is trapped at the photocathode

assembly mounted on the middle shell (not shown in Fig. 3) after passing completely through the inner shell. As the observation angle is changed, the outer shell rotates with the detector and undergoes translation along the chamber axis, guided by the helical slot, HS, and guide screw, GS. Thus, the light entrance hole is not obscured. The outer sleeve incorporates Teflon gaskets to the middle shell in order to minimize gas leakage. Mechanical interactions inside the sample chamber limit the range of permissible detector angles to 38° - 126° with respect to the light axis.

Gas samples are manipulated on a small glass inlet manifold before they are introduced into the instrument. In order that the sample chamber pressure change only slowly with time, the sample gas is stored in a 5 liter ballast bulb during operation. The samples are admitted into the sample chamber through a Granville Phillips model 203 variable leak valve. When samples are liquids at room temperature, |————— we do not use the ballast, but instead admit the vapor directly from the bulb containing the sample. The leak valve is in this case heated to 40°C to prevent condensation at the valve orifice and the accompanying irregularity of flow. In order to avoid cross contamination of one sample by preceding ones, the glass manifold is baked in an annealing oven when changing from one substance to another.

Sample gases enter the sample chamber through the base of the middle shell. A duct connected to that base leads to a Westinghouse-type WL-7903 high pressure ionization gauge mounted outside of the vacuum chamber on the 18 in. main flange. The gauge output signal

varies linearly with pressure in our normal range of operating pressures of 2 to 5 mTorr.

We have found that sulfur and halogen-containing organics damage the high pressure ionization gauge filament for sample pressures in the range 2-4 mTorr. A capacitance manometer would be a better, albeit a more expensive, sample pressure measuring device.

Detected photoelectron signal I_{pe} depends on sample pressure via a Lambert-Beer law:

$$I_{pe} = AI_{ph}(1 - e^{-Q_{pe}n\ell_{pe}})e^{-Q_{es}n\ell_{es}}, \quad (2)$$

where I_{ph} is the initial photon flux, Q_{pe} and Q_{es} are the total cross sections for photoionization and electron scattering, respectively, and ℓ_{pe} and ℓ_{es} are the pathlengths over which photoionization contributes to detected signal and electron scattering attenuates it, respectively. A is an overall detection efficiency constant. The number density of absorbers or scatterers n is proportional to pressure. The total electron scattering cross section is several orders of magnitude larger than the photoionization cross section for the typical range of electron and photon energies encountered in this experiment. As a result, a nonlinear dependence of I_{pe} on pressure can arise from electron scattering even at pressures sufficiently low for the $1 - e^{-Q_{pe}n\ell_{pe}}$ to be a linear function of pressure. In order to maximize the signal to background ratio, we operate at the maximum pressure for which the photoelectron counting rate depends linearly on pressure, which is determined separately for each substance studied. Typical maximum permissible operating pressures are 4 mTorr for nitrogen and argon.

C. Electron Energy Analyzer and Detector

The electron energy dispersion and detection system is composed of four parts: a decelerating lens, a 180° double focusing hemispherical analyzer,²⁵ an accelerating lens, and a Spiraltron electron multiplier. The whole detection system is mounted on a single 200 mm diameter worm gear and is rotated about the (horizontal) axis of the sample chamber. This gear must be lubricated periodically with molybdenum disulfide to limit wear. The lens elements and hemispheres were fabricated from OFHC grade copper and plated with 24K gold. The lenses are held rigidly in place by boron nitride spacers and aluminum mounting brackets bolted directly to the inner hemisphere. A scaled section view is shown in Fig. 4.

Apertures of diameter 1.0 mm in the inner shell of the sample chamber and the first lens element limit the detector acceptance half angle to 2.1° . The hemispherical analyzer is operated in the constant electron energy mode²⁶ in order to optimize electron energy resolution. The lens formed by elements C1 and HC decelerates photoelectrons, initially having kinetic energy T , to a fixed energy V usually chosen to be 1.5 eV. The difference $T - V$ is called the sphere center energy. Spectra are generated by sweeping the potential applied to the lenses HC, HM, and M1 and the various sphere elements with respect to C1, which is connected to the inner shell of the sample chamber. This mode has the advantage that the absolute energy resolution remains roughly constant over the full range of the spectrum.

The operation of the hemispherical energy analyzer has been discussed at length by Purcell.²⁵ Our analyzer has a mean radius of

38.1 mm and a 1.27 mm radial gap between inner and outer spheres. Space and weight restrictions have dictated that we not use full hemispheres; the sides were cut off and the hemisphere halves are surrounded by a stainless steel bracket held at the sphere center potential.

We anticipated deviations from the nominal $1/r$ analyzing field because of this modification. As a result, we incorporated correcting electrodes halfway around the hemispheres. Turner²⁷ has found correcting electrodes like these helpful in improving resolution in 127° cylindrical analyzers. To date the spectrometer has been operated with the inner sphere and outer sphere corrector electrodes left at the potentials of the corresponding spheres. Contamination of the electron energy analyzer surfaces tends to slowly reduce counting rates over periods of a month, requiring periodic cleaning.

After emerging from the analyzer, the photoelectrons are accelerated to 6.5 eV by a Herzog lens element and final cylindrical lens and focused through a 1.0 mm diameter aperture in the rear of that lens. Thereafter, they are accelerated into the front cone of a Bendix Model 4219X Spiraltron electron multiplier biased at +60 V with respect to ground. The Spiraltron is mounted on a boron nitride support by two of its electrical connecting tabs, and is enclosed in an aluminum chamber to eliminate being reached by stray electrons. We operate the Spiraltron as a two-terminal device. Its anode is connected, via a 1000 M Ω glass-encapsulated resistor to a copper collector plate and a +3200 V power supply.

Charge pulses at the copper collector are converted into voltage pulses by a differentiating network. The voltage pulses, 10-50 mV in

height, are amplified and discriminated by a specially designed pulse amplifier involving inexpensive and easily replaceable components. This facilitates its repair when it is damaged by high voltage breakdowns in the system.

The inner shell of the sample chamber, the Herzog lenses, and the hemispheres are coated with aquadag in order to reduce the probability of reflection of electrons from surfaces. The aquadag surfaces are polished in order to reduce fluctuations in contact potentials.²⁸ The spheres and lenses may be baked to 200°C by heaters mounted on the inner hemisphere.

A schematic of the lens and sphere voltage distribution system is shown in Fig. 5. To take a photoelectron spectrum we sweep the output voltage of a 12-bit digital to analog converter under computer control. This voltage is divided according to the desired energy increment between successive channels in the spectrum. Biasing power supplies and operational amplifiers supply voltages to the lens and sphere elements. The use of operational amplifiers reduces output impedance below 1 Ω and output voltage ripple below 5 mV peak to peak.

A typical spectrum obtained with an analyzing energy of 0.75 eV is shown in Fig. 6. Normally, in order to maximize signal rates and to reduce susceptibility to changing surface conditions, we operate at an analyzing energy of 1.5 eV for which the resolution is about 30 meV. Furthermore, faster electrons are less susceptible to magnetic field deflections and thus angular distributions are less prone to magnetic field-induced artifacts at this higher analyzing energy.

D. Additional Experimental Hardware

A Bodine NSH-12R reversible 1/50 horsepower dc motor provides electromechanical control of the detector angle. The motor drive shaft is linked to the main worm gear via a stainless steel worm through a rotary motion feedthrough on the instrument main flange. For each revolution of the drive shaft, the detector rotates by one degree. The drive shaft is geared to a Disc model 100 incremental shaft encoder which makes ten dry reed switch contacts for each one full shaft rotation. The detector angle is determined by counting switch closures from the previous angle and noting the direction of shaft rotation. Under operating conditions, the detector angular position is known to $\pm 0.2^\circ$. Internal alignment is assured by appropriately located positioning pins.

To eliminate the earth's magnetic field, the inside of the vacuum chamber is lined with a single layer of 1.27 mm mu-metal shielding in which holes are provided for the connections to the main diffusion pump and the main flange. The resulting magnetic field in the region traversed by the electrons is about 10 mG.

Due to the motion of the detector, this resulted in spurious asymmetries in the angular distribution. To eliminate the artifact, the main vacuum chamber was surrounded by three pairs of square Helmholtz coils whose sides measure about 3 m in length. The east-west and north-south coils are separated by the recommended distance,²⁹ 0.544 times the edge length, which minimizes field gradients between the coils along their axes. The vertical pair lie on the floor and above the e-w and n-s pairs in order to facilitate our access to the vacuum chamber. The coils were constructed from 40 km of 26 AWG copper magnet wire wound

around an aluminum channel. This brings the residual magnetic field down to 0.3 mG and makes detection efficiency become independent of detector angle.

Several times after line voltage power fails, some lasting only a fraction of a second, we found the need to perform extensive degaussing of instrument parts made of 304 stainless steel and of the mu-metal shield. The magnetic field transients resulting from transients in the primary power to the three dc regulated Helmholtz coil power supplies induced permanent magnetism in susceptible metals. The solution to this difficulty was to install a Topaz Model 315-BK-12 uninterruptible power supply rated at 300 VA maximum inverter capacity. The switching times of 10-15 msec of this device were found not to magnetize the instrument components. A 90 Ah lead-acid battery provides backup power for as long as 1 h in the event of a power failure.

The main vacuum chamber is pumped by a Varian-NRC Model VHS 6 in. oil diffusion pump trapped with a Varian-NRC 6 in. liquid nitrogen-cooled baffle. The outlet side of the main diffusion pump is backed by a CVC Model MCF 300 oil diffusion pump which acts as a booster stage. The two diffusion pumps are separated by a freon-cooled chevron baffle. Between the diffusion pumps and a rotary mechanical pump is a molecular sieve trap to limit mechanical pump oil contamination of the diffusion pump oil.

We reach a base pressure of 2×10^{-7} Torr after a day of pumping. Total sample and helium background pressures in the main chamber during operation is typically 1.5×10^{-5} Torr.

E. Data Acquisition System

1. Hardware

Low photoelectron counting rates for most of the samples studies require long data acquisition times. It was necessary to record sample chamber pressure, lamp flux, and other experimental parameters over the 1-9 h interval of a typical angular distribution. Some on-line data reduction, the location and counting rates at photoelectron peaks, as well as a paper tape record of each spectrum, were desirable in order to save data for later manipulation. The need to provide redundancy in measuring the angular distribution parameter β by a fit to intensities at more than two angles has been discussed above. In order to free us from physical presence in the lab to change the detector angle for each successive spectrum, automatic control of the angle drive system was desirable.

We found a computer-based data acquisition system ideally suited to these measurement and control functions over long periods of time. A block diagram of this data acquisition system is given in Fig. 7.

A Digital Equipment Corporation Model PDP8/e minicomputer forms the heart of the data acquisition system. It operates with 8192 words of core and semiconductor memory with a memory cycle time of 1.2 μ sec. Standard computer peripheral devices include a Teletype Model ASR33 terminal, a Decitek Model 242A7 300 character/sec photoelectric paper tape reader, a Teletype Model BRPE paper tape punch, and an interface to the Caltech Campus PDP10 computer. The two high-speed paper tape peripherals greatly facilitate handling of the large quantities of data generated by the data acquisition system.

Other standard hardware features include a real time clock and three channels of digital to analog conversion. The real time clock supplies a 120 Hz time base for measuring counting rates. One digital to analog converter channel operates the energy scanning electronics actively; we do not synchronize to an externally generated ramp. Two digital to analog converter channels permit oscilloscope display of spectra during data acquisition with counting rate along the Y axis and electron energy along the X axis. These same two digital to analog converters provide plotting capability on a Hewlett-Packard Model 7001AMR X-Y recorder. This system was used to plot Figs. 6 and 9 except for the lettering.

Three interfaces were used for control of the experiment. A counting interface includes a 12-bit counter and a digital display. The counter may be operated by recording either the time needed to obtain a fixed number of counts or the number of counts accumulated in a fixed time interval. A six-digit display is used as a digital ratemeter during data acquisition.

A second interface provides analog to digital conversion capability. Under computer control, one of ten voltages can be switched to either the high or low inputs of an autoranging $4\frac{1}{2}$ -digit Fairchild Model 7000 A digital multimeter. The autoranging feature and the inherent accuracy of dual-slope analog to digital conversion more than compensate for the long ($\frac{1}{4}$ sec) conversion times. Since the sample pressure, lamp flux, and lens and sphere voltages vary slowly with time, speed of operation was not required. The logic ground within the digital multimeter floats with the low input signal. The BCD representation of the numbers

in the multimeter display tubes, the signal polarity, and the decimal point location signals are level shifted to ground referenced logic levels.

A third interface contains a 12-bit drive register and a 4-bit sense register. The logical states of the 12 drive lines act as on-off switch states to the experiment. Under one computer instruction, all 12 logic states are transferred from the computer's accumulator to the drive buffer register. Control functions furnished by the drive lines include Teletype motor on, high speed punch motor on, X-Y plotter pen down, angle drive increase detector angle, angle drive decrease detector angle, audio alarm on, analog multiplexer under computer control, and activate "do not disturb" flashing red light near the laboratory entrance. Changes in the sense line register result from turning the resonance lamp on or off, making or breaking switch closure in the angle drive shaft feedback system, initiating or terminating a liquid nitrogen filling cycle, or setting or resetting a vacuum status logic level in the vacuum system control and interlock unit. A change in any one of these status switches causes a computer interrupt and the computer interrupt service program takes the appropriate action.

2. Software - Data Acquisition

From the standpoint of operating software, the 8K words of computer memory are divided into two 4K segments. A systems program in the first 4K of nonvolatile core memory provides access to software floating point routines, photoelectron spectrometer control functions, input-output devices, and the real time clock for higher level user programs in the second 4K of volatile semiconductor memory. To implement

this, we operate the second 4K in a time-sharing mode. Linkage to system routines from data acquisition and reduction programs is provided by pseudoinstructions which interrupt the processor (computer trap).

Data-taking software allows the PDP8/e to take data in the manner of a multichannel scaler. For a fixed dwell time, photoelectron counts are accumulated in the 12-bit counter interface. At the end of this period, the counter total is loaded into memory, the digital to analog converter that selects the detected electron energy advances by a small predetermined increment, and the counter is reset. The number of data channels for which photoelectron intensity is to be accumulated is an operator-set parameter. In order to average over fluctuations in lamp intensity and sample pressure, a dwell time of 1 sec is used and multiple passes over the spectral region are performed. Data acquisition is inhibited during liquid nitrogen filling cycles because solenoid switching transients interfere with the pulse counting.

Several features of the computer-based system provide important advantages over conventional multichannel-analyzer-based systems. First, the user can select from 1 to 511 data-taking channels, where each channel has the capacity of over 8 million counts. This flexibility allows us to scan different kinds of spectrum features with different numbers of channels. Sharp peaks over a limited range of the photoelectron spectrum are scanned with as few as 20 channels, whereas full spectra at $\theta = 54.7^\circ$ are scanned with all 511 channels. Second, all spectrum parameters, including time of day, energy range of the spectrum scanned, energy increment between channels, lens and sphere voltages, and the signals from the lamp photocathode and sample pressure

gauge are printed automatically on the teletype console. Third, at the conclusion of each single pass over the full spectrum, the computer measures the sample pressure. After the last pass, an average pressure obtained from dividing the sum of all pressure readings by the number of readings is automatically printed on the Teletype console. This feature allows one to compensate partially for pressure changes.

Computational capabilities of the computer-based data acquisition system allow for partial on-line reduction of the raw data. Spectra are smoothed by the least squares method of Savitzky and Golay.³⁰ A routine based upon the Savitzky and Golay least squares derivative algorithm³⁰ then locates the peak maxima. The apparent ionization potential and the counting rate from the convoluted spectrum at those peak maxima are printed on the Teletype console.

In the normal mode of taking angular distributions, we measure spectra at detector angles varying from 40° to 120° in 10° increments. In operation, a sequence of instructions punched on a short strip of paper tape is read by the high speed paper tape reader. These instructions direct the computer to take spectra, punch spectra and spectrum parameters on the paper tape punch, change the detector angle, and print out peak heights and apparent ionization potentials.

An experimental counting rate background of 0-2 counts/sec rises toward low electron energy but is independent of sample pressure. We measure background spectra at each of the nine detector angles just mentioned and parameterize the results as a series of three line segments. Subsequent calculation of β is made correcting for this background.

The sample chamber volume from which photoelectrons are detected varies inversely with the sine of the detector angle θ providing the lamp and energy analyzer view cones subtend small angles and that θ is near 90° . For the present view cone geometries, the deviation from the above form is less than 0.2% for θ between 40° and 120° . Thus, if the light beam and the sample chamber gas density are assumed homogeneous, multiplication of peak intensities by $\sin \theta$ should yield good fits of $I(\theta)$ to Eq.(1).

The configuration of sample chamber sliding seals and slots results in a sample pressure which is detector angle dependent. It is approximately 15% lower at 80° than it is at 40° and 120° . Pressure compensation for these large pressure changes becomes a necessity. Since our counting rate dependence on pressure is linear, it is a simple matter to compensate for angular variations of sample pressure.

3. Software - Data Reduction

We obtain values of β from the angular dependence of pressure compensated, volume corrected counting rates by a weighted least squares fit to the expression

$$I(\theta) = A + B \sin^2 \theta . \quad (3)$$

The linear parameters A and B are determined by simple linear regression theory.³¹ Weights are chosen inversely proportional to the variance in the measurement of counting rate (which is equal to the number of counts) and are normalized to 9, the number of values of θ used. The variance σ_β^2 of β is obtained from propagating the variances σ_A^2 and σ_B^2 of A and B³²:

$$\sigma_{\beta}^2 = \left(\frac{\partial \beta}{\partial A}\right)^2 \sigma_A^2 + \left(\frac{\partial \beta}{\partial B}\right)^2 \sigma_B^2 \quad (4)$$

Here σ_A^2 and σ_B^2 are obtained from diagonal elements of the weighted least squares variance-covariance matrix.³¹ The lengths of the error bars in the β curve of Fig. 9 are equal to σ_{β} .

A PDP8/e 8K system based program performs the calculation of β just described. In one mode, the user enters angles, peak heights, and sample pressures manually via the Teletype keyboard for spectrum peaks located by the peak searching feature of the data-taking program. In another mode, it reads in, via the high speed reader, a paper tape on which are tabulated intensities and sample pressures for all channels in the spectrum for which intensity exceeds a preselected threshold. It then performs the calculation of β for each of these channels.

Another PDP8/e 8K system based program provides india ink plots of spectra, energy and intensity tick marks, and the variation of β across full spectra.

III. RESULTS

Figure 8 shows an angular distribution for the $\text{Ar}^+ 2p_{3/2}$ peak. The peak intensity has been pressure compensated, volume corrected, and divided by the pressure compensated intensity at $\theta = 90^\circ$. The dashed curves correspond to the least mean square curve for which $\beta = 0.88$, and as can be seen, its fit to the experimental points is very satisfactory. The value of σ_β is 0.02.

Our results for argon ionized by the HeI line are presented in Table I. together with those of other workers and theoretical calculations. We observe a slight difference between the $j = \frac{3}{2}$ and $j = \frac{1}{2}$ spin-orbit components that is in good agreement with calculations of Kennedy and Manson.³³ Carlson *et al.*⁷ and Morgenstern *et al.*¹⁵ have observed similar behavior in HeI ionization of xenon and krypton, where the difference in β for the two spin-orbit components is appreciably larger.

In Fig. 9 we display the results for a large polyatomic molecule, 1,5-hexadiene, run with the present apparatus. This substance was obtained from the Aldrich Chemical Company. It had a stated purity of 98% and was used without further purification. The sample was degassed by several freeze, pump, thaw cycles on our sample inlet manifold using liquid nitrogen as the cooling agent. Measurement of all the indicated photoelectron angular distributions required three days. The full spectrum was divided into five segments of width approximately 1.5 eV and a nine-angle angular distribution of each segment required 9-10 h. This spectrum was energy-calibrated by taking a spectrum of a mixture of 1,5-hexadiene with argon.

Previous measurements of photoelectron angular distributions for a series of acyclic olefins have shown that β values for π electrons ejected from C-C double bonds are larger by 0.6 to 0.9 than for σ electrons ejected from C-C and C-H single bonds,^{8, 13, 34} when the photoelectrons have comparable energies. This finding and the β values of Fig. 9 lead us to assign the 9.2-10.5 eV region as arising from the ionization of C-C double bond π electrons. This use of angular distributions to interpret photoelectron spectra is an indication of the usefulness of these kinds of measurements. We also attribute the diffuse band which covers the ionization energy range from 11-17 eV and the band centered about 18.2 eV to ionization from C-C and C-H σ bonds. The band between 9.2-10.5 eV has two prominent maxima, one at 9.59 eV and the other at 10.01 eV, which have been assigned³⁵ as π_- and π_+ combinations of the weakly interacting double bonds. A more detailed analysis of this molecule will be published elsewhere.

IV. CONCLUSIONS AND SUMMARY

The design, construction, and operation of a photoelectron spectrometer used for measurements of the angular and energy distributions of photoelectrons intensity have been presented. The apparatus has sufficient sensitivity and stability to be helpful in the study of the electronic structure of a wide range of atoms and molecules. The operation of the apparatus is highly automatic which permits handling of the large quantity of information that is produced. The data are very useful for the interpretation of photoelectron spectra.

ACKNOWLEDGMENTS

We wish to express our thanks to the members of the Instrument Shop of the Division of Chemistry and Chemical Engineering for their gifted assistance in the construction of the instrument, with particular thanks to W. Schuelke and A. Stark. We also thank Dr. O. A. Mosher for his participation in the design of the pulse amplifier.

REFERENCES

1. F. I. Vilesov, B. L. Kurbatov, and A. N. Terenin, Dokl. Akad. Nauk SSSR 138, 1329 (1961).
2. D. W. Turner and M. I. Al-Joboury, J. Chem. Phys. 37, 3007 (1962); D. W. Turner, C. Baker, A.D. Baker, and C. R. Brundle, Molecular Photoelectron Spectroscopy (Wiley-Interscience, London, 1970).
3. G. V. Marr, Photoionization Processes in Gases (Academic Press, New York, 1967), Chaps. 10-12.
4. J. Cooper and R. N. Zare, J. Chem. Phys. 48, 942 (1968); J. Cooper and R. N. Zare, Lectures in Theoretical Physics, S. Geltman, K. Mahanthappa, and N. Brittin, Eds. (Gordon and Breach, New York, 1969), Vol. XI-C, p. 317.
5. J. L. Hall and M. W. Siegel, J. Chem. Phys. 48, 943 (1968).
6. J. Berkowitz and H. Ehrhardt, Phys. Letters 21, 531 (1966); J. Berkowitz, H. Ehrhardt, and T. Tekaat, Z. Physik 200, 69 (1967).
7. T. A. Carlson and A. E. Jonas, J. Chem. Phys. 55, 4913 (1971).
8. T. A. Carlson, G. E. McGuire, A. E. Jonas, K. L. Cheng, C. P. Anderson, C. C. Lu, and B. P. Pullen, Electron Spectroscopy, D. A. Shirley, Ed. (North-Holland, Amsterdam, 1972), p. 207.
9. P. Mitchell and K. Codling, Phys. Letters 38A, 31 (1972); M. J. Lynch, A. B. Gardner, and K. Codling, ibid. 40A, 349 (1972).
10. J. A. Kinsinger and J. W. Taylor, Int. J. Mass Spectrom. Ion Phys. 10, 445 (1972).
11. J. A. R. Samson, J. Opt. Soc. Am. 59, 356 (1969).

12. D. L. Ames, J. P. Maier, F. Watt, and D. W. Turner, *Faraday Discussions Chem. Soc.* 54, 277 (1972).
13. J. A. R. Samson, *Phil. Trans. Roy. Soc. London* A268, 141 (1970)
14. J. W. McGowan, D. A. Vroom, and A. R. Comeaux, *J. Chem. Phys.* 51, 5626 (1969); D. A. Vroom, A. R. Comeaux, and J. W. McGowan, *Chem. Phys. Letters* 3, 476 (1969).
15. R. Morgenstern, A. Niehaus, and M. W. Ruf, *Chem. Phys. Letters* 4, 635 (1970); R. Morgenstern, A. Niehaus, and M. W. Ruf, Electronic and Atomic Collisions, L. Branscomb, Ed. (North-Holland, Amsterdam, 1971), p. 167.
16. H. Harrison, *J. Chem. Phys.* 52, 901 (1970).
17. J. L. Dehmer, W. A. Chupka, and J. Berkowitz, Electronic and Atomic Collisions, J. S. Risley and R. Geballe, Eds. (University of Washington, Seattle, 1975), p. 565.
18. D. C. Mason, A. Kuppermann, and D. M. Mintz, see Ref. 8, p. 269; D. M. Mintz and A. Kuppermann, see Ref. 17, p. 567.
19. R. G. Houlgate, J. B. West, K. Codling, and G. V. Marr, *J. Phys. B* 7, L470 (1974).
20. W. S. Watson and D. T. Stewart, *J. Phys. B* 7, L466 (1974).
21. They cannot resolve the $^2P_{3/2} - ^2P_{1/2}$ doublet of Ar split by 177 meV.
22. R. G. Newburgh, L. Heroux, and H. E. Hinteregger, *Appl. Opt.* 1, 733 (1962).
23. J. A. R. Samson, Techniques of Vacuum Ultraviolet Spectroscopy (Wiley, New York, 1967), p. 231.
24. G. L. Weissler, Handbuch der Physik, S. Flügge, Ed. (Springer-Verlag, Berlin, 1956), Bd. 21, p. 304.

25. E. M. Purcell, Phys. Rev. 54, 818 (1938).
26. J. A. Simpson, Rev. Sci. Instr. 35, 1698 (1964).
27. D. W. Turner, Proc. Roy. Soc. (London) A 307, 15 (1968).
28. D. W. Turner, Chemical Spectroscopy and Photochemistry in the Vacuum-Ultraviolet, C. Sandorfy, P. J. Ausloos, and M. B. Robin, Eds. (D. Reidel, Dordrecht, Holland, 1974), p. 25.
29. A. H. Firester, Rev. Sci. Instr. 37, 1264 (1966).
30. A. Savitzky and M. J. E. Golay, Anal. Chem. 36, 1627 (1964).
31. N. R. Draper and H. Smith, Applied Regression Analysis (Wiley, New York, 1966), Chap. 2.
32. H. Margenau and G. M. Murphy, The Mathematics of Physics and Chemistry (D. Van Nostrand, New York, 1943), p. 498.
33. D. J. Kennedy and S. T. Manson, Phys. Rev. A 5, 227 (1972) and private communication with S.T.M.
34. R. M. White, T. A. Carlson, and D. P. Spears, J. Electron Spectrosc. 3, 59 (1974).
35. J. C. Bünzli, A. J. Burak, and D. C. Frost, Tetrahedron 29, 3735 (1973).

TABLE I. Values of β for ionization of argon by HeI light.

$^2P_{3/2}$	$^2P_{1/2}$	Source
0.88 ± 0.02	0.86 ± 0.02	Present work
0.85 ± 0.05	0.85 ± 0.05	T. A. Carlson <u>et al.</u> ^a
0.95 ± 0.02	0.95 ± 0.02	R. Morgenstern <u>et al.</u> ^b
0.9		J. W. McGowan <u>et al.</u> ^c
0.4		J. Berkowitz <u>et al.</u> ^d
0.3		J. A. R. Samson ^e
0.90_5	0.88	Hartree-Fock dipole length D. J. Kennedy and S. T. Manson ^f
0.88	0.85_5	Hartree-Fock dipole velocity ^f

^a Reference 7.^b Reference 15.^c Reference 14.^d Reference 6.^e Reference 13.^f Reference 33.

FIGURE CAPTIONS

FIG. 1. Block diagram of variable angle photoelectron spectrometer. He, cylinder of UHP helium. ZT, liquid nitrogen immersed zeolite trap for lamp helium supply. RB, lamp ballast resistor, 1320 Ω . LPS, lamp power supply, 0.555 V, 300 mA maximum. SC, sample chamber. PC, photocathode for light flux measurement. CL, electron lens elements before hemispherical analyzer. ANALYZER, 180° hemispherical electrostatic electron energy analyzer. ML, electron lens elements between hemispheres and detector. S, spiraltron electron multiplier. CPS, power supply to Spiraltron cathode. APS, power supply to Spiraltron anode. R,C, differentiating network for Spiraltron pulses: R=1 M Ω , C=500 pF. PDP8/e, Digital Equipment Corporation PDP8/e minicomputer. INTER, counting system interface to experiment. OUTPUT, computer output devices to user.

FIG. 2. Section view of lamp. Hatched and stipled parts, except for the stainless steel lamp anode, A, are of aluminum and constitute the lamp body. K, tungsten carbide cathode. C, quartz discharge capillary. HV, high voltage power lead. S, starter electrode. He, helium inlet. OA, lamp flux outlet capillary. DP, differential pumping connections. KER, kerosene cooling inlet (outlet not shown). CE, kerosene cooling envelope inside lamp body. Flows of helium and kerosene are indicated by horizontal arrows.

FIG. 3. Section and external views of sample chamber. Hatched areas are sections of the inner and outer shells. OS, outer shell. MS, middle shell. IS, inner shell. GI, gas inlet. HS, helical slot. GS, guide screw for helical slot. LI, light inlet hole. Motion of OS and flow of sample are shown with vertical arrows.

FIG. 4. Section view of electron analyzer and sample chamber in plane of electron trajectories. Hatched areas include BN, a boron nitride mounting block for S, the Spiraltron, and part of CIS, the inner shell of the sample chamber. COS, outer shell of sample chamber. PC, photocathode. LE, light entrance. C1, HC, HM, and M1, lens elements. LS, aluminum supports for lens elements. IS, inner hemisphere. OS, outer hemisphere. ISC, corrector to inner hemisphere. OSC, corrector to outer hemisphere. AL, aluminum enclosure for Spiraltron. CF, AF, electrical feedthroughs for Spiraltron. AR, resistor from Spiraltron anode to anode plate A.

FIG. 5. Circuit schematic of lens and sphere voltage distribution system. Biasing networks for inner and outer sphere correctors, ISC and OSC, are omitted. Resistances are given in ohms; K = times 1000. The amplifiers, A, are Texas Instrument's SN72741. DAC, input from a computer digital to analog converter. DRS, select digital resolution, the incremented analog voltage between DAC channels in steps of 1-5 mV. PS1, 18 V power supply. BIAS, adjustable bias voltage circuit for all lens elements that varies the accepted electron energy: C, coarse adjustment via tandem potentiometers, F, fine adjustment. PS2, 37 V power supply. B, three 1.35 V mercury cells in series. C1, HC, HM, H1, conductors to lens elements. SC, conductor to sphere mounting bracket held at sphere center voltage. IS, OS, ISC, OSC, conductors to sphere elements. DA, user adjustment of IS-OS voltage.

FIG. 6. High resolution HeI spectrum of argon $^2P_{3/2}$ (left) and $^2P_{1/2}$ at $\theta = 60^\circ$. The spectrum was taken at an analyzing energy of 0.75 eV and at 2 meV electron energy increments between successive channels. Resolution for the $^2P_{3/2}$ peak is 16 meV FWHM.

FIG. 7. Block diagram of computer-based data acquisition system. Direction of flow of information is indicated by arrows. PDP8/e, minicomputer. PUN, RDR, high speed paper tape punch and reader. TTY, Teletype ASR33 terminal. PDP10, interface to PDP10. DAC, three-channel digital to analog converter. PLOT, X,Y plotter. CRT, cathode ray tube for display of spectra. AMPS, amplifiers for lens and sphere voltage control. INT, counting interface, including counter and digital display. A, Spiratron pulse amplifier. INPUT, input for ten analog voltages from lenses, etc. MUX, dual ten-channel analog multiplexer. DVM, autoranging voltmeter. LS, logic signal level shifter. DL, drive line interface between instrument and computer. ANG, signal to angle drive for increasing or decreasing θ . XYP, signal to XY plotter to lower pen. AA, signal to audio alarm. ADMC, signal to place multiplexer under computer control. SL, sense line interface between instrument and computer. ANGF, angle drive feedback. LO, lamp status signal. N₂, liquid nitrogen baffle-filling status signal. VAC, vacuum system status signal.

FIG. 8. Signal intensity, corrected for angle-dependent scattering volume and pressure, and normalized to unity at 90° , as a function of scattering angle θ . For the upper figure the abscissa is $\cos^2 \theta$ and for the lower one, θ . The circles indicate points for $\theta > 90^\circ$ and the crosses $\theta < 90^\circ$. The dashed curves represent the least square error fit ($\beta = 0.88$) to these points according to Eq. (1).

FIG. 9. (a) HeI photoelectron spectrum of 1,5-hexadiene at $\theta = 54.7^\circ$ in lower frame. The spectrum was taken over 511 data channels with a difference of 20 meV between the electron energies for successive data channels. (b) Variation of β with ionization potential.

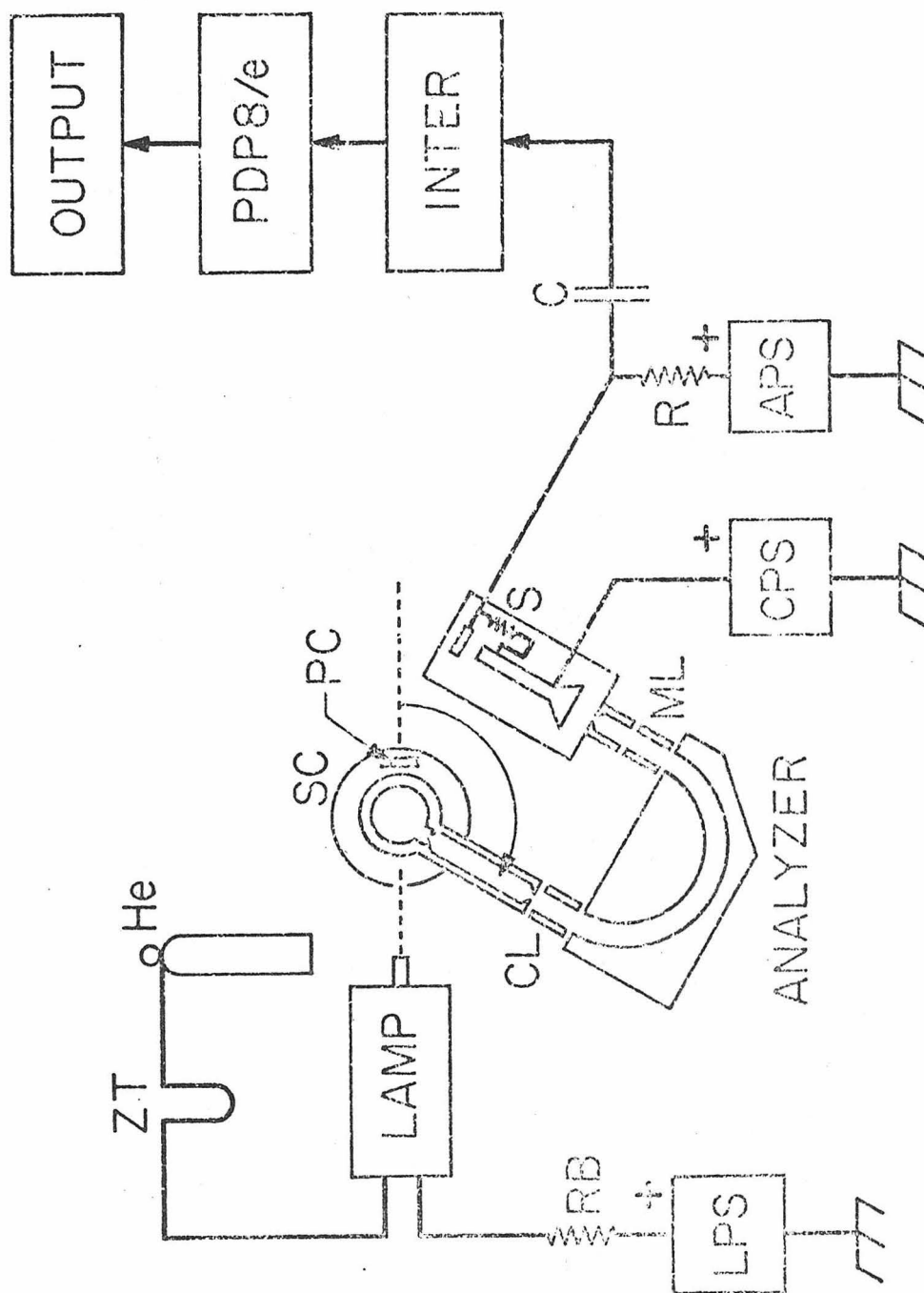


Figure 3-1

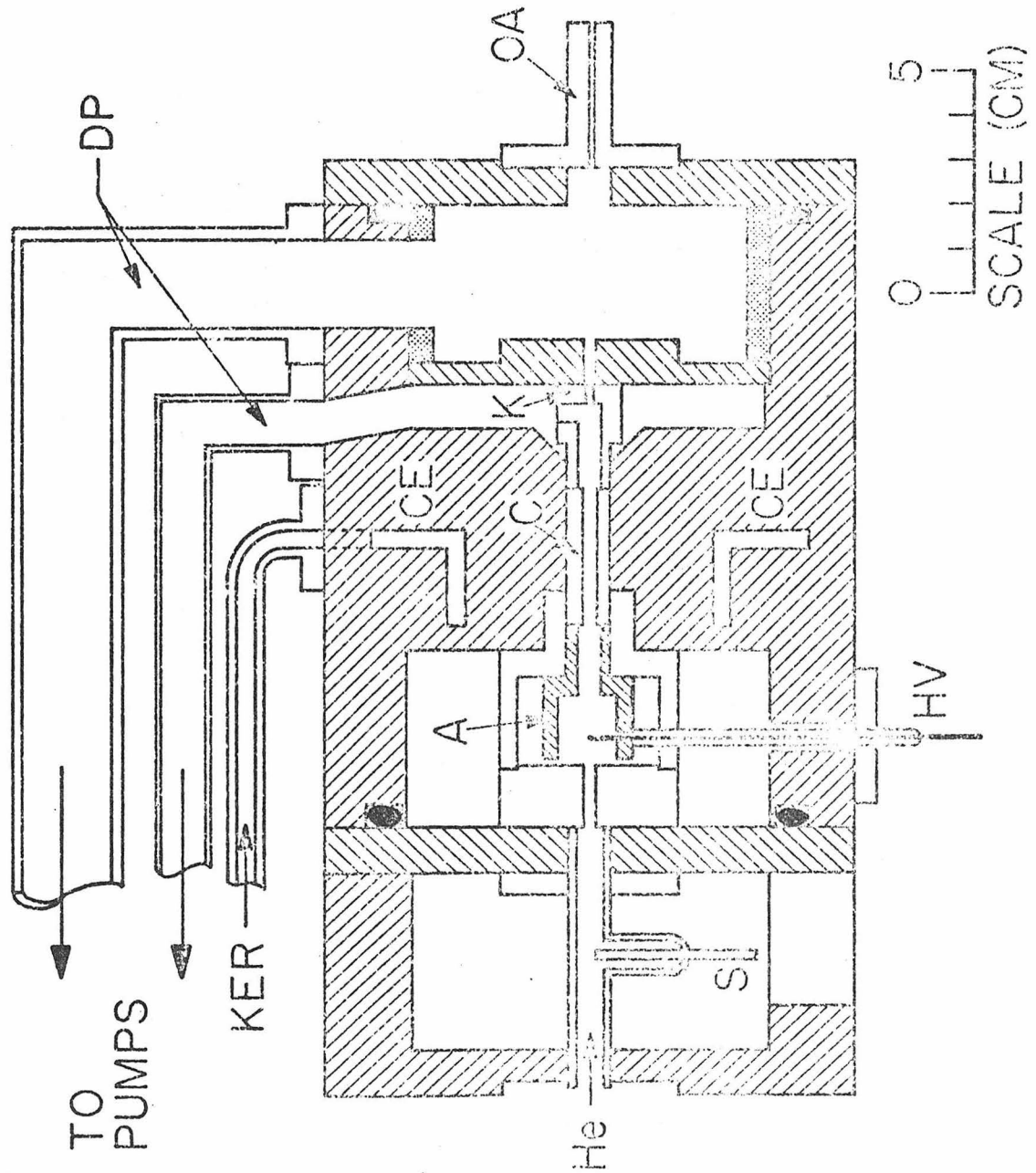


Figure 3-2

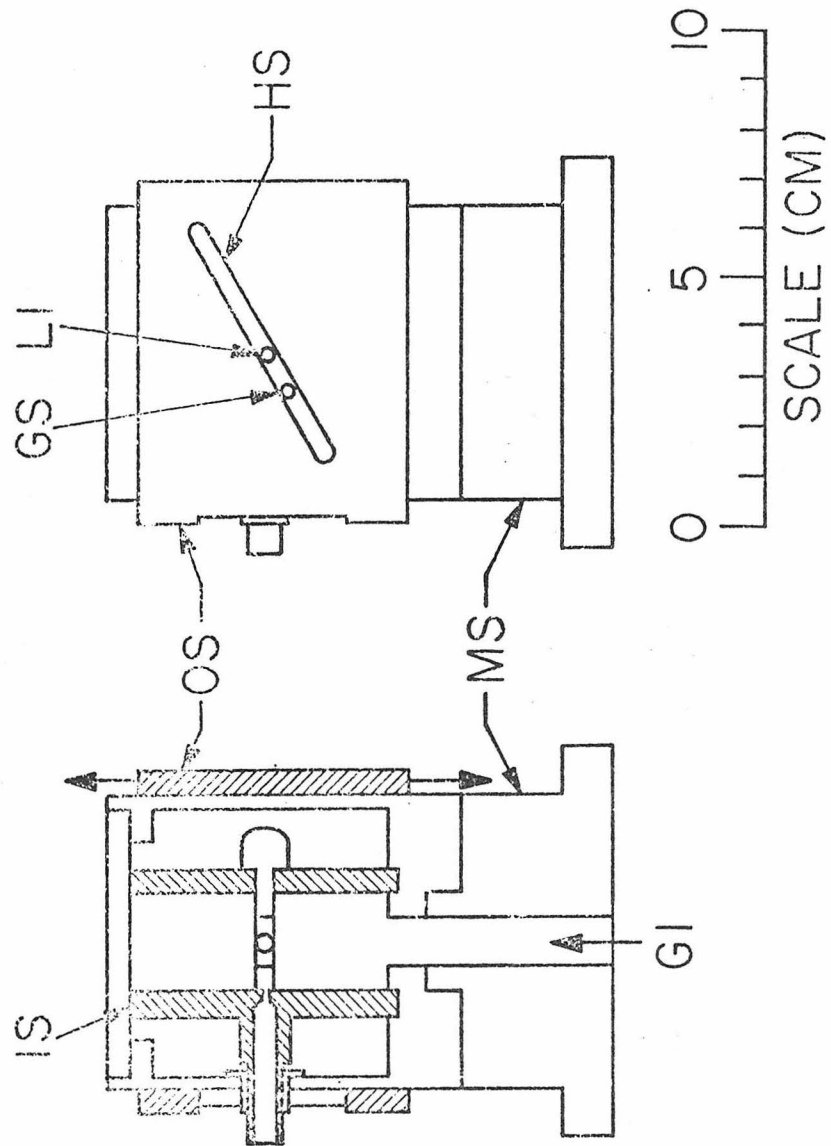


Figure 3-3

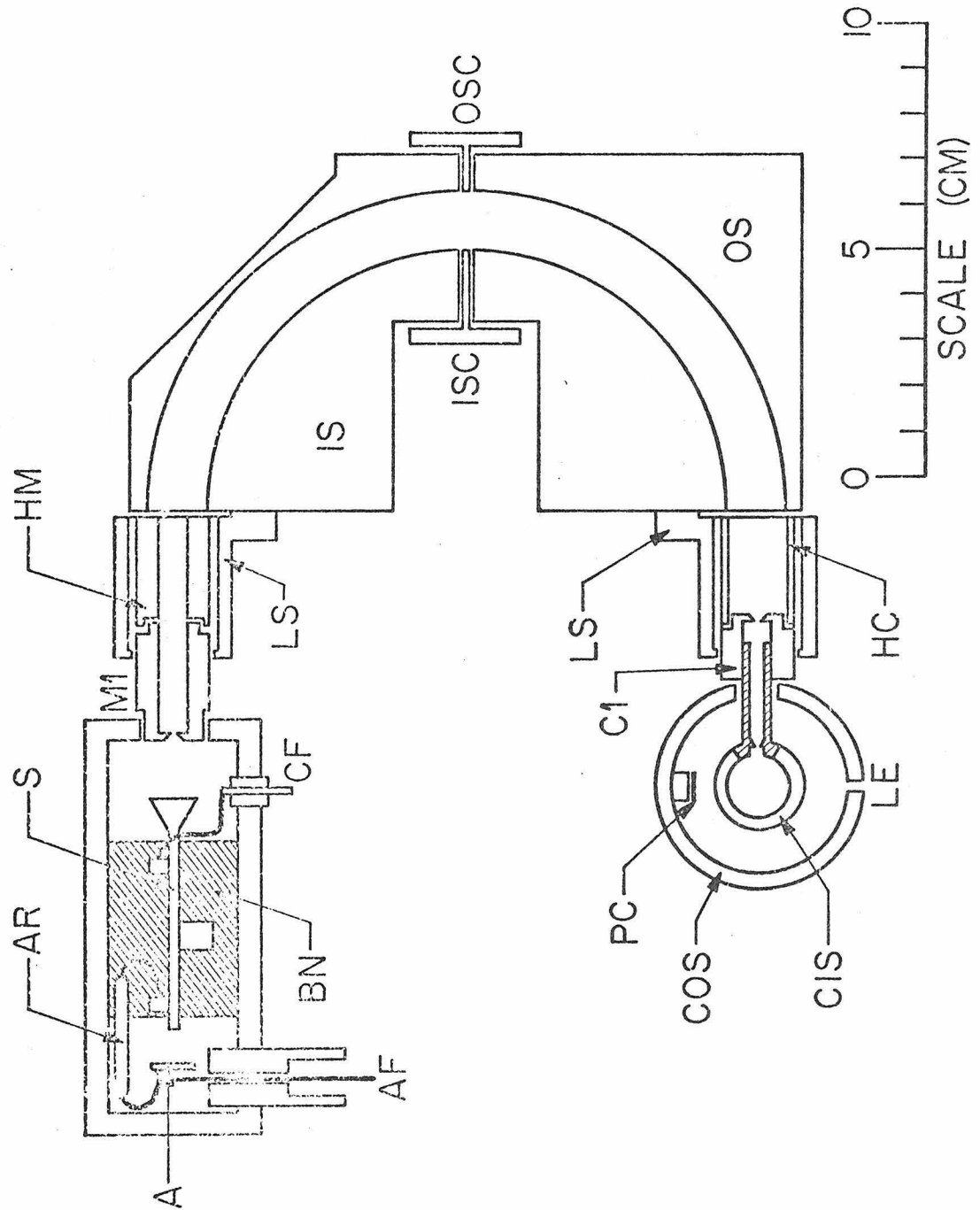


Figure 3-4

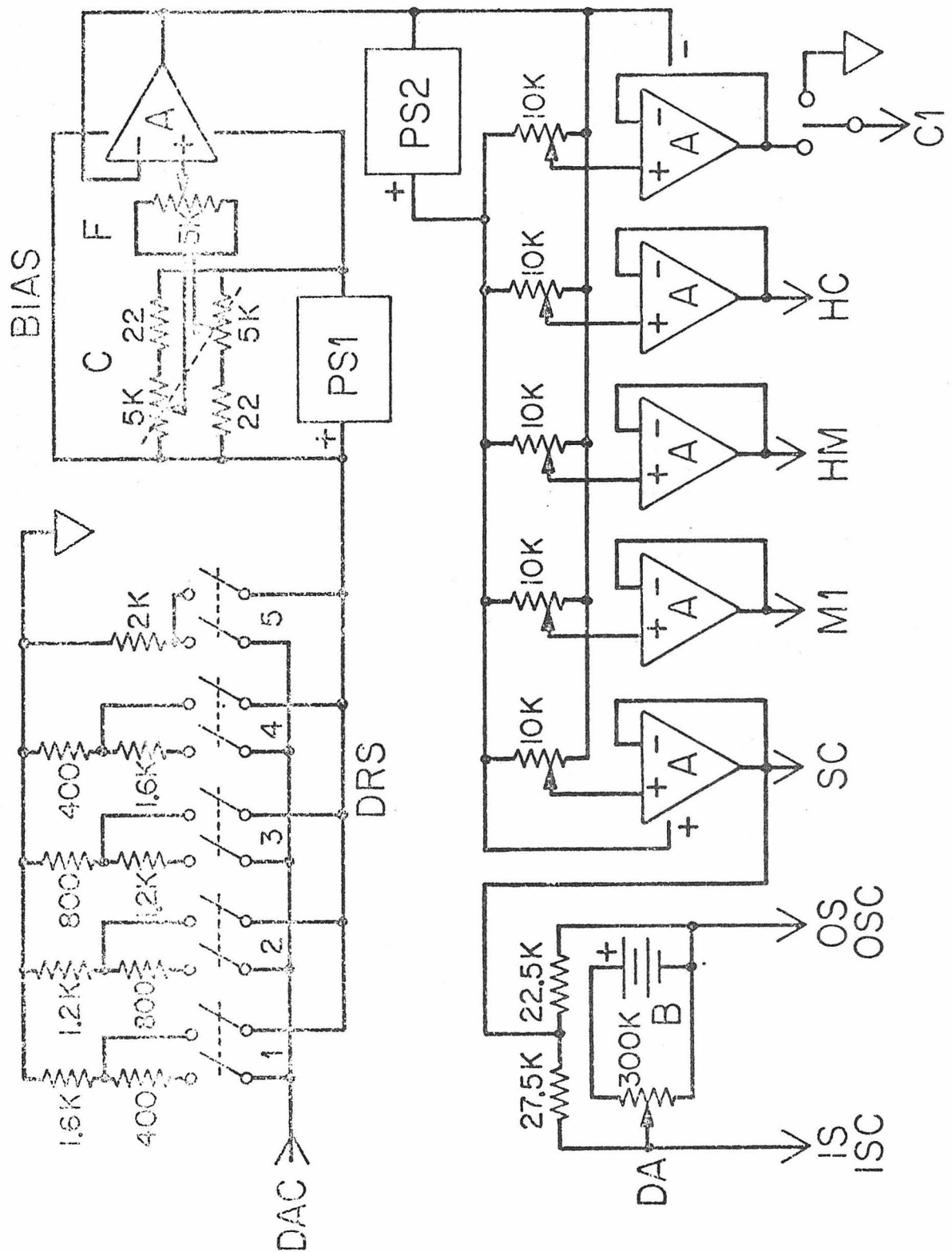


Figure 3-5

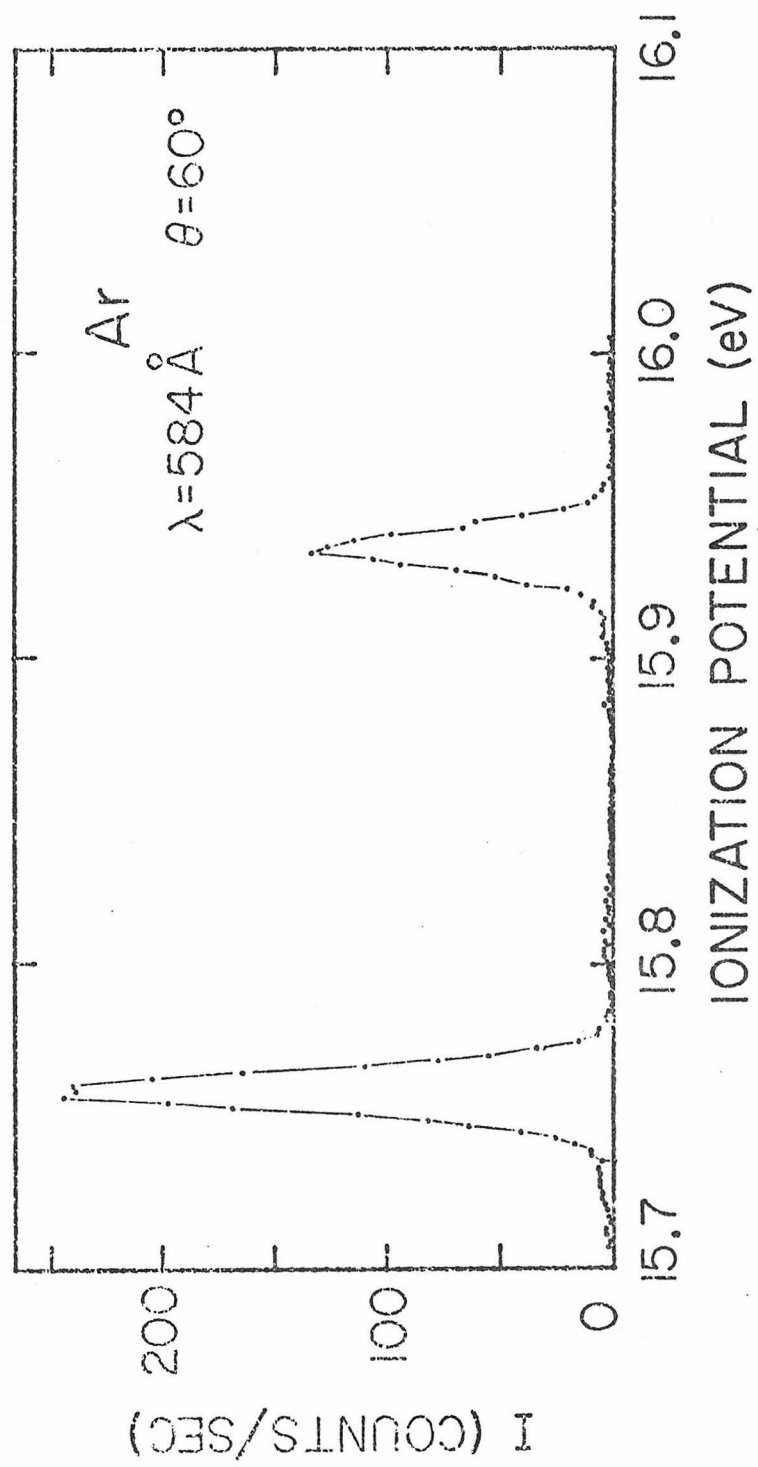


Figure 3-6

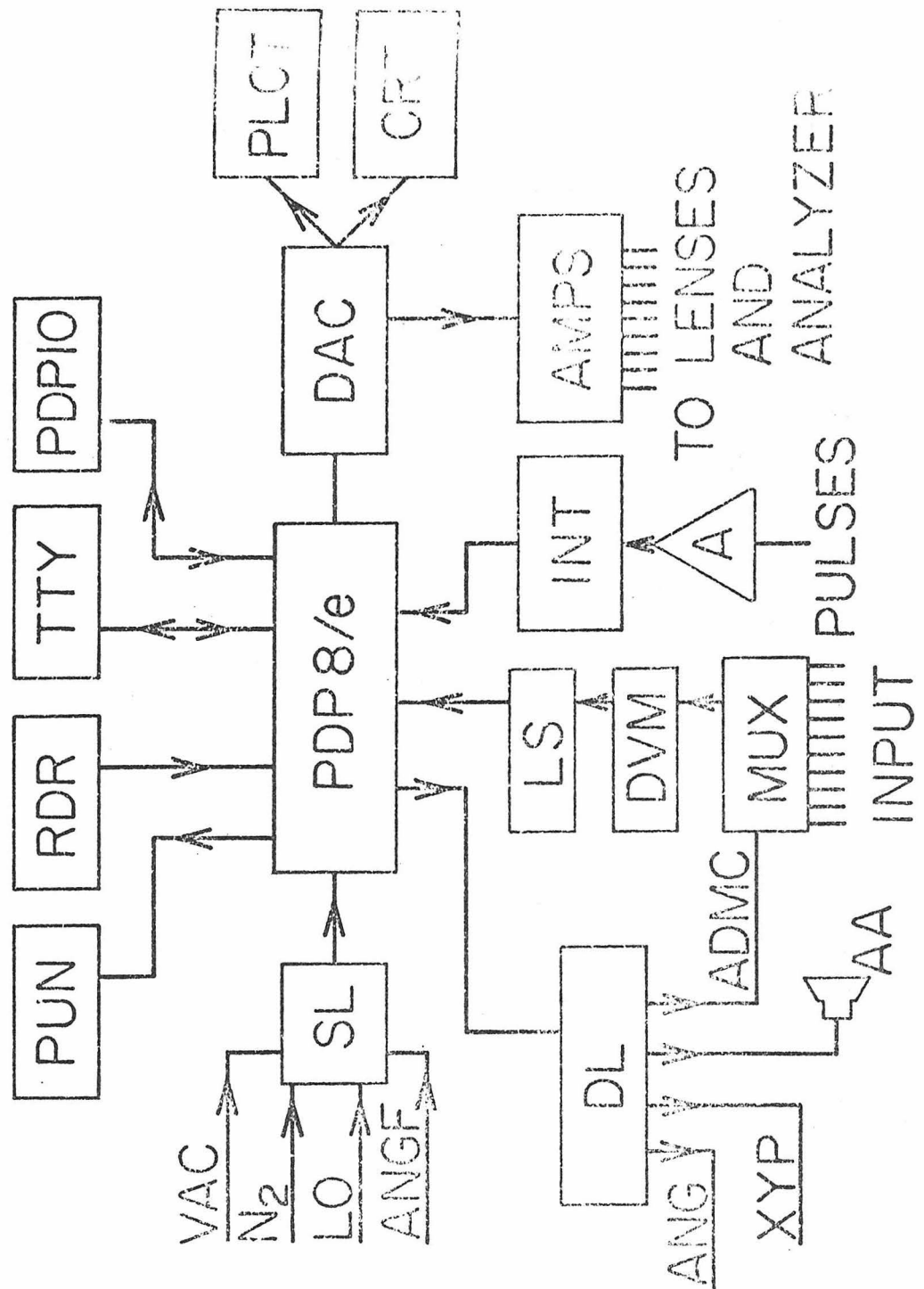


Figure 3-7

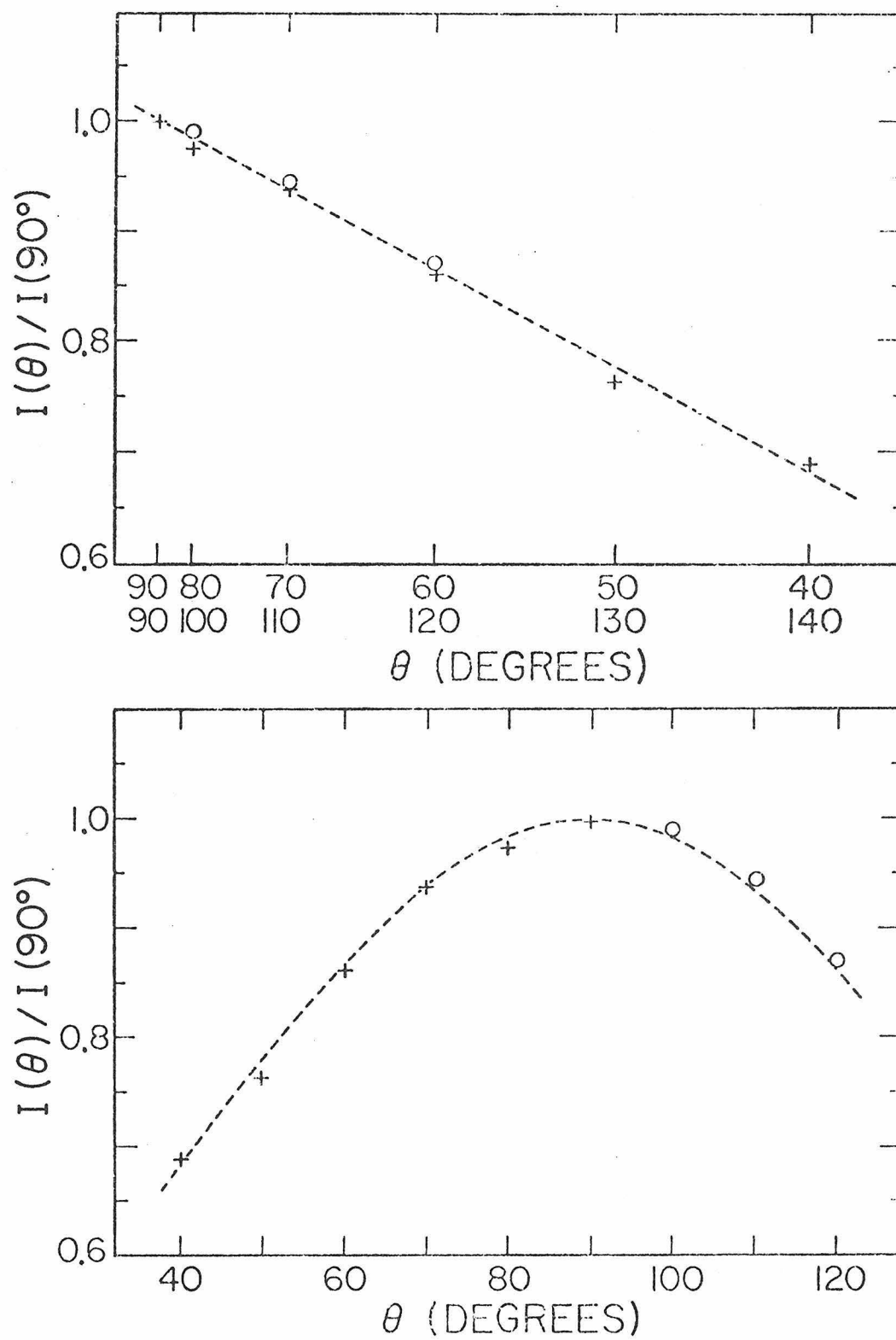


Figure 3-8

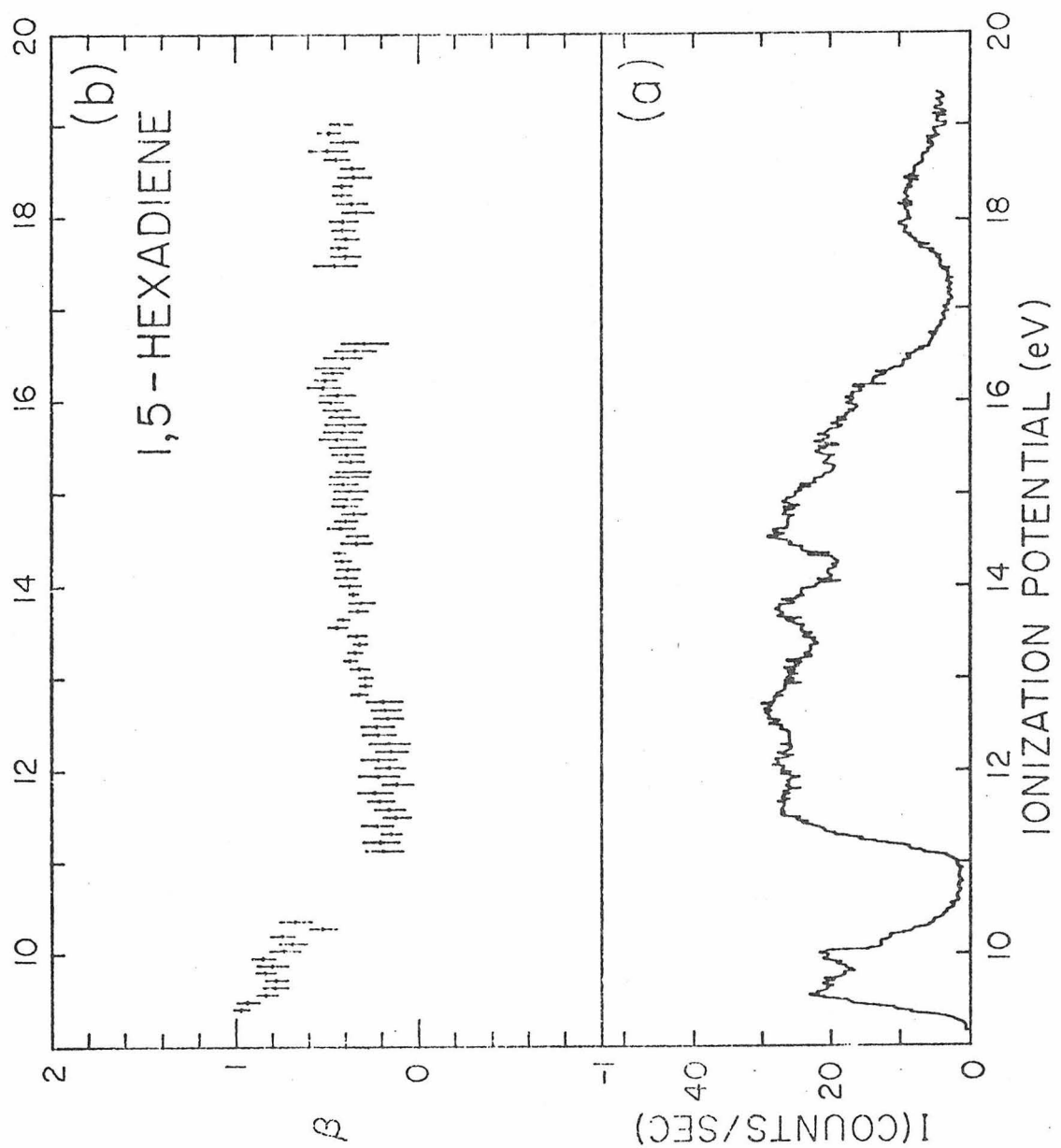


Figure 3-9

CHAPTER 4 - RESULTS AND DISCUSSION: NOBLE GASES

$$\frac{d\sigma}{d\Omega} = \frac{Q}{4} [1 - \frac{1}{2}\beta P_2(\cos\theta)]$$

4.1 Introduction

Much of the early experimental angular distribution studies included the noble gases Ar, Kr, and Xe, for which peak counting rates were high. The experiments did not require a sophisticated data acquisition system and thus were relatively easy. Still, as was seen in Table I of Chapter 3, only since 1971 have experimental results begun to agree with one another.

4.2 Argon

We present here results for argon taken with the HeI lines in the light source at 584, 537, and 522 Å. Peak counting rates for the 537 and 522 Å spectra are 2% and 0.5%, respectively, of those of the 584 Å spectrum, as shown in Fig. 4-1. The 584, 537, and 522 Å spectra are well enough separated in energy so that no interference is apparent.

Experimental asymmetry parameters for the $^2P_{3/2}$ and $^2P_{1/2}$ peaks are summarized in Table 4-I and Fig. 4-2. Experimental results using dispersed continuum^{1,2} light sources and rotatable detectors, as well as UV line sources,^{3,4} are included in Fig. 4-2. We report a previously unresolved difference between β values at 584 Å for the $^2P_{3/2}$ and $^2P_{1/2}$ peaks. The magnitude of the difference,

TABLE 4-I. Values of the Asymmetry Parameter, β , for Argon 3p Ionization

Ionic State	IP (eV)	Photon Energy (eV)	β , expt.	β , theor. ^a
$^2P_{3/2}$	15.759	21.217	0.88 ± 0.02^b ($0.85^c, 0.95^d$)	$0.90_5(0.88)$
			$0.3^e, 0.9^f, 0.4^g$	
		23.086	0.99 ± 0.03	$1.07(1.06_5)$
$^2P_{1/2}$	15.936	23.741	1.12 ± 0.04	$1.12(1.12_5)$
		21.217	0.86 ± 0.02^b ($0.85^c, 0.95^d$)	$0.88(0.85_5)$
			1.05 ± 0.06	
		23.086	1.08 ± 0.08	$1.05_5(1.05)$
		23.741		$1.10_5(1.11)$

^aRef. 5. Hartree-Fock dipole length formula. Values in parentheses from HF dipole velocity formula.

^bStandard deviation from 30 determinations for data accumulated over a period of 6 months. Other error bars reflect goodness of fit over 9 angles only.

^cRef. 3. ^dRef. 4. ^eRef. 6. ^fRef. 7. ^gRef. 8.

0.02 β units, could be due to either the variation of β with photoelectron energy or to spin-orbit effects. The variation reproduces that calculated by Kennedy and Manson,⁵ who ignored spin orbit effects. Thus, we attribute the variation in β to variation of β with electron energy alone.

Data points for 584, 537, and 522 Å ionization agree well with the theoretical curve of Kennedy and Manson.⁵ Houlgate, et al.¹ have reported a significantly better agreement with the calculation of Amusia, et al.¹¹ in the region of the Cooper minimum for 3p ionization. At the same time, Houlgate, et al.¹ report a minimum in the argon 3s integral ionization cross section within 15 eV of threshold. This agrees with the calculations of Amusia, et al.¹¹ and Lin,¹² who include effects of electron correlation. This is in gross disagreement with the calculation of Kennedy and Manson,⁵ who predict a maximum in this region. The better agreement of experimental β parameters for photoionization from the 3p subshell between 5-7 eV of threshold with the Kennedy and Manson calculation could be purely coincidental. Alternatively, it could indicate that neglect of certain many electron correlations is a reasonable approximation for certain ranges of photoelectron energy. At the same time, the lack of close agreement for experimental results over a wide range of photon energies with Amusia's¹¹ calculation remains a mystery.

4.3 Neon

The results for neon provide a severe test of both theory and experiment. The principal output line from a HeI discharge, at 584 Å, contains insufficient energy to ionize neon (IP = 21.564 eV). However, the weaker 537 and 522 Å lines do permit studies of 1 photon ionization of neon, as seen in Fig. 4-3. Branton, et al.¹³ first noticed this in 1970, when they published the 537 Å spectrum of neon. Although signal to background ratios for the present work varied over the range of 1.6 for $^2P_{\frac{1}{2}}$ ionized by 522 Å light to 13.3 for $^2P_{\frac{3}{2}}$ ionized by 537 Å light, the experimental data points cluster nicely about the Cooper and Manson⁵ calculation.

After their original results for the noble gases appeared in 1970, Manson and Cooper¹⁴ suggested that the sharp dip in β near threshold, shown in Fig. 4-4, was an artifact. Since that time, results of van der Wiel and Brion¹⁵ and Lynch, et al.¹⁶ have shown the theoretical results to be accurate as close as 3 eV of threshold. The results of the present investigation, presented in Table 4-II, show the theoretical results to be accurate as low as 1.42 eV above threshold.

TABLE 4-II. Values of the Asymmetry Parameter, β , for Neon 2p Ionization

Ionic state	IP (eV)	Photon Energy (eV)	β , expt. ^a	β , theor. ^b
$^2P_{\frac{3}{2}}$	21.564	23.086	-0.49 ± 0.05	$-0.40(-0.44_5)$
		23.741	-0.34 ± 0.14	$-0.30_5(-0.34_5)$
$^2P_{\frac{1}{2}}$	21.661	23.086	-0.51 ± 0.06	$-0.41(-0.46)$
		23.741	-0.14 ± 0.22	$-0.32(-0.36)$

^aError limits reflect goodness of fit over 9 angles only.

^bRef. 5. From Hartree-Fock dipole length formula. Values in parentheses from HF dipole velocity formula.

REFERENCES

1. R. G. Houlgate, J. B. West, K. Codling, G. V. Marr, J. Phys. B. 7, L470 (1974).
2. W. S. Watson, D. T. Stewart, J. Phys. B 7, L466 (1974).
3. T. A. Carlson, A. E. Jonas, J. Chem. Phys. 55, 4913 (1971).
4. A. Niehaus, M. W. Ruf, Z. Phys. 252, 84 (1972).
5. D. J. Kennedy, S. T. Manson, Phys. Rev. A 5, 227 (1972) and private communication with STM.
6. J. A. R. Samson, Phil. Trans. Roy. Soc. Lond. A268, 141 (1970).
7. J. W. McGowan, D. A. Vroom, A. R. Comeaux, J. Chem. Phys. 51, 5626 (1969).
8. J. Berkowitz, H. Ehrhardt, Phys. Lett. 21, 531 (1966);
J. Berkowitz, H. Ehrhardt, T. Tekaas, Z. Phys. 200, 69 (1967).
9. P. Mitchell, K. Codling, Phys. Lett. 38A, 31 (1972).
10. G. R. Branton, C. E. Brion, J. Electron Spectr. 3, 123 (1974).
11. M. Ya. Amusia, N. A. Cherepkov, L. V. Chernysheva, Phys. Lett. 40A, 15 (1972).
12. C. D. Lin, Phys. Rev. A 9, 181 (1974).
13. G. R. Branton, D. C. Frost, T. Makita, C. A. McDowell, I. A. Stenhouse, J. Chem. Phys. 52, 802 (1970).
14. S. T. Manson, J. W. Cooper, Phys. Rev. A 2, 2170 (1970).
15. M. J. van der Wiel, C. E. Brion, J. Electron Spectr. 1, 439 (1973).
16. M. J. Lynch, A. B. Gardner, K. Codling, Phys. Lett. 40A, 349 (1972).

Figure Captions

Fig. 4-1 Spectrum of argon at a detector angle of 54.7° incorporating 584, 537, and 522 Å spectra. Spectrum was taken over 511 channels at a dwell time of 20 seconds/channel. The ionization potential scale is given as if the lamp output were only 584 Å. Note that the 522 and 537 Å spectra appear with a different vertical scale.

Fig. 4-2 Variation of the asymmetry parameter β with photoelectron energy for argon 3p ionization (1 Ryd = 13.6 eV). ●, present investigation. ■, Ref. 1. ▲, Ref. 2. ✕, Ref. 3. ◇, ref. 4. Curves HF-L and HF-V from Ref. 5. Curve RPAE from Ref. 11. Not shown, for clarity's sake, are results of Refs. 9, 10, which lie along the trends visible here.

Fig. 4-3 Spectrum of neon at a detector angle of 54.7° incorporating 537 and 522 Å spectra. Spectrum was taken over 213 channels at a dwell time of 10 seconds/channel.

Fig. 4-4 Variation of the asymmetry parameter β with photoelectron energy for neon 2p ionization (1 Ryd = 13.6 eV). ●, present investigation. ■, Ref. 15. ▲, Ref. 16. Curves HF-L and HF-V from Ref. 5.

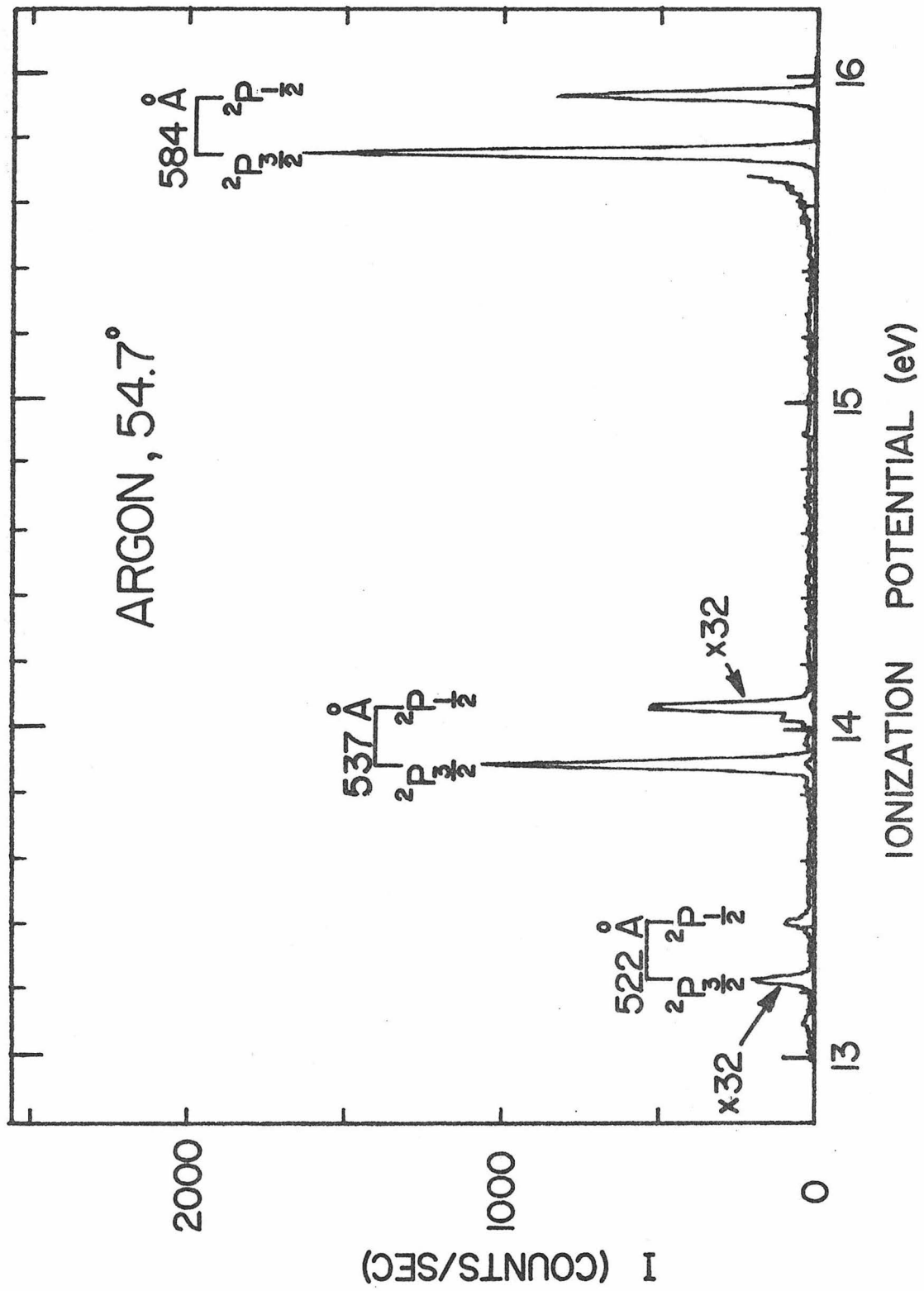


Figure 4-1

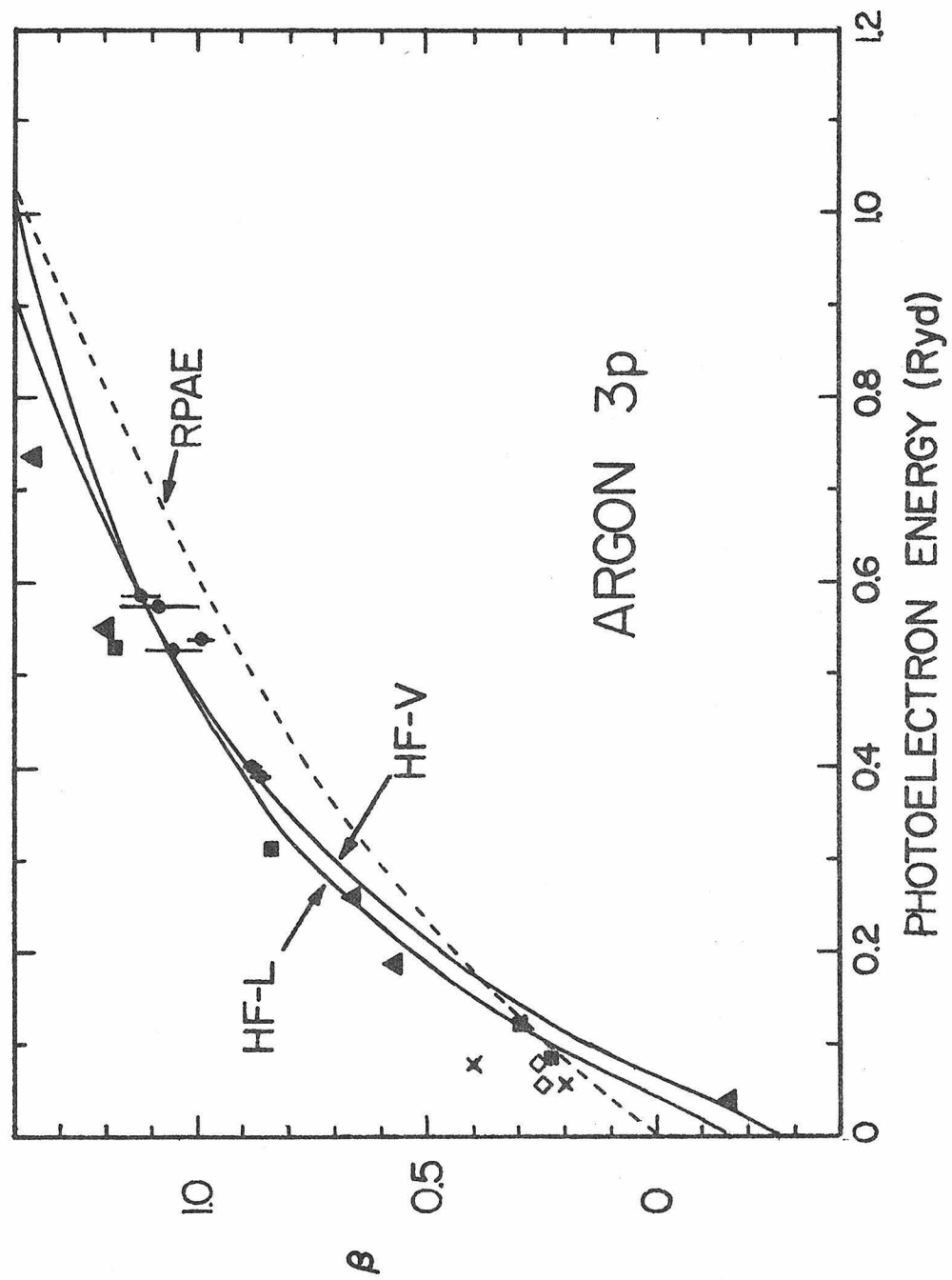


Figure 4-2

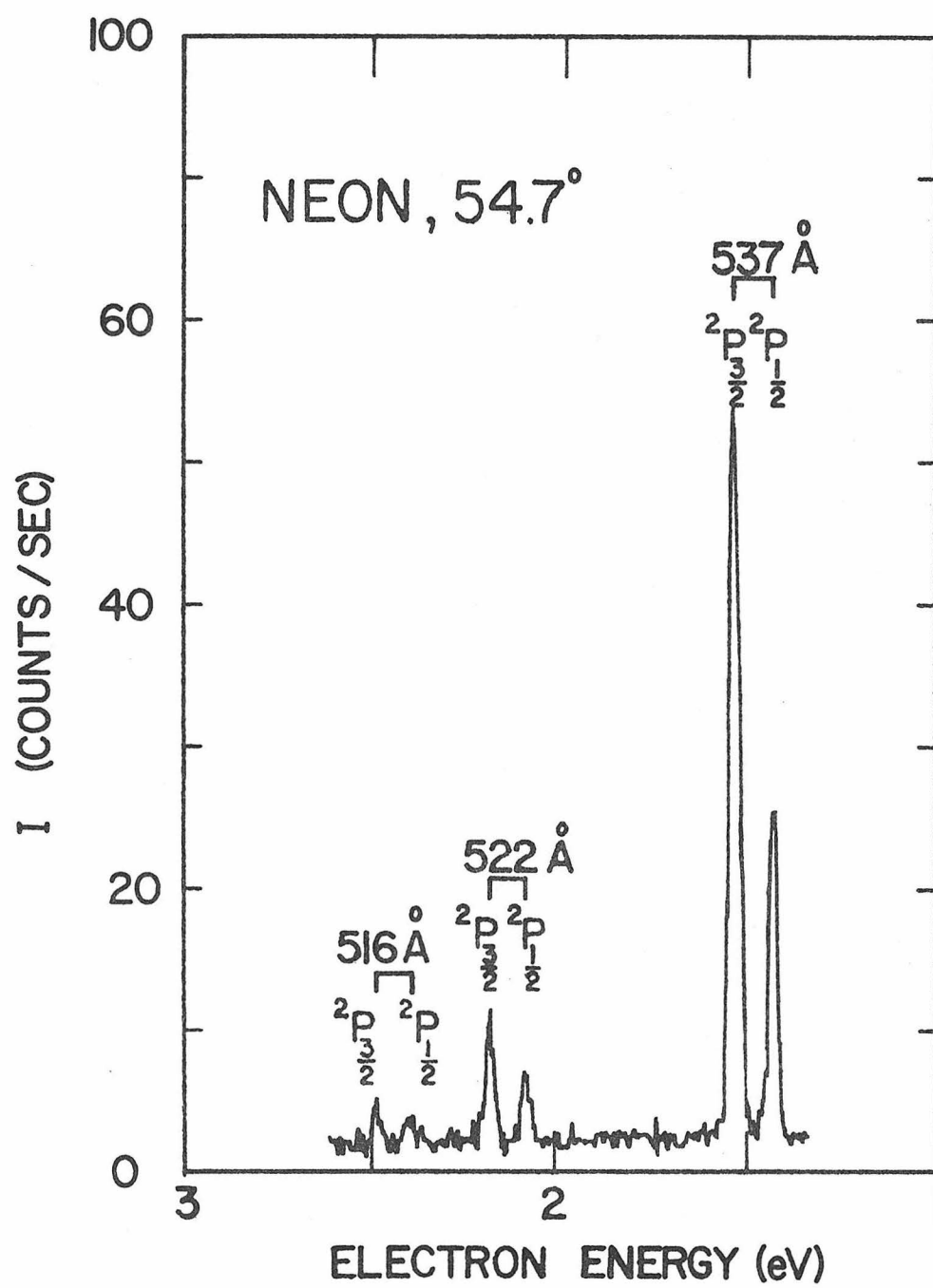


Figure 4-3

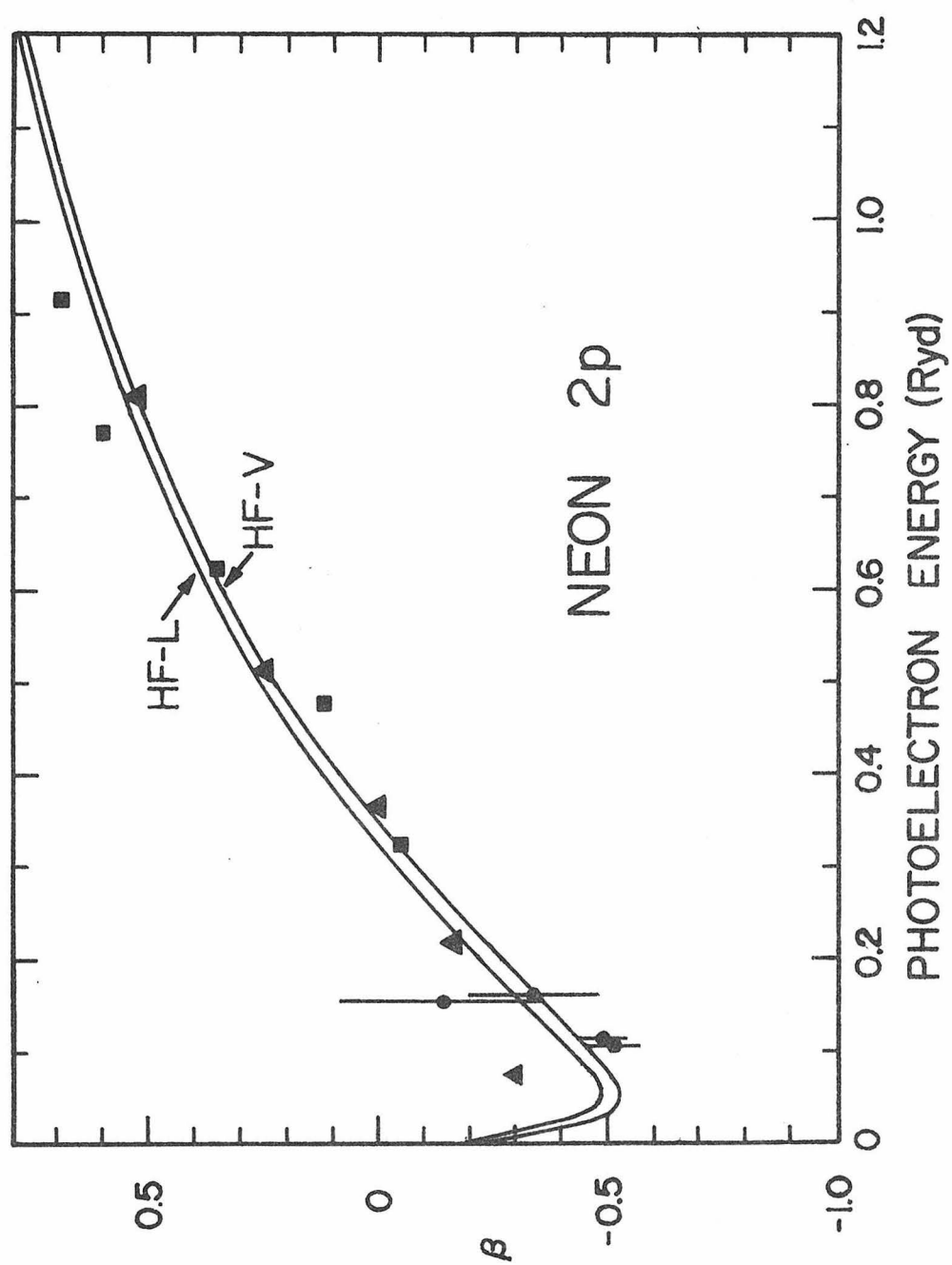


Figure 4-4

CHAPTER 5 - RESULTS AND DISCUSSION: DIATOMIC MOLECULES

$$P_{\nu'}^a \propto F_{i\nu'}^2 + K(\lambda, n_\lambda, \nu) F_{i\nu}^2 F_{\nu\nu'}^2$$

5.1 Paper II - Electron Energy Dependence of the Differential Photoelectron Cross Section of N₂.

Electron Energy Dependence of the Differential Photoelectron Cross Section of N_2 .

The angular distribution of photoelectron intensity for molecular nitrogen was studied using HeI and NeI glow discharge light sources. Studies of photoelectron angular distributions covering a range of photon energies, and thus a range of electron energies, are possible using the weaker high order lines in each discharge as well as the principal output lines. Peaks in three photoelectron bands of N_2 were studied at the photon energies: 16.85, 19.78, 21.22, 23.09, and 23.74 eV, where possible. We find that the $v' = 0$ peak of the $X^2\Sigma_g^+$ band has abnormally high intensity and an abnormally low angular distribution asymmetry parameter, β . Several mechanisms for this anomaly are discussed, including autoionization, the variation of electric dipole transition moments, and resonance phenomena. None of these explanations is completely in agreement with all theoretical and experimental evidence.

Introduction

One of the fundamental postulates introduced early in the analysis of molecular photoelectron spectra was that vibrational peak intensities were closely related to calculated Franck-Condon factors.¹ Relative vibrational peak intensities within an electronic band are presumed to depend solely on the overlap of nuclear wavefunctions for ground and ionic states. While this postulate is not exact, it has nevertheless been of considerable use in the interpretation of molecular photoelectron spectra².

Recent measurements of HeI photoelectron spectra³ and photoelectron angular distributions^{4,5} for vibrational peaks of the ground $X^2\Sigma_g$ state of N_2^+ appear to violate this postulate. We have reinvestigated the photoelectron angular distributions of N_2 at several photon wavelengths in the hopes of resolving the controversy which has arisen.

Theoretical Background

The differential photoelectron cross section for the transition from an initial state $\Psi_i(\underline{r}, \underline{R})$ to a final state $\Psi_f(\underline{r}, \underline{R})$ will be proportional to the square of a transition matrix element:

$$I(\gamma) \propto \left| \langle \Psi_f(\underline{r}, \underline{R}) \left| \hat{T} \right| \Psi_i(\underline{r}, \underline{R}) \rangle \right|^2 \quad (1)$$

averaged over rotational levels

Here, \underline{r} and \underline{R} denote the set of electronic and nuclear coordinates, respectively, \hat{T} is the operator for the interaction between the molecular electrons and the electromagnetic field, and γ is the angle between the direction of observation and the direction of polarization of the light. In the Born-Oppenheimer approximation⁶, each total

wavefunction is factored into the product of a nuclear wavefunction $\chi(\underline{R})$ and an electronic wavefunction $\psi(\underline{r};\underline{R})$. For sufficiently high temperatures and if rotational structure is not resolved, it has been shown that the average over rotational sublevels becomes an average over molecular orientations⁷. Finally, for ionization by non-polarized light, we average $I(\gamma)$ over orientations of the polarization vector with respect to the photon propagation vector. The result is the familiar form⁸:

$$I(\theta)_{\substack{v'' \rightarrow v' \\ i \rightarrow f}} = \frac{Q_{i \rightarrow f}^{v'' \rightarrow v'}}{4\pi} \left[1 - \frac{\beta}{4} (3\cos^2 \theta - 1) \right], \quad (2)$$

where θ is the angle between the direction of observation and the photon propagation vector, $Q_{i \rightarrow f}^{v'' \rightarrow v'}$ is the total cross section for transition from vibrational level v'' of the initial neutral state to level v' of the ion. The asymmetry parameter, β , is a function only of the electronic levels involved in the transition and the energy of the outgoing electron (and thus the incident photon wavelength). Franck-Condon factors are incorporated in the total cross section $Q_{i \rightarrow f}^{v'' \rightarrow v'}$. The value of β may range from -1 to +2.⁹

Theoretical calculations of the asymmetry parameter, β , have been made for an extensive collection of atoms and molecules^{10 - 14}. In all cases, very slight variation of β with electron energy for electron energies $\gtrsim 200$ eV follows somewhat more rapid variation close to ionization threshold. However, variations of β higher than +0.4 units/eV are uncommon. These normally accompany only autoionization of Rydberg states above the first ionization potential,

as has been observed in xenon¹⁵. Here, the measured β values take the form¹⁴:

$$\beta = \frac{Q_{\text{dir}}^{\beta_{\text{dir}}} + Q_{\text{auto}}^{\beta_{\text{auto}}}}{Q_{\text{dir}} + Q_{\text{auto}}} \quad , \quad (3)$$

where dir and auto index values of β and total cross sections for direct and autoionization pathways, respectively.

Thus, even for studies of photoelectron angular distributions measured near threshold, over a limited range of photoelectron energies, we expect a gradual variation of β for ionization of electrons from a single molecular orbital. Producing ions with greater degrees of vibrational excitation correspondingly lowers the measured outgoing electron energy, for ionization by light of a fixed wavelength. Thus, within the Born-Oppenheimer approximation and assuming the absence of autoionization, the variation of β across vibrational envelopes should only reflect the variation of β with electron energy. Deflections of the measured β values for certain vibrational levels within a given electronic band and corresponding gross deviations of measured vibrational intensities from the calculated Franck-Condon factors should thus indicate the presence of molecular autoionization or other interfering processes.

Experimental

Photoelectron angular distributions were measured with windowless helium and neon glow discharge lamps and a rotatable electron energy analyzer. The rotatable electron energy analyzer consists of a 6.800 cm mean radius hemispherical electrostatic analyzer, electrostatic lenses, and a channel electron multiplier mounted on a worm gear which is rotated about a horizontal axis. The analyzer is attached to an enclosed sample chamber which is normally filled with 4 millitorr of N_2 , as measured by a high pressure ionization gauge. Spectra of photoelectron intensity versus electron energy are generated using a minicomputer-based data acquisition system. A block diagram of the experimental apparatus is given in Fig. 1.

We investigated the photoelectron angular distributions for nitrogen at the wavelengths listed in Table I. Normally, photoelectron spectra taken with the unfiltered radiation of a windowless discharge must be interpreted with caution. A weak feature could be caused either by an ionization with a low transition probability, one of the He I or Ne I higher order lines, or impurity lines in the light source. Impurity lines from neutral atom emissions, as H I, N I, or O I, have energies lower than those of the principal lamp emission lines. Thus, corresponding photoelectron energies are lower than those of 584 Å spectra and lie out of the range of the present investigation. The ionic states populated by 584 Å light have been well characterized; we expect no structure due to unforeseen new ionic states in the photon range 16.85 - 23.74 eV covered by this experiment. Further, population of

high lying ionic levels, such as the $C^2\Sigma_u^+$ state¹⁷, should produce photoelectrons at low kinetic energies, again, out of the range of the present investigation.

The higher order lines present in the discharge lamp at low intensity give rise to photoelectron spectra shifted with respect to those of the principal emission by a known amount and superimposed upon that of the principal emission. Other laboratories measuring fixed angle spectra have found these higher order lines a general nuisance, but we have found them of considerable use in studying the variation of β values with electron energy. For the most part, except for $v' \geq 3$ of the $A^2\Pi_u$ band and the entire $B^2\Sigma_u^+$ band, weak structure resulting from ionization by the higher order lines does not overlap structure produced by the intense principal atomic lines. N_2 has sharp structure of high intensity and our apparatus has reasonably high sensitivity. Thus, the photoelectron intensity produced by the higher order lines and amounting to no more than 2% of the intensity of their more intense counterparts was adequate for this study. Long data acquisition times, as long as 10 hours for the study of a single peak, were still unavoidable. Fortunately, the photoelectrons arising from the higher order lines fall in a region of high electron energy where background rates are low, under 1 count per second.

We find no photoelectron peaks corresponding to weak atomic lines other than those listed by Kelley¹⁶. Spectra taken with the HeI and NeI lamps are presented in Figs. 2 and 3, respectively. Photoelectron peaks corresponding to $v' = 0$ of the $X^2\Sigma_g^+$ ion produced by

the higher order lines of the neon discharge are shown separately in Fig. 4. We measured photoelectron angular distributions in the region only for the 627 Å line which has the highest intensity. We made no attempts to measure β values for $v' = 1$ of the $X^2\Sigma_g^+$ state at 627 or 522 Å. Signal to background ratios were no better than 1:1 for $v' = 0$ and we expected the $v' = 1$ peaks to be weaker by an order of magnitude.

Spectral intensities measured as peak heights by the PDP8/e data acquisition software at each of 9 detector angles in the range $\theta = 40 - 120^\circ$ were fitted to Eq. 2 by a weighted least squares procedure. Photoelectron intensity was corrected for the volume of intersection of the lamp and detector view cones at each θ and was compensated for the linear variation of counting rate with sample pressure. The quoted error limits reflect both goodness of fit to Eq. 2 and reproducibility. Results are listed in Table II.

Correction for photoelectron background is a crucial part of making accurate measurements of β , especially when the signal to background ratio approaches 1:2. During operation, we parameterize an electron-energy-dependent background as a series of three connected line segments:

$$B(E) = T \sum_{j=1}^3 S_j(E - E_j) . \quad (4)$$

Here, T is the dwell time per data channel, S_j is the slope of the background spectrum in $\text{counts} \cdot \text{eV}^{-1} \cdot \text{sec}^{-1}$, E_j are electron energies where the slope of counting rate versus electron energy changes. The

typical background spectrum increases roughly at a rate of $1/6 \text{ count} \cdot \text{ev}^{-1} \cdot \text{sec}^{-1}$ over the range of decreasing electron energy from 13 eV (background near zero) to 1 eV.

The PDP8/e data reduction computer program then subtracts the parameterized background measured for each of the nine angles of an angular distribution before calculating β values. In the case of the 627 Å angular distributions of the $v' = 0 \text{ X}^2 \Sigma_g^+$ peak, background counting rates were measured at the corresponding electron energy immediately after measuring the angular distribution, without the above-mentioned parameterization.

We believe the background subtraction to be an accurate procedure. In the case of the ionization of the Ne 2p subshell, for signal to background ratios in the range 1.6 - 13.33, the procedure yields good agreement with previous theoretical and experimental results¹⁸.

Results

$\text{X}^2 \Sigma_g^+$ Band

In agreement with previous measurements by Morgenstern⁵ and Carlson⁴, β values for the $v' = 0$ and $v' = 1$ peaks in the 584 Å spectrum are grossly different. In addition, we find a smaller although reproducible difference in the 537 Å spectrum, as well. The β values measured for the $v' = 0$ peaks for 584 and 537 Å ionization are identical, within experimental error. For the $v' = 2$ peak in the 584 Å spectrum, we reproduce a β value significantly higher than that found earlier by Morgenstern⁵.

Results obtained using the NeI discharge agree much better

with those of Morgenstern⁵ than with those of Carlson⁴. The value obtained for $v' = 0$ at 627 Å is high and comparable to that obtained for the $v' = 1, 2$ levels in the 584 Å spectrum.

The enhancement of $v' = 2, 3, 4$ vibrational peak intensities in the NeI (16.67, 16.85 eV) spectra relative to those of the 584 Å spectrum has been attributed to autoionization¹⁹.

$A^2\Pi_u$ Band

In the 584 Å spectrum, we find a previously unresolved difference in β for the first several members of the vibrational progression. For the 537 Å peaks, β values are significantly higher than at 584 Å. We report the first measurement of β for the $v' = 0$ peak produced by the 736 Å line. The corresponding electron energy is exceedingly low, 0.16 eV. Angular distributions for such low electron energies are easily distorted by stray electric and magnetic fields, yet we obtain a reasonable fit to Eq. 2.

$B^2\Sigma_u^+$ Band

Measured β values at 584 Å are in good agreement with those reported earlier. Because of the high value for the ionization potential of this band, the 537 and 522 Å spectra heavily overlap the 584 Å spectrum of the $A^2\Pi_u$ band. Thus we are unable to report β values at the photon wavelengths of the higher order lines.

Discussion

A²Π_u Band

We can infer the variation of β with electron energy for the A²Π_u band from the variation of β across a vibrational progression as long as the possibility of autoionization can be eliminated. We should be able to detect the presence of autoionization or other processes competing with direct autoionization on the basis of the vibrational peak intensities for a given band.

In general, Franck-Condon factors linking neutral states to ionic states for processes of direct ionization and autoionization will be different, as Smith²⁰ and Kinsinger²¹ have discussed for autoionization of molecular oxygen. The potential energy curves, and especially the change in r_e , were found to determine which vibrational peaks were enhanced.

Gardner and Samson³ have measured vibrational peak intensities in the 584 Å spectrum of the A²Π_u band, corrected for analyzer electron energy discrimination, and compared results to calculated Franck-Condon factors uncorrected for the variation of the electronic dipole transition moment. They find reasonable agreement between theory and experiment, so we presume that autoionization should not contribute to observed intensities. Vibrational peak intensities measured for the 537 Å spectrum do not differ noticeably from those for the 584 Å spectrum. Thus, the β values obtained for the 537 Å spectrum are probably not contaminated by autoionization.

There may be autoionizing levels which contribute intensity to the $v' = 0$ peak of the A²Π_u band of the 736 Å spectrum. As a means

of identifying the autoionizing levels at 16.847 eV, we list the possible Rydberg state energies which may fall in this energy region in Table III. Rydberg electrons do not participate heavily in molecular bonding. Thus, we assume that the energy levels of neutral Rydberg states can be calculated from energy levels of the ion to which they converge and from transferable term values $T(n_\lambda, l, \lambda)$, by:

$$E(\nu; n_\lambda, \ell, \lambda) = I_b(\nu) - T(n_\lambda, \ell, \lambda) \quad . \quad (5)$$

Here, $I_b(\nu)$ is the ionization potential for ions in electronic state b and in vibrational state ν .

The ionization potential of $v' = 0$ of the $B^2\Sigma_u^+$ band is high, 18.76 eV. Electronically autoionizing states incorporating the $B^2\Sigma_u^+$ ion would have $ns\sigma_g$ or $nd\lambda_g$ Rydberg levels for the state to be optically allowed. In no case do Lindholm's term values²² for the only experimentally known strong series ($nd\pi_g$) give resulting energies within 100 meV of 16.85 or 16.67 eV. Franck-Condon factors for $v' = 1$ $B^2\Sigma_u^+ \leftarrow v' = 0$ $X^1\Sigma_g^+$ are too low for autoionization from the corresponding Rydberg states to be important. Thus, all autoionizing states at 16.67 or 16.85 eV have $A^2\Pi_u$ ionic cores.

In the photoionization mass spectrometry study of Berkowitz and Chupka²³, no evidence for vibrational autoionization was detected for N_2 . Indeed, they confirm the presence of vibrational autoionization only in H_2 , where it had been previously predicted to occur. We conclude that the $A^2\Pi_u$ peak in the 736 Å spectrum is probably not contaminated by electronic or vibrational autoionization.

In considering all of the $A^2\Pi_u$ peaks for which angular distri-

butions were measured, it is possible to draw a straight line connecting the data points. The solid line of Fig. 5 represents this trend. This is an encouraging sign that we have determined the variation of β for the $A^2\Pi_u$ state for all electron energies below 6.3 eV. The observed trend suggests that β for any vibrational peak within the band increases from a value close to -0.25 at threshold at a rate of roughly 0.15 0.15 units/eV over the range where experimental determinations have been made. The energy dependence we observe is reminiscent of the behavior of β for carbon 2p electrons calculated by Manson¹⁰ for this energy range. The experimental β values of π orbitals of olefin olefins^{21,24,25} behave similarly.

$X^2\Sigma_g^+$ Band

Encouraged by the results for the $A^2\Pi_u$ ionic state, we next may look for trends in β values for the $X^2\Sigma_g^+$ peaks. Here, experimental measurements were made for a 7 eV range of electron energy over which trends should be clearly visible. Examining all of the data points corresponding to $v' = 0$ peaks of the $X^2\Sigma_g^+$ band, we find a discontinuity in Fig. 5 at an electron energy near 4.5 eV. The experimental β values for $v' = 1$ and $v' = 2$ show no such discontinuities, where data points have been taken. Indeed, $v' = 1$ data points at 736 Å and 584 Å and the $v' = 2$ data point at 584 Å lie consistently along the extrapolated variation of $\beta(v' = 0)$ with electron energy in the range below 4.5 eV. The role of autoionization in deflecting β values for each of the data points for the $^2\Sigma_g^+$ ionization band should next be investigated.

As previously mentioned, autoionization is likely responsible for enhancement of $v' = 2, 3, 4$ peaks of the $X^2\Sigma_g^+$ ionization in the 736 and 744 Å photoelectron spectra¹⁹. To a certain extent, $v' = 0$ and $v' = 1$ peaks, for which accurate values of β were measured, are enhanced as well. In examining peak intensities $I(v' = 0)/I(v' = 1)$ at different wavelengths, Carlson⁴ regarded ratios measured at 736 Å as of doubtful value for comparisons to 584 Å spectra in view of this contamination.

We may infer the extent of autoionization-induced enhancement of $v' = 0$ and $v' = 1$ if we can discover which Rydberg states are autoionizing and to which vibrational states of the ion the autoionizing states decay. We neglect autoionization from $\nu \geq 5$ levels of Rydberg states converging to the $A^2\Pi_u$ ion because the corresponding Franck-Condon factors, $F_{i\nu}^2$, will be small. Smith²⁰ has shown that rates of autoionization of Rydberg states can be proportional to Franck-Condon factors to the corresponding ion. Bardsley²⁶ has shown that rates of autoionization are lower for higher members of a given Rydberg series. Thus, we note that the dominant contribution to vibrational peak enhancement will be made by autoionization of lower members of the Rydberg series. Values of $E(\nu; n_\lambda, \ell, \lambda)$ calculated by Eq. 5 are listed in Table III. Only two strong Rydberg series, $ns\sigma_g$ and $nd\sigma_g$, have been found in optical spectra²². Thus, only term values for these two series have been entered in the table.

We note that $E(\nu = 4, 4d\sigma_g)$ is equal to the energy of one of the two principal lines in the NeI discharge, 743.7 Å, lying at 16.67 eV. This photon energy corresponds well to the peak in the photoionization

spectrum of Berkowitz and Chupka²³ which lies at 743.5 Å. We calculate that $E(\nu = 2, 7d\sigma_g)$ is equal to the energy of the 736 Å NeI line. Near 736 Å in the photoionization spectrum, assignments are more difficult because structure in this region is weak.

Since we have estimated which vibrational levels are responsible for the electronic autoionization, we can estimate relative enhancements of the various vibrational peaks in the NeI spectrum. Smith²⁰ has shown that rates of autoionization of Rydberg states to ionic states can be proportional to Franck-Condon factors from the ion limit of the Rydberg series to that final ion. The appropriate Franck-Condon factors here thus correspond to Meinel band emission ($A^2\Pi_u \rightarrow X^2\Sigma_g^+$) and are tabulated by Nicholls²⁷ and listed in part in Table IV. For autoionization of $\nu = 2 - 4$ vibrational levels, factors to $v' = 0$ of the $X^2\Sigma_g^+$ ion are in general lower than those to $v' = 2, 3, 4$ by a factor of 2 - 10. Franck-Condon factors to $v' = 1$ are somewhat higher, but are generally lower than those to $v' = 2, 3, 4$ by a factor of 1.5.

We can calculate β for the direct process, to which we hope to establish a trend for the variation of β with electron energy, by applying Eq. 3. We assume that β_{auto} is 0.2, as measured for $v' = 2, 3$ at 736 Å, and thus can estimate β_{dir} for $v' = 0, 1$. We assume that electron energy discrimination in our electron energy analyzer will be small in the limited energy range covered. Thus, peak heights for $\theta = 54.7^\circ$ should correspond to $Q_{\text{auto}} + Q_{\text{dir}}$. Corrections to the β value for $v' = 0$ should not exceed 0.04 upwards and lie practically within the range of experimental error. The correction to the β value for $v' = 1$ could possibly be as large as 0.1, assuming that

$I(v' = 0)/I(v' = 1) = 10$ for direct ionization, corresponding to Franck-Condon factors calculated by Nicholls²⁷.

For experiments at 627 Å, unlike 736 Å, we assert that there is no possibility of competing autoionization. The corresponding energy, 19.779 eV, lies well above all Rydberg states which converge to $v' = 0$ and $v' = 1$ of the $N_2^+ B^2\Sigma_u^+$ state (18.76 and 19.05 eV, respectively). Furthermore, no Rydberg states with r_e close to 1.1 Å, converging to higher ionization potentials, are known in this region. First, the absorption cross section curves of Lee, *et al.*²⁸, Sasanuma, *et al.*²⁹, and Watson, *et al.*³⁰ are remarkably structureless in the 580 - 660 Å region. Rydberg states converging to the $C^2\Sigma_u^+$ ion are not found spectroscopically for $\lambda > 550$ Å³¹. Second, there is a possibility that neutral states might be Rydberg states converging to the $D^2\Pi_g$ ion. In this case, the potential energy curves are expected to be similar to those of the $D^2\Pi_g$ ion, which has a large (1.471 Å) equilibrium internuclear distance, r_e ³². As a result, Franck-Condon factors to vibrational levels in this well are calculated to be exceedingly low³³. Vertical transitions from ground neutral N_2 to these Rydberg states necessarily intersect the potential energy curves above the dissociation limit, 20.089 eV (corresponding to $N^4S_0 + N^4P$). However, the photon energy, 19.779 eV, lies below this value.

For photon energies above 20.089 eV, the possibility that autoionization might enhance vibrational peaks can not be eliminated. Thus, we must interpret data for $\lambda = 584, 537$, and 522 Å in the light of β values for the direct process obtained from experiments at other

wavelengths. Roughly speaking, the peaks for $v' = 1, 2$ produced by the 584 Å line lie along the extrapolation of the results for $\lambda > 584$ Å. The β value for $v' = 2$ at 584 Å is reproducible and may lie slightly below the trend line for ionization by the direct process. The β values obtained for $v' = 0$ at 584, 537 and 522 Å lie significantly below this trend line.

Where autoionization dominates direct ionization and the autoionization lifetime exceeds the molecular rotational period, the photoelectron angular distribution should tend to isotropy. The measured values will tend to 0 in this case. This effect predominates in the 736 Å ionization of N_2 for $v' = 2, 3$ of the $X^2\Sigma_g^+$ state, reported here and previously⁵, as well as in the 736 Å ionization of O_2 for $v' \geq 4$ of the $X^2\Pi_g$ state reported previously^{4,5}. Eq. 3 should be used in cases of ionization where direct and autoionization contributions are both substantial. Experimental β values in this situation lie intermediate between the extremes of β_{dir} and β_{auto} . Thus, we might attribute deviations below the trend line for $^2\Sigma_g^+$ ionization to a partial contribution from autoionization.

A Consideration of Autoionization

Carlson⁴ has discussed the possibility that autoionization could be responsible for the different values of β for $v' = 0$ and 1 at 584 Å. He concluded that evidence for autoionization is meager based upon the following arguments:

1. Resonance absorption via Rydberg states converging to the $\sigma_g 2s$ ionization at 37.3 eV should not be possible at a photon energy of 21.2 eV.

2. Double excitation processes are conceivable, but less probable.
3. Samson and Cairns³⁴ observe no resonance absorption at 584 Å in their absorption experiment.
4. Vibrational intensity ratios for $v' = 0$ and $v' = 1$ at 584 Å and 304 Å were compared. Autoionization processes would have to selectively produce N_2^+ in $v' = 0$ and autoionization would have to contribute at least 40% of the total band intensity, assuming $\beta_{\text{auto}} = 0$, to explain the vibrational intensity ratios. Carlson regarded this as improbable.

Carlson suggested that a breakdown of the Born-Oppenheimer approximation was likely responsible for the observed anomaly. In a subsequent publication, Thomas³⁵ derived the dependence of photoelectron angular distributions on the degree of vibrational and rotational excitation in the ion. He based his derivation on the breakdown of the dipole approximation.

Carlson's arguments 1 and 3 above assume that the autoionizing state is a vibrational level of an electronic state resonant with the HeI radiation. In the discussion of the 627 Å spectrum earlier, we suggested that neutral states in the spectral region for $\lambda > 550$ Å and in the Franck-Condon envelope accessible from the ground neutral state are probably repulsive. Here, the intersection of the Franck-Condon envelope with the potential curves for the excited neutrals lies above the dissociation limit, as long as $\lambda < 617.1$ Å.

Argument 2 is fundamentally sound. In the 304 Å photoelectron spectra of N_2 , several peaks are seen which correspond to double

excitation processes¹⁷. Here one bonding electron is promoted to an antibonding $\sigma_u 2p$ or $\pi_g 2p$ orbital and another bonding electron is ejected. The spectral peaks are substantially weaker than those corresponding to the $X^2\Sigma_g$, $A^2\Pi_u$, or $B^2\Sigma_u^+$ ionic states. Production rates for double excitation neutrals, where one electron is promoted to a higher valence orbital and one may be promoted to a Rydberg orbital, have not been as well characterized. Electron^{36,37} and photon^{38,39} impact fluorescence studies have detected atomic emission at 1200 Å ($^4P \rightarrow ^4S_0$) above a threshold of 20.089 eV. Aarts and de Heer³⁶ have suggested that Rydberg states lying below the $D^2\Pi_g$ ion are likely responsible for this emission. Lee, et al.³⁸. in a photon impact study, measured an atomic fluorescence cross section of $2 \times 10^{-19} \text{ cm}^2$ near 584 Å. This compares with the partial photoionization cross section for the production of $N_2^{+2}\Sigma_g^+$ in all vibrational levels of $7.5 \times 10^{-18} \text{ cm}^2$ at 584 Å as measured by Blake and Carver⁴⁰. The atomic fluorescence cross section is thus a small, but appreciable fraction of the $X^2\Sigma_g^+$ photoionization cross section, where the intervening neutral states must arise from double electron excitations. Conceivably, the same neutral states could autoionize in competition with the dissociative process. For N_2 , the lifetimes with respect to autoionization for autoionizing Rydberg states may typically be $n^3 \times 10^{-14} \text{ sec}$,⁴¹ where n is an effective principal quantum number. For lower ($n = 3, 4$) Rydberg states, autoionization can compete effectively with dissociation, which occurs on a time scale of $10^{-12} - 10^{-13} \text{ sec}$.

In focussing on Carlson's argument 4, the 40% figure he quotes

as the fraction of ionization in the $^2\Sigma_g^+$ region that might be attributed to autoionization is probably too high. On the basis of the trend line of β for $^2\Sigma_g^+$ ionization in Fig. 6, we can presume that $v' = 1$ is not appreciably enhanced by autoionization. Then, the relative amounts of autoionization may be calculated from the extent to which $v' = 0$ and $v' = 2$ peaks are enhanced. Table V lists a number of vibrational peak intensity ratios measured and calculated for the vibrational peaks of the $X^2\Sigma_g^+$ band. Gardner and Samson³ have published vibrational intensity factors at 584 Å, corrected for electron energy analyzer discrimination effects and the different angular distributions for $v' = 0, 1, 2$ transitions. They also tabulate vibrational peak intensity ratios using accurate numerical vibrational wavefunctions, but without electric dipole transition moment corrections. We neglect the contribution of autoionization which enhances $v' = 2$, since vibrational intensity ratios are of low accuracy. We further assume that the theoretical results furnish vibrational intensity ratios in the absence of autoionization. We then calculate that $23 \pm 7\%$ of the total $X^2\Sigma_g^+$ intensity at 584 Å might be attributed to autoionization. Correspondingly, 25% of the $v' = 0$ intensity might be attributed to autoionization.

The fraction of $^2\Sigma_g^+$ photoelectron intensity at 584 Å that we have attributed to autoionization need not be considered inordinately large. The intervening neutral autoionizing state is dissociative. Hence, the corresponding density of states may be very high.

We have several means of evaluating the importance of autoionization. The photoabsorption cross section curves might show

extra structure in this spectral region. Photoelectron experiments at different wavelengths could shed light on the problem. We can formulate and apply a theoretical model for the enhancement of structure in the photoelectron spectrum.

Samson has measured the photoionization yield for N_2 at 584 Å to be close to unity³⁴. Correspondingly, the measurements of Blake and Carver⁴⁰ give the partial cross section to the $X^2\Sigma_g^+$ state as approximately $7.5 \times 10^{-18} \text{ cm}^2$ out of a total cross section of approximately $2.2 \times 10^{-17} \text{ cm}^2$. Thus, on the basis of vibrational enhancement arguments alone, autoionization would have to be responsible for $23\% \times (7.5/22)$, or 7.8% of the total absorption cross section (about $1.6 \times 10^{-18} \text{ cm}^2$). As discussed earlier, the spectral region where the autoionization may be occurring, to shorter wavelengths than 617.1 Å, is remarkably free of structure²⁸⁻³⁰ except for $\lambda < 550 \text{ Å}$ ^{28,29,31}. The region between 617 - 560 Å (20 - 22 eV) is generally flat and featureless. A significant amount of diffuse band structure could underlie this region and be undetectable. Thus, the conventional absorption experiment may not be sufficiently sensitive to processes which may compose a small fraction of the total cross section.

A comparison of photoelectron intensities in the $X^2\Sigma_g^+$ and $A^2\Pi_u$ bands may shed light on the issue. In the usual molecular orbital scheme, the $3\sigma_g$ and $1\pi_u$ orbitals are composed primarily of nitrogen 2p electrons. In the same scheme, the $2\sigma_u$ orbital is composed primarily of nitrogen 2s. According to arguments of Price⁴² the variation of photoelectron intensity with energy within

50 eV of threshold should depend on the s/p character of the orbitals. Intensity for orbitals with dominant s-character increases relative to orbitals with dominant p-character on changing the lamp from HeI (584 Å) to HeII (304 Å). The spectra of Katrib, *et al.*⁴³ shows this effect in a comparison of the $A^2\Pi_u$ and $B^2\Sigma_u^+$ bands of N_2 . However, ignoring effects of different angular distributions on observed intensities, the $X^2\Sigma_g^+$ band ($-\sigma_g 2p$), which should not vary greatly in intensity relative to the $A^2\Pi_u$ band ($-\pi_u 2p$), shows a marked decrease in changing lamps from HeI to HeII. Significantly, the relative intensities of $v' = 1$ of the $X^2\Sigma_g^+$ band and the $A^2\Pi_u$ band do not show marked change with photon energy. In the HeII photon energy range (40.8 eV), autoionization should not be of any practical importance. The $v' = 0$ $X^2\Sigma_g^+$ peak is thus significantly enhanced in the HeI spectrum in a region where autoionizing states may exist.

The ratio of autoionization to the direct process for the $v' = 0$ $X^2\Sigma_g^+$ peak in the 584 Å spectrum may allow us to evaluate β_{auto} of Eq. 3. Experimental β values for the NeI photoelectron studies of O_2 ⁴ and N_2 ^{5,44} suggest that β_{auto} tends to 0 where the lifetime of the autoionizing state exceeds one rotational period. For N_2 , using a HeI light source, the β value for $v' = 0$, 0.74 ± 0.02 , could represent a β value in the presence of direct ionization and autoionization. We assume that $\beta = 1.43$ for $v' = 1$ furnishes β_{dir} and the above analysis of vibrational peak intensities for $v' = 0$ and $v' = 1$ furnishes the fraction of autoionization in the $v' = 0$ peak, 0.25. Applying Eq. 3, we find $\beta_{\text{auto}} = -1.16 \pm 0.43$, significantly below 0, but within the error bars of the permissible⁹ range of β , $-1 \leq \beta \leq 2$. This

result may seem odd until we realize that the neutral autoionizing state would not persist for a full rotational period (10^{-11} sec.).

Competing dissociation would take place on a time scale shorter than 10^{-12} sec. The β_{auto} near -1 is extremely interesting in the context of Dill's treatment of angular momentum transfers¹⁴ in photoionization. This theory was applied to the ionization of xenon, for which resonances in β accompany resonances in the ionization cross section. In the cases of relatively long lived autoionizing states, at the extrema of the cross sections, the normally forbidden angular momentum transfers mix heavily with the allowed transfers. The asymmetry parameter for a forbidden angular momentum transfer is -1.

We have performed a calculation of the enhancement of vibrational peaks due to autoionization. We sought to determine whether autoionization could account for the enhancement of $v' = 0$ and the dependence of β on photoelectron energy for the $v' = 0, 1, 2$ peaks in the $X^2\Sigma_g^+$ band. We based the calculation on the Fano theory of configuration interaction⁴⁵. This theory has only been applied previously to the autoionization of discrete states imbedded in the ionization continuum. Extensions of the theory to molecules by Mies⁴⁶ and Bardsley⁴⁷ permitted Smith²⁰ to express vibrational intensities as the sum of two terms involving Franck-Condon factors:

$$I \propto F_{i\nu'}^2 + aF_{i\nu}^2 F_{\nu\nu'}^2, \quad (6)$$

where i , ν , and ν' index vibrational quantum numbers for initial, autoionizing, and final states, respectively, and a is a parameter. This expression is valid only in two cases. In the first case, the

energy width of the light source is small compared to the width of the resonance, and the photon energy is tuned to the resonance maximum. In the second case the energy width of the light source greatly exceeds the width of the resonance and the photon bandwidth encompasses the entire resonance. We assumed that Eq. 6 above would furnish vibrational intensity for the autoionization of continuum nuclear states if the Franck-Condon factors were calculated using energy-normalized nuclear continuum wavefunctions. Further, we assumed that the parameter a was independent of photon energy.

We made assumptions about the potential energy curves for the autoionizing state or states since neutral states in the region above 20 eV have not been well characterized. Dipole selection rules permit $np\sigma_u$ and $np\pi_u$ Rydberg orbitals to accompany a $D^2\Pi_g$ ion core. In the calculation, we allowed absorption to the $np\sigma_u + \text{core}$ and $np\pi_u + \text{core}$ electronic states to occur with equal probabilities. Electronic autoionization of neutral Rydberg states varies inversely with the cube of the effective principal quantum number²⁶. Correspondingly, we considered only the $3p\sigma_u + \text{core}$ and $3p\pi_u + \text{core}$ Rydberg states. We defined the potential curves subject to several constraints. First, both potential energy curves were forced to dissociate into $N(^4S) + N(^4P)$ at 20.089 eV, corresponding to the observed threshold for 1200 Å emission, $^4P \rightarrow ^4S$ ³⁶⁻³⁹. Second, we required the potential energy curve to be repulsive in the Franck-Condon region as was expected for Rydberg states lying below the $D^2\Pi_g$ ion. The curve for $r < r_e$ was given Morse potential parameters fitted to the $v = -\frac{1}{2}, 5$, and 10 RKR classical turning points and vibrational term values

calculated by Namioka, et al.³², for the $D^2\Pi_g$ ion. Finally, the potential energy curves at $r_e = 1.471 \text{ \AA}$ of the Rydberg states were taken to lie directly below that of the $D^2\Pi_g$ ion by 3.898 ($np\pi_u$) and 4.158 ($np\sigma_u$) eV. The difference in energy was chosen to agree with the difference between $3p\sigma_u$ and $3p\pi_u$ term values for the Rydberg series lying below the $X^2\Sigma_g^+$ first ionization potential²². The mean of 3.898 and 4.158 was chosen to give sizeable values of $F_{i\nu}^2$, $F_{\nu v'}^2$ for $v' = 0$ and small values for $v' = 1, 2$.

Based on these assumptions, the potential energy curves for $r > r_e$ were taken to be of Morse form, where the dissociation energy, D_e , and range parameter, α , were different than for $r < r_e$. The two potential energy functions were thus:

$$V_o(r) = \begin{cases} 17.77 + 1.236(1 - e^{-2.81326\Delta r})^2 & r < 1.471 \text{ \AA} \\ 17.77 + 2.319(1 - e^{-2.05400\Delta r})^2 & r > 1.471 \text{ \AA} \end{cases} \quad (7)$$

$$V_\pi(r) = \begin{cases} 18.03 + 1.236(1 - e^{-2.81326\Delta r})^2 & r < 1.471 \text{ \AA} \\ 18.03 + 2.059(1 - e^{-2.17983\Delta r})^2 & r > 1.471 \text{ \AA} \end{cases} \quad (8)$$

where $\Delta r = r - 1.471 \text{ \AA}$ and energies are given in eV and distances in Angstroms. The potential energy curve specified by Eq. 7 for one of the Rydberg states, as displayed in Fig. 6, resembles that of the $D^2\Pi_g$ ion for $r < r_e$, yet switches smoothly at $r = r_e$ into a curve which dissociates into $N(^4S) + N(^4P)$.

Continuum nuclear wavefunctions were calculated by Runge-Kutta integration of the radial Schrödinger equation. The wavefunctions were energy normalized by requiring the asymptotic form $\sin(kr + \delta)$, where δ is a phase shift and $\hbar k$ is the momentum of the nuclear motion

asymptotically. Nuclear wavefunctions for the bound N_2 and N_2^+ levels were taken to be the Morse oscillator wavefunctions of Nicholls²⁷.

Potential parameters μ_A , ω_e , $\omega_e x_e$, and r_e were taken from Herzberg⁴⁹. For the Franck-Condon factors obtained, the normalization in momentum space is expressed as:

$$\int_0^{\infty} F_j(k) dk = 1, \quad (9)$$

where j labels the vibrational level of the discrete nuclear state.

The resulting products of Franck-Condon factors, $F_{i\nu}^2 F_{\nu v'}^2$, were calculated as a function of photon energies over a range of 7 eV above the 20.089 eV dissociation limit. We converted the variation of $F_{i\nu}^2 F_{\nu v'}^2$ with photon energy to curves for β with energy assuming that the theoretical curve should agree with the experimental β values for $v' = 0$ of the $X^2\Sigma_g^+$ band at 584 Å. Since Q_{dir} and Q_{auto} of Eq. 3 are related to $F_{i\nu}^2$ and $aF_{i\nu}^2 F_{\nu v'}^2$, respectively, this normalization fixes the value of a . Further, we assumed $\beta_{auto} = -1.16$ and $\beta_{dir} = 1.43$ in Eq. 3, independent of photoelectron energy.

Theoretical results are compared to experimental data points in Figs. 7 - 9. The model predicts large deviations from $\beta = 1.43$ for all vibrational levels, where the minima in β occur at different photon energies for different v' . Furthermore, since for several energy regions, the factors $F_{i\nu}^2 F_{\nu v'}^2$ are similar for $v' = 0, 1, 2$, where the factors F_v^2 remain fixed, the model predicts significant enhancement of $v' = 1, 2$ for photon energies larger than 21.21.

The results of the model calculation do not fare well in a comparison with experimental results. For $v' = 0$, β values at 537 and

522 Å lie along the calculated curve in Fig. 7. However, experimental and theoretical results for $v' = 1$ do not match. The experimental result for $v' = 1$ lies significantly above that calculated at the electron energy appropriate for 537 Å, as seen in Fig. 8. The match for $v' = 2$ peaks at 584 Å in Fig. 9 is not good, and probably could not be improved by increasing β_{auto} or by shifting the potential curves. Gardner and Samson³ have measured the vibrational peak intensities for $v' = 0$ and 1 over a range of photon energies ($\lambda = 584, 537$, and the lines of an Ar arc source, for λ as high as 645 Å). The ratio of $v' = 0$ intensity to $v' = 1$ intensity was found to be roughly independent of photon energy in this range.

We rationalize the failure of the model to accurately describe the variation of β and vibrational peak heights in the following manner. First, we really do not have accurate potential curves for the neutral states in the 20 - 25 eV region. Recent calculations of Thulstrup and Andersen⁵⁰ and Cartwright and Dunning⁵¹ have accurately characterized the double excitation ionic states in this region. Rydberg states converging to these ions certainly exist. Second, we only guessed at the theoretical expressions for vibrational intensities in the autoionization of continuum nuclear states. Theoretical efforts in this area are needed. Finally, autoionization of continuum nuclear states may not be the mechanism for the enhancement of $v' = 0$ and the different β values for $v' = 0$ and $v' = 1$.

Eq. 6 might be relatively accurate for describing autoionization of Rydberg states converging to the $C^2\Sigma_u^+$ ion. Here, the levels which autoionize are discrete states imbedded in the ionization continuum.

Since the conventional Franck-Condon factors determine the relative enhancement of the various vibrational peaks, the suggestions by Wacks⁵² become appropriate. The dominant factor affecting the distribution of Franck-Condon factors for an excitation process is the change in r_e of the transition. When the change of r_e exceeds 10%, as in the case of a $C^2\Sigma_u^+ + \text{Ryd.} \leftarrow X^1\Sigma_g^+$ excitation, the transition probabilities become small to any particular vibrational level and spread over many vibrational levels. Correspondingly, the enhancement of ionic vibrational peaks in the vibrational envelope would be spread over many high vibrational levels, as is observed in CO ionization⁵³, rather than being concentrated in the enhancement of $v' = 0$.

Other Sources for the Anomaly

The source of the anomalous behavior of photoelectron intensity in the $v' = 0$ peak of the $X^2\Sigma_g^+$ band may lie elsewhere. The electric dipole transition moment may be varying with vibrational transition, and thus, with the r -centroid of the transition. Accompanying the Born-Oppenheimer factorization of a molecular wavefunction into electronic and nuclear wavefunctions and an integration over the electronic coordinates in Eq. 1, the transition amplitudes take the following form:

$$\underline{T} = \int \chi_f(\underline{R}) \chi_i(\underline{R}) \underline{D}(\underline{R}) d^3 \underline{R} \quad . \quad (10)$$

Here, the functions χ are nuclear wavefunctions and $\underline{D}(\underline{R})$ is an electric dipole transition moment:

$$\underline{D}(\underline{R}) = \int \psi_f(\underline{r}; \underline{R}) \hat{\underline{T}} \psi_i(\underline{r}; \underline{R}) d^3 \underline{r} \quad , \quad (11)$$

where the ψ are electronic wavefunction. Frequently, \underline{T} is factored into a product of a Franck-Condon amplitude and a transition moment:

$$\underline{T} = F_{if} \overline{D(\underline{R})} \quad , \quad (12)$$

by the theorem of the mean. The \underline{R} dependence of $\underline{D(\underline{R})}$ will then yield a dependence of $\overline{D(\underline{R})}$ on the vibrational quantum number of the final state.

This effect was investigated previously by Itikawa⁵⁴ and Berkowitz and Spohr⁵⁵ for molecular hydrogen. Here, vibrational intensities in the $X^2\Sigma_g^+$ progression of H_2 differ significantly from accurate Franck-Condon factors. Systematically, over the range of vibrational levels in the ion, the ratio of experimental or accurate (corrected for variations of the electric dipole transition moment) theoretical vibrational intensities to the Franck-Condon factors increased by 4 - 5% with each increasing quantum of vibrational energy in the molecular ion. At the same time, Carlson⁴ has reported no change in the asymmetry parameter over the range of vibrational peaks for H_2 .

The intensity effect observed for N_2 is significantly larger than for H_2 and the change of β is substantial. An explanation for the N_2 anomalies based upon changes in the electron dipole transition moment would thus be unprecedented.

Another possibility is that the resonance phenomenon seen in the K-shell ionization of N_2 may be occurring in the valence shell. Dehmer and Dill⁵⁶ calculate a significant drop in β and a corresponding increase in intensity in the region 6 - 15 eV above ionization threshold.

The dip in β in the region 9 - 10 eV above threshold is comparable to that observed in the $X^2\Sigma_g^+$ band for $v' = 0$. However, the intensity enhancement appears to be much larger (an increase of 200%) than is observed in the $X^2\Sigma_g^+$ band. In addition, the magnitude of the effect would have to depend on the vibrational level of the ion if resonance excitation were the mechanism for the present N_2 anomaly. The paper presents no evidence to suggest that the effect could vary with the degree of vibrational level in the ion. Finally, Dehmer and Dill suggest that the effect may be present in core L-shell or core M-shell ionization. Resonance phenomena of this sort have not been observed in valence shell ionization.

$B^2\Sigma_u^+$ Band

The only β values for the $B^2\Sigma_u^+$ ionization, measured at 584 Å, lie along the curve of the $X^2\Sigma_g^+$ ionization. This may be mere coincidence or may indicate that curves for $^2\Sigma_g^+$ and $^2\Sigma_u^+$ should be the same near ionization threshold, since both ionic states produced are $^2\Sigma$ states.

This possibility is interesting in light of theoretical calculations of photoelectron angular distributions for molecules. Ritchie⁵⁷ has suggested that for high photoelectron energies (> 100 eV), a torque caused by high order terms in a multipole expansion about the molecular ionic center has only a small effect. In this energy range, the potential is dominated by a spherically symmetric monopole term and for molecules having a center of symmetry, the form of the angular distribution for ionization from a molecular orbital of gerade and ungerade symmetry is very much different.

Assuming that the wavefunction for the outgoing photoelectron is a plane wave orthogonalized to filled molecular orbitals (OPW)¹² yields β values for the $B^2\Sigma_u^+$ state which are significantly lower than those calculated for the $X^2\Sigma_g^+$ state. The present experimental values lie intermediate between the OPW results for the $B^2\Sigma_u^+$ and $X^2\Sigma_g^+$ states.

Conclusion

The photoelectron angular distributions have been measured for N_2 for both the strong and very weak emission lines of neon and helium glow discharge lamps. The wide range of photon energies covered has allowed us to measure the electron energy dependence of β .

We have discussed several mechanisms for the anomalous variation of β with vibrational peak in the $X^2\Sigma_g^+$ photoelectron spectrum at 584 Å. The autoionization pathway through Rydberg states converging to the $D^2\Pi_g$ ion might enhance $v' = 0$ intensity in the $X^2\Sigma_g^+$ ionization band by as much as a third. Alternatively, other mechanisms are possible. However, an explanation consistent with all experimental results is not available yet. Any mechanism should account for the anomalous HeI/HeII effect on the $v' = 0$ peak, the enhancement of $v' = 0$ relative to $v' = 1$ in the energy region near 21 eV, and the anomalous difference between β values between $v' = 0$ and $v' = 1$.

We suggest that further angular distribution experiments for $\lambda > 617$ Å, corresponding to the $N(^4S) + N(^4P)$ dissociation limit, will help more firmly establish the trend observed here for the $X^2\Sigma_g^+$

band. In addition, experiments for $\lambda < 660 \text{ \AA}$, corresponding to the threshold for the $\text{N}_2^+ \text{ B } ^2\Sigma_u^+$ state, should be performed to examine for further similarities in the energy dependence of β for loss of electrons from $\sigma_g 2p$ and $\sigma_u 2s$ orbitals.

Acknowledgment

We are grateful to Dr. Thomas Rescigno for supplying a computer program to calculate energy normalized nuclear continuum wavefunctions.

References

1. M. I. Al-Joboury, D. W. Turner, J. Chem. Soc. 5141 (1963).
2. D. W. Turner, C. Baker, A. D. Baker, C. R. Brundle, Molecular Photoelectron Spectroscopy (Wiley-Interscience, London, 1970).
3. J. L. Gardner, J. A. R. Samson, J. Chem. Phys. 60, 3711 (1974).
4. T. A. Carlson, Chem. Phys. Lett. 9, 23 (1971); T. A. Carlson, A. E. Jonas, J. Chem. Phys. 55, 4913 (1971).
5. R. Morgenstern, A. Niehaus, M. W. Ruf, in L. Branscomb (editor) Electronic and Atomic Collisions (North-Holland, Amsterdam, 1971) p. 167.
6. M. Born, J. R. Oppenheimer, Ann. Physik 84, 457 (1927).
7. D. C. Cartwright, A. Kuppermann, Phys. Rev. 163, 86 (1967).
8. J. W. Cooper, S. T. Manson, Phys. Rev. 177, 157 (1969).
9. J. Cooper, R. N. Zare, in S. Geltman, K. Mahanthappa, N. Brittin (editors) Lectures in Theoretical Physics Vol. III-C (Gordon and Breach, New York, 1969) p. 317.
10. S. T. Manson, J. Electron Spectr. 1, 413 (1972).
11. S. Iwata, S. Nagakura, Mol. Phys. 27, 425 (1974).
12. J. W. Rabalais, T. P. Debies, J. L. Berkosky, J.-T. J. Huang F. O. Ellison, J. Chem. Phys. 61, 529 (1974); 62, 4588 (1975).
13. B. Schneider, R. S. Berry, Phys. Rev. 182, 141 (1969).
14. D. Dill, Phys. Rev. A 7, 1976 (1973).
15. J. A. R. Samson, J. L. Gardner, Phys. Rev. Lett. 31, 1327 (1973).
16. R. L. Kelley, Atomic Emission Lines Below 2000 Angstroms, Hydrogen Through Argon (Naval Research Laboratory, Washington, 1968) NRL Report 6648.

17. L. Åsbrink, Faraday Disc. Chem. Soc. 54, 142 (1973); A. W. Potts, T. A. Williams, W. C. Price, Faraday Disc. Chem. Soc. 54, 104 (1972); M. Okuda, N. Jonathan, J. Electron Spectr. 3, 19 (1974).
18. D. M. Mintz, A. Kuppermann, in J. S. Risley, R. Geballe (editors) Electronic and Atomic Collisions (U. of Washington, Seattle, 1975) p. 567.
19. P. Natalis, J. Delwiche, J. E. Collin, Chem. Phys. Lett. 13, 491 (1972); J. E. Collin, P. Natalis, Int. J. Mass Spectrom. Ion Phys. 2, 231 (1969).
20. A. L. Smith, Phil. Trans. Roy. Soc. Lond. A268, 169 (1970); J. Quant. Spectr. Radiat. Transfer 10, 1129 (1970).
21. J. A. Kinsinger, J. W. Taylor, Int. J. Mass Spectrom. Ion Phys. 11, 461 (1973).
22. E. Lindholm, Arkiv för Fysik 40, 111 (1968).
23. J. Berkowitz, W. A. Chupka, J. Chem. Phys. 51, 2341 (1969).
24. R. M. White, T. A. Carlson, D. P. Spears, J. Electron Spectr. 3, 59 (1974).
25. D. M. Mintz, A. Kuppermann, in preparation.
26. J. N. Bardsley, Chem. Phys. Lett. 1, 229 (1967).
27. R. W. Nicholls, J. Res. Nat. Bur. Stds. 65A, 451 (1961).
28. L. C. Lee, R. W. Carlson, D. L. Judge, M. Ogawa, J. Quant. Spectrosc. Radiat. Transf. 13, 1023 (1973).
29. M. Sasanuma, E. Ishiguro, Y. Morioka, M. Nakamura, in Y. Nakai (editor) Conference Digest of the Third International Conference on Vacuum Ultraviolet Radiation Physics, Tokyo, 1971,

p. 1pA2 - 3.

30. W. S. Watson, J. Lang, D. T. Stewart, J. Phys. B. 6, L148 (1973).
31. K. Codling, Astrophys. J. 143, 552 (1966).
32. T. Namioka, K. Yoshino, Y. Tanaka, J. Chem. Phys. 39, 2629 (1963).
33. R. W. Nicholls, J. Quant. Spectrosc. Radiat. Transfer 2, 433 (1962).
34. J. A. R. Samson, R. B. Cairns, J. Geophys. Res. 69, 4583 (1964).
35. I. L. Thomas, Phys. Rev. A 4, 457 (1971).
36. J. F. M. Aarts, F. J. de Heer, Physica 52, 45 (1971).
37. M. J. Mumma, E. C. Zipf, J. Chem. Phys. 55, 5582 (1971);
J. M. Ajello, J. Chem. Phys. 53, 1156 (1970); W. Sroka,
Z. Naturforsch. 24a, 398 (1969).
38. L. C. Lee, R. W. Carlson, D. L. Judge, M. Ogawa, J. Chem. Phys. 61, 3261 (1974); Chem. Phys. Lett. 19, 183 (1973).
39. K. D. Beyer, K. H. Welge, J. Chem. Phys. 51, 5323 (1969).
40. A. J. Blake, J. H. Carver, J. Chem. Phys. 47, 1038 (1967).
41. K. C. Smith, J. A. Schiavone, R. S. Freund, J. Chem. Phys. 59, 5225 (1973).
42. W. C. Price, A. W. Potts, D. G. Streets in D. Shirley (editor)
Electron Spectroscopy (North Holland, Amsterdam, 1972) p. 187.
43. A. Katrib, T. P. Debies, R. J. Colton, T. H. Lee, J. W. Rabalais, Chem. Phys. Lett. 22, 196 (1973).

44. cf. Table II.
45. U. Fano, Phys. Rev. 124, 1866 (1961).
46. F. H. Mies, Phys. Rev. 175, 164 (1968).
47. J. N. Bardsley, Chem. Phys. Lett. 2, 329 (1968).
48. F. R. Gilmore, J. Quant. Spectrosc. Radiat. Transfer 5, 369 (1965).
49. G. Herzberg, Molecular Spectra and Molecular Structure I. Spectra of Diatomic Molecules (Van Nostrand Reinhold, New York, 1939).
50. E. W. Thulstrup, A. Andersen, J. Phys. B 8, 965 (1975).
51. D. C. Cartwright, T. H. Dunning, J. Phys. B 8, L100 (1975).
52. M. E. Wacks, J. Chem. Phys. 41, 930 (1964).
53. D. M. Mintz, A. Kuppermann, unpublished results.
54. Y. Itikawa, J. Electron Spectr. 2, 125 (1973).
55. J. Berkowitz, R. Spohr, J. Electron Spectr. 2, 143 (1973).
56. J. L. Dehmer, D. Dill, Phys. Rev. Lett. 35, 213 (1975).
57. B. Ritchie, J. Chem. Phys. 61, 3291 (1974).

Table I. Table of atomic emission lines used in present study.

Light Source	Wavelength (Å)	Energy (eV)	Intensity ^a
He I	584.334	21.217	100
	537.030	23.086	2
	522.213	23.741	0.5
Ne I	735.895	16.847	100
	626.822	19.779	0.3

^a Relative photoelectron intensity for $X^2\Sigma_g^+$, $v' = 0$, for each lamp fill gas.

Table II. Asymmetry parameter β for ionization of N_2 by photons of different wavelength.

Ionic State	v'	I.P. (eV)	584 Å		736 Å		537 Å		522 Å		627 Å	
			Expt.	Theory	Expt.	Theory	Expt.	Theory	Expt.	Theory	Expt.	Theory
$X^2\Sigma_g^+$	0	15.53	0.74±0.02 (0.5 ^a , 0.69 ^b)	1.91 ^c , 0.95 ^d	1.00±0.03 (1.20 ^a , 0.99 ^b)	1.93 ^c , 0.34 ^d	0.72±0.03		0.95±0.05		1.3±0.2	
	1	15.85	1.43±0.02 (1.4 ^a , 1.40 ^b)		0.93±0.04 (0.92 ^b)		1.1±0.2					
	2	16.12	1.3±0.1 (0.73 ^b)		0.22±0.04							
	3	16.39			0.14±0.04							
$A^2\Pi_u$	0	16.59	0.36±0.02 (0.43 ^{b†})	0.72 ^c	-0.26±0.11		0.7±0.1					
	1	16.92	0.29±0.02 (0.30 ^{a†})				0.6±0.1					
	2	17.15	0.25±0.03									
	3	17.38	0.25±0.04									
$E^2\Sigma_u^+$	4	17.60	0.24±0.04									
	5	17.81	0.35±0.05									
	6	18.02	0.31±0.09									
	0	18.76	1.29±0.04 (1.23 ^a , 1.25 ^b)	-0.861 ^c								
	1	19.04	1.25±0.04 (1.27 ^b)									

^a Ref. 4.^b Ref. 5.^c Ref. 12.^d Ref. 13.† Measured constant over vibrational envelope. Others have measured β for a vibrational average in this band; results from these groups is not included in this table.

Table III. Predicted Rydberg state energy levels^a.

Ion Core	Vib. Quantum Number	Series	I. P. of Ion (eV)	Principal Quantum Number				
				n=3	n=4	n=5	n=6	n=7
$A^2\Pi_u$	1	$s\sigma_g$	16.92	13.33	15.37	16.05	16.37	16.54
	1	$d\sigma_g$	16.92	15.24	16.00	16.34	16.52	16.63
	2	$s\sigma_g$	17.14	13.55	15.59	16.27	16.59	16.76
	2	$d\sigma_g$	17.14	15.46	16.22	16.56	16.74	<u>16.85</u>
	3	$s\sigma_g$	17.37	13.78	15.82	16.50	16.82	16.99
	3	$d\sigma_g$	17.37	15.69	16.45	16.79	16.97	17.08
	4	$s\sigma_g$	17.59	14.00	16.04	16.72	17.04	17.21
	4	$d\sigma_g$	17.59	15.91	<u>16.67</u>	17.01	17.19	17.30
$B^2\Sigma_u^+$	0	$d\sigma_g$	18.76	17.15	17.87	18.19		

^a Using the following quantum defects from Ref. 26: $s\sigma_g$, 1.04; $d\sigma_g$, 0.18; $d\pi_g$, 0.07.

Table IV. Meinel band Franck-Condon factors^a.

Vibrational Level, $A^2\Pi_u$	Vibrational Level, $X^2\Sigma_g^+$				
	$v'' = 0$	$v'' = 1$	$v'' = 2$	$v'' = 3$	$v'' = 5$
1	0.3255	0.0312	0.3358	0.2368	0.0080
2	0.1360	0.2245	0.0214	0.1851	0.1171
3	0.0453	0.1990	0.0797	0.1048	0.2929
4	0.0133	0.1032	0.1745	0.0072	0.0058

^a From Ref. 27.

Table V. $X^2\Sigma_g^+$ vibrational peak intensities at 584 Å.

Peak	Experimental Ratios ^a	Franck-Condon Factor ^a
0	100.0	100.0
1	6.94±0.66	9.27
2	0.32±0.21	0.59

^a Normalized to 100.0 at $v' = 0$, from Ref. 3.

Figure Captions

1. Block diagram of variable angle photoelectron spectrometer.
 HE cylinder of UHP helium. ZT, liquid nitrogen immersed zeolite trap for lamp helium supply. BR, lamp ballast resistor, 1320 Ω . LPS, lamp power supply, 555 V, 300 mA maximum. SC, sample chamber. PC, photocathode for light flux measurement. CL, electron lens elements before hemispherical analyzer. ANALYZER, 180° hemispherical electrostatic electron energy analyzer. ML, electron lens elements between hemispheres and detector.
2. HeI photoelectron spectrum of N₂ at $\theta = 120^\circ$. The spectrum was accumulated over 511 data channels, an incremented energy of 15 meV between successive channels, and a dwell time per channel of 30 seconds. Background was not subtracted from the spectrum displayed here.
3. NeI photoelectron spectrum of N₂ at $\theta = 54.7^\circ$, including only the 736 and 744 Å spectra. The spectrum was accumulated with 10 meV incremented between channels, and with a dwell time of 45 sec. Background was not subtracted from the spectrum displayed here.
4. NeI spectrum of N₂ at $\theta = 54.7^\circ$, showing $v' = 0$ X²Σ_g⁺ peaks produced by the 619, 627, and 630 Å lines in the discharge. Spectrum was accumulated over 218 channels, an incremented energy of 4 meV per channel, and at a dwell time of 90 sec. The lower trace is the raw spectrum and the upper trace is a 13 point smoothing of the lower trace.

5. Plot of experimental β values versus photoelectron energy for N_2 ionized by 736, 627, 584, 537, and 522 Å light. \odot , $v' = 0$, $^2\Sigma_g^+$. \triangle , $v' = 1$, $^2\Sigma_g^+$. \bullet , $v' = 2$, $^2\Sigma_g^+$. \square , peaks of the $A^2\Pi_u$ state. \blacktriangle , peaks of the $B^2\Sigma_u^+$ state. Solid line represents variation of β for vibrational peaks of the $A^2\Pi_u$ band for experiments at three photon energies. Dashed line represents variation of β for the $v' = 0$ peak of the $X^2\Sigma_g^+$ band for experiments at five photon energies.
6. Potential energy curves for the lower of the two proposed auto-ionizing states (heavy solid line) and the low-lying ionic states of N_2 , after Gilmore⁴⁸. The dashed horizontal line lies at 21.21 eV (584 Å).
7. Variation of β with photoelectron energy for $v' = 0$ of the $X^2\Sigma_g^+$ band. Experimental data points are indicated in relation to the calculated variation. The dashed line represents $\beta = 1.43$.
8. Variation of β with photoelectron energy for $v' = 1$ of the $X^2\Sigma_g^+$ band as in Fig. 7.
9. Variation of β with photoelectron energy for $v' = 2$ of the $X^2\Sigma_g^+$ band as in Fig. 7.

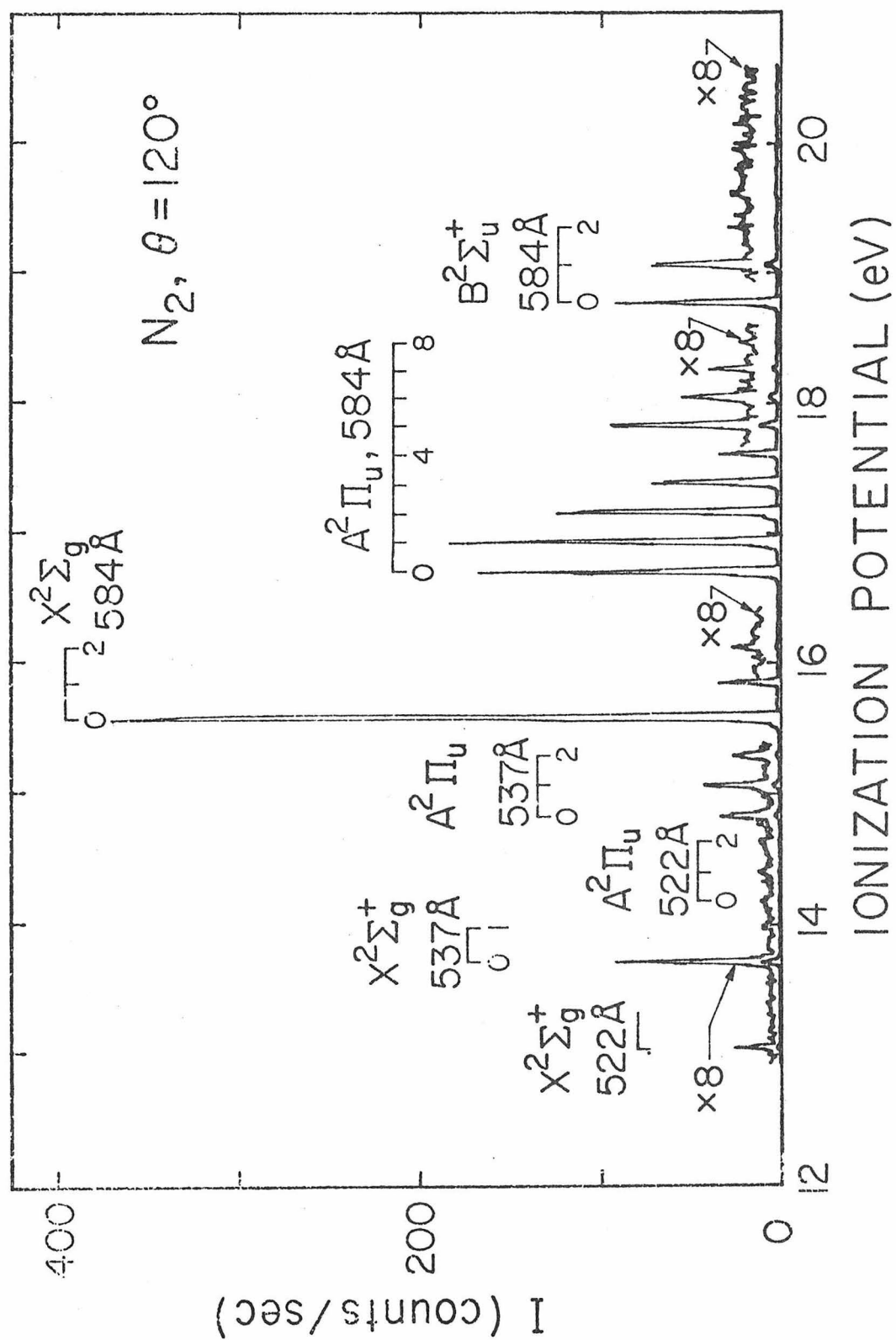


Figure 5.1-2

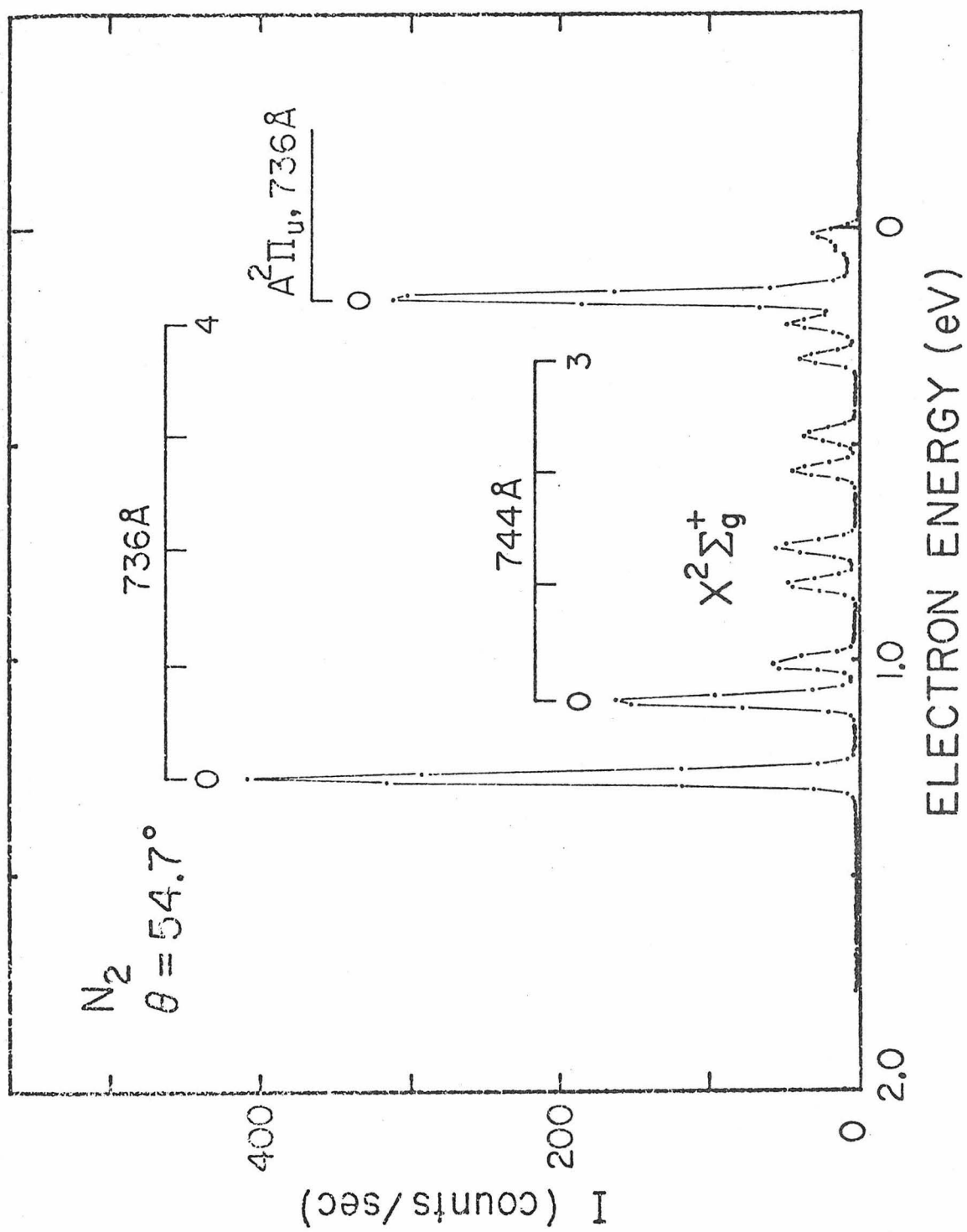


Figure 5.1-3

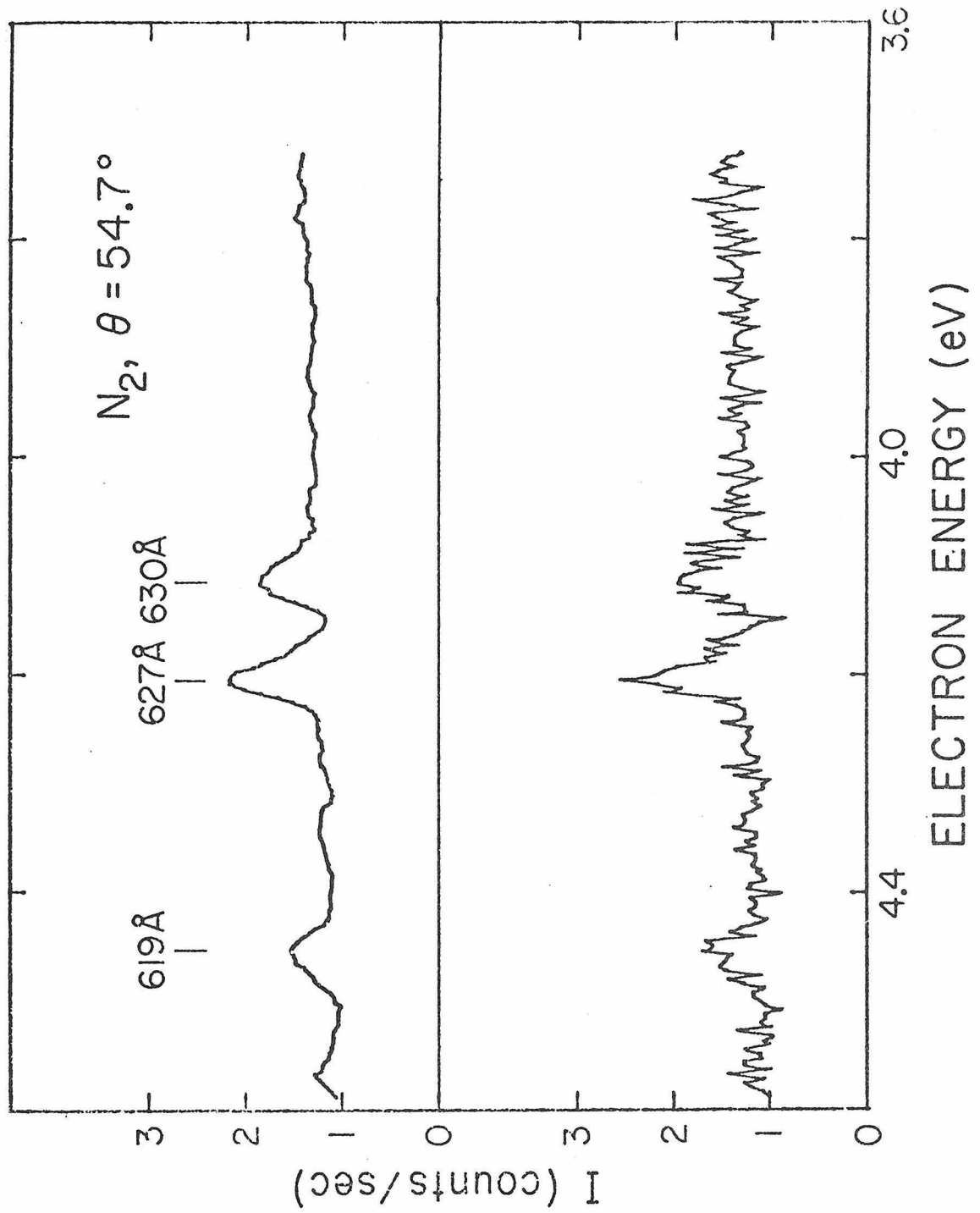


Figure 5.1-4.

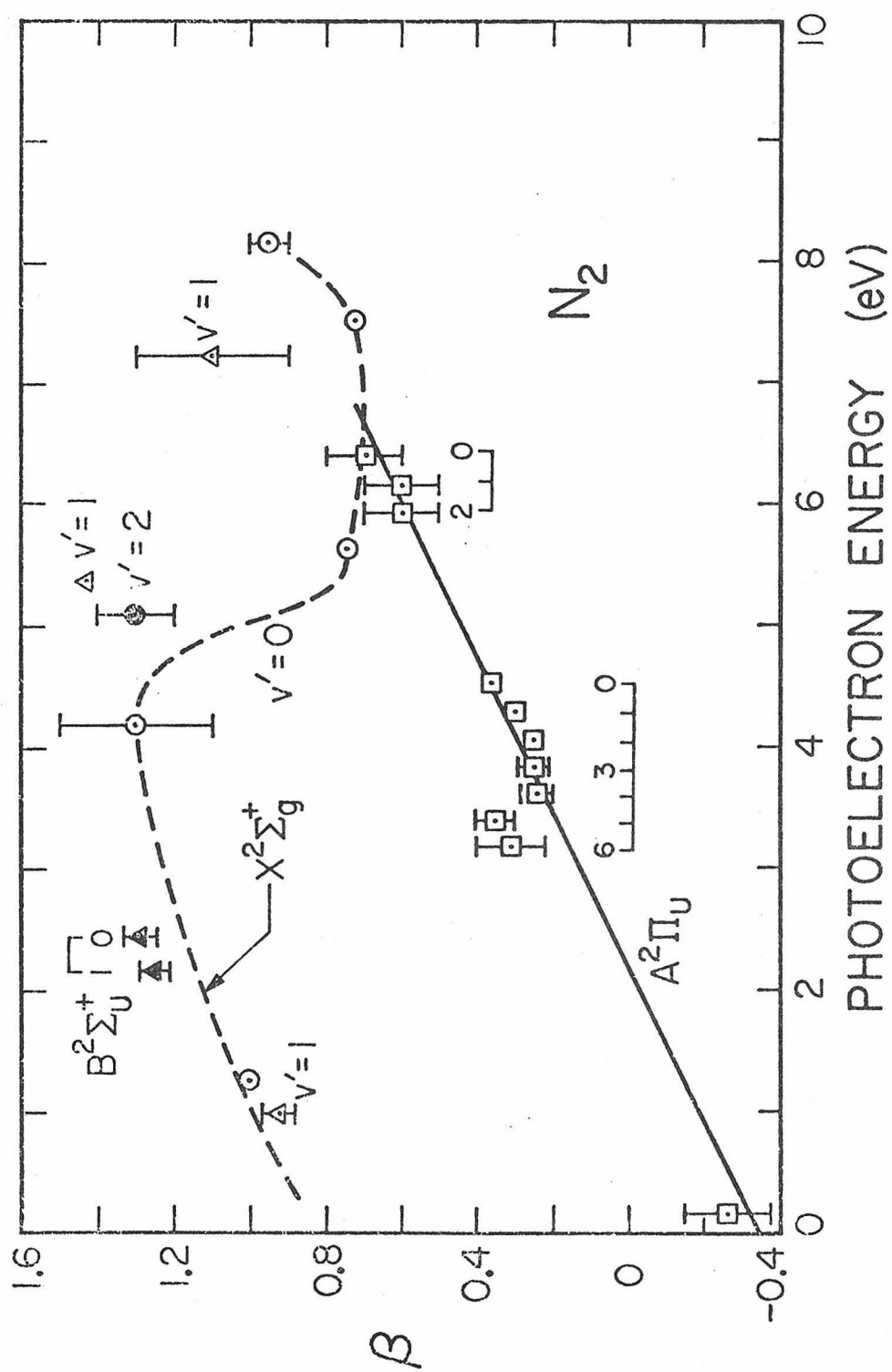


Figure 5.1-5

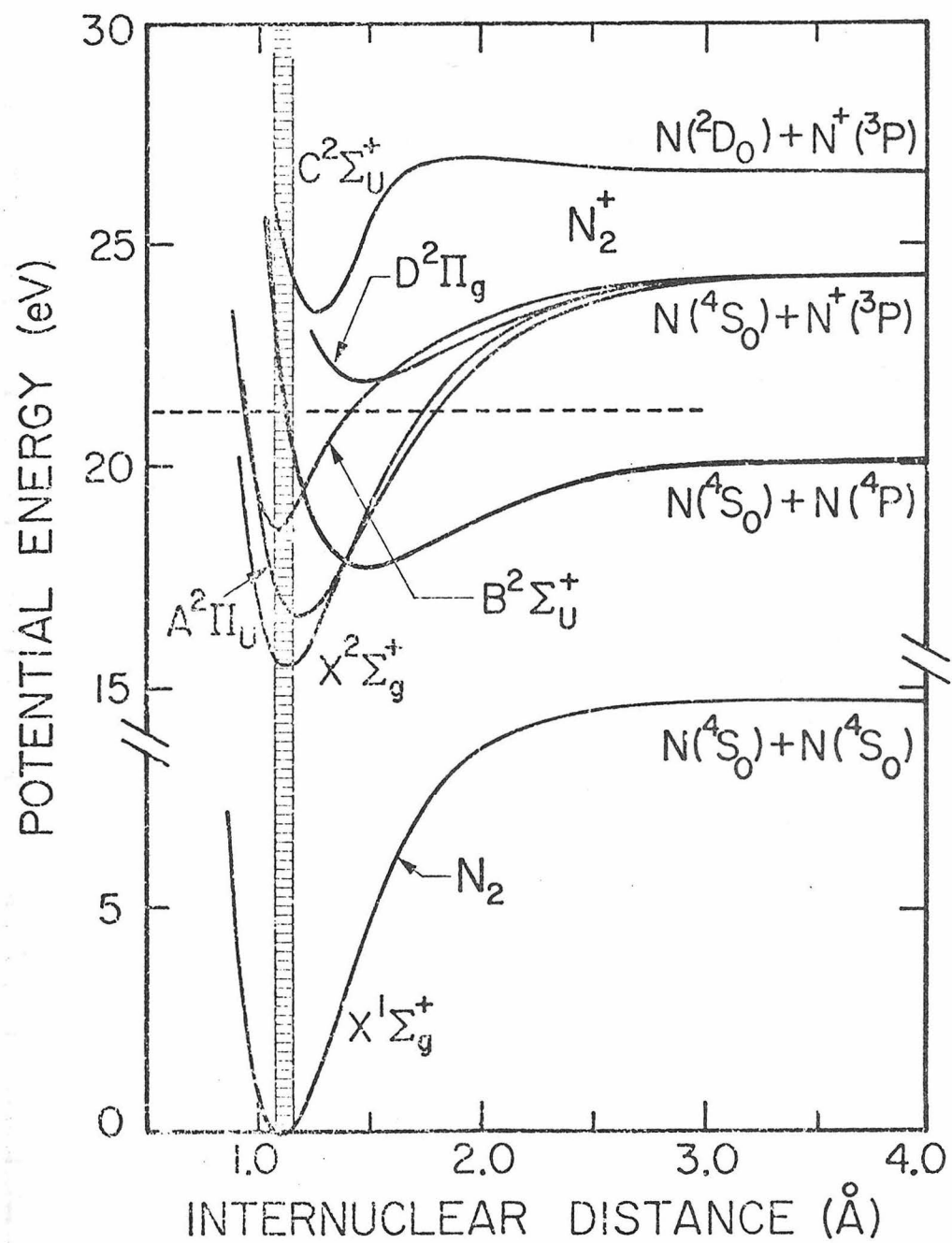


Figure 5.1-6

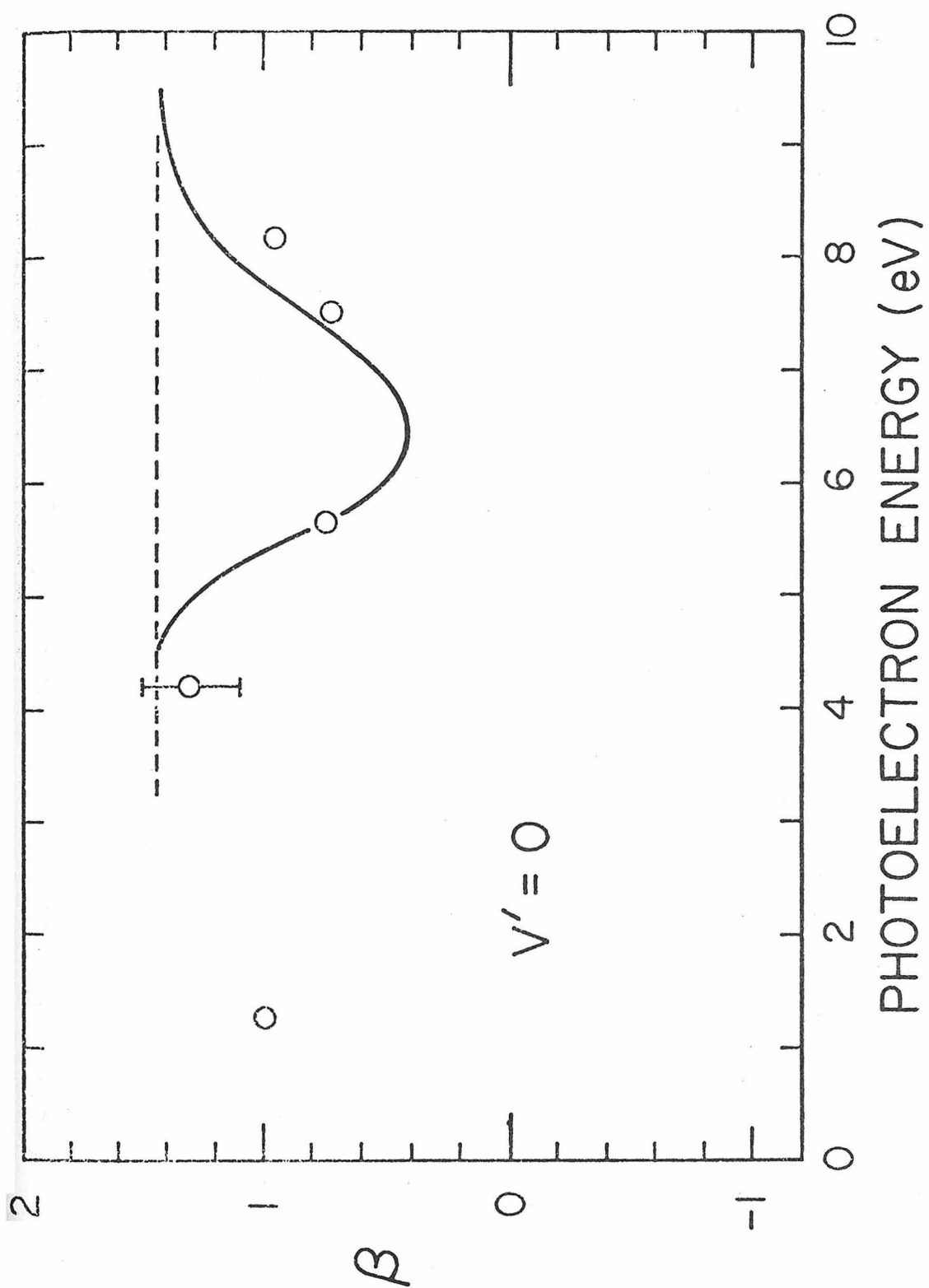


Figure 5.1-7

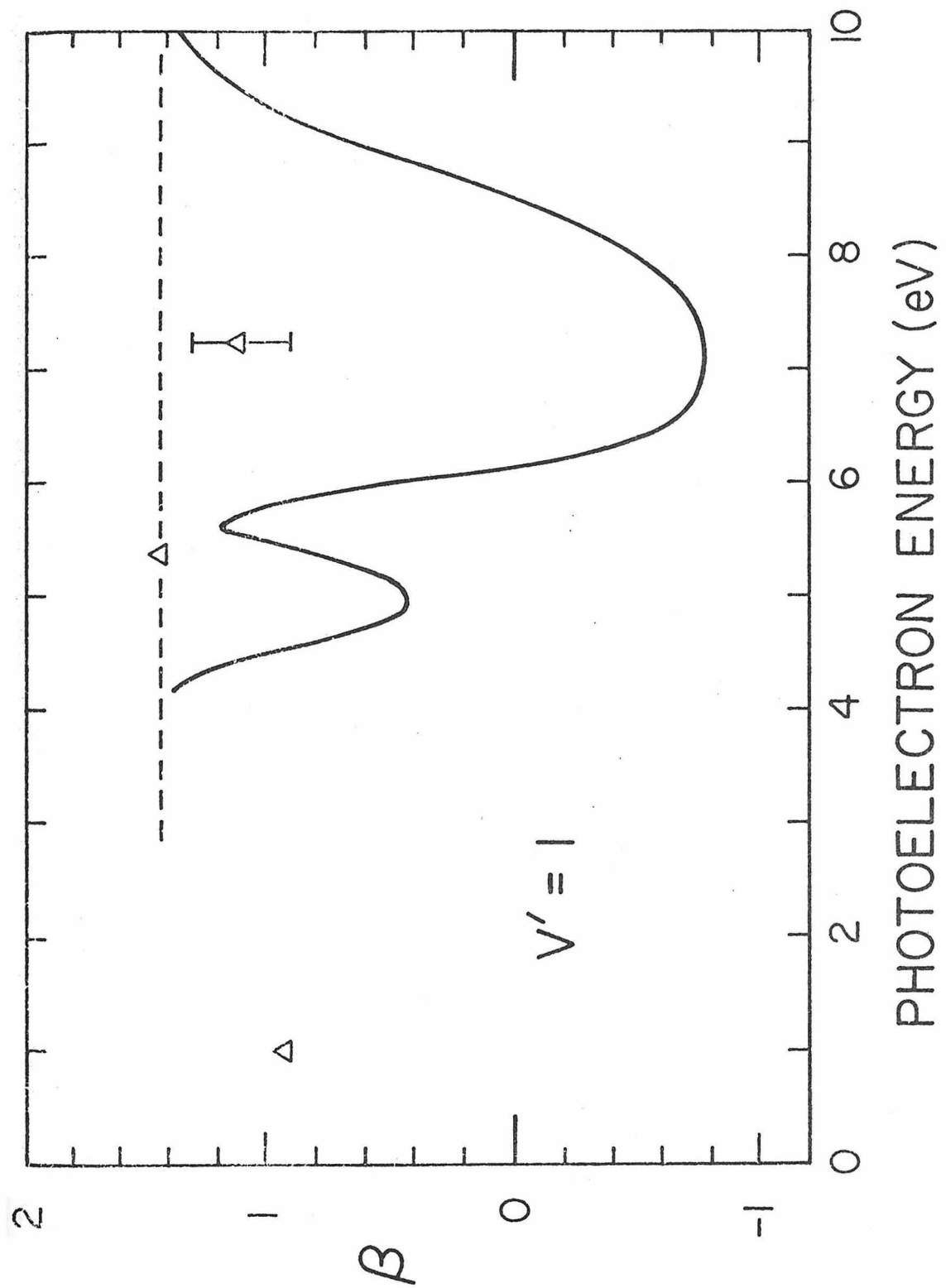


Figure 5.1-8

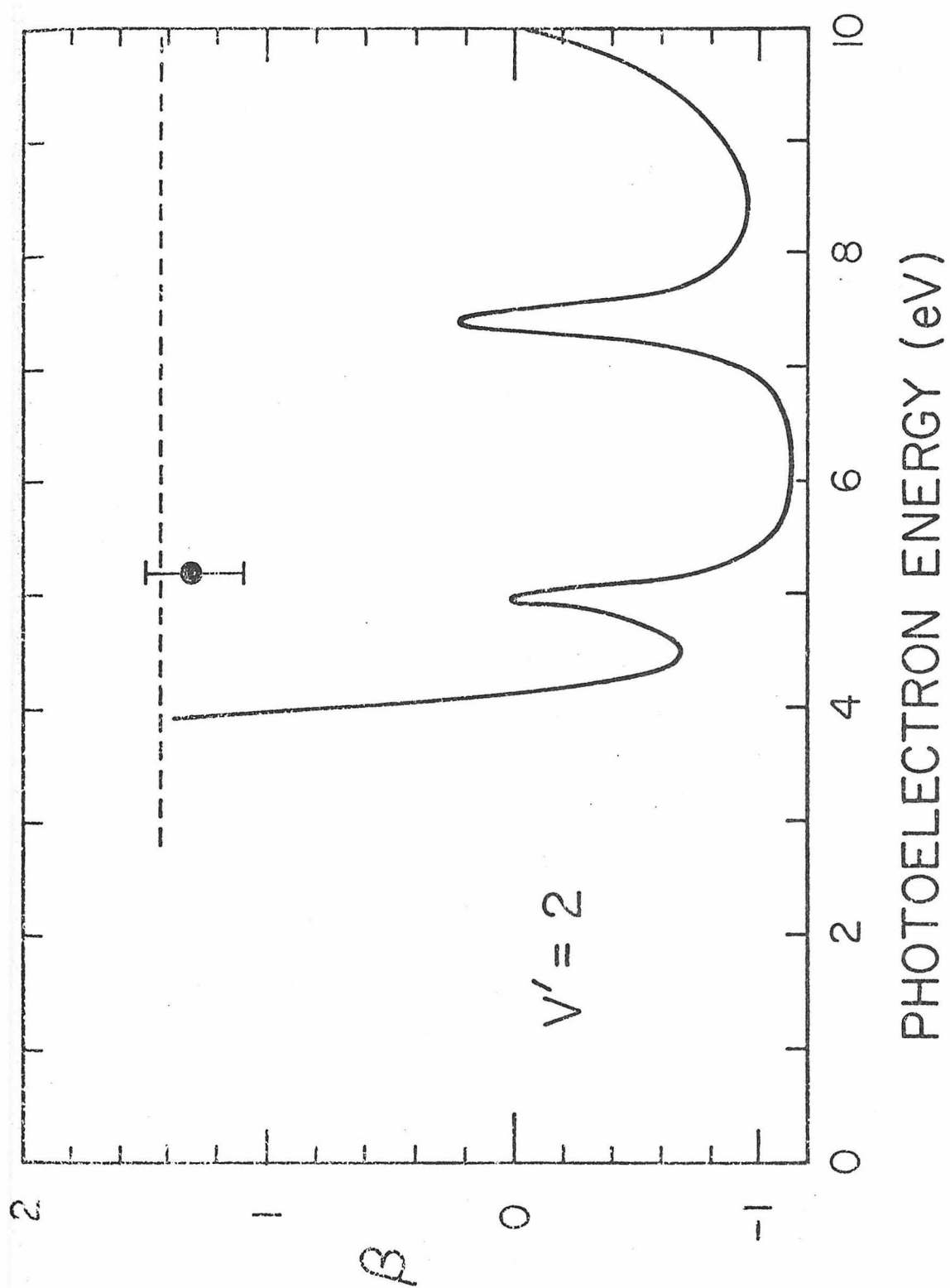


Figure 5.1-9

5.2 Carbon monoxide

We might expect photoionization experiments on carbon monoxide to reproduce many of the trends found with N_2 . That the two molecules are isoelectronic and have roughly the same reduced masses makes their 584 Å photoelectron spectra virtually identical. The CO spectrum in Fig. 5.2-1 may be compared to that of Fig. 2 in paper II. The CO spectrum using the principal NeI output lines at 736 Å and 744 Å shows the same enhancement of vibrational peaks for $v' = 2$ due to autoionization.¹ Nominally forbidden states, populated by a two-electron process, are seen in the HeII photoelectron spectrum of CO,²⁻⁴ just as in N_2 .^{2,3,5} Dissociative ionic states, both neutral and ionic, are found in the energy region 20-25 eV above ground neutral CO. Collision induced dissociation of CO^+ into $C^+ + O$ probably proceeds via a $D^2\Pi$ state,⁶ just as the process in N_2^+ proceeds by the $D^2\Pi_g$ state.⁶ Freund's group found dissociation of high Rydberg states of CO^7 in the 20-25 eV region, just as in N_2 ,⁸ and can attribute both to double excitation neutrals. The absorption spectra of both N_2 and CO are principally strong continua in the 20-25 eV region.^{9,10}

Earlier it had been noted that vibrational intensities in the $N_2^+ X^2\Sigma_g^+$ band did not agree with calculated Franck-Condon factors^{11,12} and spectra at other wavelengths.^{13,14} Angular distribution asymmetry parameters for $v' = 0$ and $v' = 1$ of this band are different.^{14,15} Vibrational intensities for $v' = 0,1$ peaks for the $X^2\Sigma^+$ band of CO are in better agreement with Franck-Condon factors for the transition.¹¹ However, the ratio of Franck-Condon factors lies slightly

outside of the error range of the vibrational peak intensities. Carlson has reported different β values for the $v' = 0$ and $v' = 1$ peaks.¹⁵ Preliminary results from this laboratory reproduce this trend, but our β values lie 0.15-0.35 above Carlson's.

We report here previously unresolved anomalous structure in the HeI photoelectron spectrum of CO in the 4.8-6.8 eV range of electron energy. This spectral region lies intermediate between the strong peaks of the $X^2\Sigma^+$ and $A^2\Pi$ states produced by 584 Å ionization. As seen in Fig. 5.2-2, some of the structure in this region corresponds to production of CO^+ in the $A^2\Pi$ state by the 537 Å line in the lamp. The other structure in this region forms a vibrational progression with roughly the same spacings as the $v' = 0-1$ spacing of the $X^2\Sigma^+$ band. The additional structure did not change in intensity when research grade gas was substituted for CP grade gas. Furthermore, the peak positions of the anomalous peaks did not correspond to that of any common diatomics or triatomics whose spectra are given by Turner.¹⁶ Thus, we attribute the additional anomalous structure completely to transitions in CO. Spectra produced by the 522 Å line have $\frac{1}{4}$ of the intensity of those produced by the 537 Å line. However, the additional structure has peak intensities comparable to or greater than the 537 Å spectrum. Thus we ascribe the structure to the 584 Å lamp emission line.

The Birge-Sponer plot¹⁷ of Fig. 5.2-3 suggests that the additional peaks are high vibrational members of the $X^2\Sigma^+$ progression. The slope of the variation of $E(V) - E(V-1)$ with V gives the

spectroscopic parameter $\omega_e x_e$, where:¹⁷

$$\frac{d[E(V) - E(V-1)]}{dV} = -2\omega_e x_e . \quad (5.13)$$

An approximate linear fit to the data points gives $\omega_e x_e = 14 \text{ cm}^{-1}$, comparable to Herzberg's value of 15.164 cm^{-1} .¹⁸

Wacks¹⁹ has calculated Franck-Condon factors for the $X^2\Sigma^+ \leftarrow X^1\Sigma^+$ transition using Morse vibrational wavefunctions. He calculates that Franck-Condon factors for vibrational peaks 1:2:3,... will vary by 100:0.3:0,... . Peaks assigned as $v' = 2, 3, \dots$ in Fig. 5.2-2 are much stronger than the intensities predicted by Franck-Condon factors for the direct ionization alone.

Enhancement of high vibrational levels in the 736/744 Å spectra of N_2 , CO, and O_2 ^{1, 14, 20} has previously indicated the presence of autoionization. By the theory of Smith²¹ the production rate of ion a in vibrational state v' can take the form:

$$P_{v'}^a \propto F_{iv'}^2 + K(\lambda, n_\lambda, \nu) F_{i\nu}^2 F_{\nu v'}^2 , \quad (5-14)$$

where autoionization through vibrational state ν of Rydberg member n_λ of progression λ accompanies direct ionization. In Eq. 5-14, the F's are Franck-Condon factors and K is a constant. The theory assumes that the narrow bandwidth excitation line of light source is tuned to a maximum in the absorption profile. Vibrational peak enhancement here in CO is distributed over a broad range of

vibrational peaks to high v' . Wacks¹⁹ has suggested that the dominant factor affecting the distribution of Franck-Condon factors for an excitation process is the change in r_e of the transition. When the change of r_e exceeds 10%, the transition probabilities become small to any particular vibrational level and spreads over many vibrational levels. Thus, we reason that the intervening Rydberg state has an equilibrium internuclear distance at least 10% different from those of the $X^2\Sigma^+$ state of CO^+ (1.115 \AA)¹⁸ and the $X^1\Sigma^+$ state of CO (1.128 \AA).¹⁸ Åsbrink, et al.⁴ have used the HeII photoelectron spectrum between 20-24 eV to make assignments in the high resolution absorption experiments of Codling and Potts.²² They assign the peak at 21.241 eV in the absorption spectrum as the $v = 10$, 3p member of a Rydberg series converging to the $C^2\Sigma^+$ state of CO^+ . This energy is very close to 21.217 eV (584 \AA). Thus, we attribute the anomalous structure in the 584 \AA spectrum to autoionization of a Rydberg state converging to the $C^2\Sigma^+$ ionic state.

Angular distribution studies over the peaks assigned as high vibrational members of the $X^2\Sigma^+$ progression will be helpful. If autoionization is populating the high CO^+ vibrational levels, β values for the corresponding peaks should be near zero, by analogy to the results of paper II and elsewhere.^{14, 23}

REFERENCES

1. P. Natalis, J. Delwiche, J. E. Collin, Chem. Phys. Lett. 13, 491 (1972); J. E. Collin, P. Natalis, Int. J. Mass Spectrom. Ion. Phys. 2, 231 (1969).
2. A. W. Potts, T. A. Williams, W. C. Price, Faraday Disc. Chem. Soc. 54, 104 (1972); A. W. Potts, T. A. Williams, J. Electron. Spectr. 3, 3 (1974).
3. M. Okuda, N. Jonathan, J. Electron Spectr. 3, 19 (1974).
4. L. Åsbrink, C. Fridh, E. Lindholm, K. Codling, Phys. Script. 10, 183 (1974).
5. L. Åsbrink, C. Fridh, Phys. Script. 9, 338 (1974).
6. T. F. Moran, F. C. Petty, A. F. Hedrick, J. Chem. Phys. 51, 2112 (1969).
7. K. C. Smyth, J. A. Schiavone, R. S. Freund, J. Chem. Phys. 60, 1358 (1974).
8. K. C. Smyth, J. A. Schiavone, R. S. Freund, J. Chem. Phys. 59, 5225 (1973).
9. L. C. Lee, R. W. Carlson, D. L. Judge, M. Ogawa, J. Quant. Spectrosc. Radiat. Transf. 13, 1023 (1973).
10. M. Sasanuma, E. Ishiguro, Y. Morioka, M. Nakamura, in Y. Nakai (editor) Conference Digest of the Third International Conference on Vacuum Ultraviolet Radiation Physics, Tokyo, 1971, p. 1pA2-3.
11. J. L. Gardner, J. A. R. Samson, J. Chem. Phys. 60, 3711 (1974).

12. T. H. Lee, J. W. Rabalais, J. Chem. Phys. 61, 2747 (1974).
13. A. Katrib, T. P. Debies, R. J. Colton, T. H. Lee, J. W. Rabalais, Chem. Phys. Lett. 22, 196 (1973).
14. T. A. Carlson, Chem. Phys. Lett. 9, 23 (1971).
15. T. A. Carlson, A. E. Jonas, J. Chem. Phys. 55, 4913 (1971).
16. D. W. Turner, C. Baker, A. D. Baker, C. R. Brundle, Molecular Photoelectron Spectroscopy (Wiley-Interscience, London, 1970).
17. H. B. Dunford, Elements of Diatomic Molecular Spectra (Addison-Wesley, Reading, Mass., 1968) p. 67.
18. G. Herzberg, Molecular Spectra and Molecular Structure I. Spectra of Diatomic Molecules (Van Nostrand-Reinhold, New York, 1950) p. 438.
19. M. E. Wacks, J. Chem. Phys. 41, 930 (1964).
20. J. A. Kinsinger, J. W. Taylor, Int. J. Mass Spectrom. Ion Phys. 11, 461 (1973).
21. A. L. Smith, J. Quant. Spectrosc. Radiat. Transf. 10, 1129 (1970); Phil. Trans. Roy. Soc. Lond. A268, 169 (1970).
22. K. Codling, A. W. Potts, J. Phys. B 7, 163 (1974).
23. R. Morgenstern, A. Niehaus, M. W. Ruf, in L. Branscomb (editor) Electronic and Atomic Collisions (North Holland, Amsterdam, 1971) p. 167.

Figure Captions

Fig. 5.2-1 Spectrum of carbon monoxide at a detector angle of 54.7° incorporating 584, 537, and 522 Å spectra. Spectrum was taken over 510 channels at a dwell time of 50 seconds/channel. The ionization potential scale is given as if the lamp output were only 584 Å.

Fig. 5.2-2 Spectrum of the ionization potential region lying between prominent peaks of the $X^2\Sigma^+$ and $A^2\Pi$ bands of the 584 Å spectrum of carbon monoxide. Spectrum was taken over 376 channels at a dwell time of 35 seconds/channel.

Fig. 5.2-3 Birge-Sponer plot of the energy spacings of anomalous structure in the HeI spectrum of CO.

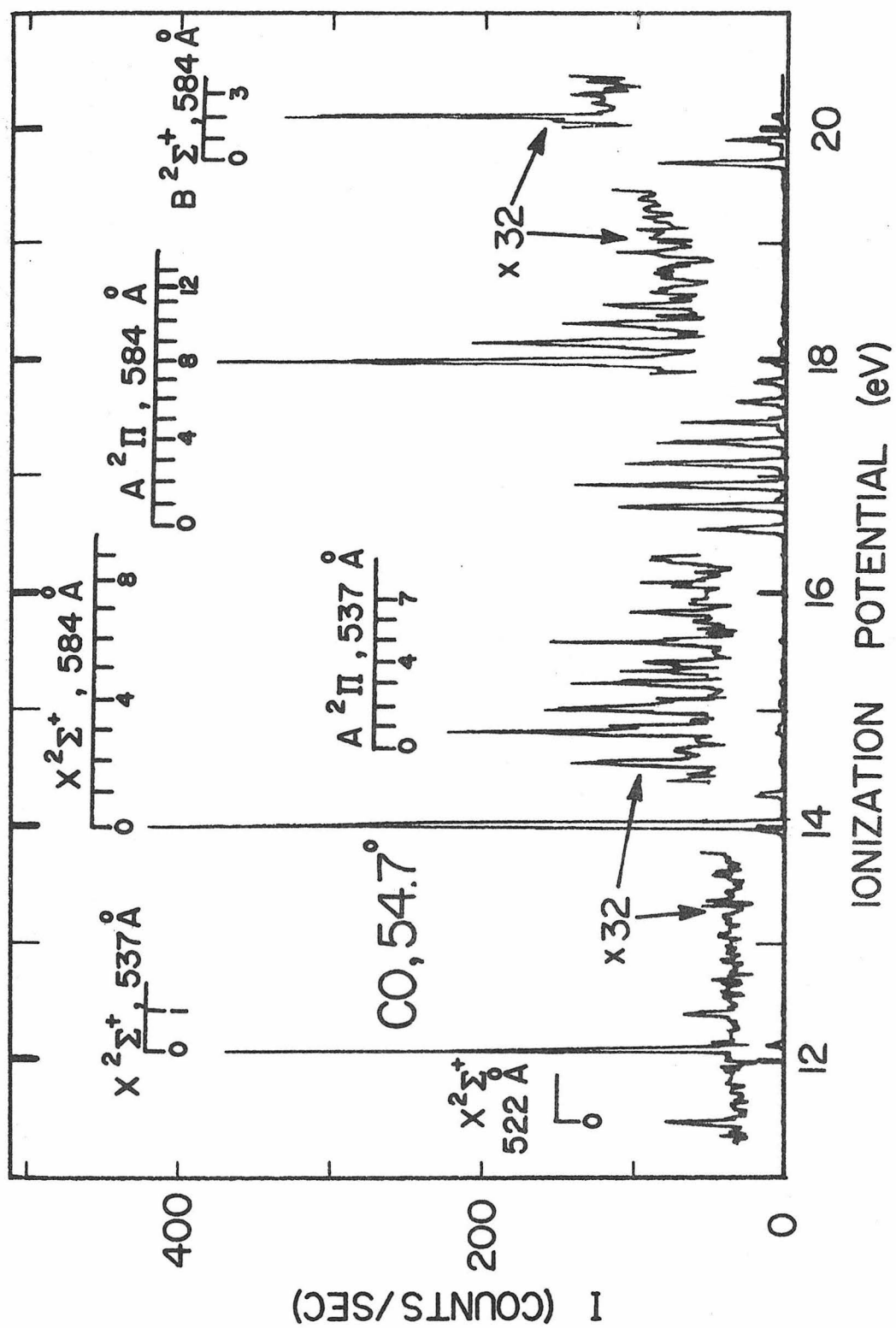


Figure 5.2-1

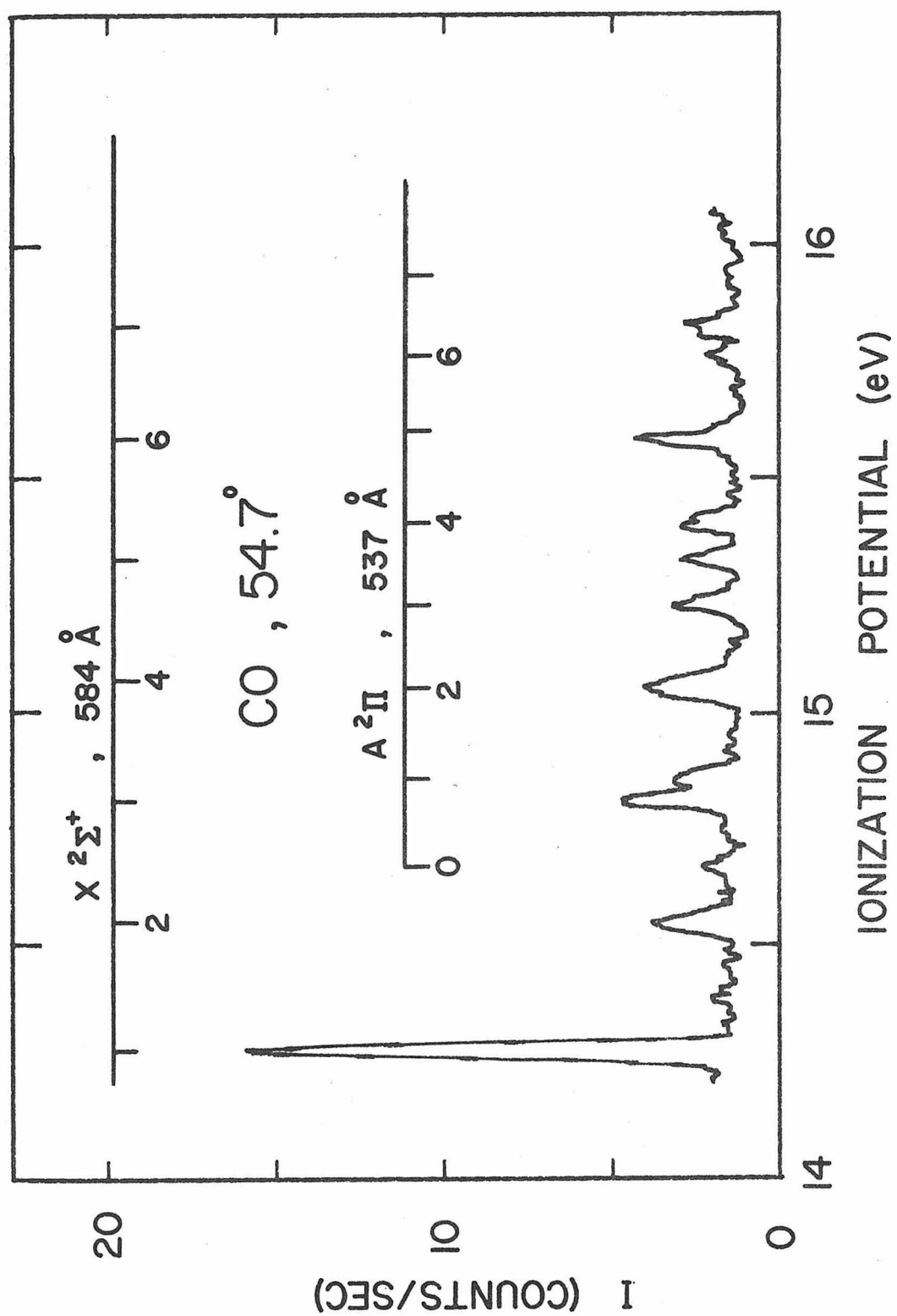


Figure 5.2-2

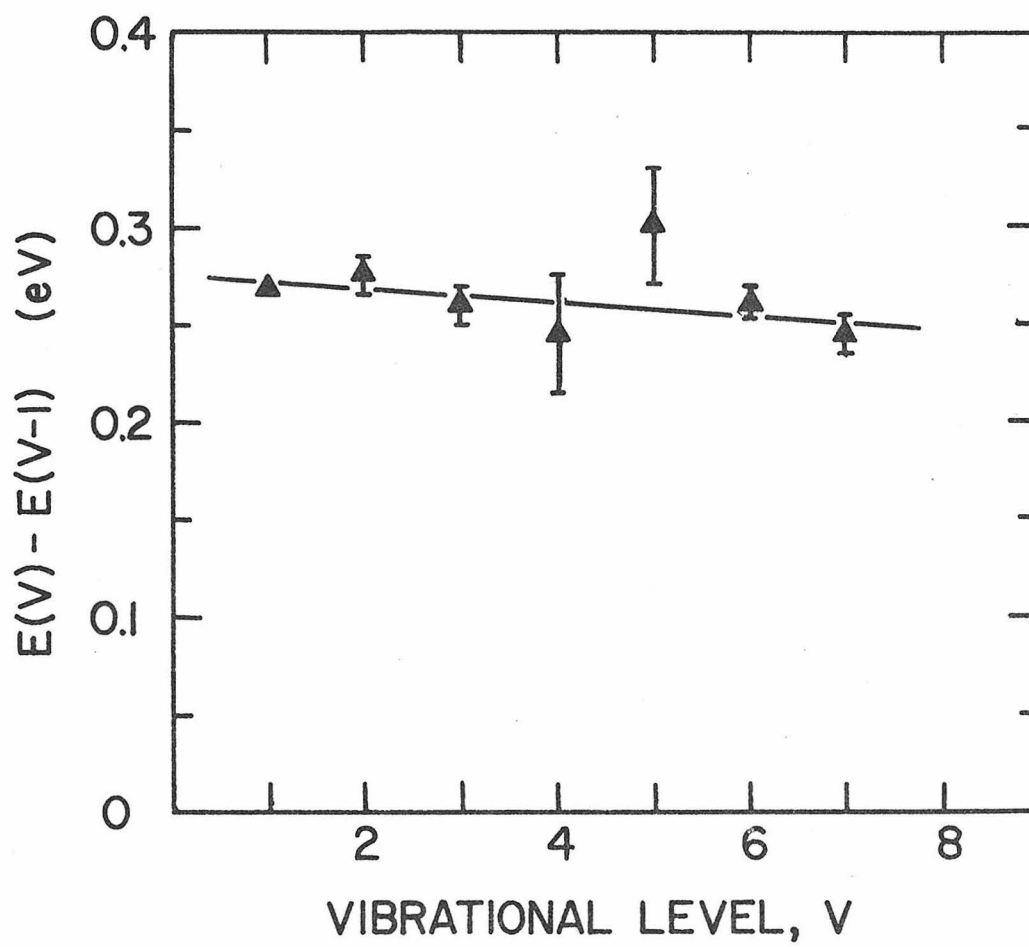


Figure 5.2-3

CHAPTER 6 - RESULTS AND DISCUSSION: POLYATOMIC MOLECULES

$$\left| E_{ij} - \lambda \delta_{ij} \right| = 0$$

6.1 Paper III - Variable Angle Photoelectron

Spectroscopy of Ethylene, Isobutylene, 2-Methyl,
2-butene, and 2,3-Dimethyl,2-butene.

Variable Angle Photoelectron Spectroscopy of Ethylene

Isobutylene, 2-Methyl,2-butene, and 2,3-Dimethyl,2-butene

Using a HeI line source lamp, photoelectron angular distributions were measured for the series of olefins: ethylene, isobutylene, 2-methyl,2-butene, and 2,3-dimethyl,2-butene. The variation of the asymmetry parameter β with electron energy was inferred by a comparison of the four structurally similar molecules. In the $\sigma 2p$ orbital ionization region of the spectrum, we find a similar variation of β with electron energy over bands corresponding to widely varying orbital symmetries. In the π orbital ionization region of the spectrum, β increases with increasing electron energy, taken from the variation of β across the vibrational envelopes. Accompanying the drop in β for π ionization with increasing methyl substitution is an anomalous drop in β at the high ionization potential end of the $\sigma 2p$ region which may indicate the presence of σ/π orbital mixing.

INTRODUCTION

The assignment of structure observed in the vacuum ultraviolet photoelectron spectra of polyatomic molecules is complicated by the density of ionic electronic states in the ionization potential range 8-20 eV. In the orbital approximation, each band in a molecular photoelectron spectrum corresponds to ionization from a particular molecular orbital.

Several useful experimental techniques have been presented for the explication of structure in photoelectron spectra. These include analysis of vibrational fine structure,^{1,2} comparison of photoelectron spectra of related compounds,³⁻⁵ and the observation of variation of band intensities with photon energy.⁶⁻⁸ Analysis of vibrational structure is normally only possible for simple molecules. Franck-Condon factors linking the ground neutral states to many different normal modes of ionic states are frequently large. Commonly studied series of related molecules have varying degrees of substitution of bulky alkyl groups or highly electronegative fluorines. Substituent effects must be interpreted with caution,⁵ since it is easy for substituents to grossly perturb geometries and electronic densities. The study of band intensity variation with photon energy has firm theoretical grounds only in the energy range well above 100 eV,⁶ though it has been applied for comparisons of He I and He II spectra.^{7,8}

In 1968, Hall and Siegel⁹ found that ejected electron angular distributions in the laser photodetachment of H^- and O^- were very much different. They attributed this to the extensive s-character in the H^- electrons and extensive p-character in the outer shell O^- electrons.

Guided by the Hall and Siegel findings, we hope that similar relationships might be found for photoelectron angular distributions of neutral polyatomic molecules. In the beginning, it is necessary to formulate empirical rules for the variation of photoelectron angular distributions with the type of electron photoejected and with photon wavelength, where the electronic structure is known beforehand. Then, if a sufficient number of empirical rules can be found, we can explicate structure in photoelectron spectra where ambiguities have arisen. At the same time, we can test the various theoretical models which too frequently have made conflicting assignments of the energy ordering of ionic excited states.

Carlson's group^{10,11} has compared angular distributions of molecular photoelectrons arising from a given molecular orbital to values of the most probable angular momentum in a single center expansion of that orbital. As Rabalais¹² has pointed out, this correlation can be made correctly for only high energy ionizations. To date, most experimental angular distribution studies of molecules have focused on the ionization of valence electrons within 15 eV of threshold.

We include in this study experimental measurements of photoelectron angular distributions of isobutylene, 2-methyl,2-butene, and 2,3-dimethyl,2-butene as an extension of earlier work on ethylene.¹³ Ethylene photoelectron angular distributions were remeasured for comparison purposes.

EXPERIMENTAL

Photoelectron angular distributions were measured with a windowless helium glow discharge lamp (majority emission at 584 Å) and a rotatable electron energy analyzer. The rotatable electron energy analyzer consists of a 6.800 cm mean radius hemispherical electrostatic analyzer, electrostatic lenses, and a Spiraltron¹⁴ detector. The entire electron energy analyzer is mounted on a worm gear which is rotated about a horizontal axis. The analyzer is attached to an enclosed sample chamber which is normally filled with 3-5 millitorr of the sample gas under study. Spectra of photoelectron intensity versus electron energy are generated using a minicomputer-based data acquisition system built around a Digital Equipment Corporation PDP8/e.¹⁵ A block diagram of the experimental apparatus is given in Fig. 1.

Sample materials were obtained from the following sources and at the minimum purities indicated in parentheses: ethylene (J. T. Baker, CP 99.5%), isobutylene (Matheson, CP 99%), 2-methyl,2-butene (Aldrich, 99+%), and 2,3-dimethyl,2-butene (Aldrich, Gold Label 99+%). Full spectra of these compounds were taken at a detector angle of 54.7° with respect to the light axis and are reproduced in Figs. 2-5. The spectra of ethylene¹⁶ and isobutylene¹⁷ are identical in all respects to published high resolution spectra.

Liquid samples were degassed by several freeze-pump-thaw

cycles before use. Gas samples were distilled into a liquid nitrogen immersed cold finger from the gas cylinder and were further degassed by several freeze-pump-thaw cycles. The glass manifold which constituted the inlet system was baked in a glassblower's annealing oven between successive samples in order to avoid cross contamination.

Spectra were taken at an analyzing energy of 1.5 eV and corresponding resolution of 30-35 meV FWHM, as measured at the argon $^2P_{3/2}$ peak. Spectra were energy calibrated with the argon $^2P_{3/2}$ line at 15.759 eV.¹ The linearity of the energy scale was checked with a spectrum taken of a 1/3 : 1/3 : 1/3 mixture of ethylene, xenon, and argon.

Total data acquisition times averaged 4 days. This allowed for the high pressure ionization gauge to become acclimated to each sample gas, a number of 9-angle angular distributions covering detector angles of 40-120° in increments of 10°, and a spectrum of background at each of the 9 angles. Each spectrum in the angular distribution consists of intensity measurements over 80-160 channels and scanning a range of ionization potentials of 0.5-1.5 eV. During the period of 4 days, the lamp flux, as measured at a tungsten photocathode mounted in the sample chamber, did not vary by more than 5%. Over shorter periods of 6-10 hours during which an angular distribution was run, the lamp flux did not vary typically by more than 1%. Contact potential shifts of sharp features did not change by more than 0.01 eV over 6-10 hours.

Spectral intensities at each of 9 angles and at each channel of the spectrum were then fitted to the theoretical expression:¹⁸

$$I(\theta) \propto 1 - \frac{\beta}{4} (3 \cos^2 \theta - 1) , \quad (1)$$

where θ is the detector angle with respect to the (unpolarized) light axis, $I(\theta)$ is the photoelectron intensity corrected for the volume of intersection of lamp and detector view cones at each θ and compensated for the linear variation of counting rate with sample pressure, and β is the fitted asymmetry parameter.

Photoelectron intensity is corrected for an energy parameterized background which is different at each detector angle. Photoelectron angular distributions were measured over at least a 10 eV range starting below the first adiabatic ionization potential. Intensities at electron energies corresponding to ionization potentials above 19 eV were in general too low for the organic molecules listed above for adequate signal to background ratios.

RESULTS

Ethylene

The low resolution photoelectron spectrum of ethylene first appeared in 1964.¹⁹ Since that time, several groups^{16,20} have analyzed the vibrational fine structure in the high resolution spectrum of ethylene. The 584 Å spectrum consists of five bands of which the four at lowest ionization potential are reproduced in Fig. 2. The first band at a vertical ionization potential of 10.51 eV, as is typical of unsaturated hydrocarbons,²¹ corresponds to the loss of a carbon-carbon bonding π electron. Features at vertical ionization potentials of 12.82, 14.69, and 15.90 eV correspond to the loss of σ orbital electrons in the plane of the molecule. All three bands correspond to the loss of electrons which are at least partially CH bonding. The band which appears near 19 eV is extremely weak¹⁶ and we expected poor signal to background ratios. As a result, we did not include results for this band in the discussion below.

As we¹³ and the group of T. A. Carlson^{11,22} have previously observed, the angular distributions corresponding to the removal of the ethylene π electrons are noticeably different from those corresponding to the removal of the σ electrons. Table I contains values of β measured by both groups. The β value corresponding to the removal of the π electron is large, 1.25 ± 0.05 . The measured β values in the σ region are very much lower and lie in the range 0.30-0.65.

Isobutylene

The high resolution photoelectron spectrum of isobutylene has been published previously only by Kimura, et al.¹⁷ The spectrum consists of 5 distinct bands and one broad band and is shown in Fig. 3. The only bands which display vibrational fine structure are those at vertical ionization potentials of 9.45 and 17.27 eV. The former corresponds to the loss of a π electron and has a CC stretching frequency of $1400 \pm 50 \text{ cm}^{-1}$. The latter corresponds to the loss of an electron from an orbital with a large component of 2s character and shows a CH_n deformation frequency²³ of $1350 \pm 50 \text{ cm}^{-1}$.

The number of ionization bands in the full 584 Å spectra for methylated ethylenes is $2C+1$, where C is the number of carbon atoms. This assumes that we should see one photoelectron band per orbital and that only one carbon 2s band is present. In the region between ionization potentials of 11-17 eV must fall 7 ionizations of orbitals with varying degrees of CH and CC bonding character.

We list β values at selected vertical ionization potentials of isobutylene given by Kimura, et al.¹⁷ and quoted in Table II. The β value for the π ionization is noticeably higher than that corresponding to the loss of the σ electron at 11.81 eV (vertical). If β values measured at many of the σ vertical ionization potentials listed by Kimura et al.,¹⁷ (except carbon 2s), are plotted against the corresponding electron energy (in Fig. 6), the result is a straight line, with one exception. The β corresponding to the shoulder at 15.7 eV is slightly low.

2-Methyl, 2-butene

The high resolution photoelectron spectrum of 2-methyl, 2-butene is published in Fig. 4 for the first time. Adiabatic and vertical ionization potentials derived from low resolution spectra appeared previously in a publication by Frost and Sandhu.²⁴ The only distinct vibrational fine structure occurs at the π ionization at 8.86 eV (vertical) and corresponds to the symmetric CC stretch ($1450 \pm 50 \text{ cm}^{-1}$). The spectrum contains one recognizable feature at 16.83 eV (vertical), corresponding to the removal of an electron with extensive carbon 2s character. We expect that 9 ionizations of orbitals with varying degrees of CH and CC bonding character must fall in the spectral range between ionization potentials of 10-16.6 eV. The bands at 11.35, 12.55, and 15.60 eV (vertical) may represent one ionic state each by band intensity arguments. Thus 6 ionizations probably lie in the generally structureless region between 12.7-15.3 eV.

We list β values at selected vertical ionization potentials of 2-methyl, 2-butene in Table III. The β value for the π ionization is again higher than that measured at 11.35 eV (vertical) corresponding to the lowest lying σ ionization. Experimental β values measured at peaks and shoulders of the σ region between 10-16.6 eV vertical IP versus the corresponding electron energy are plotted in Fig. 7. The result is a straight line, and again with one exception. The β corresponding to the peak at 15.60 eV IP is anomalously low.

2,3-Dimethyl, 2-butene

The high resolution photoelectron spectrum of 2,3-dimethyl, 2-butene is shown in Fig. 5 for the first time, although again, adiabatic and vertical ionization potentials derived from low resolution spectra had appeared previously.²⁴ The only distinct vibrational fine structure occurs at the π ionization at 8.44 eV IP and corresponds to the symmetric CC stretch ($1430 \pm 50 \text{ cm}^{-1}$). The spectrum contains one well separated feature at 10.96 eV IP, corresponding to the removal of a σ electron of undetermined CH and CC character since vibrational fine structure is not resolved. In addition, a shoulder at 16.4 eV IP probably corresponds to the removal of an electron of extensive carbon 2s character, on the basis of comparisons to other methylated ethylenes. The other component of this high ionization potential band, with a vertical ionization potential of 15.85 eV, probably results from the ionization of a single electron of undetermined CH and CC character. Since we must account for ionizations of 13 electron orbitals between ionization potentials of 8-17 eV, the broad, generally featureless region between 11.7-15.5 eV must contain ionizations of 9 electrons.

We list β values at selected recognizable peaks and shoulders of 2,3-dimethyl, 2-butene in Table IV. The β value for the π ionization is now only slightly higher than that measured at the vertical ionization potential of the lowest lying σ ionization. A plot of β values at selected peaks and shoulders of the σ region between 10-16 eV versus electron energy appears in Fig. 8. We find a

straight line with one exception; the β corresponding to the peak at 15.85 eV ionization potential is anomalously low.

DISCUSSION

Examination of Figs. 2-5 reveals that the variation of β across non-overlapping bands is slight, but in many cases, measurably non-zero. This is consistent with the Born-Oppenheimer approximation²⁵ which states that electronic wave functions should vary relatively slowly over the range of equilibrium interatomic coordinates. Relative vibrational peak intensities are then determined primarily by Franck-Condon factors. Born-Oppenheimer breakdown should generally be a small effect for large molecules in photoelectron spectroscopy. Consideration of Born-Oppenheimer breakdown yields a minor correction to vibrational peak intensities due to variation of electronic transition moments with vibrational level.²⁶ By the Born-Oppenheimer approximation, the angular distribution parameter β is determined solely by the electronic wavefunction. The energy of the ejected photoelectron is lower if some of the original photon energy has gone into vibrational excitation of the ion. We then can study the variation of β with electron energy for a given photoelectron band by examining the variation of β across the vibrational fine structure of that band.

We then have the capability of measuring the energy variation of β in the region of the molecular vertical ionization potential if apparatus sensitivity can allow measurement of variation of β as a function of vibrational level. This was accomplished with the present apparatus on previous studies of the $N_2^+ A^2\Pi_u$ state.²⁷

The use of the variation of β across a given vibrational band to infer the variation of β with electron energy is not valid if autoionization occurs. As seen previously in spectra of N_2 and O_2 at $\lambda = 736 \text{ \AA}$, autoionization grossly distorts Franck-Condon envelopes.²⁸ If the lifetime of an autoionizing state exceeds one molecular rotation, preferred directions in space are averaged out and β tends to 0, as Carlson has discussed.²⁹ Measured β values at photoelectron peaks which are enhanced due to autoionization thus are closer to 0 than values measured in the absence of autoionization.

The vibrational envelopes of the first π band of isobutylene, 2-methyl, 2-butene, and 2,3-dimethyl, 2-butene bear strong resemblance to each other and to those of isomeric butenes studied by Kimura et al.¹⁷ and White et al.²² All show a minor decrease in β with increasing vibrational excitation in the ion. Thus, all of the bands are affected by autoionization or none of the bands is so affected. Selection rules for autoionization are based solely on symmetries and spin multiplicities of the states involved.³⁰ The variety of molecular symmetries of the ground neutral and ground ion in the collection of methylated ethylenes suggests that if one band were autoionized, at least one of the set would not be autoionized. Thus we conclude that vibrational structure in the lowest π bands is not enhanced due to autoionization. The dependence of β on vibrational excitation of these ions should accurately reflect variations in β with electronic energy. Autoionization need not be

considered for most of the σ structure, since β generally varies smoothly in this energy range.

Vibrational Franck-Condon envelopes are typically narrow. Infrequently does a vibrational envelope extend over more than a 1 to 1.5 eV range of electron energy. This gives us a limited chance to extrapolate variations of β with electron energy too far.

The variation of β over the range of photoelectron structure from 11-17 eV labelled $\sigma 2p^{22}$ is remarkably uniform. White, et al.²² noticed the gradual rise in spectra of ethylene, propylene, and several of the isomeric butenes. We confirm the observation for the three members of the methyl-substituted ethylenes that the previous workers omitted. The gradual rise is linear, as was seen in Figs. 6-8, except for an unexplained anomaly near an electron energy of 5.5 eV.

In the $\sigma 2p$ region, taking isobutylene as a typical case, we expect an assortment of A_1 , A_2 , and B_2 excited ionic states. In the orbital approximation, each band corresponds to the photoejection of an electron from a σ molecular orbital. The molecular orbitals are related only in their CH and CC σ bonding character. The relative proportions of CH and CC σ bonding are unspecified for the moment. Measured values of β for all of the a_1 orbital ionizations taken as a group are expected to vary similarly with electron energy. Similarly, measured values of β for all of the b_2 ionizations taken as a group are expected to vary similarly with electron energy. This is an

assumption, but is expected to be a good one. Yet all of the β values for $\sigma 2p$ ionizations, to the sensitivity limits of our apparatus, lie along a single line. For the $\sigma 2p$ region, we conclude that, for isobutylene, as for the rest of the methylated ethylenes, the variation of β over bands corresponding to differing ionic symmetries, $\beta_{\sigma p}$, reflects the variation of β for any of the bands $\beta(E)$.

Kinsinger and Taylor³¹ measured photoelectron angular distributions for benzene at the NeI and HeI resonance lines. They found that for orbitals of the same type (π, r, t, s classification of Jonsson and Lindholm),³² the corresponding β values can be connected by a smooth curve. Significantly, orbitals within each group were of different group theoretical designations. As an example, the π orbitals included those of e_{2g} and a_{2u} symmetry.

The present work and that of White et al.²² was done on acyclic hydrocarbons of lower symmetry than D_{6h} . Nevertheless, assuming only that β for all of the σ ionizations yielding ions of the same group theoretical designation lie along a single $\beta(E)$ curve yields the same conclusion. Within a given orbital type, $\sigma 2p$ in the case of planar olefins and (π, r, s, t) of benzene, the electron energy variation of β is independent of group theoretical designations of the molecular orbital ejected.

The variation of $\beta_{\sigma p}$ versus electron energy for the entire series of methyl substituted ethylenes is plotted in Fig. 9. We include results from the study of propylene and cis- and trans-2-butene of

White et al.²² for completeness. Significantly, all lines are parallel and lie within ± 0.1 units of β of each other. The lines thus lie almost within experimental error of each other. This result is striking in view of the diverse collection of molecular symmetry groups (C_{2v} , C_{2h} , C_s , D_{2h}) that is represented. These results suggest that the variation of $\beta_{\sigma p}$ is a general phenomenon and is very much symmetry independent. The linear variation of $\beta_{\sigma p}$ is likely due only to the planar character of the σ electrons which are photoejected. The similarities observed in the electron energy variation of $\beta_{\sigma p}$ suggest that curves for β for other families of ionization, such as carbon 2s or π , should show some clear internal consistencies as well.

The carbon 2s assignment of the band in the HeI photoelectron spectra at highest ionization potential is based on similarities in peak positions for families of hydrocarbons.^{33,34} As seen in Figs. 3-5, the carbon 2s peak at lowest ionization potential shifts to lower ionization potential with increasing molecular size. Thus HeI spectra usually have only one carbon 2s band at moderate intensity.

We can thus extract the variation of β with electron energy only from the vibrational energy dependence of β , providing the bands are not enhanced by autoionization. For the series of molecules studied, this is difficult because poor signal to background ratios yield large error bars and we notice only the absence of gross trends. Results of the benzene study mentioned earlier³¹ showed similar results for the electron energy dependence of s-type bands. Reported values of

β of 0.5 for the $2b_{1u}$ band at 25.5 eV IP and 0.70 for the $2e_{2g}$ band at 18.9 eV IP indicate a slight energy dependence.

Upon methyl substitution, $\beta_{\sigma S}$ is roughly independent of the size of the molecule, in agreement with earlier findings of White, et al.²² Values of $\beta_{\sigma S}$ for the series of methyl substituted ethylenes are shown in Fig. 10. The similarities in measured β values over a 2 eV range of electron energy and a similar anticipated energy dependence suggest that the curves containing the variation of $\beta_{\sigma S}$ with electron energy should be virtually identical.

Adiabatic ionization potentials in the carbon $\pi 2p$ region have been studied systematically for a series of 63 alkylated ethylenes by Masclet, et al.³⁵ For methylated ethylenes, they found a systematic decrease in adiabatic first ionization potential with increasing methyl substitution. This agrees with the behavior of vertical ionization potentials reported here and in the work of Kimura, et al.¹⁷ That methylated ethylenes have only one π ionization per molecule means that the variation of β_{π} over the vibrational envelope is the only direct source of the electron energy variation of β . The increase in β_{π} with increasing electron energy in the electron energy range between 10.7-12.7 eV is represented in Fig. 11 and in Table V.³⁶

We extrapolate β values to an electron energy of 10.71 eV in Table V for comparison purposes. We do not expect errors to exceed $\pm .1$. White, et al.²² measured β at the vertical ionization potentials of the two π bands of 1,3-butadiene. They measured β values at the

b_g ionization at 9.0 eV and the a_u ionization at 11.5 eV. On the basis of peak positions and β values, the slope of the interpolated line, +0.08 units/eV, is comparable to the rate of change of β across the isolated b_g band. The variation of β_π in benzene³¹ and in cis-2-butene²² is much more rapid, +0.4 units/eV, and indicates a variability in the dependence of β_π on electron energy.

In comparisons of β_π before or after extrapolation, we notice that β_π is a strongly decreasing function of the number of attached methyl groups. This was first noted by White et al.²² in their study of ethylene, propylene, and cis- and trans-2-butene. In contrast to the behavior of β for $\sigma 2p$ and $\sigma 2s$ ionizations, values of β_π do not lie within error bars of each other. The extrapolation of β_π to 10.71 eV electron energy accentuates the decrease in β_π with increasing methyl substitution.

The difference between the angular distributions of π and σ ionizations was the first hoped-for regularity sought on the basis of the original Hall and Siegel experiment. The comparisons need to be made at the same electron energy to be truly valid. A slight extrapolation of the $\sigma 2p$ line for ethylene yields a difference between β_π and β_σ of 1.2 units. The ability to distinguish π ionizations from σ ionizations on the basis of β values alone diminishes upon methyl substitution. The molecular geometries are no different, however. As an example, electron diffraction studies of 2,3-dimethyl,2-butene³⁷ reveal that the neutral molecule is planar.

The unexpected dip in β at an ionization potential near 15.7 eV is yet unexplained. We should expect that all $\sigma 2p$ ionizations should lie along the same smooth line. The amplitude of the dip, the difference between the measured $\beta_{\sigma p}$ and that estimated from linear extrapolation to an electron energy of 5.5 eV, increases with increasing methyl substitution. Results are listed in Table VI. This is especially clear in the plots of β versus electron energy for tri- and tetra-substituted ethylene, but is also apparent in the plot for isobutylene. The trend is not obvious from examining the lower members of the methyl-substituted ethylenes alone.²² Any deviation is slight and could be interpreted as natural variation with electron energy. Also, any anomalous variation could easily be obscured by overlapping structure. In isobutylene and the tri- and tetra-substituted ethylenes, the drop occurs for photoelectron structure at the upper end of the $\sigma 2p$ region. Here, the corresponding photoelectron band or shoulder does not overlap excessively with neighboring $\sigma 2p$ structure.

MIXING MODEL

We attribute the change of β_{π} with increasing methyl substitution and increasing drop of $\beta_{\sigma p}$ in the 5.5 eV range of electron energy with increasing methyl substitution to the mixing of π and σ orbitals called hyperconjugation³⁸ or through-bond interaction.³⁹ The model which makes predictions about the extent of mixing has been called linear combination of bonding orbitals (LCBO),^{34,40} structure representation,⁴¹ or the group orbital method²⁴ and is based on the equivalent orbital theory of Hall and Lennard-Jones.⁴² This empirical model has been extensively used previously in photoelectron spectroscopy to predict vertical ionization potentials on the basis of parameters derived from photoelectron spectra of model compounds.^{34,40,41} The orbital electrons which are photoejected, corresponding to each band in the spectrum, are interpreted as linear combinations or mixtures of appropriate structural units in the molecule which might transform the same way with respect to one of the several symmetry operations of the molecular symmetry group. For planar unsaturated molecules, the structural units, termed "out-of-plane localized orbitals" by Kimura, et al.,¹⁷ are π bonds and linear combinations of CH bonds. Linear combinations of CH bonds, called $\pi(\text{CH}_3)$, are antisymmetric under reflection in the molecular plane and take the form:⁴⁰

$$\pi(\text{CH}_3) = \frac{1}{\sqrt{2}}(\text{CH1} - \text{CH2})\cos\gamma + \frac{1}{\sqrt{6}}(\text{CH1} + \text{CH2} - 2\cdot\text{CH3})\sin\gamma, \quad (2)$$

where γ is a phase factor related to the rotational orientation of the CH_3 structure. This yields a secular equation:

$$|E_{ij} - \lambda \delta_{ij}| = 0, \quad (3)$$

where E_{ij} are structural energy parameters taken from spectral peak positions of model compounds, λ represents an eigenvalue, and δ_{ij} is the usual Kronecker delta.

The relevant parameters here are the energies E of a carbon-carbon double bond (d), the $\pi(\text{CH}_3)$ structure (m), the interaction of a $\pi(\text{CH}_3)$ with a carbon-carbon double bond (x), and the interaction of two $\pi(\text{CH}_3)$ structures attached to the same sp^2 hybridized carbon (y). Uncertainties about the vertical ionization potential of methane have yielded a wide variation ($m = 13.7\text{--}14.3 \text{ eV}$)^{17,24,41} of parameters for the energy of an isolated $\pi(\text{CH}_3)$ structure. Typically, the other parameters take the values:

$$d = 10.51 \text{ eV}$$

$$x = 1.5 - 2.0 \text{ eV}$$

$$y \sim 0.2 \text{ eV}.^{43}$$

A list of sample eigenvalues and eigenfunctions is given in Table VII.

We find trends in the eigenvalues and eigenfunctions which are independent of the choice of parameters and are expected to be valid even if the collection of parameters is not optimized for fits to peak positions in the photoelectron spectra of related compounds. The π

ionization potential, corresponding to the lowest eigenvalue, is lowered with increasing methyl substitution. The largest eigenvalue is typically in the range 14.5-16.5 eV, depending on the choice of parameters. It increases with increasing methyl substitution. When two or more methyl groups are substituted on the ethylene frame, all other eigenvalues cluster about m . All but the lowest eigenvalue correspond to band structure within the carbon $\sigma 2p$ region. The eigenfunctions corresponding to the highest and the lowest eigenvalues have coefficients of both $\pi(C=C)$ and the various $\pi(CH_3)$. All other eigenfunctions have zero coefficient of $\pi(C=C)$, a consequence of symmetry, rather than fortuitous choice of structural parameters. With increasing methyl substitution, the coefficient of $\pi(CH_3)$ character increases in the eigenfunction corresponding to the lowest eigenvalue (largely π ionization) with increasing methyl substitution. Conversely, with increasing methyl substitution, the coefficient of $\pi(C=C)$ character increases in the eigenfunction corresponding to the highest eigenvalue.

Eigenvalue trends have been tested against experimental vertical ionization potentials of the $\pi 2p$ and $\sigma 2p$ bands in the photoelectron spectra of methylated ethylenes.^{17,24} Much of the σ structure overlaps grossly and it is very difficult to assign particular features to loss of out-of-plane orbital electrons unambiguously. In isobutylene, 2-methyl, 2-butene, and 2,3-dimethyl, 2-butene, the highest eigenvalue is predicted to lie at the upper end of the $\sigma 2p$ region where overlap with neighboring bands would be minimized.

In ionization potential regions close to 14.2 eV, $\beta_{\sigma p}$ varies smoothly for the complete set of methylated ethylenes. The mixing model predicts out-of-plane orbital electron ionizations in this region. Two explanations are possible. First, the β parameter for $\pi(\text{CH}_3)$ ionization may be different from that for in-plane ionization corresponding to the other $\sigma 2p$ structure. Because of the high degree of overlap between bands, our apparatus might then be insensitive to small changes. However, in the case of 2,3-dimethyl,2-butene, we expect three bands from out-of-plane ionization within a narrow region. Our apparatus finds no such gross deviations expected in this case. Second, and more plausible, β for unmixed out-of-plane $\pi(\text{CH}_3)$ subunits is identical to or very similar to that for in-plane ionizations. This explanation predicts the absence of deviations in β in the ionization potential region near 14.2 eV.

For ionizations of orbital electrons of mixed π/σ character, we have no rigorous theoretical guide to the expected β in terms of β values of un-mixed subunits. Replacing the initial wavefunction by a linear combination:

$$\psi_i = C_a \psi_a + C_b \psi_b \quad (4)$$

does not yield:

$$\beta = C_a^2 \beta_a + C_b^2 \beta_b ,$$

where β_a and β_b could be calculated or measured for ψ_a and ψ_b

separately. The expression for β in the work of several theoreticians^{18,44,45} would contain numerous cross terms in $C_a C_b$ which are not expected to disappear except at high photoelectron energy.⁴⁶

Nevertheless, we can look for qualitative trends which are expected to be of more use in examining olefins other than methylated ethylenes. First, we need values of β_π , extrapolated to 10.71 eV electron energy from Table V. Next, the fractional deviation from ethylene, f , is calculated from:

$$f = \frac{\beta_\pi - \beta_\pi(\text{ethylene})}{\beta_{\sigma p}(\text{mean}) - \beta_\pi(\text{ethylene})},$$

where $\beta_{\sigma p} = 0.06$, the mean of the set of methylated ethylenes, extrapolated to 10.71 eV electron energy, and $\beta_\pi(\text{ethylene})$ is the experimental value of β for the π ionization in ethylene. The values of f are compared with fractions of σ character calculated from squares of subunit coefficients from mixing model eigenfunctions in Table V. Measured β values are deflected in the direction of $\beta_{\sigma p}$, but only in qualitative agreement with amounts predicted on the basis of coefficients of $\pi(\text{CH}_3)$ and $\pi(\text{C}=\text{C})$ in the mixed wavefunction.

We may apply the model to account for the sudden drop in $\beta_{\sigma p}$ in the electron energy range near 5.5 eV. We found earlier that the amount that $\beta_{\sigma p}$ drops in this spectral region increases with increasing methyl substitution. The model would predict that the unmixed value of β_π for ethylene is lower than the unmixed value of β

for a typical $\sigma 2p$ ionization here.

Independently of the model above, we can estimate the value of β_π for ethylene within 5 eV of threshold on the basis of previous calculations and experiments for related carbon-containing molecules. Kinsinger and Taylor³¹ found a β value of -0.5 for the benzene π orbitals in this energy region. Lohr's calculation⁴⁷ of C_2 as a model for ethylene gives a β value near -0.8. This value should be shifted upwards on the basis of his error (0.5-0.8 units) at an electron energy of 10.7 eV. Kennedy and Manson's β for the carbon atomic 2p sub-shell⁴⁸ goes to zero at threshold and rises with increasing electron energy.

We can thus estimate that the β value for ethylene at 5 eV electron energy should be close to 0. This value is lower than the corresponding unmixed value of $\beta_{\sigma p}$ for $\sigma 2p$ ionization at the same electron energy and is consistent with the mixing model.

CONCLUSION

From first principles, we would expect the necessity to measure photoelectron angular distributions at a number of photon wavelengths in order to determine the electron energy variation of β . The photoelectron angular distributions measured at a single photon energy incorporate much of this information already. If we are judicious, we can infer the variation of β across vibrational envelopes. Also, the variation of β within a set of ionizations of closely related orbitals should reflect the energy variations for any of the members of the set. Thus, for the low electron energy region, photoelectron angular distributions can be independent of group theoretical symmetry designations of corresponding ionic states.

Complications arise due to through-bond mixing of orbitals of different types. Measured values of β in these mixed systems take on values intermediate between β values measured for unmixed systems. The deviation from the unmixed value of β for the principal unmixed subunit, as the deviations of β_{π} for the set of methyl substituted ethylenes from the measured ethylene value, indicates the extent of through-bond mixing. The effects of mixing are reciprocal. The σ region is perturbed in these cases, as well.

Several significant assumptions were made in the course of deriving the above conclusions. The assumption about β values for ionization of electrons from orbitals of the same symmetry within the $\sigma 2p$ region should be tested with photoelectron angular distribution

measurements at a different wavelength. The absence of auto-ionization in the 21.2 eV region for the set of methylated ethylenes is easily verified using the technique of photoionization mass spectrometry.

REFERENCES

1. D. W. Turner, C. Baker, A. D. Baker, C. R. Brundle, Molecular Photoelectron Spectroscopy (Wiley-Interscience, London, 1970).
2. M. I. Al-Joboury, D. W. Turner, J. Chem. Soc. 5141 (1963).
3. P. Bischof, J. A. Hashmall, E. Heilbronner, V. Hornung, Helv. Chim. Acta 52, 1745 (1969).
4. A. D. Baker, D. P. May, D. W. Turner, J. Chem. Soc. (B) 22 (1968).
5. C. R. Brundle, M. B. Robin, J. Amer. Chem. Soc. 92, 5550 (1970); C. R. Brundle, M. B. Robin, N. A. Kuebler, J. Amer. Chem. Soc. 94, 1451 (1972).
6. F. Wuilleumier, M. O. Krause, Phys. Rev. A 10, 242 (1974).
7. W. C. Price, A. W. Potts, D. G. Streets, in D. A. Shirley (editor) Electron Spectroscopy (North-Holland, Amsterdam, 1972) p. 187.
8. M. B. Robin, N. A. Kuebler, C. R. Brundle, in D. A. Shirley (editor) Ibid., p. 351.
9. J. L. Hall, M. W. Siegel, J. Chem. Phys. 48, 943 (1968).
10. T. A. Carlson, C. P. Anderson, Chem. Phys. Lett. 10, 561 (1971).
11. T. A. Carlson, G. E. McGuire, A. E. Jonas, K. L. Cheng, C. P. Anderson, C. C. Lu, B. P. Pullen, in D. A. Shirley (editor) op. cit., p. 207.

12. J. W. Rabalais, T. P. Debies, J. L. Berkosky, J.-T. J. Huang, F. O. Ellison, J. Chem. Phys. 61, 529 (1974).
13. D. C. Mason, A. Kuppermann, D. M. Mintz, in D. A. Shirley (editor) op. cit., p. 269.
14. Galileo Electro-optics Corp., Sturbridge, Mass.
15. Digital Equipment Corporation, Maynard, Mass.
16. a) A. D. Baker, C. Baker, C. R. Brundle, D. W. Turner, Int. J. Mass Spectrom. Ion Phys. 1, 285 (1968).
b) G. R. Branton, D. C. Frost, T. Makita, C. A. McDowell, I. A. Stenhouse, J. Chem. Phys. 52, 802 (1970).
17. K. Kimura, S. Katsumata, T. Yamazaki, H. Wakabayashi, J. Electron Spectr. 6, 41 (1975).
18. J. Cooper, R. N. Zare, in S. Geltman, K. Mahanthappa, N. Brittin (editors) Lectures in Theoretical Physics Vol. XI-C (Gordon and Breach, New York, 1969) p. 317.
19. M. I. Al-Joboury, D. W. Turner, J. Chem. Soc. (B) 4434 (1964).
20. M. B. Robin, Higher Excited States of Polyatomic Molecules Vol. II (Academic Press, New York, 1975) Chap. 4.
21. M. J. S. Dewar, S. D. Worley, J. Chem. Phys. 50, 654 (1969).
22. R. M. White, T. A. Carlson, D. P. Spears, J. Electron Spectr. 3, 59 (1974).
23. a) A. W. Potts, D. G. Streets, J. Chem. Soc. Faraday II 70, 875 (1974).
b) D. G. Streets, A. W. Potts, J. Chem. Soc. Faraday II 70, 1505 (1974).

24. D. C. Frost, J. S. Sandhu, *Ind. J. Chem.* 9, 1105 (1971).
25. G. Herzberg, Molecular Spectra and Molecular Structure: II. Electronic Spectra and Electronic Structure of Polyatomic Molecules (Van Nostrand, New York, 1967), p. 128.
26. T. H. Lee, J. W. Rabalais, *J. Chem. Phys.* 61, 2747 (1974).
27. D. M. Mintz, A. Kuppermann, in J. S. Risley, R. Geballe (editors) Electronic and Atomic Collisions (U. of Washington, Seattle, 1975) p. 567; Chap. 5, this work.
28. P. Natalis, J. E. Collin, *Chem. Phys. Lett.* 2, 414 (1968);
P. Natalis, J. Delwiche, J. E. Collin, *Chem. Phys. Lett.* 13, 491 (1972); J. E. Collin, P. Natalis, *Int. J. Mass Spectrom. Ion Phys.* 2, 231 (1969).
29. T. A. Carlson, *Chem. Phys. Lett.* 9, 23 (1971).
30. G. Herzberg, op. cit., p. 458.
31. J. A. Kinsinger, J. W. Taylor, *Int. J. Mass Spectrom. Ion Phys.* 10, 445 (1972); they used HeI data of Ref. 10 to calibrate their instrument.
32. B.-Ö. Jonsson, E. Lindholm, *Ark. Fys.* 39, 65 (1969).
33. W. C. Price, in P. Hepple (editor) Molecular Spectroscopy (Institute of Petroleum, London, 1968) p. 221.
34. H. Bock, B. G. Ramsey, *Angew. Chem. Internat. Ed.* 12, 734 (1973).
35. P. Masclet, D. Grosjean, G. Mouvier, J. Dubois, *J. Electron Spectr.* 2, 225 (1973).

36. In propylene, the data in Fig. 2 of Ref. 22 show a slight decrease of β_{π} with increasing electron energy.
37. J. L. Carlos, Jr., S. H. Bauer, J. Chem. Soc. Faraday II 70, 171 (1974).
38. R. S. Mulliken, J. Chem. Phys. 7, 339 (1939).
39. R. Hoffmann, Accts. Chem. Res. 4, 1 (1971).
40. M. Beez, G. Bieri, H. Bock, E. Heilbronner, Helv. Chim. Acta 56, 1028 (1973).
41. T. Koenig, H. Longmaid, J. Org. Chem. 39, 560 (1974) and references cited therein.
42. a) G. G. Hall, Proc. Roy. Soc. Lond. A205, 541 (1951); Trans. Faraday Soc. 49, 113 (1953).
b) J. Lennard-Jones, G. G. Hall, Proc. Roy. Soc. Lond. A213, 102 (1952).
43. The large value of γ (1.2 eV) used by R. A. Wielessek and T. Koenig, Tet. Lett. 28, 2429 (1974), was obtained from ethane and is probably inappropriate for describing the interaction of methyl groups in 2-methyl olefins.
44. S. Iwata, S. Nagakura, Mol. Phys. 27, 425 (1974).
45. F. O. Ellison, J. Chem. Phys. 61, 507 (1974).
46. J.-T.J. Huang, F. O. Ellison, Chem. Phys. 7, 473 (1975).
47. L. L. Lohr, Jr., in D. Shirley (editor) op. cit., p. 245.
48. S. T. Manson, J. Electron Spectr. 1, 413 (1972).

TABLE I. Ethylene

Vertical IP (eV)	Orbital ^a D _{2h}	Description	β , this work ^d	β , previous work ^b
10.51	1b _{3u}	π	1.25 \pm 0.05	1.20
12.82	1b _{3g}	C σ 2p; ^b CH bonding ^c	0.30 \pm 0.05	0.35
14.69	3a _g	C σ 2p; CC bonding	0.60 \pm 0.10	0.60
15.90	1b _{2u}	C σ 2p; CH bonding	0.65 \pm 0.05	0.65
19.1	2b _{1u}	C σ 2s; CC antibonding		

^aOrbital designation from Ref. 16a.^bRef. 22.^cRef. 16.^dEvaluated at vertical ionization potential.

TABLE II. Isobutylene

Vertical IP (eV)	Orbital ^b C _{2v}	Description	β , this work ^d
9.45	2b ₁	π	0.75 ± 0.05
11.81	a'	C σ 2p	0.25 ± 0.05
12.90	a'	C σ 2p	0.30 ± 0.05
(13.2) ^a	a'	C σ 2p	0.35 ± 0.05
(13.8) ^a	1a ₂	C σ 2p; π (CH ₃) ^c	0.40 ± 0.05
15.03	a'	C σ 2p	0.60 ± 0.05
(15.3) ^a	a'	C σ 2p	0.55 ± 0.05
(15.7) ^a	1b ₁	C σ 2p; π (CH ₃) ^c	0.45 ± 0.05
17.27	a'	C σ 2s ^c	0.55 ± 0.10

^aShoulders indicated in Ref. 17.

^bIn-plane orbitals assigned using point group C_s and include a₁ and b₂ of C_{2v}.

^cAssigned by Kimura, et al., Ref. 17.

^dEvaluated at vertical ionization potential.

TABLE III. 2-Methyl, 2-butene

Vertical IP (eV)	Orbital ^b C _s	Description	β , this work ^c
8.86	4a''	π	0.80 ± 0.05
11.35	a'	C σ 2p	0.25 ± 0.05
12.55	a'	C σ 2p	0.30 ± 0.05
12.90	a'	C σ 2p	0.40 ± 0.05
(13.6) ^a	2a'', 3a'', a'	C σ 2p; in plane and $\pi(\text{CH}_3)^b$	0.50 ± 0.05
14.73	a'	C σ 2p	0.6 ± 0.1
15.60	1a''	C σ 2p; $\pi(\text{CH}_3)^b$	0.45 ± 0.10
16.83	a'	C σ 2s	0.5 ± 0.1

^aShoulder^bAssignments of out-of-plane structure based upon LCBO eigenvalues, eigenfunctions. Extent of overlap in C σ 2p region hinders isolation of all 11 expected features.^cEvaluated at vertical ionization potential.

TABLE IV. 2,3-Dimethyl, 2-butene

Vertical IP (eV)	Orbital ^b D _{2h}	Description	β , this work ^c
8.44	2b _{3u}	π	0.60 \pm 0.05
10.96	a'	C σ 2p	0.25 \pm 0.05
12.71	a'	C σ 2p	0.40 \pm 0.05
(13.5) ^a	1b _{1g} , 1a _u , 1b _{2g}	C σ 2p; π (CH ₃) ^b	0.5 \pm 0.1
(14.2) ^a	a'	C σ 2p	0.6 \pm 0.1
14.85	a'	C σ 2p	0.7 \pm 0.1
15.85	1b _{3u}	C σ 2p; π (CH ₃) ^b	0.4 \pm 0.1
(16.4) ^a	a'	C σ 2s	0.5 \pm 0.1

^aShoulder.

^bIn-plane orbitals assigned using point group C_s and include a_g, b_{1u}, b_{2u}, b_{3g} of D_{2h}. Out-of plane orbitals assigned using point group D_{2h} and LCBO eigenfunctions and eigenvalues.

^cEvaluated at vertical ionization potential.

TABLE V. Variation of asymmetry parameter, β , over vibrational envelopes of π bands

Compound	Orbital	$d\beta/dE_e$	β Extrapolated to $E_e = 10.71$	Fraction dev. of β from 1.25	LCBO σ character
ethylene	$1b_{3u}$	0.10 ± 0.05	1.25	0	0
propylene	$2a''$	-0.10^a	1.0 ± 0.1	0.2	0.14
<u>cis</u> -2-butene	$2b_2$	0.4^a	0.2 ± 0.1	0.9	0.20
<u>trans</u> -2-butene	$2a_u$	0.1^a	0.7 ± 0.1	0.5	0.20
isobutylene	$2b_1$	0.30 ± 0.05	0.5 ± 0.1	0.6	0.19
2-methyl, 2-butene	$4a''$	0.20 ± 0.05	0.5 ± 0.1	0.6	0.23
2, 3-dimethyl, 2-butene	$2b_{3u}$	0.10 ± 0.05	0.4 ± 0.1	0.7	0.26

^aMeasured from Figs. 2, 3, 4 of Ref. 22.^b $1-C_\pi^2$ ($C=C$), where C_π is evaluated by the LCBO method.

TABLE VI. Variation of asymmetry parameter, β , over $\sigma 2p$ region

Compound	Pseudo- π orbital	IP, ^a of corresponding band	$d\beta/dE_e$	$\beta_{\text{extrap}}^{-\beta_{\text{expt}}}$
isobutylene	$1b_1$	15.7 ^c	-0.12	0.20 ± 0.05
2-methyl, 2-butene	$1a''$	15.60	-0.11	0.25 ± 0.10
2, 3-dimethyl, 2-butene	$1b_{3u}$	15.85	-0.12	0.40 ± 0.10

^aVertical, in eV.

^bMeasured from variation over other $\sigma 2p$ structure.

^cMeasured at a shoulder.

TABLE VII. Eigenvalues and Eigenvectors of LCBO model

Molecule	Orbital	Eigenvalue ^a	Subunit coefficient in eigenvector ^a				
			$C_{\pi}(C=C)$	$C_H(CH_3^{(1)})$	$C_H(CH_3^{(2)})$	$C_H(CH_3^{(3)})$	$C_H(CH_3^{(4)})$
propylene	2a''	9.812	0.9289	-0.3704			
	1a''	14.898	0.3704	0.9289			
<u>cis</u> 2-butene	2b ₂	9.268	0.8938	-0.3171			-0.3171
	1a ₂	14.200	0.0	0.7071			-0.7071
	1b ₂	15.412	0.4485	0.6319			0.6319
<u>trans</u> 2-butene	2a _u	9.268	0.8938	-0.3171		-0.3171	
	1b _g	14.200	0.0	0.7071		-0.7071	
	1a _u	15.442	0.4485	0.6319		0.6319	
isobutylene	2b ₁	9.307	0.8994	-0.3091	-0.2091		
	1a ₂	14.000	0.0	0.7071	-0.7071		
	1b ₁	15.603	0.4372	0.6360	0.6360		
2-methyl, 2-butene	4a''	8.838	0.8755	-0.2754	-0.2754	-0.2858	
	3a''	14.000	0.0	0.7071	-0.7071	0.0	
	2a''	14.263	0.0302	-0.3862	-0.3862	0.8371	
	1a''	16.009	0.4822	0.5244	0.5244	0.4664	
2, 3-dimethyl, 2-butene	2b _{3u}	8.451	0.8619	-0.2536	-0.2536	-0.2536	-0.2536
	1b _{1g}	14.000	0.0	0.5000	-0.5000	-0.5000	0.5000
	1a _u	14.000	0.0	0.5000	-0.5000	0.5000	-0.5000
	1b _{2g}	14.400	0.0	0.5000	0.5000	-0.5000	-0.5000
	1b _{3u}	16.459	0.5071	0.4310	0.4310	0.4310	0.4310

^aUsing the parameters: $d = 10.51$
 $m = 14.2$
 $x = 1.75$
 $y = 0.2$

and the geometry



Figure Captions

Figure 6.1-1 Block diagram of variable angle photoelectron spectrometer. HE, cylinder of UHP helium. ZT, liquid nitrogen immersed zeolite trap for lamp helium supply. BR, lamp ballast resistor, 1320 Ω . LPS, lamp power supply, 555 V, 300 mA maximum. SC, sample chamber. PC, photocathode for light flux measurement. CL, electron lens elements before hemispherical analyzer. ANALYZER, 180° hemispherical electrostatic electron energy analyzer. ML, electron lens elements between hemispheres and detector. S, Spiraltron channel electron multiplier. CPS, power supply to Spiraltron cathode. APS, power supply to Spiraltron anode. R, C, differentiating network for Spiraltron pulses: R = 1 M Ω , C = 500 pf. PDP8/e, Digital Equipment Corporation PDP8/e minicomputer. INTER, counting system interface to experiment. OUTPUT, computer output devices to user.

Figure 6.1-2 HeI photoelectron spectrum of ethylene at $\theta = 54.7^\circ$ in lower frame. The variation of β with ionization potential of spectrum features on the lower frame is shown on the upper frame.

Figure 6.1-3 HeI photoelectron spectrum of isobutylene at $\theta = 54.7^\circ$ in lower frame. The variation of β with ionization potential of spectrum features on the lower frame is shown on the upper frame.

Figure 6.1-4 HeI photoelectron spectrum of 2-methyl,2-butene at $\theta = 54.7^\circ$ in lower frame. The variation of β with ionization potential

of spectrum features on the lower frame is shown on the upper frame.

Figure 6.1-5 HeI photoelectron spectrum of 2,3-dimethyl,2-butene at $\theta = 54.7^\circ$ in lower frame. The variation of β with ionization potential of spectrum features on the lower frame is shown on the upper frame.

Figure 6.1-6 Variation of the asymmetry parameter, β , over the σ 2p region of isobutylene.

Figure 6.1-7 Variation of the asymmetry parameter, β , over the σ 2p region of 2-methyl,2-butene.

Figure 6.1-8 Variation of the asymmetry parameter, β , over the σ 2p region of 2,3-dimethyl,2-butene.

Figure 6.1-9 Variation of the asymmetry parameter, β , over the σ 2p region of the complete set of methyl substituted ethylenes.

●, ethylene. ▲, propylene. ◇, cis 2-butene. ◆, trans 2-butene. ○, isobutylene. □, 2-methyl,2-butene. △, 2,3-dimethyl,2-butene. Data for propylene, cis, and trans 2-butene are from Ref. 22.

Figure 6.1-10 Asymmetry parameter, β , for the σ 2s region of the set of methyl substituted ethylenes. Data for ethylene have not been included.

Figure 6.1-11 Variation of the asymmetry parameter, β , over the π region of the complete set of methyl substituted ethylenes. Lines represent the variation of β over each vibrational envelope. Symbols are the same as those of Fig. 9. Data of propylene, cis-, and trans-2-butene are from Ref. 22.

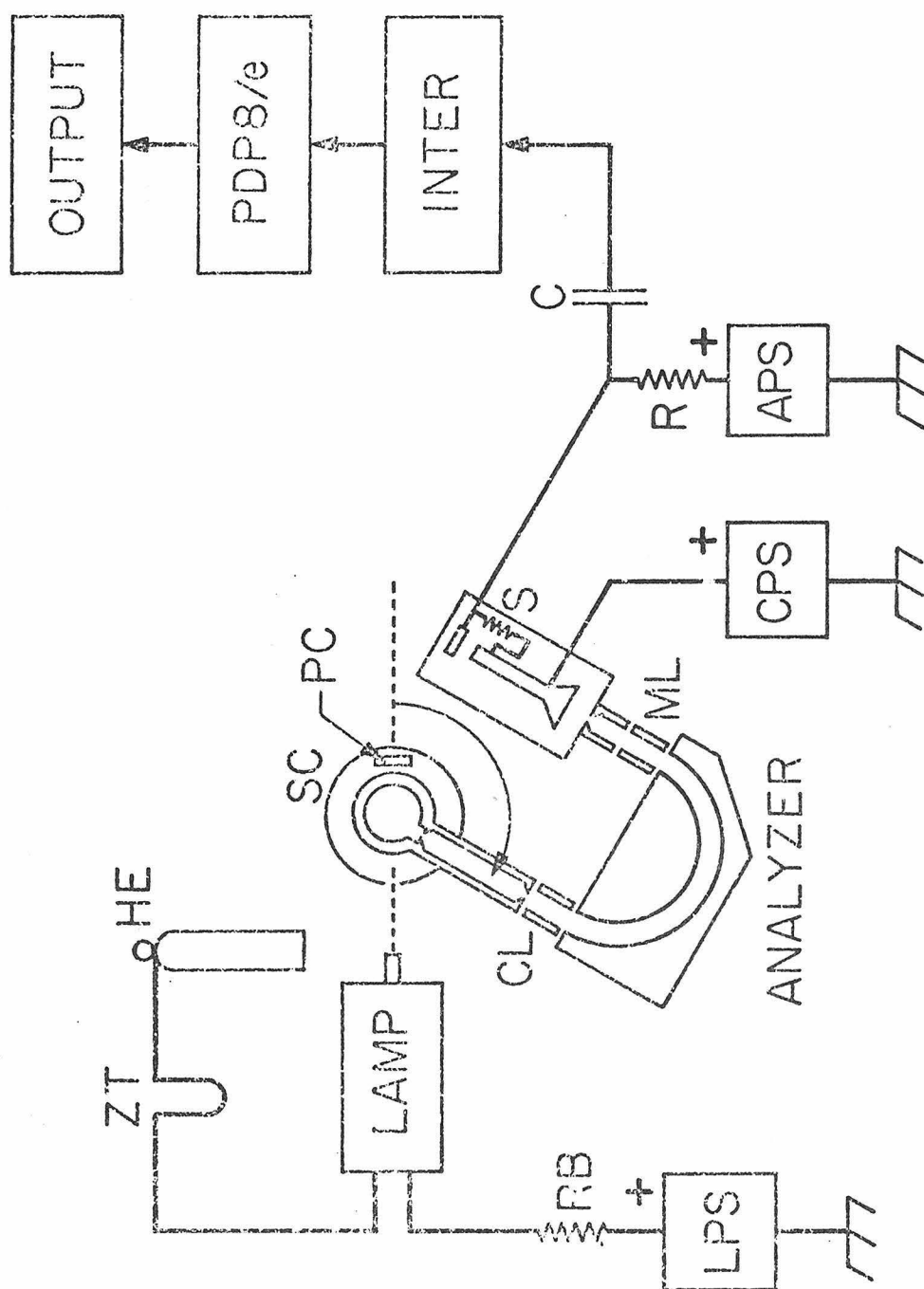


Figure 6.1-1

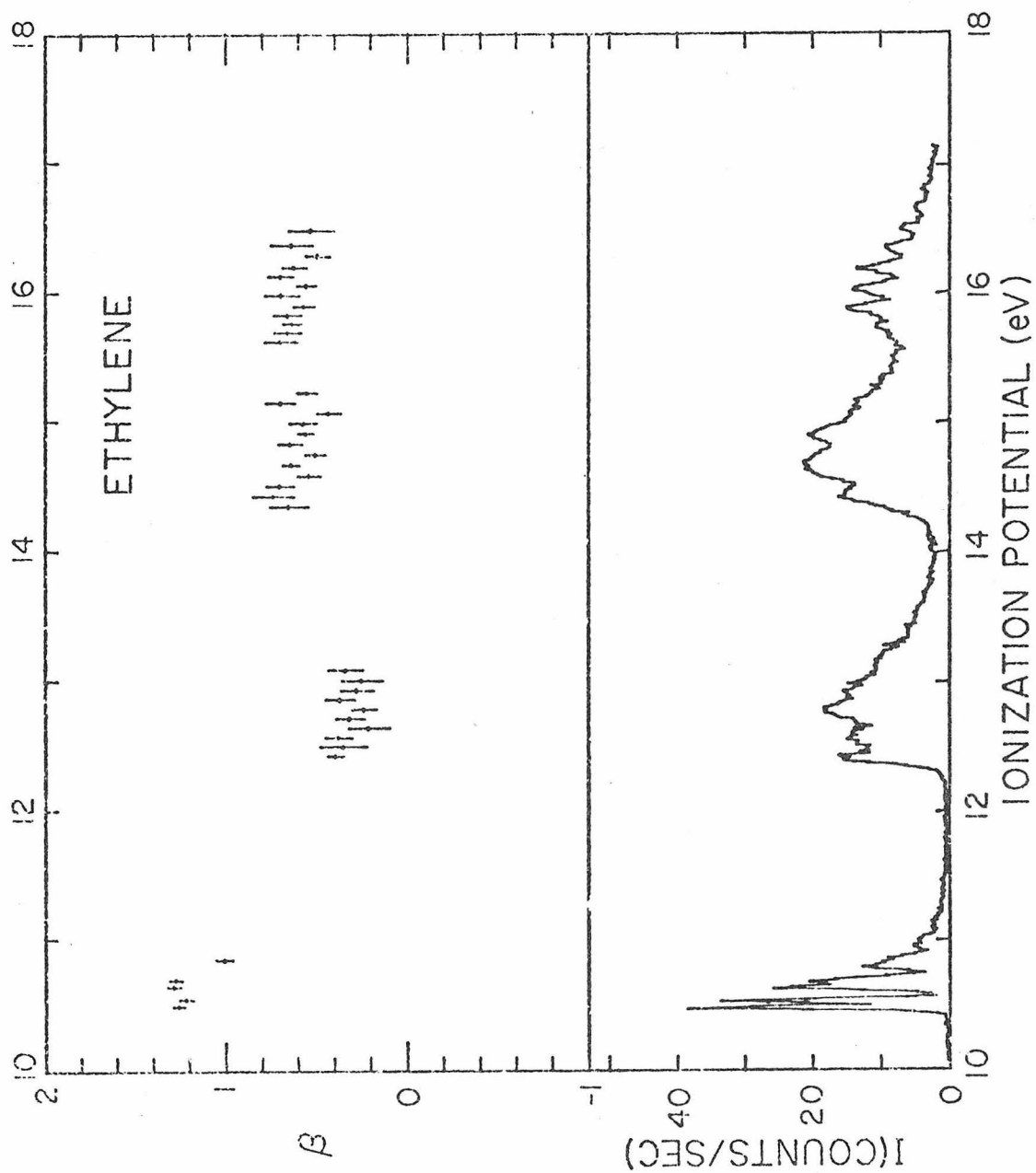


Figure 6.1-2

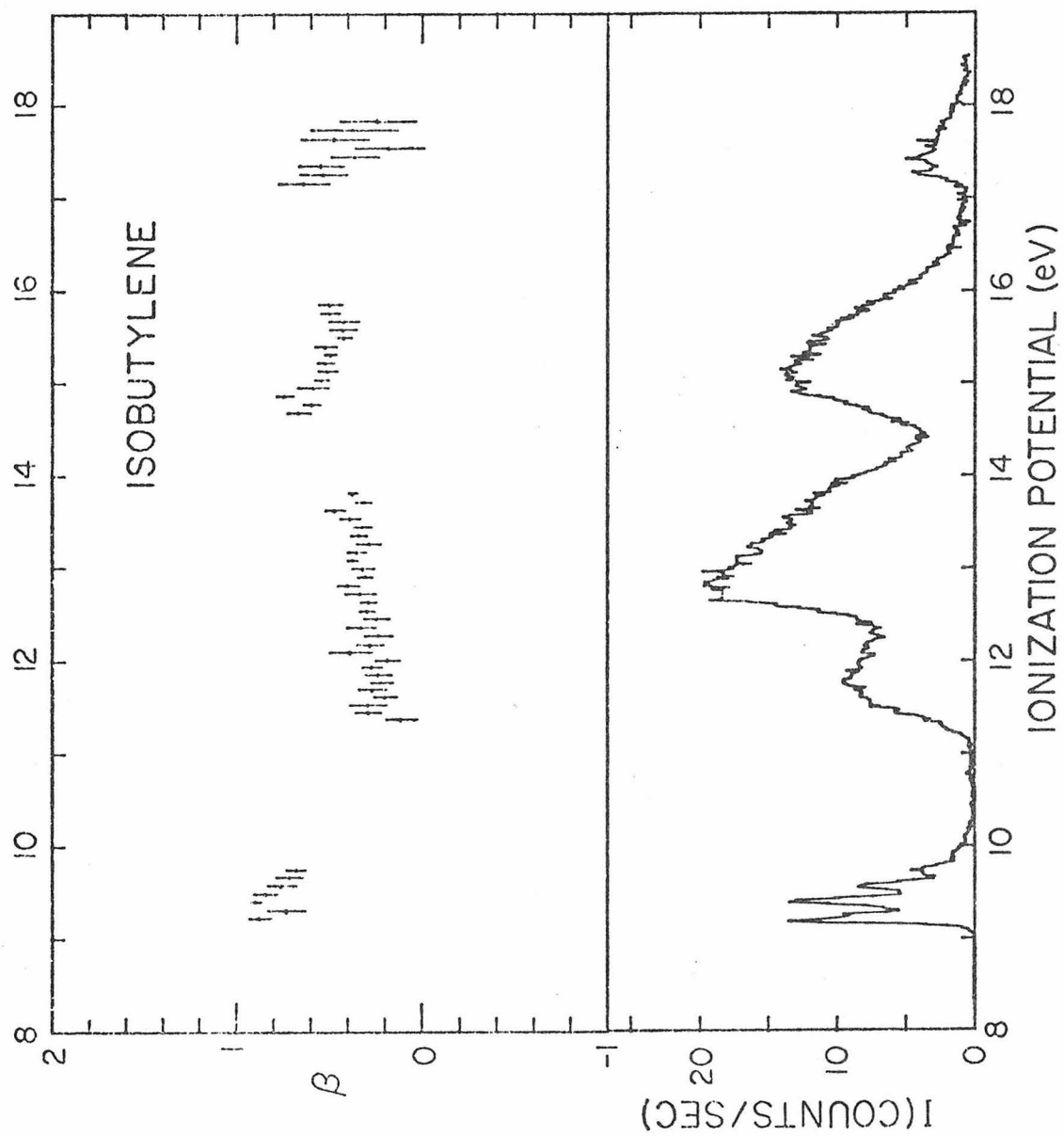


Figure 6.1-3

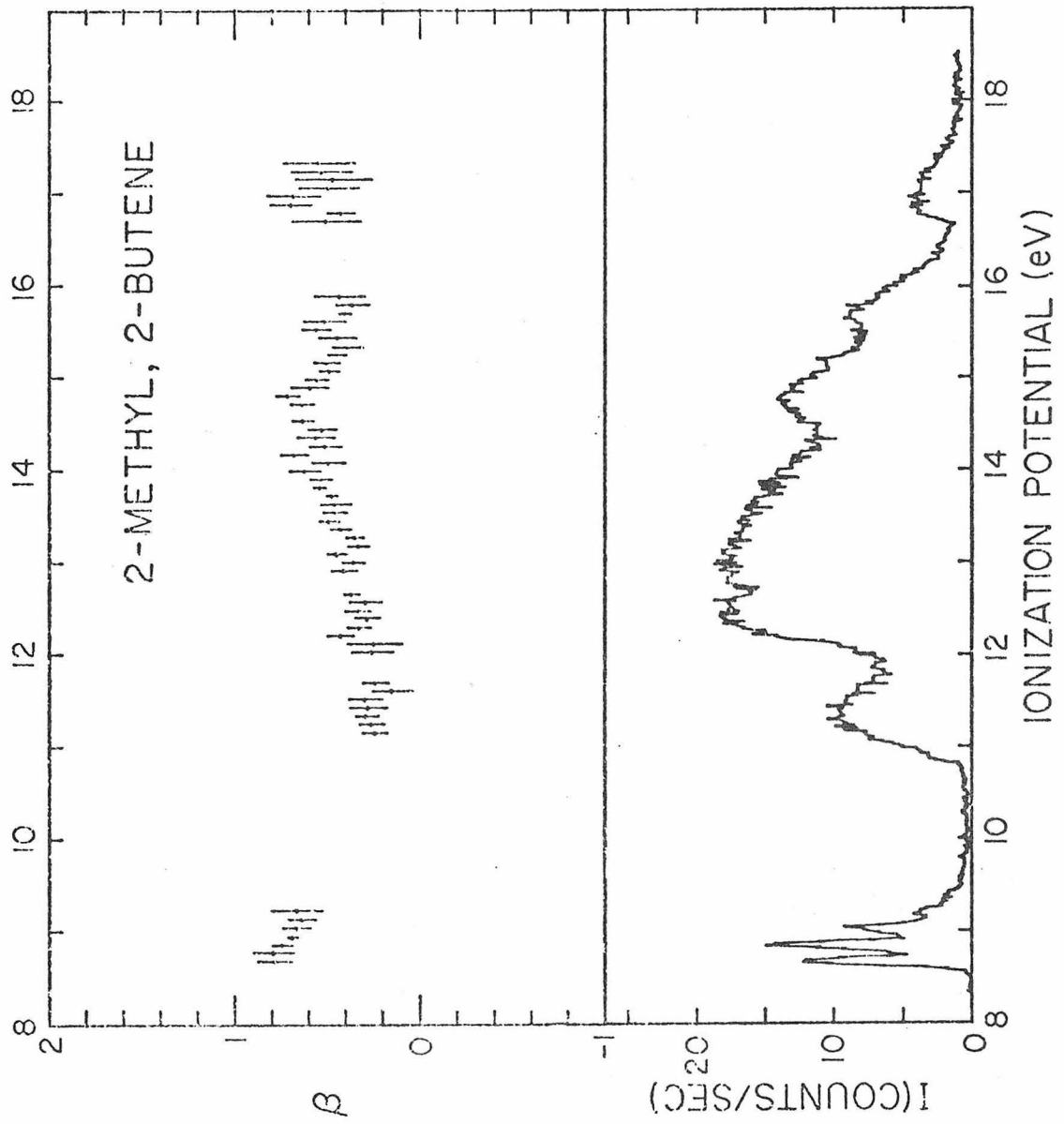


Figure 6.1-4

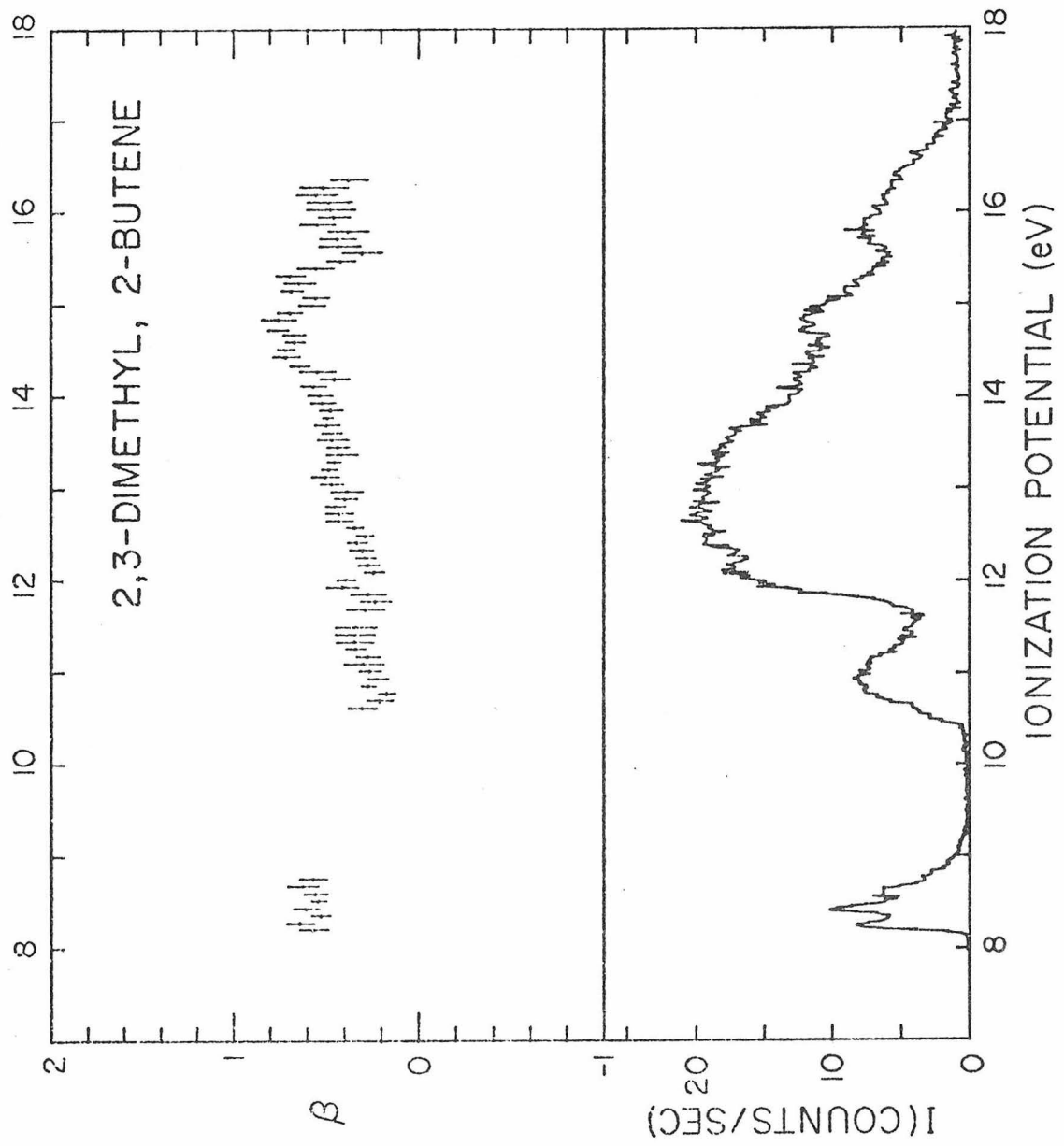


Figure 6.1-5

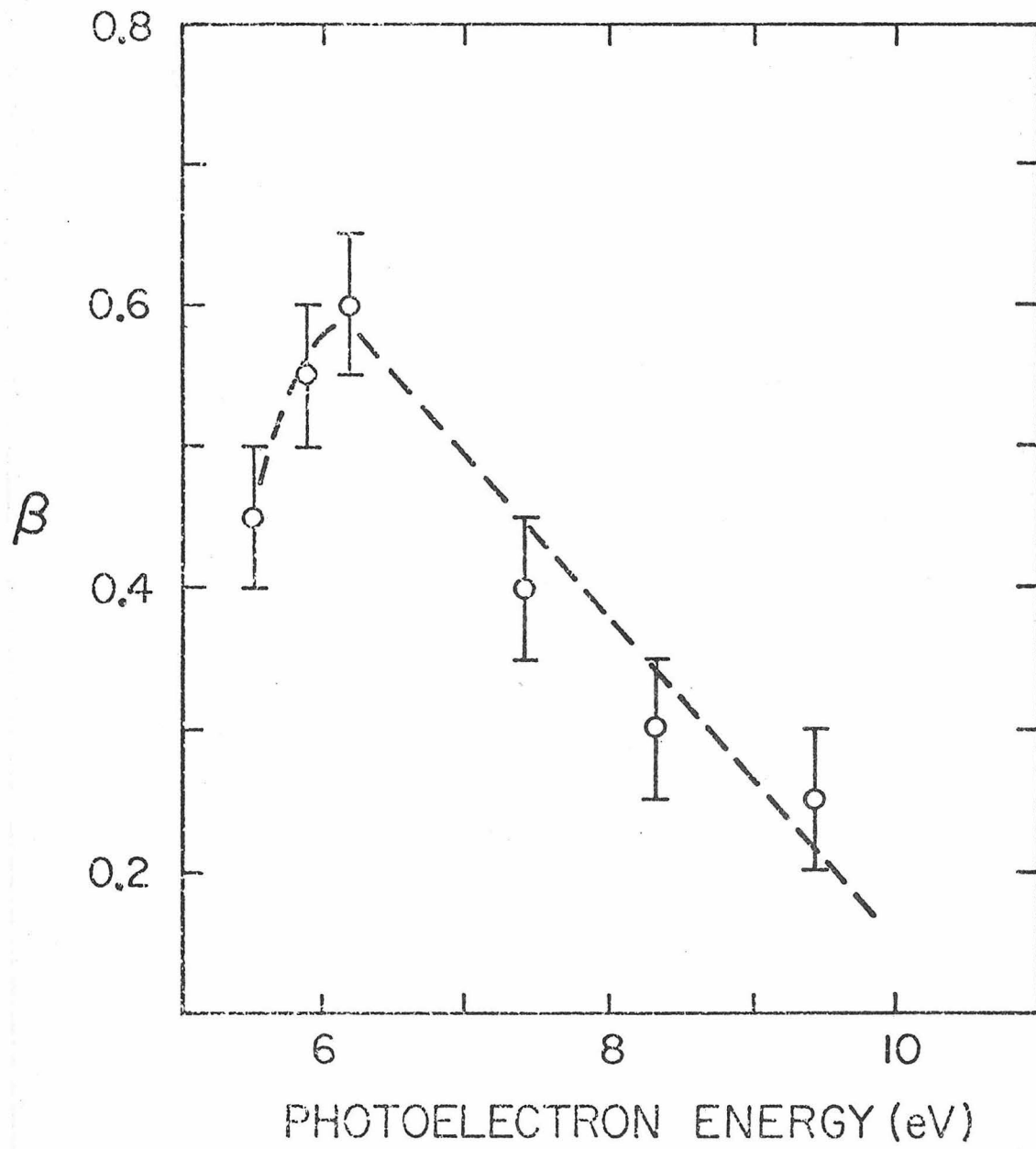


Figure 6.1-6

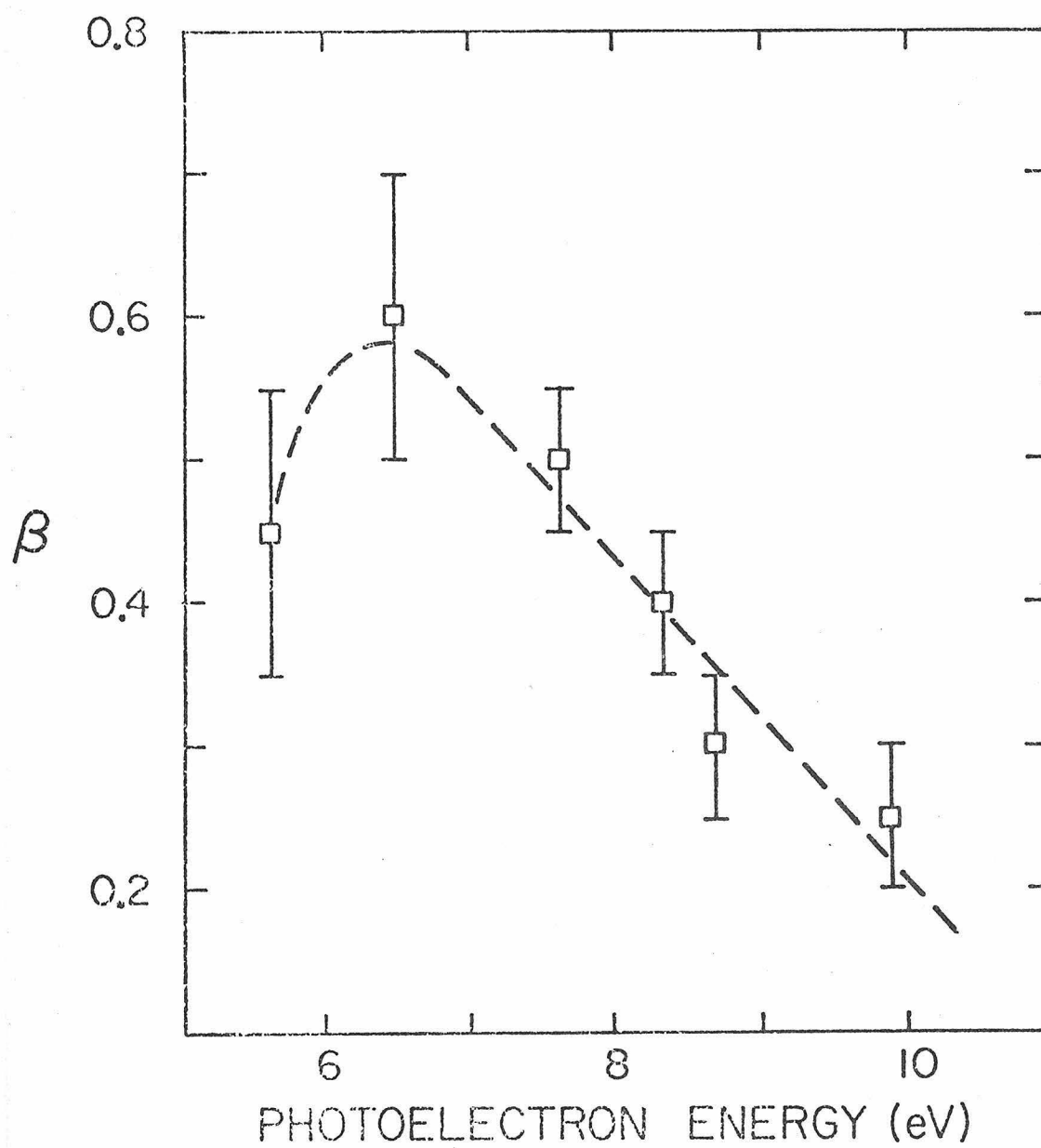


Figure 6.1-7

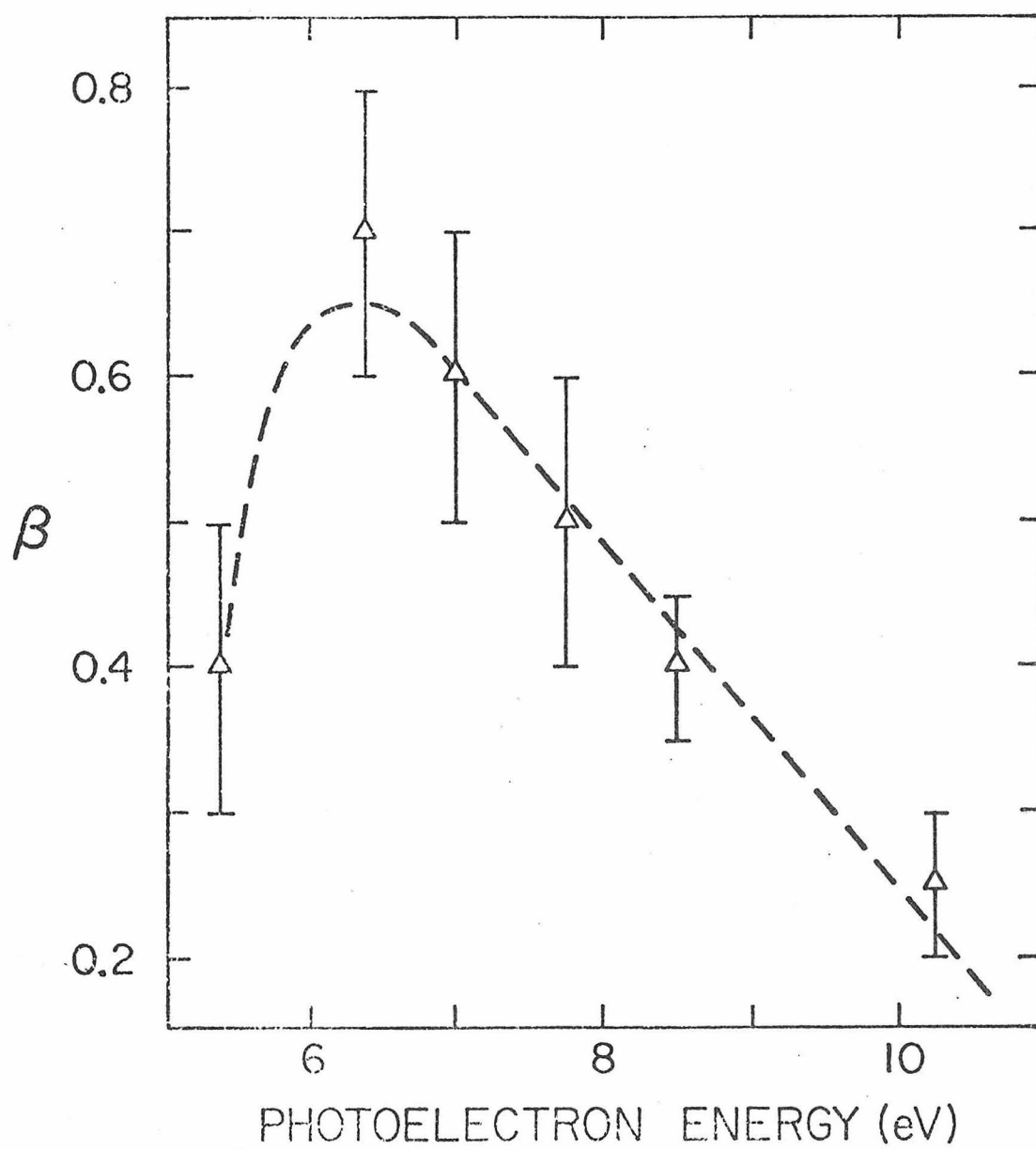


Figure 6.1-8

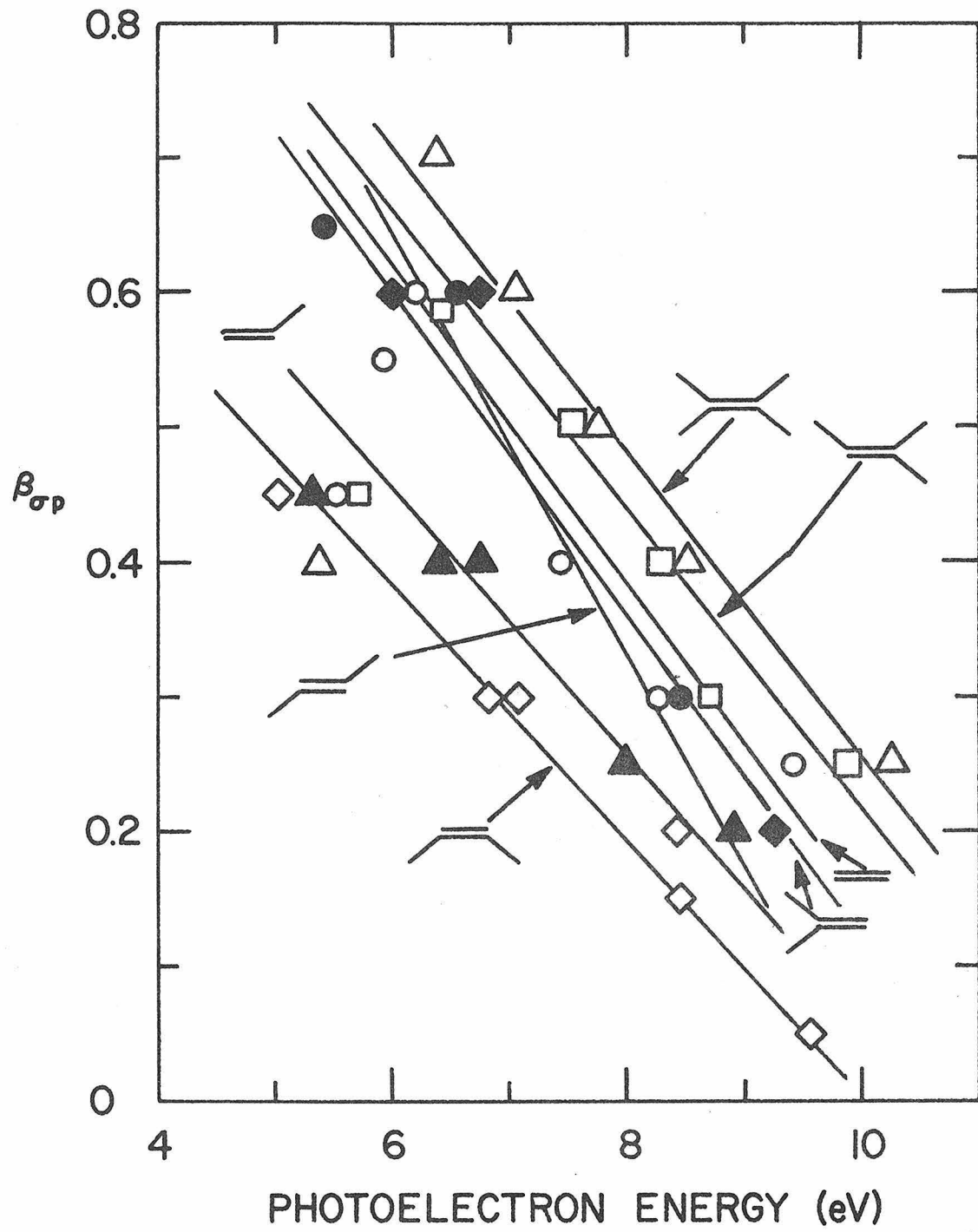


Figure 6.1-9

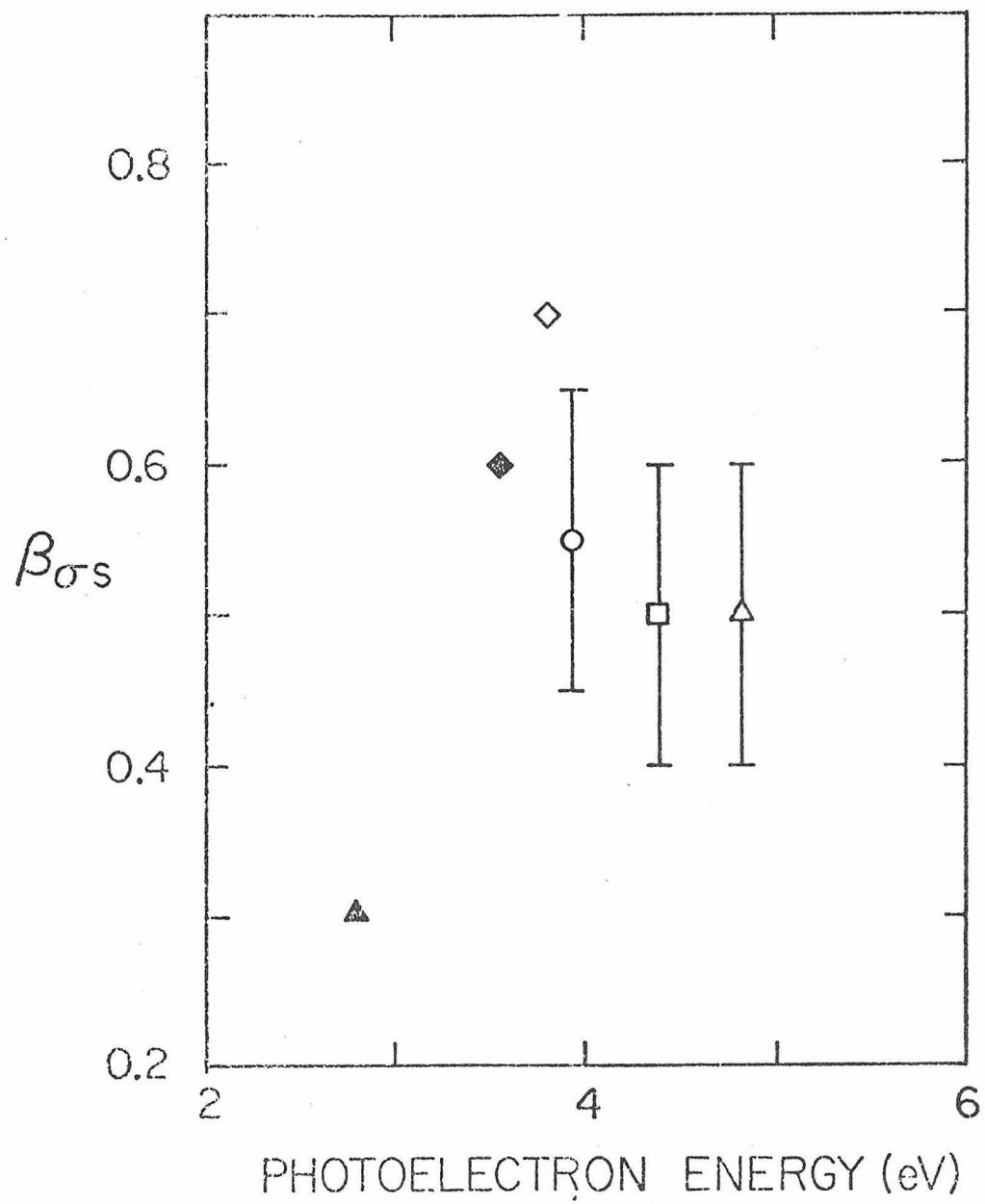


Figure 6.1-10

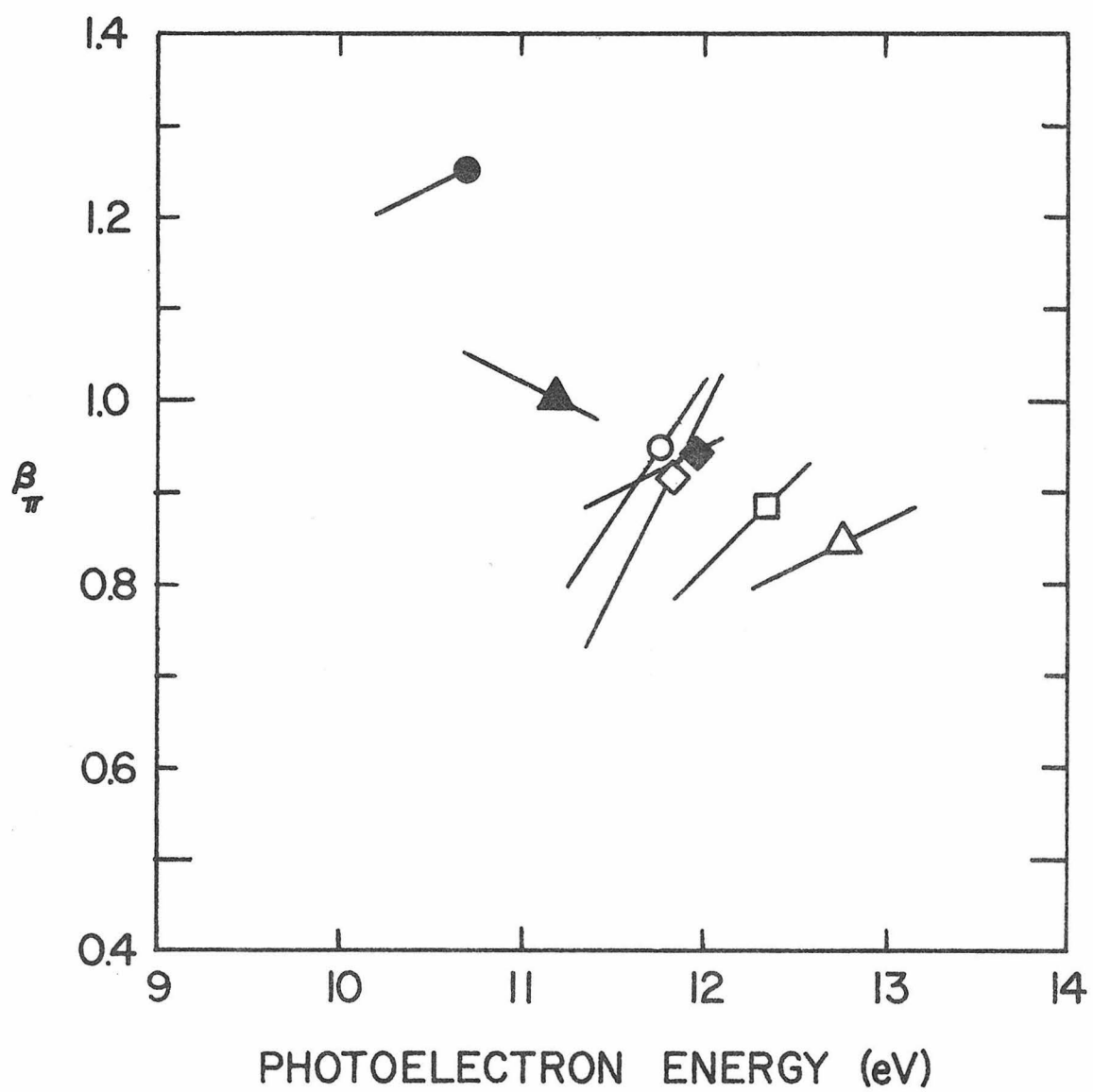


Figure 6.1-11

6.2 Paper IV - Variable Angle Photoelectron Spectroscopy
of Allene, 1,3-Butadiene, 1,4-Pentadiene, and 1,5-Hexadiene

Variable Angle Photoelectron Spectroscopy of Allene,
1,3-Butadiene, 1,4-Pentadiene, and 1,5-Hexadiene

Using a HeI line source lamp, photoelectron angular distributions were measured for a series of di-olefins. In the case of allene, we propose the ordering $2e$, $3b_2$, $1e$ for the three lowest lying orbitals on the basis of a deconvolution of the band in the ionization potential range 14-16.5 eV. A re-examination of 1,3-butadiene supports the π , π , σ energy ordering of low lying molecular orbitals. The variation of the asymmetry parameter, β , across the $\sigma 2p$ region in the photoelectron spectra of 1,4-pentadiene and 1,5-hexadiene supports an earlier notion that through-space interaction of the π -bonds dominates through-bond interaction. Spectra of the π region taken at higher sensitivity than previously suggests that the interaction between π moieties decreases in going from 1,4-pentadiene to 1,5-hexadiene.

INTRODUCTION

The kinetic energy analysis of photoelectrons, as Turner has discussed,¹ encouraged a fresh view of the electronic structure of molecules. In the orbital approximation, each band in the spectrum of a closed shell molecule corresponds to the ionization of an electron from one of the occupied molecular orbitals. Too frequently, however, the overlap of neighboring bands has hindered spectral assignments. For complex polyatomic molecules, the experimentalist needs another degree of freedom besides knowledge of peak positions and resolution of vibrational fine structure in order to explicate his spectra.

We² and several other groups³⁻⁵ have found the angular distributions of photoelectrons a sensitive probe of molecular electronic structure. Briefly, for non-polarized light, the angular distribution must take the following form:⁶

$$\frac{d\sigma}{d\Omega} = \frac{Q}{4\pi} \left[1 - \frac{\beta}{4} (3\cos^2\theta - 1) \right], \quad (1)$$

where Q is the total cross section, θ is the angle between the light axis and the velocity vector of the outgoing photoelectron, and β is a single asymmetry parameter. The asymmetry parameter, β , ranges between -1 and +2 and describes the deviation from isotropy. The value of β depends on the electronic structure of initial neutral and final ionic states and on the energy of the outgoing photoelectron (and thus upon the wavelength of the incident photon).

In a previous publication from this laboratory,⁷ we suggested several empirical rules for explicating photoelectron spectra based upon regularities in the variation of the asymmetry parameter β for HeI photoelectron spectra of the series of methyl-substituted ethylenes. The dependence of β on electron energy can be inferred from the dependence of β on ionic vibrational excitation for a given band. The possibility of autoionization must be eliminated for this to hold rigorously. A second rule pertains to closely lying photoelectron bands, where each corresponds to the loss of electrons from orbitals of similar character. Here, the energy dependence of β for any band in the series can be inferred from β measured at the vertical ionization potential of all ionization bands in the series. Energy dependence of β may be extrapolated a limited distance.

Mixing between orbitals of different types, as σ/π hyperconjugation, displaces the corresponding β values from those values obtained from unmixed systems. Measured β values lie intermediate between those of unmixed types. The extent of displacement, where it can be measured, serves as a gauge of the interaction.

In this paper, we present results for the HeI photoelectron angular distributions of a set of four dienes: allene, 1,3-butadiene, 1,4-pentadiene, and 1,5-hexadiene. We expected that this set of compounds would present a variety of molecular electronic structures and bond-bond interactions which could be analyzed profitably from the standpoint of the empirical rules listed above.

EXPERIMENTAL

Photoelectron angular distributions were measured with a windowless helium glow discharge lamp (majority emission at 584 Å) and a rotatable electron energy analyzer. Photoelectron angular distributions are measured with the aid of a minicomputer-based data acquisition system built around a DEC PDP8/e. Details of the design and construction of our apparatus were given in previous publications.^{7,8}

Spectra were taken at an analyzing energy of 1.5 eV and corresponding resolution of 30-35 meV FWHM, as measured at the Argon $^2P_{3/2}$ peak. Spectra were energy calibrated with the argon $^2P_{3/2}$ peak at 15.759 eV⁹ ionization potential.

Spectral intensities were measured at each of nine detector angles in 10° increments from 40° to 120° with respect to the light axis. Intensities were then fitted to Eq. 1 by expression:

$$I(\theta) \propto 1 - \frac{\beta}{4} (3 \cos^2 \theta - 1), \quad (2)$$

where $I(\theta)$ is photoelectron intensity corrected for the volume of intersection of the lamp and detector view cones at each θ and compensated for the linear variation of counting rate with sample pressure. Photoelectron intensity is also corrected for an energy parameterized background which is different at each detector angle. Photoelectron angular distributions were measured over at least a 10 eV range starting below the first adiabatic ionization potential. Intensities at

electron energies corresponding to ionization potentials above 19 eV were in general too low for the sample molecules for adequate signal to background ratios.

Sample materials were obtained from the following sources and at the minimum purities indicated in parentheses: allene (Matheson, 97%), 1,3-butadiene (Matheson, instrument grade 99.5%), 1,4-pentadiene (Aldrich, 99%), and 1,5-hexadiene (Aldrich, 98%). The spectra of allene and 1,3-butadiene are identical in all respects to published high resolution spectra.⁸ Photoelectron spectra for these four compounds are presented in Figs. 1-4.

Liquid samples were degassed by several freeze-pump-thaw cycles before use. Gas samples were distilled into a liquid nitrogen immersed cold finger from the gas cylinder and were further degassed by several freeze-pump-thaw cycles. The glass manifold which constituted the inlet system was baked in a glassblower's annealing oven between successive samples in order to avoid cross contamination.

RESULTS

Allene

The high resolution spectrum of allene was first published in 1969.¹⁰ The spectrum consists of three distinct bands. Previous and present experimental results are included in Table I. The band at lowest ionization potential corresponds to ionization from the degenerate pair of perpendicular π orbitals. The lack of regular vibrational structure in the latter half of the band and the pronounced double peaking have been attributed to Jahn-Teller distortion of the ion.^{10,11} The second broad band which starts at an adiabatic ionization potential of 14.10 eV consists of two overlapping features, as has been suggested by a number of theoretical treatments.^{12,13} The only vibrational fine structure in this region, measured as 1090 cm^{-1} by Turner,¹⁰ is attributed to a CH_2 scissors deformation in the corresponding ion. Thus, the corresponding molecular orbital depopulated by photoionization must have some CH bonding character. On the basis of its peak position, the weak band at 17.4 eV vertical ionization potential probably corresponds with significant carbon 2s character.

Measured β values for the first band are typical of the ionization from a π orbital. The variation of β across this band is slight and contradicts any suggestion that the complexity of observed vibrational structure is due to autoionization. The value measured for the second ionization band decreases rapidly from a value of

0.65 for early members of the vibrational progression to a value of 0.10 for the second component within the band.

We have deconvoluted the band which lies between 14-16.5 eV according to the following prescription. Let photoelectron intensity in a region of overlap be the sum of two contributions:

$$I(\theta) = I_1(\theta) + I_2(\theta) = \frac{Q_1}{4\pi} \left[1 - \frac{\beta_1}{2} P_2(\cos \theta) \right] + \frac{Q_2}{4\pi} \left[1 - \frac{\beta_2}{2} P_2(\cos \theta) \right], \quad (3)$$

where 1 and 2 index the total cross sections and asymmetry parameters for the ionization of electrons from two different molecular orbitals. Assume that the variation of β with ionic vibrational excitation (and photoelectron energy) in the band can be neglected in comparison to the variation due to band overlap. Then the measured total cross section and asymmetry parameters in Eq. 1 will be:

$$Q = Q_1 + Q_2 \quad (4a)$$

$$\beta = \frac{\beta_1 Q_1 + \beta_2 Q_2}{Q_1 + Q_2} \quad (4b)$$

Measurement of β across a broad photoelectron band can furnish the ratio Q_1/Q_2 :

$$\frac{Q_1}{Q_2} = \frac{\beta - \beta_2}{\beta_1 - \beta}, \quad (5)$$

providing that β_1 and β_2 can be extracted from a spectral region

where mixing can be presumed small. Intensities of the two overlapping components can be isolated, providing the variation of Q_1/Q_2 across a band is known and a spectrum taken at $\theta = 54.7^\circ$ is available. Current reproducibility and sensitivity does not allow vibrational fine structure to be resolved in a region of overlap of two bands where both have closely spaced strong character.

Figure 5 shows a deconvolution of the band between 14-16.5 eV. In making the deconvolution, we assumed that β takes constant values of 0.65 for all vibrational structure in the first components and 0.10 for all structure in the second component. The two components have the intensity ratio 1:2.4. On the basis of our deconvolution, Table I gives experimental vertical ionization potentials of the two components in this band for the first time.

1,3-butadiene

The high resolution photoelectron spectrum of 1,3-butadiene first appeared in 1969.¹⁴ Extensive theoretical^{15,16} and experimental^{17,18} work assigns the bands at lowest ionization potential as removal of electrons from orbitals in the order, π, π, σ . Previous workers had proposed the ordering π, σ, π ,^{14,19} but a re-examination^{17,20} of experimental results supports the π, π, σ ordering. Figure 2 show the photoelectron spectrum of 1,3-butadiene taken at a detector angle of 54.7° . Measured β values are in generally good agreement with those reported by White, et al.¹⁸ earlier. However, we measure a reproducible β value of 0.35 ± 0.10

for the 18.5 eV band corresponding to an orbital with extensive carbon 2s character, in gross disagreement with the value measured earlier. A summary of experimental vertical ionization potentials and β values appears in Table II.

The second and third bands are deconvoluted in Fig. 6, assuming that β for each component does not vary over the region of band overlap. The resulting bands are roughly of comparable area.

The first ionization band bears strong resemblance to the corresponding band of ethylene, so the influence of autoionization is presumed small.

1,4-pentadiene

The full spectrum of 1,4-pentadiene appears here for the first time in Fig. 3. A list of vertical ionization potentials and experimental β values appears in Table III. A spectrum of the π region at lowest ionization potential was reported earlier by Bünzli, et al.,²¹ but vibrational structure was not as well resolved as in the present work. The π region contains two maxima, corresponding to ionizations from π_+ and π_- linear combinations of the double bonds. Vibrational frequencies of $1200 \pm 50 \text{ cm}^{-1}$ and $1500 \pm 50 \text{ cm}^{-1}$ are seen in the first and second components, respectively, probably corresponding to CC stretching frequencies.

A structureless series of overlapping bands lies between the vertical ionization potentials of 11.3-17 eV. By analogy to similar structure seen in the set of methyl-substituted ethylenes, the corre-

sponding molecular orbitals are assigned as $\sigma 2p$ and contain unspecified amounts of CH and CC bonding character. Definitive assignments in the $\sigma 2p$ region are difficult, except in cases where there is a high degree of symmetry and orbital degeneracy reduces the number of bands.

On the basis of comparisons to other olefins and dienes, we assign the structure near 18 eV vertical ionization potential to ionizations of the carbon 2s type. The band is slightly double peaked so that two electronic states may lie in this spectral region.

The molecule is probably non-planar. Bünzli, *et al.*²¹ suggest that the equilibrium neutral geometry probably belongs to point group C_s , based upon their Extended Hückel calculation.

Measured β values decrease over the π region with increasing ionization potential at a rate of 0.15 ± 0.05 units/eV. Thereafter, β in the $\sigma 2p$ region rises smoothly over the entire range.

1,5-hexadiene

The spectrum of 1,5-hexadiene resembles that of 1,4-pentadiene very closely. The full spectrum of 1,5-hexadiene appears here in Fig. 4 for the first time. Vertical ionization potentials and experimental β values are listed in Table IV. A spectrum of the π region at lowest ionization potential was reported earlier by Bünzli, *et al.*,²¹ but again at lower sensitivity.

The π region contains two maxima, corresponding to ionizations from π_+ and π_- linear combinations of the double bonds.

Vibrational fine structure is seen in the first ($1050 \pm 50 \text{ cm}^{-1}$) and second ($1500 \pm 50 \text{ cm}^{-1}$) component of the band. The structure probably corresponds to excitation of CC stretching modes in the molecular ion.

The $\sigma 2p$ region is slightly broader than that encountered in 1,4-pentadiene. A featureless carbon $\sigma 2s$ band lies near 18 eV vertical ionization potential.

In the π region, β values decrease at a rate of 0.15 ± 0.05 units/eV, comparable to the value observed in 1,4-pentadiene. Thereafter, β rises gradually over the entire $\sigma 2p$ region. In the carbon 2s region β is roughly constant.

The calculations of Bünzli, et al.²¹ suggest that the equilibrium neutral geometry is non-planar and that the molecule probably belongs to the point group C_2 .

DISCUSSION

In the absence of autoionization, the variation of β across vibrational envelopes should reflect the variation of β with respect to electron energy.⁷ Table V lists the variations of β across non-overlapping π bands for the four dienes discussed here. In general, the variation does not exceed 0.3 units/eV and is consistent with the behavior seen in methyl substituted ethylenes.^{7,18} For π ionizations, β increases with increasing electron energy. For $\sigma 2p$ ionizations, bands corresponding to different ionic states overlap too much for the variation of β across single isolated bands to be measured. For $\sigma 2s$ ionizations, β is constant with electron energy or else increases very slightly with increasing electron energy.

That the variation of β with vibrational level of the b_g band of 1,3-butadiene can be smoothly extrapolated to the a_u band is in good agreement with data presented earlier by White, et al.¹⁸

Figure 7 summarizes the variation of β in the $\sigma 2p$ ionization region with increasing electron energy for the series of olefins studied here and previously.^{7,18} Measured β values for the $\sigma 2p$ region presented here for 1,3-butadiene, 1,4-pentadiene, and 1,5-hexadiene vary roughly linearly over the electron energy range from 6-10 eV. The slope, -0.11 units/eV, is the same as for the $\sigma 2p$ structure of the methyl substituted ethylenes.⁷ The lines lie practically within experimental error of each other.

The measured β for the third ionization band of 1,3-butadiene

at 12.4 eV is markedly lower than that of the first two bands at 9.1 eV and 11.7 eV, as was noticed by White, *et al.*¹⁸ On this basis, they assigned the bands as removal of electrons from orbitals in the order π , π , σ . An additional justification for the $\pi\pi\sigma$ ordering emerges. The value of β at the vertical ionization potential of the third band places it along an extrapolation of the $\sigma 2p$ line, rather than an extrapolation from the vibrational dependence of β from the first π band.

The splitting between π_+ and π_- peaks, in no specified order yet, decreases in going from 1,4-pentadiene to 1,5-hexadiene, as shown in Fig. 8. Bünzli, *et al.*²¹ found the opposite trend with spectra taken at a lower apparatus sensitivity. We observe no anomalous variation in β over the $\sigma 2p$ region for either compound. Variation of β for $\sigma 2p$ ionizations can be attributed completely to natural energy variation, to the sensitivity limits of our apparatus. Earlier studies of methyl substituted ethylenes revealed that hyperconjugation or through-bond mixing of π and σ structures is reflected in anomalous changes in β in the $\sigma 2p$ region. That we see no effect for 1,4-pentadiene and 1,5-hexadiene here suggests that hyperconjugation is relatively weak in the through-bond coupling of the two double bonds. We conclude that the decrease in π_+/π_- splitting in going from 1,4-pentadiene to 1,5-hexadiene is principally due to decreased through-space coupling. This suggests a greater spatial separation or less favorable overlap between the two interacting double bonds in the case of 1,5-hexadiene. Therefore, the π_- linear combination of

the π orbitals gives rise to the lower of the two ionization potentials observed for both non-conjugated dienes.

Among the set of dienes discussed here, β in the 2s region, 0.35 - 0.6, lies in the same range as that observed in the set of methyl-substituted ethylenes.^{7,18}

Allene deserves to be discussed separately, because the variation of β in the σ 2p region does not fit easily into the pattern of the other dienes or the substituted ethylenes. The β value measured at the vertical ionization potential of the first band is typical of π ionizations. That measured for the carbon σ 2s region lies within the range observed in the set of substituted ethylenes and dienes. However, β decreases with increasing ionization potential over the band between 14-16.5 eV. Normally, β in the carbon σ 2p region increases with increasing ionization potential.

In the 14-16.5 eV range of ionization potentials, previous theoretical work^{12,13} predicted two electronic states of the ion, those arising from ionization of electrons from the 1e and 3b₂ orbitals. The 1e results from mixing of the anti-symmetric combination of CH σ bonds on one carbon with the π orbital on the other two carbon atoms.¹² The two antisymmetric combinations lie at right angles with respect to each other and are thus degenerate. The 3b₂ results from mixing of the symmetric combinations of CH bonds on the two outer carbon centers with a carbon 2p_z on the middle carbon, where the C-C-C axis is taken to be the symmetry z axis. The 3b₂ orbital

is non-degenerate.

Deconvoluted peak intensities should be roughly in the ratio of degeneracies of the ion, for ionizations of molecular orbitals of similar character.^{22,23} The 2.4:1 observed ratio is thus consistent with the orbital ordering $2e, 3b_2, 1e$. Table VI summarizes the results of Lindholm's SPINDO¹² and several ab initio calculations.¹³

Significantly, all of the calculations, after applying Koopmans' Theorem, predict the orbital ordering $2e, 1e, 3b_2$ or predict that the $1e$ and $3b_2$ orbitals will be degenerate. Requiring the $2e, 1e, 3b_2$ ordering unreasonably necessitates that the transition probability for the $3b_2$ orbital ionization be roughly 5 times that of the $1e$ orbital ionization. Electron energy discrimination effects in the electron energy analyzer should be minor for such a narrow range of electron energies.

The β value of the first component of the 14-16.5 eV band is typical of the unmixed $\sigma 2p$ ionizations of the other olefins and diolefins at a comparable electron energy.⁷ The value measured for the other component of the 14-16.5 eV band, if the $2e, 3b_2, 1e$ ordering is correct, should reflect extensive mixing with the π orbital. In our earlier study of methyl-substituted ethylenes,⁷ the magnitude of an anomalous drop in β for the $\sigma 2p$ region could be correlated with the extent of mixing predicted by a simple "linear combination of bonding orbitals" model. Molecular geometry favors extensive mixing in the case of allene. The CC bonds are shorter (1.308 \AA)²⁴ than in

ethylene (1.337 \AA)²⁵, and thus, through-bond π/σ interactions are expected to be very substantial. The value of β for the unmixed CC π bond is probably near 0 for this range of electron energy, if analogies can be made to the methyl substituted ethylenes.⁷

Thus, on the basis of the mixing model and knowledge of the molecular geometry alone, we conclude that the second component in the 14-16.5 eV band arises from ionization from the 1e orbital. We also conclude that extensive mixing of a methylene group with a π orbital on the other two carbons is responsible for the low value of β we observe here.

Neither the band intensity argument nor the mixing model based on photoelectron angular distributions has yet accounted for the distinct vibrational fine structure observed on the low ionization potential edge of the 14-16.5 eV band. The structure indicates that the corresponding molecular orbital must have significant amounts of CH bonding character. This requirement is satisfied if the molecular orbital contains either symmetric or antisymmetric combinations of CH bonding character. Thus, both orbital orderings (2e, 3b₂, 1e or 2e, 1e, 3b₂) are consistent with the observed vibrational fine structure.

CONCLUSION

We have analyzed the photoelectron angular distributions of a collection of dienes within a model based on an earlier study of methyl substituted ethylenes. On the basis of the model and considerations of molecular geometries and deconvoluted band intensities, we propose a re-ordering of the ionic states of allene. The $\pi\pi\sigma$ ordering of the ionization potentials of 1,3-butadiene is consistent with the model. The model suggests that through-bond interactions between the two double bonds of 1,4-pentadiene and 1,5-hexadiene are small. Thus, the π_- linear combination has the lower ionization potential for both compounds. The decrease in π_+/π_- splitting on going from 1,4-pentadiene to 1,5-hexadiene reflects decreasing through-space interaction.

We expect that the present model will be useful in studies of a wide range of hydrocarbons. We apply it cautiously, knowing that only angular distribution measurements over a wide range of photon energies can confirm the correctness of the model and the validity of our conclusions based upon the model.

REFERENCES

1. D. W. Turner in P. Hepple (editor) Molecular Spectroscopy (Institute of Petroleum, London, 1968) p. 209.
2. D. C. Mason, A. Kuppermann, D. M. Mintz, in D. A. Shirley (editor) Electron Spectroscopy (North Holland, Amsterdam, 1972) p. 269; D. M. Mintz, A. Kuppermann, in Proceedings, IX ICPEAC, 1975.
3. T. A. Carlson, G. E. McGuire, A. E. Jonas, K. L. Cheng, C. P. Anderson, C. C. Lu, B. P. Pullen, in D. A. Shirley (editor) op. cit., p. 207.
4. A. Niehaus, M. W. Ruf, in L. Branscomb (editor) Electronic and Atomic Collisions (North Holland, Amsterdam, 1971) p. 167.
5. J. A. Kinsinger, J. W. Taylor, Int. J. Mass Spectrom. Ion Phys. 10, 445 (1972).
6. J. Cooper, R. N. Zare, in S. Geltman, K. Mahanthappa, N. Brittin (editors) Lectures in Theoretical Physics Vol. XI-C (Gordon and Breach, New York, 1969) p. 317
7. D. M. Mintz, A. Kuppermann, submitted J. Chem. Phys.
8. D. M. Mintz, D. C. Mason, A. Kuppermann, submitted Rev. Sci. Instrum.
9. D. W. Turner, C. Baker, A. D. Baker, C. R. Brundle Molecular Photoelectron Spectroscopy (Wiley-Interscience, London, 1970).
10. C. Baker, D. W. Turner, Chem. Commun. 480 (1969).

11. F. Brogli, J. K. Crandall, E. Heilbronner, E. Kloster-Jensen, S. A. Sojka, J. Electron Spectr. 2, 455 (1973); E. Haselbach, Chem. Phys. Lett. 7, 428 (1970).
12. E. Lindholm, C. Fridh, L. Åsbrink, Faraday Disc. Chem. Soc. 54, 127 (1972).
13. a) R. J. Buenker, J. Chem. Phys. 48, 1368 (1968).
b) S. D. Peyerimhoff, R. J. Buenker, Theor. Chim. Acta 14, 305 (1969).
c) L. J. Schaad, L. A. Burnelle, K. P. Dressler, Theor. Chim. Acta 15, 91 (1969).
d) J. M. André, M. C. André, G. Leroy, J. Weiler, Int. J. Quant. Chem. 3, 1013 (1969).
14. J. H. D. Eland, Int. J. Mass.Spectrom. Ion Phys. 2, 471 (1969).
15. a) R. J. Buenker, J. L. Whitten, J. Chem. Phys. 49, 5381 (1968).
b) B. Dumbacher, Theor. Chim. Acta 23, 346 (1972).
c) L. Åsbrink, C. Fridh, E. Lindholm, J. Amer. Chem. Soc. 94, 5501 (1972).
16. F. Brogli, E. Heilbronner, Theor. Chim. Acta 26, 289 (1972).
17. M. Beez, G. Bieri, H. Bock, E. Heilbronner, Helv. Chim. Acta 56, 1028 (1973).
18. R. M. White, T. A. Carlson, D. P. Spears, J. Electron Spectr. 3, 59 (1974).
19. C. R. Brundle, M. B. Robin, J. Amer. Chem. Soc. 92, 5550 (1970); M. J. S. Dewar, S. D. Worley, J. Chem. Phys. 49,

- 2454 (1968); R. Sustmann, R. Schubert, Tet. Lett. 2739 (1972).
20. C. R. Brundle, M. B. Robin, N. A. Kuebler, H. Basch, J. Amer. Chem. Soc. 94, 1451 (1972).
 21. J. C. Bünzli, A. J. Burak, D. C. Frost, Tetrahedron 29, 3735 (1973)
 22. W. C. Price in P. Hepple (editor) op. cit. p. 221.
 23. D. Betteridge, M. Thompson, J. Mol. Struct. 21, 341 (1974).
 24. A. G. Maki, R. A. Toth, J. Mol. Spect. 17, 136 (1965).
 25. J. L. Carlos, Jr., S. H. Bauer, J. Chem. Soc., Faraday II 70, 171 (1974).

TABLE I. Allene

Vertical I. P. (eV)	Orbital ^a	Description	β
10.05	2e	π	0.70 ± 0.05^c
14.51 ^b	3b ₂	σ 2p	0.65 ± 0.05^d
15.6 ^b	1e	σ 2p; π (CH ₂)	0.10 ± 0.05^d
17.38	4a ₁ ^e	σ 2s	0.55 ± 0.10^c
19.5 ^f	2b ₂ ^e		

^aIn point group D_{2d}.

^bBased upon deconvolution of 14-16.5 eV region.

^cMeasured at vertical ionization potential.

^dMeasured away from the vertical ionization potential in a region where β is stationary.

^eOrdering from Ref. 12.


^fWeak structure seen in Ref. 10.

TABLE II. 1,3-Butadiene

Vertical I. P. (eV)	Orbital ^a	Description	β^b
9.07	1b _g	π	1.10 ± 0.05 (0.95)
11.54	1a _u	π	0.80 ± 0.05 (0.75)
12.26	7a _g	σ 2p	0.15 ± 0.05 (0.10)
13.52	6b _u , 6a _g	σ 2p	0.25 ± 0.05 ^c , 0.35 ± 0.05 ^d (0.10)
15.32	5a _g , 5b _u	σ 2p	0.35 ± 0.05 ^c , 0.35 ± 0.05 ^d (0.35)
17.81	4b _u	σ 2s	0.35 ± 0.10 (1.4)

^aFrom Ref. 15c.^b β Values from Ref. 18 in parentheses.^cFirst component of band.^dSecond component of band.

TABLE III. 1,4-Pentadiene

Vertical I. P. (eV)	Orbital ^a	Description	β^b
9.61	$a''; \pi_-$	π	0.80 ± 0.05
10.14	$a'; \pi_+$	π	0.75 ± 0.05
11.96	 a', a''	$\sigma 2p$	0.10 ± 0.05
12.44		$\sigma 2p$	0.20 ± 0.05
13.29		$\sigma 2p$	0.30 ± 0.05
14.67		$\sigma 2p$	0.45 ± 0.05
15.57		$\sigma 2p$	0.50 ± 0.05
16.03		$\sigma 2p$	0.50 ± 0.10
17.99		$\sigma 2s$	0.5 ± 0.1

^aAssumes C_s point group proposed in Ref. 21.

^bMeasured at vertical ionization potential.

TABLE IV. 1,5-Hexadiene

Vertical I. P. (eV)	Orbital ^a	Description	β^b
9.59	$b; \pi_-$	π	0.90 ± 0.05
10.01	$a; \pi_+$	π	0.75 ± 0.05
11.57	} a, b	$\sigma 2p$	0.15 ± 0.05
12.11		$\sigma 2p$	0.15 ± 0.05
12.74		$\sigma 2p$	0.30 ± 0.05
13.75		$\sigma 2p$	0.35 ± 0.05
14.55		$\sigma 2p$	0.40 ± 0.05
15		$\sigma 2p$	0.35 ± 0.05
15.55		$\sigma 2p$	0.40 ± 0.05
17.87		$\sigma 2s$	0.40 ± 0.10

^a Assumes C_2 point group proposed in Ref. 21.

^b Measured at vertical ionization potential.

TABLE V. Variation of β over vibrational envelopes of π bands

Sample	Orbital	$d\beta/dE$
allene	$2e$	0.10 ± 0.05
1,3-butadiene	$1b_g$	0.10 ± 0.05
1,4-pentadiene	π_+/π_-	0.15 ± 0.05
1,5-hexadiene	π_+/π_-	0.15 ± 0.05

TABLE VI. Theoretical calculations of orbital energies for the molecular orbitals of allene.

Orbital	SPINDO ^{a, b}	Form	AB INITIO ^b			
			c	d	e	f
2e	9.91	π	11.4	10.2	10.2	12.5
1e	14.49	$\sigma 2p^g$	17.6	16.7	16.4	17.8
3b ₁	14.89	$\sigma 2p^h$	17.8	16.9	16.4	19.0
4a ₁	16.78	$\sigma 2s$	20.0	19.3	19.4	21.0
2b ₁	21.96	$\sigma 2s; \sigma 2p$	27.0	26.2	26.6	27.7
3a ₁	24.02	$\sigma 2s$	30.0	29.2	30.2	30.8

^aRef. 12.

^bNegative of orbital energy listed, in eV.

^cRef. 13a.

^dRef. 13b.

^eRef. 13c.

^fRef. 13d.

^gIncludes antisymmetric combinations of CH bonds on the same terminal carbon atom.

^hIncludes symmetric combination of CH bonds on the same terminal carbon atom.

Figure 6.2-1 He I photoelectron spectrum of allene at $\theta = 54.7^\circ$ in the lower frame. The variation of β with ionization potential of spectrum features on the lower frame is shown on the upper frame.

Figure 6.2-2 He I photoelectron spectrum of 1,3-butadiene at $\theta = 54.7^\circ$ in the lower frame. The variation of β with ionization potential of spectrum features on the lower frame is shown on the upper frame.

Figure 6.2-3 He I photoelectron spectrum of 1,4-pentadiene at $\theta = 54.7^\circ$ in the lower frame. The variation of β with ionization potential of spectrum features on the lower frame is shown on the upper frame.

Figure 6.2-4 He I photoelectron spectrum of 1,5-hexadiene at $\theta = 54.7^\circ$ in the lower frame. The variation of β with ionization potential of spectrum features on the lower frame is shown on the upper frame.

Figure 6.2-5 Deconvolution of spectrum intensity for the 14-16.5 eV region of allene, based upon the variation of β with ionization potential and a spectrum taken at 54.7° . -----, intensity due to the first component of the band., intensity due to the second component of the band.

Figure 6.2-6 Deconvolution of spectrum intensity for the 11-13 eV region of 1,3-butadiene. -----, intensity due to the first com-

ponent of the band. , intensity due to the second component of the band.

Figure 6.2-7 Variation of β in the σ_{2p} region for a series of olefins and di-olefins. The series includes ethylene, isobutylene, 2-methyl, 2-butene, 2,3-dimethyl, 2-butene from Ref. 7, propylene, cis-2-butene, and trans-2-butene from Ref. 18, and 1,3-butadiene (●), 1,4-pentadiene (■), 1,5-hexadiene (◆), and allene (▲) from the present work.

Figure 6.2-8 Spectra of 1,4-pentadiene and 1,5-hexadiene taken at a detector angle of 90° .

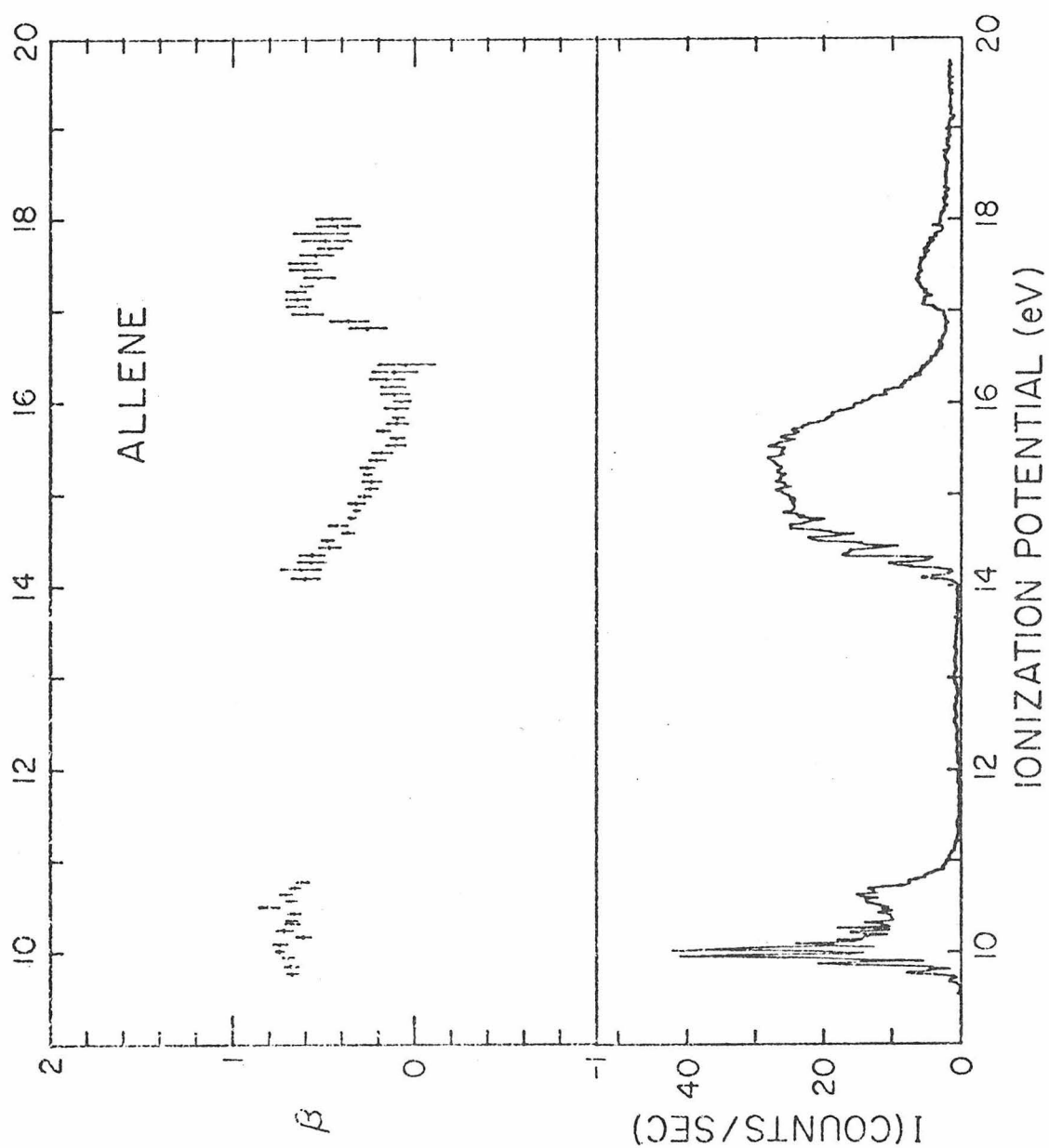


Figure 6.2-1

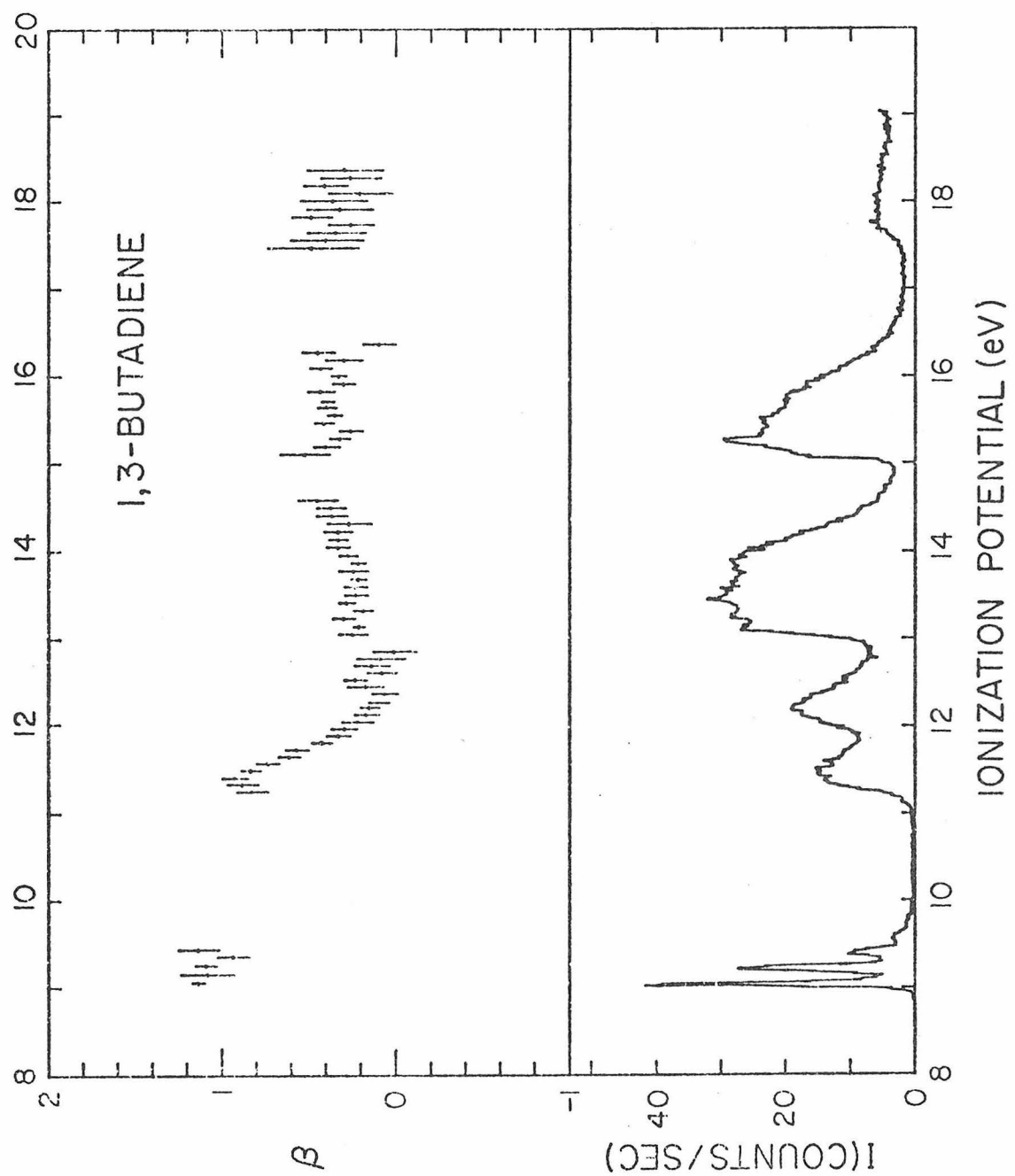


Figure 6.2-2

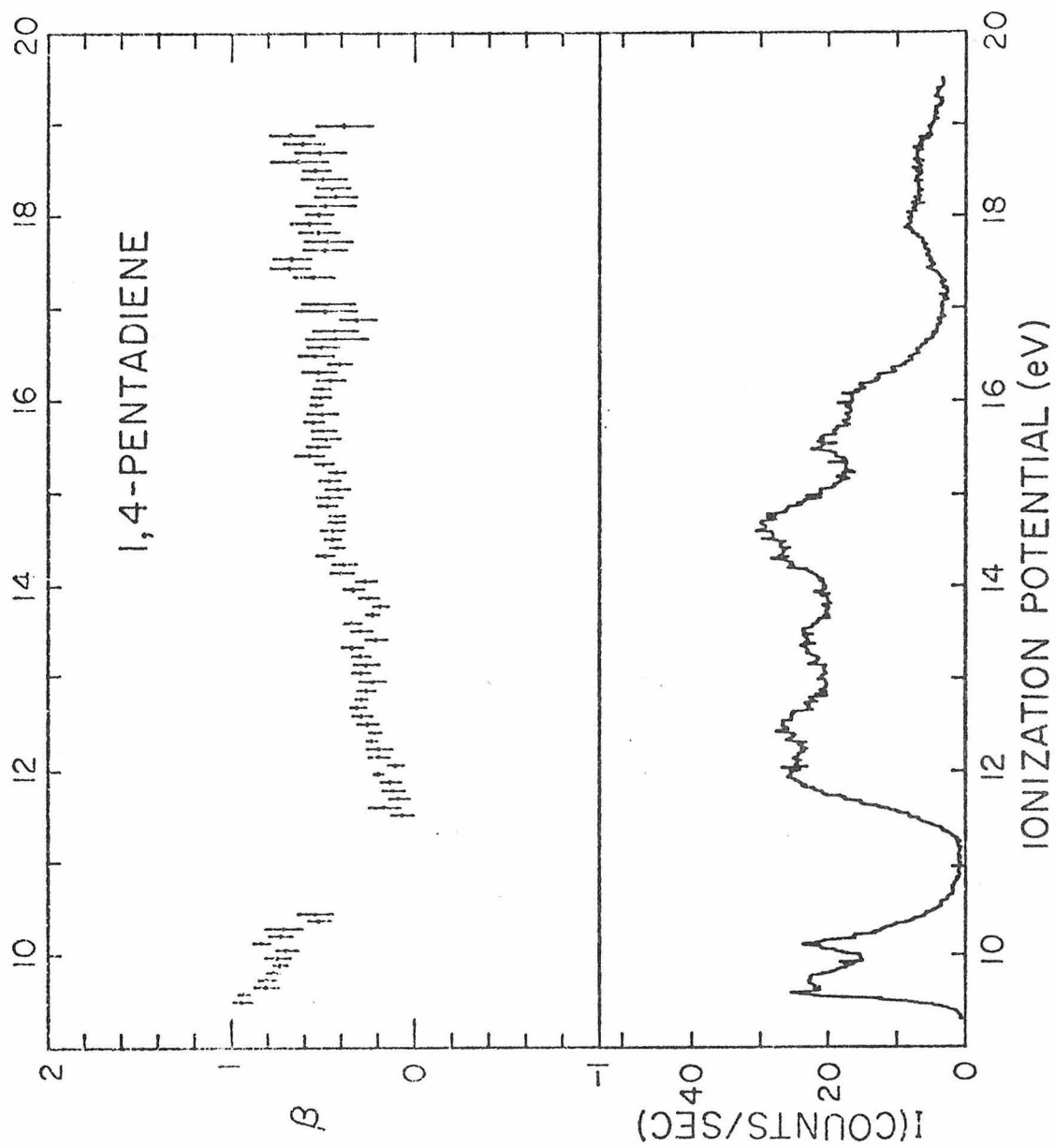


Figure 6.2-3

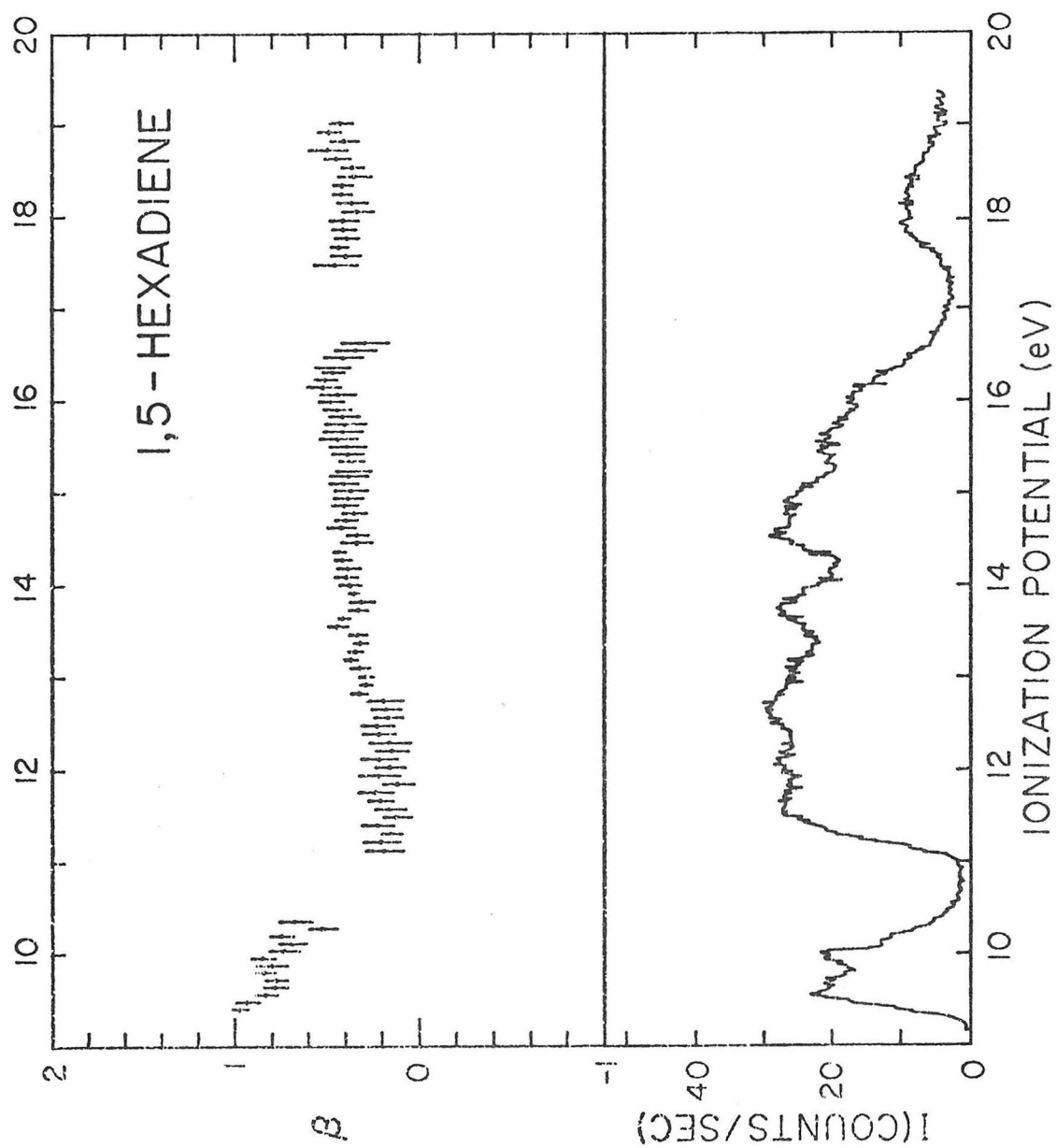


Figure 6.2-4

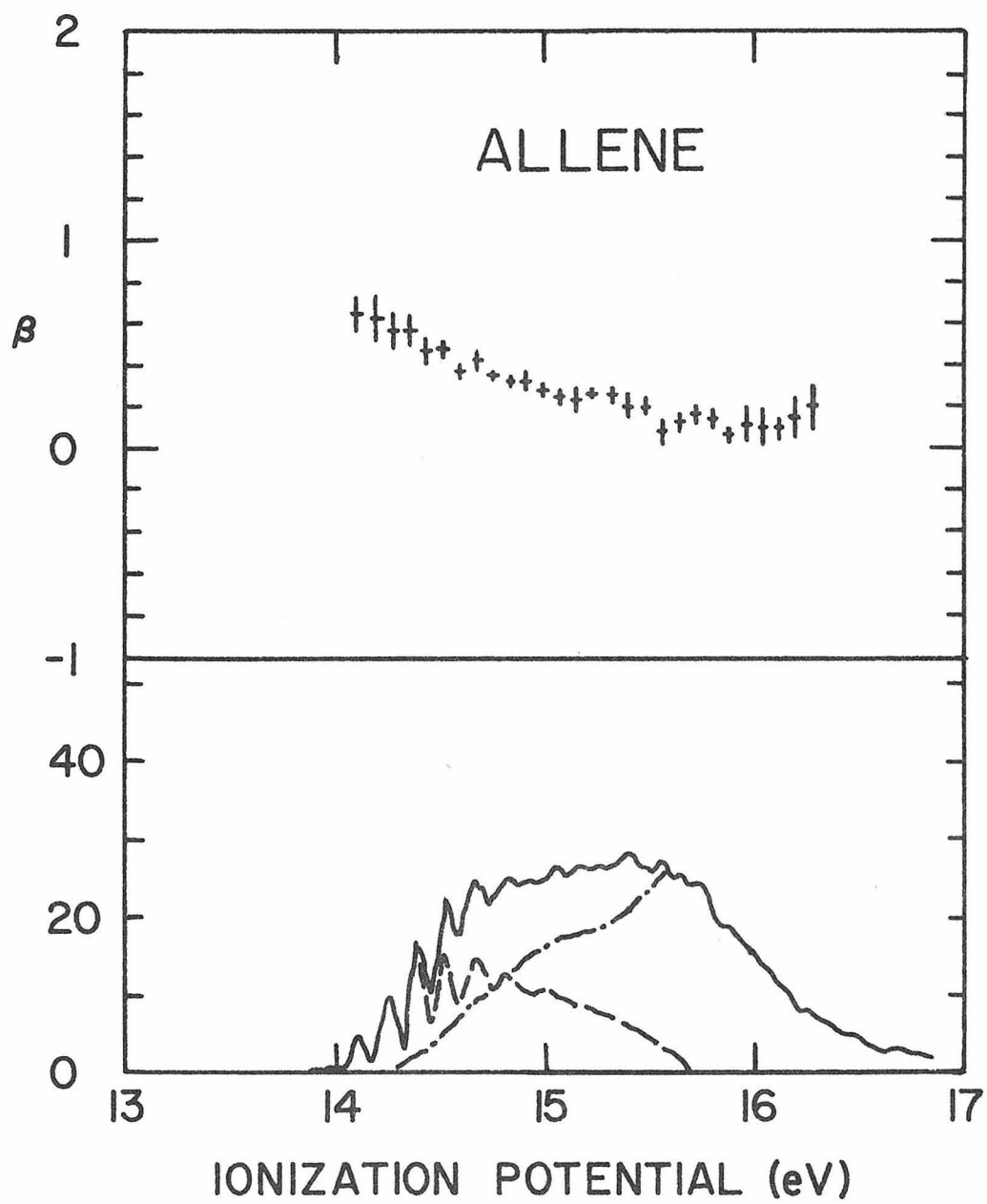


Figure 6.2-5

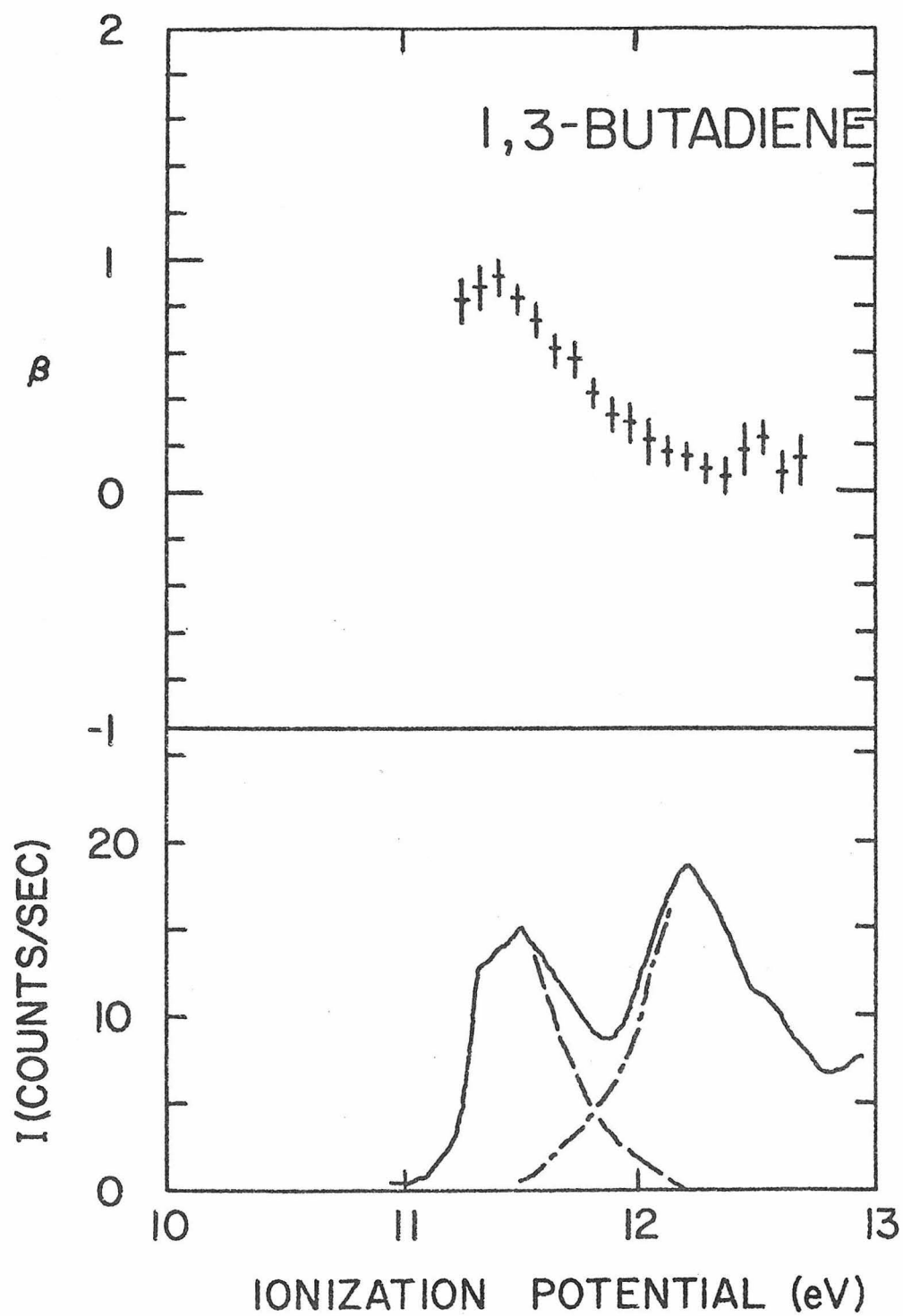


Figure 6.2-6

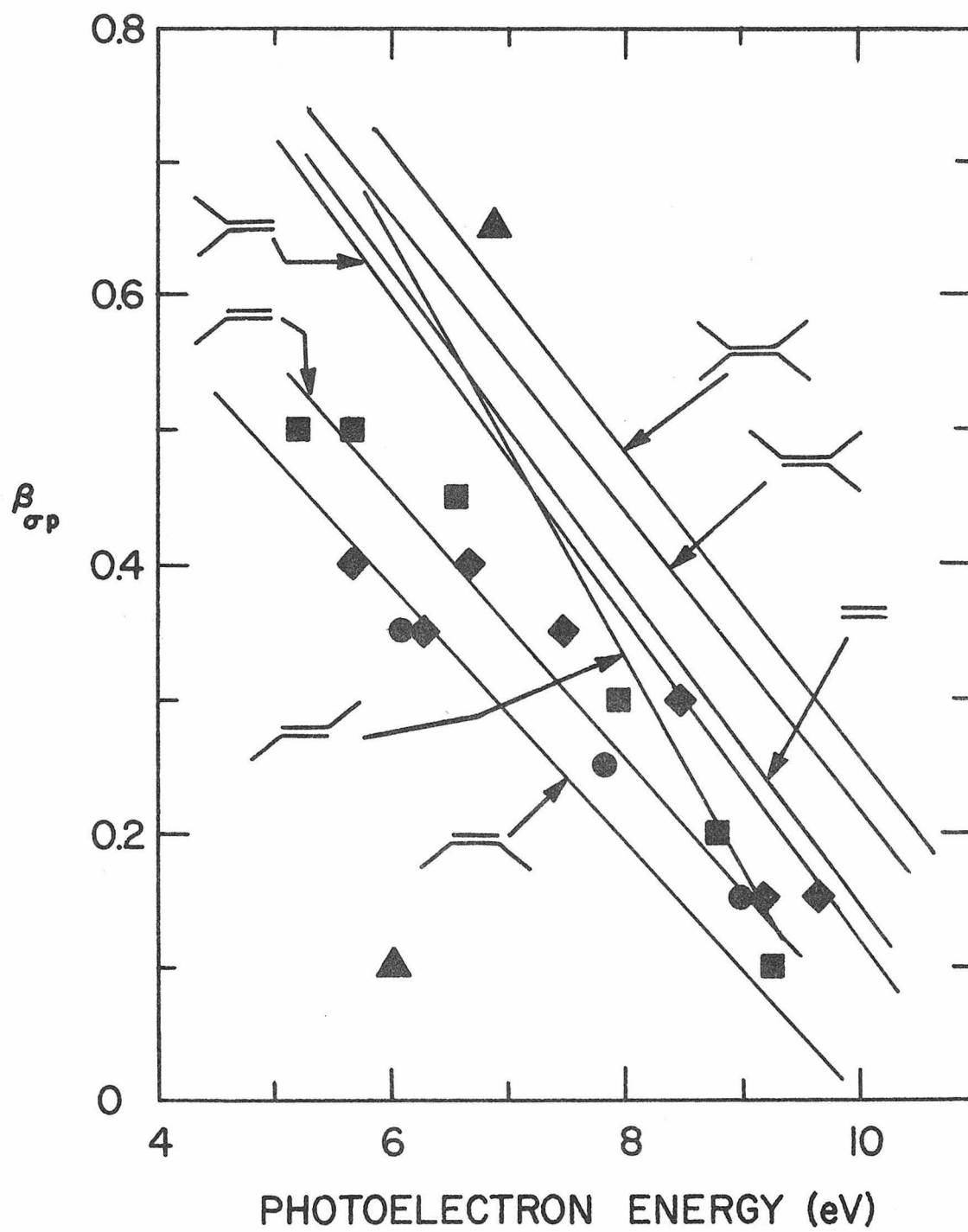


Figure 6.2-7

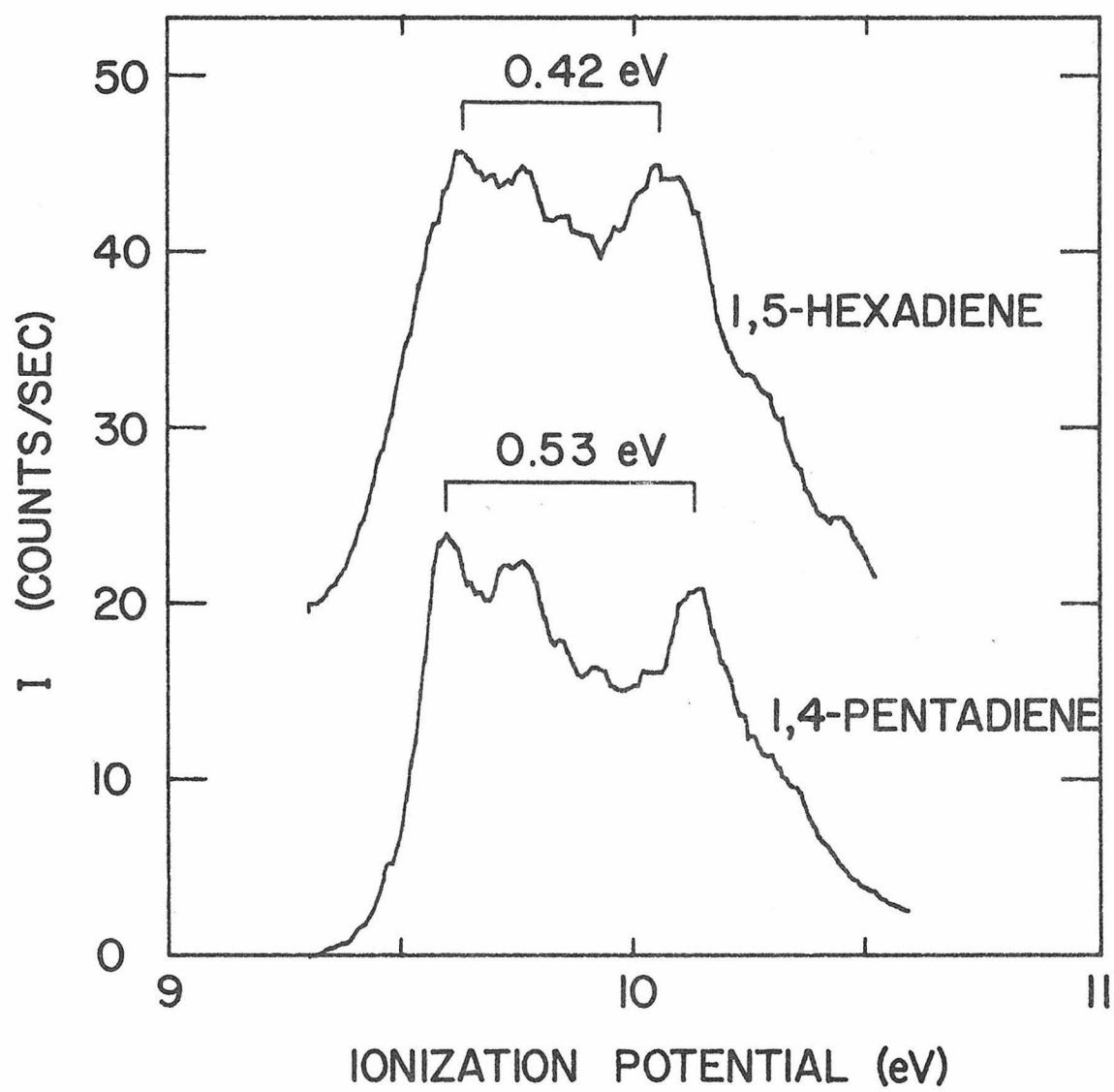


Figure 6.2-8

6.3 1,4-Cyclohexadiene

1,4-Cyclohexadiene has been used as a prototype molecule for through-bond interaction (hyperconjugation) of double bonds.¹⁻³ No orbital ordering disputes have arisen over the low-lying structure in the 584 Å photoelectron spectrum. Nevertheless, we included this compound in the present study since σ/π interactions might be expected to perturb the angular distribution β parameter for bands of mixed character.

1,4-Cyclohexadiene was obtained in 99% purity from PCR, Inc. and was degassed by repeated freeze-pump-thaw cycles in the inlet system before use. A photoelectron spectrum of the first four bands taken at a detector angle of 54.7° is given in Fig. 6.3-1. The spectrum is identical in all respects to those previously published.^{1,4} Each of the four bands was studied over 9 detector angles from 40 - 120° .

Measured β values for the first two bands are significantly higher, 0.3 ± 0.1 and 0.5 ± 0.1 , than those of the third and fourth bands, -0.4 ± 0.1 and -0.25 ± 0.10 . This is consistent with previous assignments of the first two bands as arising from π ionization¹ and the high values of β found for π ionization of other dienes.^{5,6} Experimental values rise in going from the third band to the fourth band, in agreement with previous results for σ 2p ionization. However, the β value for the second π band is significantly higher than that of the first band. This reverses the order found in the previous studies.

Figure Caption

Figure 6.3-1 Photoelectron spectrum of 1,4-cyclohexadiene, taken at a detector angle of 54.7° over 511 data channels and at a dwell time of 30 sec/channel. Variation of β for structure in the lower frame is given in the upper frame.

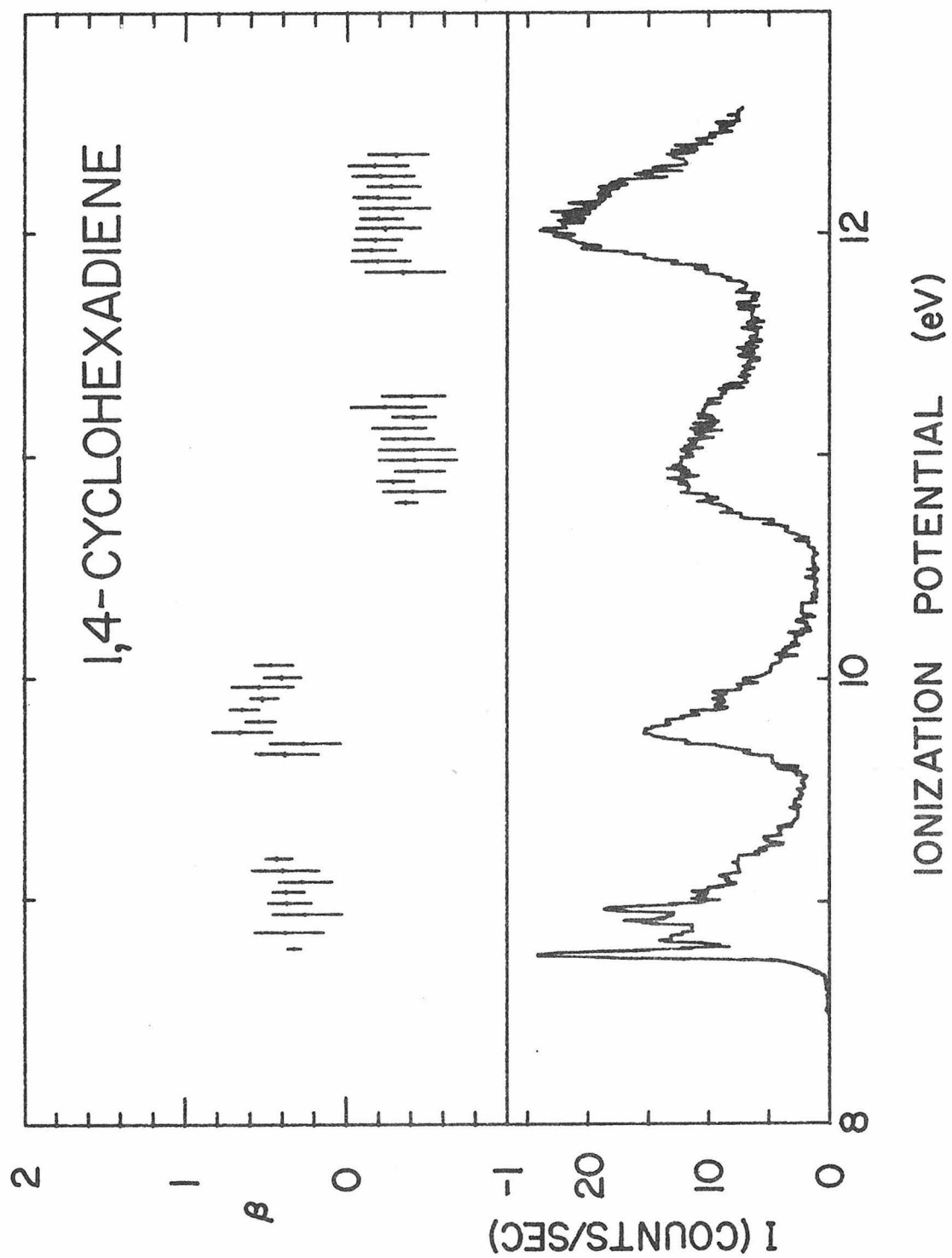


Figure 6.3-1

In paper III, a study of the methyl-substituted ethylenes, β values associated with π ionization decreased roughly monotonically upon increasing methyl substitution. At the same time, β values measured at the high ionization potential end of the $\sigma 2p$ region dropped below the otherwise linear variation in the $\sigma 2p$ region in increasing amounts upon increasing methyl substitution. Both effects were attributed to σ/π mixing of methylene subunits with the double bond.

We suggest that in the absence of interaction of the two double bonds through the bridging methylene group, β values for the first π band would be higher than that of the second π band, as in the other di-olefins. The effect of hyperconjugation, which shifts the π_+ combination of π bonds to lower ionization potential than the π_- combination,^{2,3} should also deflect β values downward for the π_+ combination. The experimental β values measured cannot be rigorously viewed as a sum of a term from π ionization and a term from σ ionization, except where the photoelectron energy is large,⁷ perhaps over 100 eV. However, this idea may have practical merit in explicating the otherwise disordered mass of data measured in angular distribution studies of olefins.

The present study examined only the first four photoelectron bands of 1,4-cyclohexadiene. We suggest that angular distribution studies at the high IP end of the $\sigma 2p$ region should be performed. By analogy to results obtained for the olefins of Paper III, hyperconjugation of the double bonds should manifest itself in a downward

discontinuity in β there. In addition, other related molecules, the series of cyclic and bridged olefins and diolefins, should be studied by the technique of variable angle photoelectron spectroscopy in order to determine whether the phenomenon reported here is general.

REFERENCES

1. P. Bischof, J. A. Hashmall, E. Heilbronner, V. Hornung, *Helv. Chim. Acta* 52, 1745 (1969).
2. R. Hoffmann, E. Heilbronner, R. Gleiter, *J. Amer. Chem. Soc.* 92, 706 (1970).
3. E. Heilbronner, *Isr. J. Chem.* 10, 143 (1972).
4. L. Åsbrink, C. Fridh, E. Lindholm, *J. Amer. Chem. Soc.* 94, 5501 (1972).
5. See paper IV.
6. R. M. White, T. A. Carlson, D. P. Spears, *J. Electron Spectr.* 3, 59 (1974).
7. J.-T. J. Huang, F. O. Ellison, *Chem. Phys.* 7, 473 (1975).

6.4 Pyridine

Low-lying structure in photoelectron spectra of many polyatomic molecules has not been fully explicated. Often bands lie closely enough in energy that assignments by conventional means are difficult. The azabenzenes have presented particular problems in band assignment. Spectral features from the ionization of π orbitals fall in the same energy range as those of the largely non-bonding (n) orbitals localized on the nitrogen atoms. Assignments based on the shapes of band envelopes have been made,^{1,2} but this procedure is extremely risky if bands overlap to a sizeable degree. Assignments based upon quantum mechanical calculations have frequently been contradictory.³⁻⁶ Assignments based upon studying series of related compounds have been made,^{7,8} are often reliable, but assume that all of the molecular electronic and steric interactions can be understood.

Previously, the angular distribution study of Ames, et al.⁹ showed that vibrational peak ratios at the two detector angles of their experiments changed over the first of the two photoelectron bands of pyridine lying at lowest ionization potential. We decided to investigate this spectral region with the present apparatus in the hope that angular distributions could be profitably interpreted in the light of previous olefin data.

Pyridine was obtained as a sample of 99+% (Spectroquality) purity from Matheson, Coleman, and Bell and was degassed by repeated freeze-pump-thaw cycles in the instrument inlet system

before use. A full spectrum of pyridine, taken at a detector angle of 54.7° , was identical in all respects to published high resolution spectra.

We present in Fig. 6.4-1 the variation of the asymmetry parameter, β , over the first two distinct photoelectron bands which lie in the 9-11 eV range of ionization potential. Angular distributions for each of the two bands were taken over a range of 9 detector angles from 40 - 120° . Experimental β values for the first band increase dramatically from -0.1 ± 0.1 to 0.45 ± 0.05 with increasing ionization potential. The experimental β value for the second band is 0.60 ± 0.05 . Ionization from a total of three valence orbitals should lie in this range of ionization potentials.^{3,4,11} Two are π orbitals and one is an n orbital.

Previously, in the photoelectron studies of 1,3-butadiene, an ordering dispute had arisen. At the same time, angular distribution studies of White, et al.¹² and Paper IV of this work found high β values for the first two bands and lower (by 0.65) β values for the third band. Over the range of other olefins studied in papers III and IV and by White, et al.,¹² π ionization gives higher β values than σ ionization in the same range of ionization potentials. This suggested the ordering π, π, σ in 1,3-butadiene and may indicate a general trend in families of hydrocarbons.

The β values of the second component of the first band and the second band are both high compared to that of the first component of the first band. Although pyridine is not a hydrocarbon, we might

Figure Caption

Figure 6.4-1 Photoelectron spectrum of pyridine, taken at a detector angle of 54.7° over 470 data channels and at a dwell time of 60 sec/channel. Variation of β for structure in the lower frame is given in the upper frame. The rise in β at the onset of the 10.5 eV band is a reproducible artifact related to the rapid change in intensity.

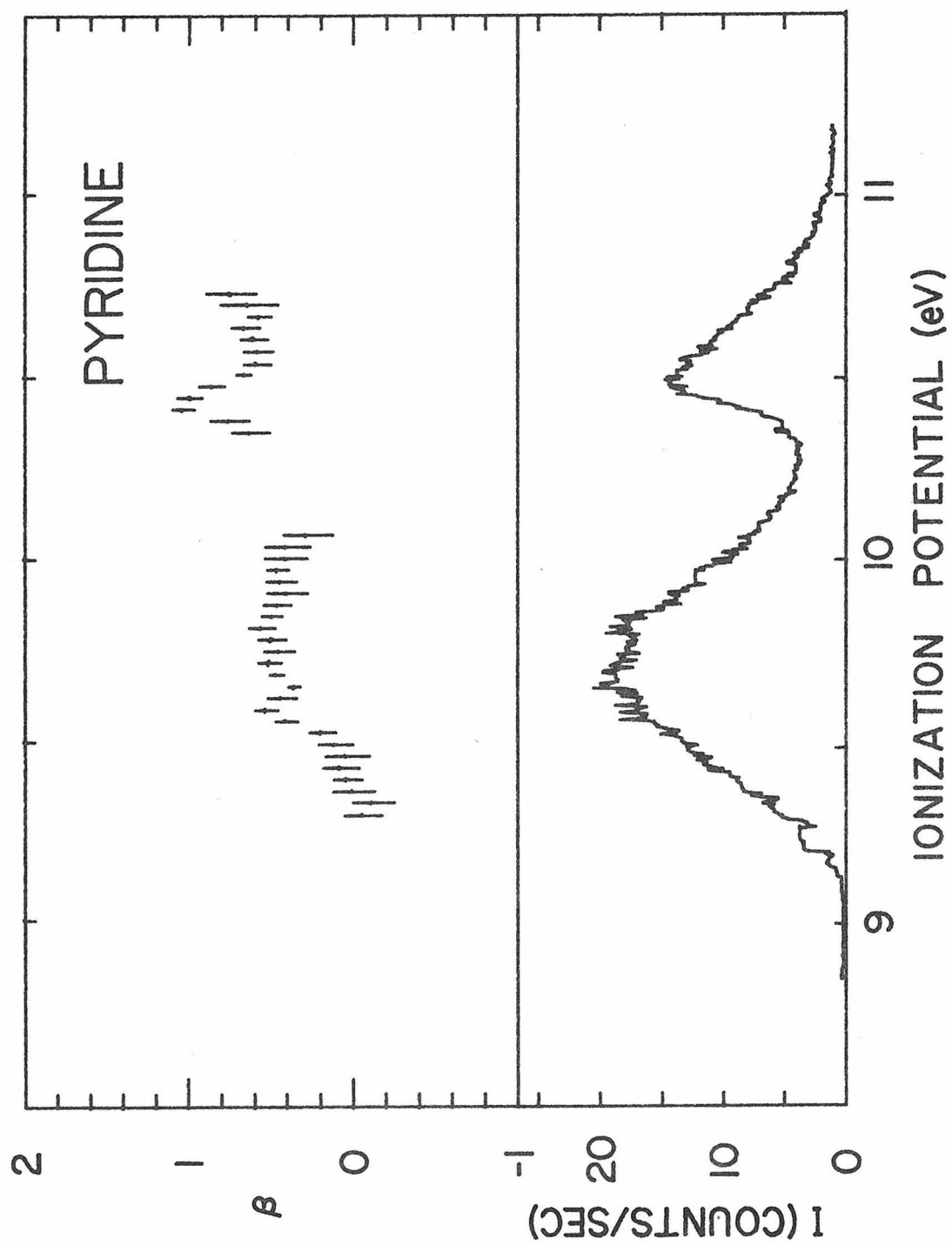


Figure 6.4-1

expect the β difference between σ and π orbitals to hold for pyridine. Electronegativities for N and C atoms are similar and pyridine is isoelectronic to benzene, for which the β value¹³ for the first degenerate π band at 9.25 eV IP is high, 1.15 ± 0.10 . Thus, we assign the orbital ordering as n, π, π , in agreement with several previous experimental studies.^{7, 8, 11}

REFERENCES

1. R. Gleiter, E. Heilbronner, V. Hornung, *Helv. Chim. Acta* 55, 255 (1972).
2. E. Haselbach, Z. Lanyiova, M. Rossi, *Helv. Chim. Acta* 56, 2889 (1973).
3. J. Spanget-Larsen, *J. Electron Spectr.* 2, 33 (1973).
4. J. Almlöf, B. Roos, U. Wahlgren, H. Johansen, *J. Electron Spectr.* 2, 51 (1973).
5. E. Clementi, *J. Chem. Phys.* 46, 4731, 4737 (1967).
6. W. R. Wadt, W. A. Goddard, *J. Amer. Chem. Soc.* 97, 1649 (1975).
7. C. R. Brundle, M. B. Robin, N. A. Kuebler, *J. Amer. Chem. Soc.* 94, 1466 (1972).
8. G. H. King, J. N. Murrell, R. J. Suffolk, *J. Chem. Soc. Dalton* 564 (1972).
9. D. L. Ames, J. P. Maier, F. Watt, D. W. Turner, *Faraday Disc. Chem. Soc.* 54, 277 (1972).
10. D. W. Turner, C. Baker, A. D. Baker, C. R. Brundle, Molecular Photoelectron Spectroscopy (Wiley-Interscience, London, 1970).
11. L. Åsbrink, C. Fridh, B. Ö. Jonsson, E. Lindholm, *Int. J. Mass Spectrom. Ion Phys.* 8, 229 (1972).
12. R. M. White, T. A. Carlson, D. P. Spears, *J. Electron Spectr.* 3, 59 (1974).

13. T. A. Carlson, C. P. Anderson, Chem. Phys. Lett. 10, 561 (1971); T. A. Carlson, G. E. McGuire, A. E. Jonas, K. L. Cheng, C. P. Anderson, C. C. Lu, B. P. Pullen, in D. Shirley (editor) Electron Spectroscopy (North-Holland, Amsterdam, 1972) p. 207.

APPENDIX A - HELMHOLTZ COIL DESIGN AND SPECIFICATIONS

After we realized the necessity of more magnetic field compensation than a single mu-metal¹ shield, two solutions presented themselves. We could either add a second magnetic shield or surround the current magnetic shield with Helmholtz coils. Coils were constructed because of the high expense of purchasing and annealing magnetic shield materials.

Three pairs of square Helmholtz coils about the three mutually perpendicular directions were built. The coils were constructed of $1'' \times 1'' \times \frac{1}{8}''$ aluminum channel and wound with 40 km (40 kg) of 26 AWG magnet wire. Coil specifications are given in Table A-I.

We chose square coils because of several design advantages:²

1. Ease of construction of coil forms
2. Greater central accessibility
3. Ease of field computation.

Firester² has calculated the optimal separation of square Helmholtz coils to be $1.0890a$ where the edge length is $2a$.³ He does not give a derivation, so that it is presented here. The Firester result is obtained by applying the law of Biot and Savart:

$$\underline{dB} = \frac{\mu_0 I d\underline{S} \times \underline{r}}{4\pi r^3}, \quad (A-1)$$

to calculate the magnetic induction due to a current I in a line segment $d\underline{S}$ at a distance \underline{r} from the line segment. For a calculation in MKS units, $\mu_0 = 4\pi \times 10^{-7}$ Weber \cdot amp⁻¹ \cdot meter⁻¹, and the magnetic

TABLE A-1. Helmholtz Coil Specifications

Coil Pair	Outer Dimension (feet-inches)	Coil Separation (feet-inches)	Turns	Initial B (milligauss)	Initial ^a Voltage	Recent ^d Voltage
NORTH-SOUTH	9-10	5-4	567	230 ± 10	68.84 ^b	63.98 ^b
EAST-WEST	9-8	5-3	300	50 ± 10	13.63 ^b	79.69 ^c
UP-DOWN	10-0	9-9	633	375 ± 10	345.5 ^c	367.5 ^c

^aOn April 12, 1973, adjustment made to null field inside coils with no magnetic shield present.

^bCoils operated in parallel.

^cCoils operated in series.

^dOn June 16, 1975, adjustments made to null field inside mu-metal shield.

induction is measured in Webers \cdot meter⁻² (1 Weber \cdot meter⁻² = 10⁴ Gauss). For two coils, and thus 8 line segments of finite length, the magnetic field along the mutual axis of the coils will be:

$$B = \frac{2\mu_0 I a^2 N}{\pi} \left\{ \frac{1}{(a^2 + x^2)(2a^2 + x^2)^{\frac{1}{2}}} + \frac{1}{(a^2 + [\ell - x]^2)(2a^2 + [\ell - x]^2)^{\frac{1}{2}}} \right\} . \quad (\text{A-2})$$

Here, N is the number of turns in each coil, x is the distance along the central axis from one of the coils, and ℓ is the coil separation. Minimizing the field gradient along the field axis with respect to the coil separation:

$$\frac{\partial}{\partial \ell} \left(\frac{\partial B}{\partial x} \right) = 0 , \quad (\text{A-3})$$

yields a cubic equation in Z^2 :

$$3Z^6 + 18Z^4 + 22Z^2 - 20 = 0 , \quad (\text{A-4})$$

where $Z^2 = \ell^2/2a^2$. A solution is $\ell = 1.0890a$.

Periodic adjustments of the Helmholtz coil power supplies⁴ may be necessary in order to zero the magnetic field inside the mu-metal shield. The laboratory ambient magnetic field does drift with time. The uninterruptible power supply⁵ which maintains continuous AC power to the Helmholtz coil power supplies requires periodic maintenance as well. Normally, when the power is available from the City of Pasadena, the backup battery⁶ is continuously charged. The water lost by electrolysis should be replaced monthly.

REFERENCES

1. Allegheny Ludlum Steel Corp., Pittsburgh, Pa.
2. A. H. Firester, Rev. Sci. Instrum. 37, 1264 (1966).
3. The UP-DOWN pair are separated by more than the recommended 5' 5" in order to improve central accessibility and allow the coils to be firmly anchored to the floor.
4. John Fluke Model 407, Electronic Measurements Model TR212A, Power Designs Model 1010T.
5. Topaz Model 315B-12-60.
6. Sears "Die Hard" battery, Model 27C.

APPENDIX B - VOLUME CORRECTION

The volume of intersection of two cylinders of arbitrary diameter is described exactly by:

$$\frac{V(\theta)}{V(90^\circ)} = \frac{1}{\sin \theta} , \quad (\text{B-1})$$

where θ is the angle between the intersecting axes. If the light and electron beams were cylinders, for detector angles other than 90° , the detector views photoelectrons arising from a larger ionization region than at 90° . It is possible to correct for the larger intersection region in data reduction software by multiplying counting rates by $\sin \theta$.

In truth, however, the light and electron beams are divergent, so that the view cylinders become view cones for real experiments. The deviation from Eq. B-1 above was earlier calculated to take the form:¹

$$\frac{V(\theta)}{V(90^\circ)} = \frac{1 + C(\theta)}{\sin \theta} . \quad (\text{B-2})$$

Here $C(\theta)$ is small for view cones subtending small solid angles and for detector angles close to 90° .

We wished to evaluate the extent that artifacts in the angular distribution could be due to imperfections in the pure $\sin \theta$ volume correction. Thus, we undertook a calculation of the area of intersection of two cones in a plane as a worst case estimate of deviations from Eq. B-1. The view cone geometry is presented in Fig. B-1.

Figure Caption

Figure B-1 Drawing illustrating the plane trigonometry of the intersection of the light and photoelectron beams.

Let the lamp and detector cone angles be α and γ , respectively.

Let the distances from vertices of the lamp and detector cones to the point of intersection of their bisecting rays be m' and ℓ' , respectively.

Thus, we define:

$$\sphericalangle CAF = \gamma \quad (\text{B-3})$$

$$\sphericalangle CBD = \alpha \quad (\text{B-4})$$

$$\sphericalangle CAA' = \sphericalangle A'AF = \frac{1}{2}\gamma \quad (\text{B-5})$$

$$\sphericalangle DBB' = \sphericalangle B'BC = \frac{1}{2}\alpha \quad (\text{B-6})$$

$$AP = \ell' \quad (\text{B-7})$$

$$BP = m' \quad (\text{B-8})$$

Draw auxiliary lines GE , GG' , BQ , and HH' such that:

$$GE \parallel BC \quad (\text{B-9})$$

$$GG' \perp GE, BC \quad (\text{B-10})$$

$$HH' \parallel BC \text{ and bisects } GG' \quad (\text{B-11})$$

$$\text{point } Q \text{ is intersection of } AA' \text{ and } HH' \quad (\text{B-12})$$

$$AQ = \ell \quad (\text{B-13})$$

$$BQ = m \quad (\text{B-14})$$

$$\sphericalangle CBQ = \beta \quad (\text{B-15})$$

$$GG' = d \quad (\text{B-16})$$

$$\sphericalangle APB' = \phi = \text{detector angle} \quad (\text{B-17})$$

$$\sphericalangle ACB = \rho \quad (\text{B-18})$$

$$\sphericalangle AA'B = \theta \quad (\text{B-19})$$

Then a modicum of plane trigonometry yields the following results:

$$\theta = \pi - \phi - \frac{1}{2} \gamma \quad (\text{B-20})$$

$$\rho = \theta - \frac{1}{2} \gamma \quad (\text{B-21})$$

$$\rho = \tan^{-1} \left\{ \frac{(1 - C') \sin \gamma}{2 \cos \gamma - \sin \gamma [\cot \theta (1 - C') - 2 \cot(\rho + \alpha)]} \right\} \quad (\text{B-22})$$

$$\text{where } C' = \frac{[\cos \theta - \sin \theta \cot(\theta + \frac{1}{2} \gamma)] (\ell' \sin \theta + m' \sin \frac{1}{2} \gamma)}{m' \sin(\theta + \frac{1}{2} \gamma)} \quad (\text{B-23})$$

$$m = m' \left\{ \frac{\sin(\theta + \frac{1}{2} \gamma)}{\sin(\theta + \beta)} \right\} \quad (\text{B-24})$$

$$d = 2m \sin \beta \quad (\text{B-25})$$

$$\ell = \ell' - \frac{1}{2} d / \sin \theta + m' \sin \frac{1}{2} \gamma / \sin \theta \quad (\text{B-26})$$

$$\text{GE} = \frac{\ell \sin \alpha (\sin \theta - m \sin \beta / \ell)}{\sin^2 \theta - \sin^2 \frac{1}{2} \alpha} \quad (\text{B-27})$$

$$\text{HH}' = \frac{\ell \sin \theta \sin \alpha}{\sin^2 \theta - \sin^2 \frac{1}{2} \alpha} \quad (\text{B-28})$$

$$\text{Area CDEF} = d \cdot \text{HH}' + \frac{1}{2} (\text{GE})^2 \sin \rho \sin \gamma / \sin(\rho + \gamma) \quad (\text{B-29})$$

For the beam parameters:

$$\begin{aligned} \ell' &= 2.15'' \quad \alpha = 1.83^\circ \\ m' &= 0.845'' \quad \gamma = 4.17^\circ \end{aligned} \quad (\text{B-30})$$

measured for the experimental geometry, values of $C(\theta)$ are listed in Table B-I for $\theta = 40^\circ - 120^\circ$ in steps of 10° . The maximum $C(\theta)$ in the normal range of detector angles is $C(120^\circ) = 0.0013$. Thus the $\sin \theta$ volume correction is very accurate for the normal range of detector angles.

TABLE B-1. Intersection Area

Detector Angle (degrees)	Area (in ²)	C(θ)
40	6.57399 (-3)	.00007
50	5.51489 (-3)	-.00018
60	4.87780 (-3)	-.00026
70	4.49545 (-3)	-.00025
80	4.28987 (-3)	-.00017
90	4.22539 (-3)	0
100	4.29167 (-3)	.00026
110	4.49953 (-3)	.00066
120	4.88543 (-3)	.00131

REFERENCES

1. James K. Rice, Ph.D. Thesis, California Institute of Technology
(1969) p. 239.

APPENDIX C - DATA ACQUISITION PROCEDURES

The method of data taking depends to a large extent on which sample gas is being studied. For a number of atomic and diatomic samples, a small amount of strong structure appears in the photoelectron spectrum. The principal information content lies in the variation of peak heights with angle. For many organic samples, on the other hand, sharp structure appears in few of the many weak bands in the photoelectron spectrum. Information lies in variation of β across broad bands.

This section will discuss the strategy for optimizing the quality and quantity of angular distribution data. Strongly emphasized is the time order of activities. The text here will refer to the various PDP8/e computer software packages available and operation as of September, 1975. A detailed discussion of operating software is available in a reference manual in the laboratory. Thus, the material will not be duplicated here.

With the lamp on and stable, admit the sample gas from the inlet manifold. For an electron impact ionization cross section of $X \text{ \AA}^2$ at 70 eV incident energy, the sample pressure, as read by the uncalibrated high pressure ionization gauge, can be set initially at $1.5X$ millitorr. Do not exceed full scale (11 millitorr) on the analog panel meter of the gauge controller.

Take a full spectrum of the compound at a detector angle of 54.7° in order to get the pressure gauge acclimated to the sample gas. The spectrum should run over as many channels as possible for a minimum

of 6 hours. The spectrum, if taken using the HeI lamp, should contain only the 584 Å spectrum for polyatomic molecules, and the 584, 537, and 522 Å spectra for noble gases and diatomics. This spectrum can be used later for plotting purposes.

If any regions of the spectrum look unusual, spectra should be taken next at a higher digital resolution (fewer meV incremented between successive data channels).

Determine the optimal operating pressure. The instrument should be operated at the highest possible pressure for which counting rate varies linearly with sample pressure. Operation at high pressures, especially for organic samples, is desirable in order to optimize the signal to background ratio.

The optimal pressure is determined by an examination of the counting rate at a prominent peak at low ionization potential. Total electron scattering cross sections for atomic and molecular targets generally rise over the range of increasing electron energies produced in the 584 Å ionization.¹ Thus, a peak at low IP will usually show the worst case intensity versus pressure variation.

After loading EDITION 15² and then POISSON CHECK,² enter POISSON CHECK and type "G" to measure the mean counting rate in a given 64 second interval. This procedure may be used to locate the peak maximum as well as to measure the variation of counting rate with pressure. The peak may be located roughly with option "G" of EDITION 15. Varying pressures may cause counting rate fluctuations due to slight variations of potentials felt by the electrons. Thus the

exact maximum should be sought. Fine adjustment of SWEEP BIAS on the lens/sphere panel will permit locating this maximum. Then, with all of the lens and sphere voltages tuned to the peak, measure counting rate for two 64-second periods. To measure the sample pressure, re-enter EDITION 15 and execute option "P". Vary the pressure by adjusting the variable leak valve, item 4 in Fig. D-1. Include in the series counting rate measured at zero sample pressure. Then plot the resulting variation of counting rate versus sample pressure corrected for the zero sample pressure gauge reading. Typical results for argon, on the $^2P_{3/2}$ peak, are shown in Fig. C-1. The arrow in Fig. C-1 indicates the maximum pressure for which counting rate varies linearly with pressure. This pressure, 6 millitorr, as read from the gauge controller, corresponds to roughly 4 millitorr absolute.

Samples may interact with the Schulz-Phelps³ high-pressure ionization gauge. Filament pyrolysis of the sample may increase the thermionic work function or deposit an insulating layer on the electron collector. In this case, time hysteresis in the variation of counting rate versus pressure is a good indication of gas/gauge interaction. Figure C-2 presents the example of tetrafluoroethylene, for which time hysteresis is clearly manifest. Arrows indicate the time order of data acquisition. Eventually, the interactions can destroy the pressure gauge.

With the sample leak adjusted to give the optimal pressure at a detector angle of 40° , data acquisition can commence. For noble

Figure Captions

Figure C-1 Variation of counting rate, $^2P_{\frac{3}{2}}$ peak, with gas pressure in the 584 Å spectrum of argon.

Figure C-2 Variation of counting rate with gas pressure in the low IP π band of tetrafluoroethylene. Arrows indicate the time sequence of the measurements.

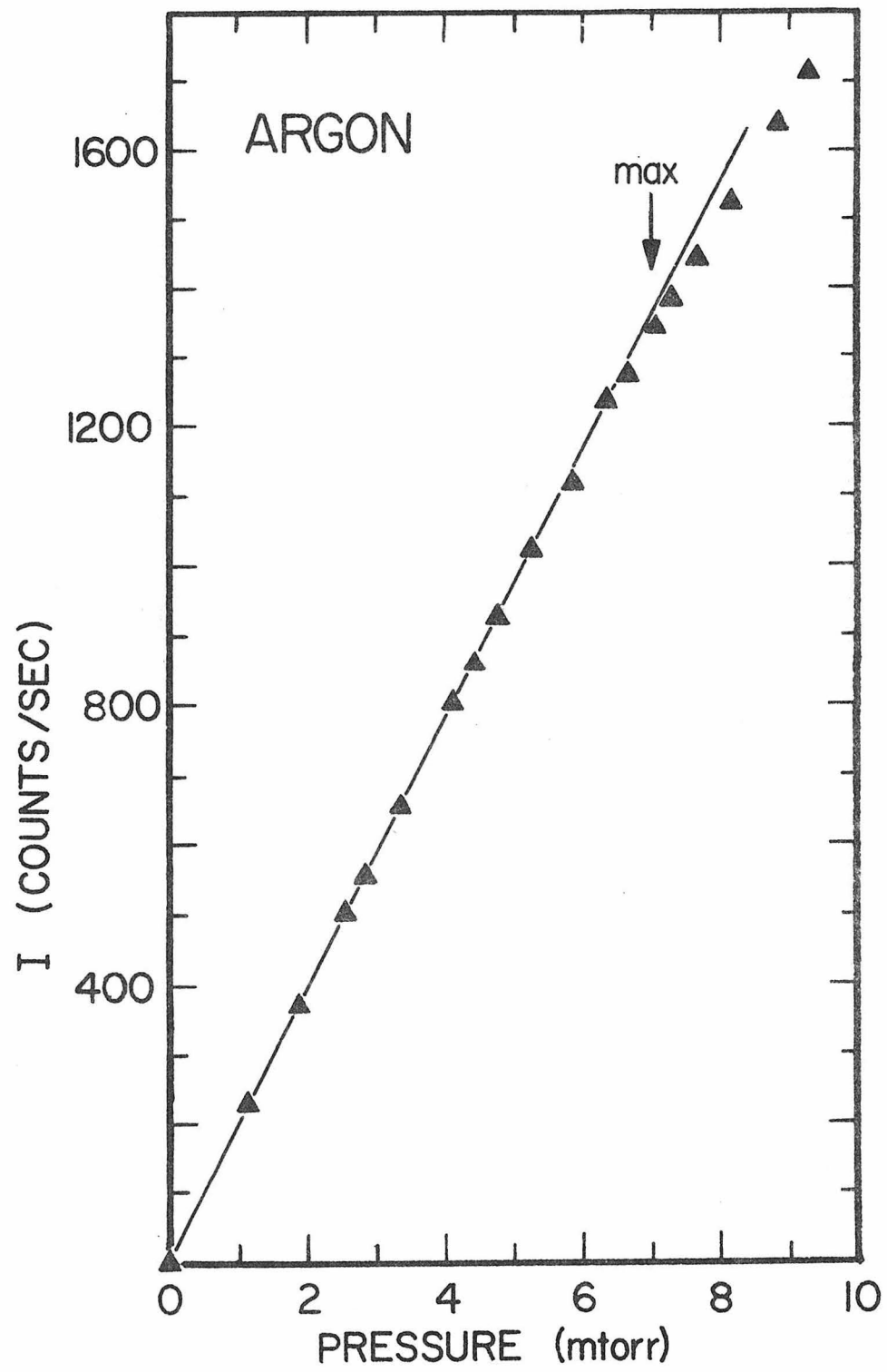


Figure C-1

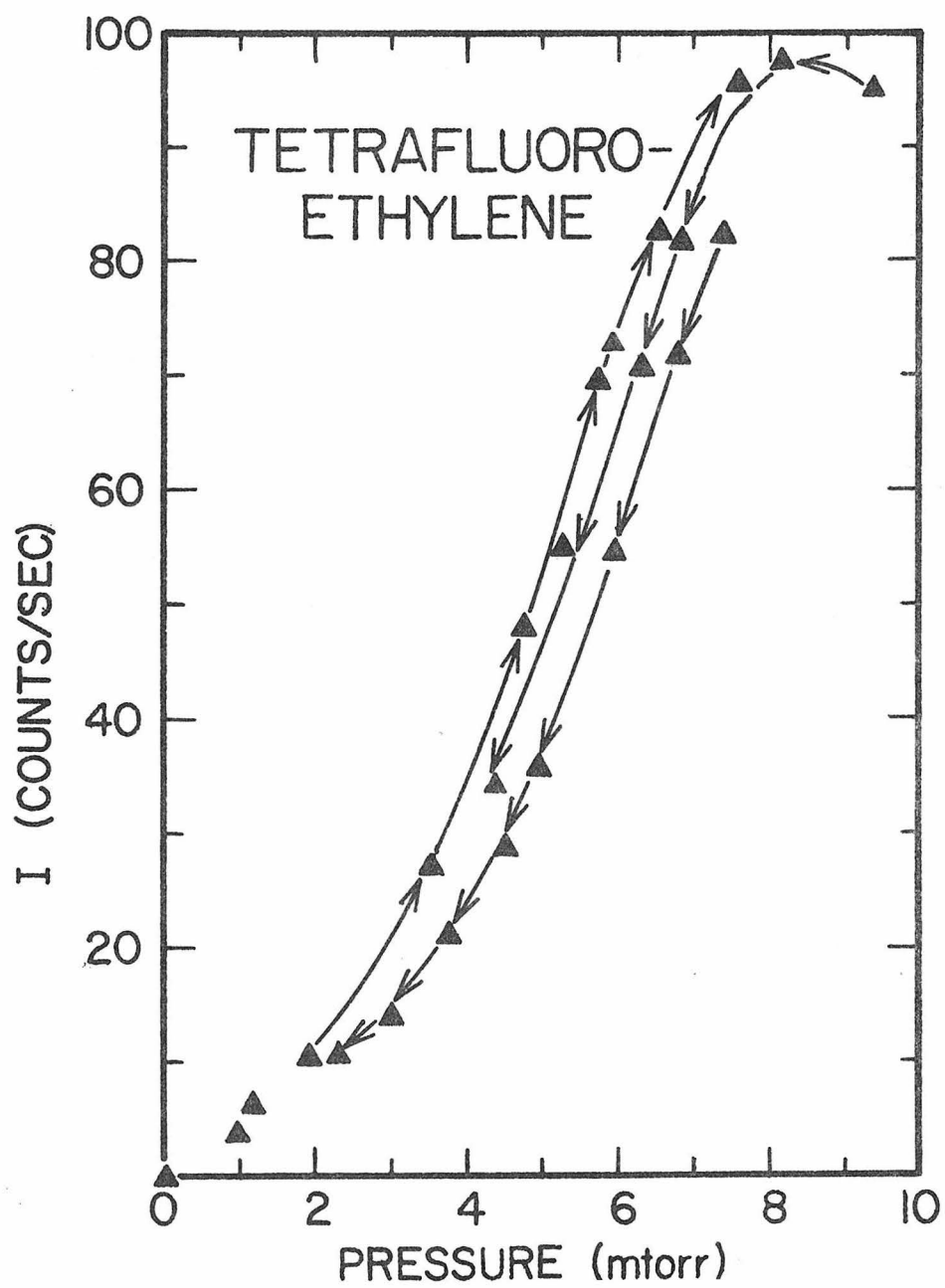


Figure C-2

gases and diatomics, data acquisition is straightforward. Merely take an angular distribution over each peak starting from the strongest and finishing at the weakest. The angular distribution or background follows, so that background compensation can be performed for the weaker peaks. For polyatomic molecules, the full spectrum should be divided into 4-6 partially overlapping regions of approximately 0.5-2 eV width centered about band structure. The regions should be studied in order of increasing ionization potential. An angular distribution of background follows that of the last band.

The angular distribution of background is always studied last in order to improve the accuracy of the background subtraction procedure. Lamp intensity and surface cleanliness vary slowly with time as long as the sample gas does not chemisorb strongly to surfaces. Thus, for spectral regions where the signal to background ratio is poor, under 2:1, the background should be measured and parameterized as soon after taking data as possible. An extreme case is offered by the 627 Å spectrum of N_2 , for which the NeI lamp intensity was dropping with time more rapidly than previously encountered with the HeI lamp. Background at the location of the $v' = 0$ peak of the $X^2\Sigma_g^+$ band was measured over 5 channels immediately after the angular distribution was run. Still, goodness of fit to the theoretical Bethe-Cooper-Zare formula was only ± 0.2 .

For some angular distributions over peaks within a single band, β values will be compared and differences in β values will be important. Here, the spectra should include both peaks, even if the

intervening spectral region has little or no structure. A typical example is the $^2P_{3/2} - ^2P_{1/2}$ doublet of argon. The band-at-a-time strategy for studying polyatomic molecules is a corollary of this suggestion.

A full angular distribution should not exceed 9-10 hours, although up to 12 hours may be acceptable if the lamp is extraordinarily stable. For a band of a polyatomic molecule, for which the maximum counting rate is 30 counts/sec, an accumulated count total of 1000 might be considered acceptable. Thus, the maximum of 3600 seconds per spectrum limits the number of data channels to 100-120. If the band contains very sharp structure, a digital resolution of 5-10 meV might be desirable. This would limit the ionization potential region scanned to 0.5 eV. For the sharp structure of noble gas and diatomic samples, a different strategy is employed. If the peak is extremely weak and isolated, the data acquisition system should be set to 20 channels covering 40 meV about the peak.

Common sense and the nature of the sample gas or type of structure being investigated may dictate deviations from the procedures outlined above.

Background parameterization fits the variation of counting rate with no sample gas present to a set of three line segments. Background is normally measured with the following spectral parameters:

starting SPHERE CENTER voltage	-11.731
sphere potential difference	0.600
SCAN	12 eV
MV (digital resolution)	5
MULT (multiplier)	20
dwel	30×1 second

After the 9 point angular distribution is completed, it should be plotted onto $8\frac{1}{2}'' \times 11''$ paper in raw and convoluted (7 point) form. The horizontal scale for spectra plotted by option "O" of EDITION 15 covers 11.9 eV. The vertical scale for the convoluted spectra to be parameterized may be determined using the memory examination feature of the debugging option of MON8K.012.² For prominent maxima in several spectra, determine the corresponding counting rates in the convoluted data buffer, which starts at location $14001_8 \times 2 \times$ (number of channels). Next, draw three line segments through each convoluted spectrum as shown in Fig. C-3. The slopes of each of the three segments can be converted to the unit counts $\cdot \text{eV}^{-1} \cdot \text{sec}^{-1}$, using scale factors for the vertical and horizontal scales as well as the dwell time per channel. The effective ionization potentials of the X intercept and first two slope break-points can be determined using their X coordinates and the horizontal scale factors. The quantities loaded into the background parameter buffer of AUTOBETA,² starting at 16717_8 , are given in Table C-I. The parameters are loaded in floating point form using the debugging feature in the order

Figure Caption

Figure C-3 Illustration of the background parameterization procedure. Ends of the spectra, A and B, represent the apparent IP's 8 and 19.9 eV.

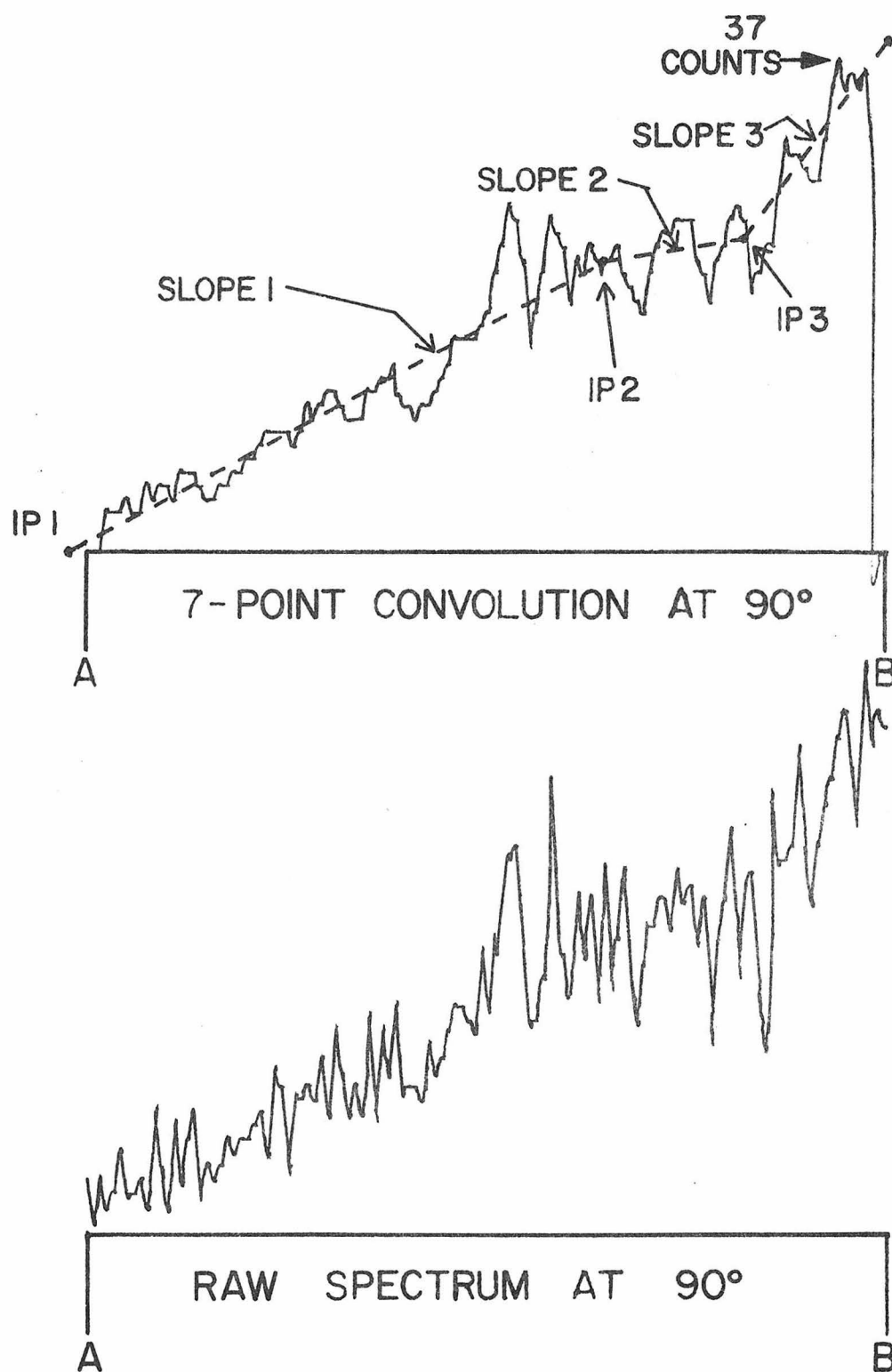


Figure C-3

TABLE C-1. Background Parameterization

j	starting location of storage of E_j (octal) ^a	starting location of storage of DS_j (octal) ^b
1	16717	17043
2	16753	17077
3	17007	17133

^aStore apparent IP's, eV

^bStore slope changes, counts \cdot eV⁻¹ \cdot sec⁻¹

40°-120° in steps of 10°.

Although the background parameterization may seem cumbersome, the background evaluation at a given apparent ionization potential becomes extremely simple. For an angular distribution at a given apparent ionization potential, the break points less than the apparent IP and the X intercept are subtracted from the apparent IP. The vector of energy differences for that detector angle and apparent IP is dot-product multiplied (multiply and add) by the corresponding vector of slope changes. The resulting scalar is finally multiplied by the dwell time per channel to recover the background counting rate. Thus:

$$\text{background} = \text{DWELL} \cdot \sum_{j=1}^3 (E - E_j) \cdot \text{DS}_j \cdot S_j, \quad (\text{C-1})$$

where E is the apparent IP of the data channel under study, E_j are the apparent IP's of the X intercept and slope break points, DS_j are the changes in slope at the slope break points, and $S_j = 0$ if the j^{th} break point apparent IP exceeds that of the current data channel, and $= 1$ otherwise. The apparent IP at some setting of the sphere center voltage, V, is defined as:

$$\text{apparent IP} = 21.217 + V - 2.475 \text{ (sphere difference)} \quad (\text{C-2})$$

Electrical charging of surfaces in the electron optics will shift spectra in energy relative to the positions expected on the basis of voltages applied by power supplies. These contact potential shifts

relative to the apparent IP can be measured and a true IP scale established via noble gas energy calibration.⁴ The ionization potentials of the noble gases are known very accurately from optical spectroscopy, so that the gases are suitable for energy calibration when mixed with the sample. A commonly used calibration is the argon $^2P_{3/2}$ peak at an ionization potential of 15.759 eV.

A relative energy calibration should be performed daily during the data acquisition period in order to correct for drifts with time. Select the sharpest spectral feature and locate the corresponding apparent IP to within 5-10 meV using EDITION 15 data taking options. Finally, when angular distributions over all spectral bands are completed, load roughly 1 psi partial pressure of argon into the inlet system and place the energy calibration of the sharp spectra feature on an absolute basis.

Current data reduction software, AUTOBETA, allows for calculation of β over a maximum of 9 detector angles. Memory limitations for internal arrays for storage of angles, counting rates, and background parameters cause this restriction. In most cases, however, an angular distribution covering 9 detector angles from 40° to 120° adequately provides for internal redundancy in the fit to the Bethe-Cooper-Zare formula. At the same time the data acquisition time for each angular distribution is not inordinately long.

REFERENCES

1. H. S. W. Massey, E. H. S. Burhop, Electronic and Ionic Impact Phenomena, Oxford, London, 1969) Vol. I, p. 25; H. S. W. Massey, Electronic and Ionic Impact Phenomena (Oxford, London, 1969) Vol. II, pp. 699-704; Low energy shape resonances, as in N_2 and CO, provide an exception, however.
2. see MAPS reference manual.
3. G. J. Schulz, A. V. Phelps, Rev. Sci. Instr. 28, 1051 (1957).
4. D. W. Turner, C. Baker, A. D. Baker, C. R. Brundle, Molecular Photoelectron Spectroscopy (Wiley-Interscience, London, 1970) p. 32.

APPENDIX D - SAMPLE HANDLING

Like data acquisition procedures, sample handling techniques depend to a large extent on sample gas. The atomic and diatomic samples run in the course of this investigation have large vapor pressures at liquid nitrogen temperatures. Thus, the need to eliminate structure from gas cross contamination requires meticulous handling procedures. On the other hand, the organic samples have extremely low vapor pressures at liquid nitrogen temperature. Gaseous samples (ethylene, isobutylene, allene, and 1,3-butadiene) and liquid samples (the balance) could be loaded into the inlet system without extraordinary precautions against air contamination. Later freeze-pump-thaw cycles could remove gaseous contamination.

The instrument gas inlet system consists of three principal elements: a rotary mechanical pump, a glass inlet manifold, and a sample leak valve. The rotary mechanical pump allows the inlet manifold pressure to be pumped down to 1 millitorr, adequate for all of the samples run during this investigation. The glass inlet system allows for maximum flexibility in gas handling. At the same time, in order to avoid cross contamination of sample gases, the glass manifold can be disassembled and baked in the glassworking shop annealing oven in between successive samples. The inlet manifold consists of a 5 liter gas ballast (1), glass joints (2) to accommodate sample bulbs, $\frac{1}{4}$ inch kovar tube connections (3) to a pressure gauge and the leak valve (4), and a liquid nitrogen trap (5). A schematic¹

of the inlet system appears in Fig. D-1.

Permanent gases are loaded in the following sequence:

1. With valve (4) and stopcocks (2) closed and valve (7) and stopcocks (6) and (8) open, evacuate the inlet system to a base pressure under 10 millitorr.
2. Close stopcock (8) in order to isolate the 5L volume at a good vacuum.
3. a) Attach the transfer line from the gas cylinder to a joint below a stopcock (2);
b) Leaving the gas regulator off, open a stopcock (2)
or
- 3'. a) Close valve (7) and attach the transfer line by substituting a Swagelok "T" for the detachable coupling (9);
b) Leaving the gas regulator off, open valve (7).
4. Check for leaks, then pump out the internal volume of the regulator with the cylinder valve closed.
5. Shut off the regulator and open the cylinder valve. Set the outlet pressure to approximately 10 psi.
6. Flush a small amount of the sample gas through the inlet system.
7. Close stopcock (6), open stopcock (8), and fill the inlet system to 1 Atm. pressure.
8. Close stopcock (8). Isolate the transfer line from the inlet (2) or (7), where appropriate, and open stopcock (6) to evacuate inlet manifold.

Figure Caption

Figure D-1 Schematic of the spectrometer inlet system.

Graphic symbols are taken from Ref. 1.

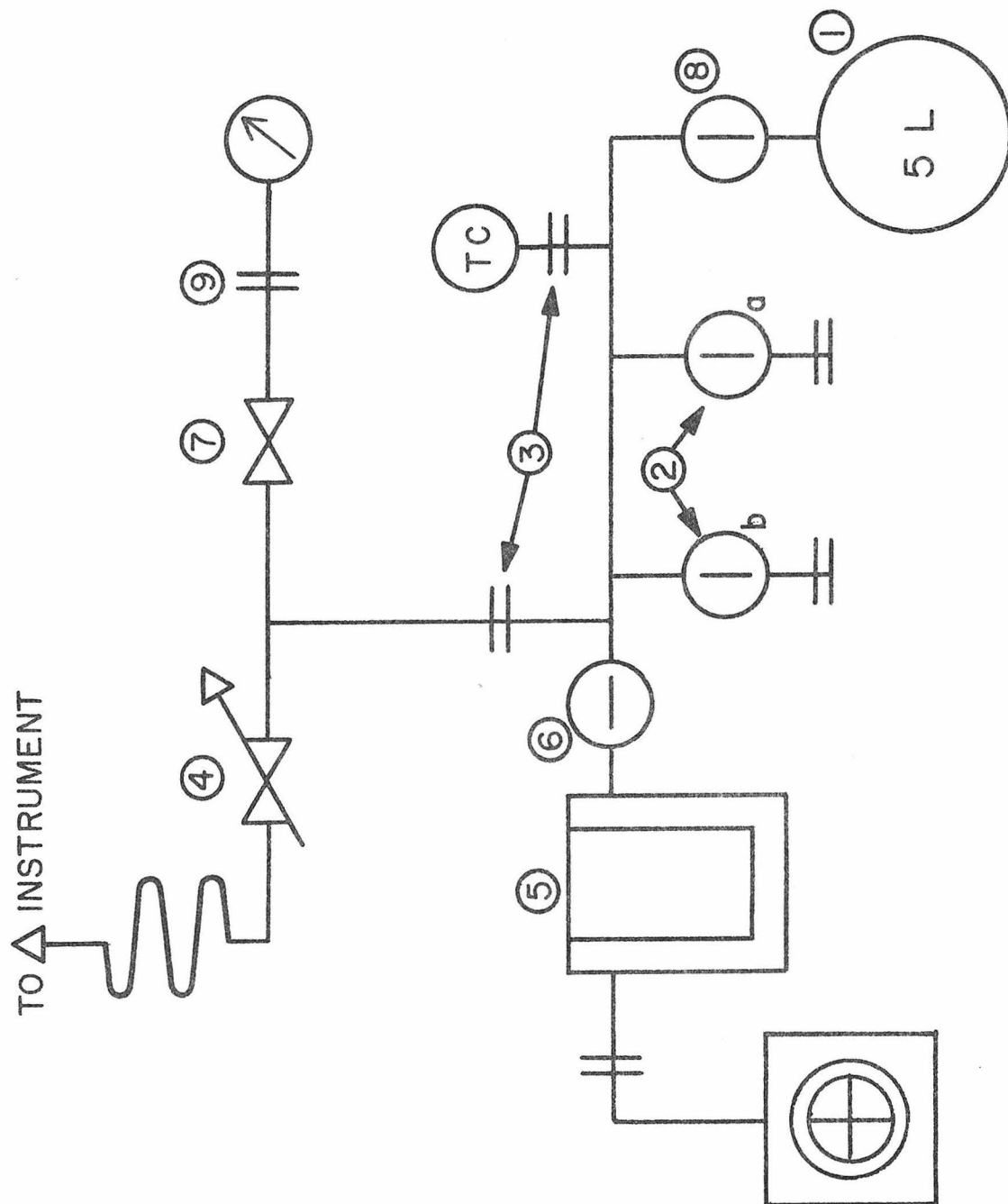


Figure D-1

9. Reattach the demountable coupling at (9) and open valve (7) if the transfer took place via (9).
10. Repeat step 1. Close valve (7) and stopcock (6), and open stopcock (8). The manifold pressure will be slightly less than 1 Atm.

For samples which are liquids or solids at room temperature, it is unnecessary to fill the 5L bulb. The samples are loaded in the following sequence:

1. With valves (4) and (7) and stopcocks (2) and (8) closed and stopcock (6) open, evacuate the inlet system to a base pressure under 10 millitorr.
2. Attach the sample bulb to a standard taper joint below one of the stopcocks (2).
3. Freeze the sample with liquid nitrogen.
4. Open the stopcock (2) and pump away the gas phase to below 10 millitorr.
5. Close the stopcock (2), remove the liquid nitrogen cooling, and allow the cold finger of the sample bulb to warm slowly to room temperature.
6. Repeat steps 3-5 twice.
7. Close stopcock (6), open the stopcock (2), and allow the inlet system pressure to rise to its room temperature value.
8. While spectra are being taken, the variable leak valve (4) must be heated to 40-50° C.

The samples which are gases at room temperature, but have low vapor pressure at liquid nitrogen temperature, are loaded through one of the two stopcocks (2a). Both a sample bulb and the 5 L reservoir are used as gas ballast.

1. Attach an empty sample bulb to the free joint below the other stopcock (2b).
2. Evacuate the sample bulb and the 5 L ballast by opening stopcocks (2b), (6), and (8). Evacuate the pressure gauge by opening valve (7). The other stopcock (2a), as well as valve (4), should be closed.
3. Close stopcocks (2b) and (8) and valve (7).
4. Attach a transfer line to the joint below stopcock (2a), evacuate the transfer line, check for leaks, and finally, pump out the regulator with the cylinder valve closed.
5. Shut off the regulator and bring the outlet pressure to 10 psi.
6. Close stopcock (6), open valve (7) and stopcocks (2b) and (8), and admit slightly less than 1 Atm. of the sample gas into the inlet system.
7. Isolate the sample transfer line by closing stopcock (2a) and shutting off the regulator and gas cylinder.
8. Freeze the sample gas into the finger of the sample bulb with liquid nitrogen. When no more condenses, close stopcock (2b), but **KEEP THE COLD FINGER UNDER LIQUID NITROGEN. IT IS A POTENTIAL BOMB.**

9. Exhaust the inlet manifold, except for the sample bulb. When the base pressure reaches 10 millitorr, close valve (7).
10. Follow the freeze-pump-thaw procedure of steps 3-5 of the previous section several times.
11. Close stopcock (6), open stopcocks (2b) and (8), and allow the sample to warm to room temperature.

REFERENCES

1. Graphic symbols per American Vacuum Society Standard,
J. Vac. Sci. Tech. 4, 139 (1967).

APPENDIX E - STATISTICAL TREATMENT OF DATA

E.1 Weighted least squares calculation of β values

The Bethe-Cooper-Zare expression for the angular distribution of photoelectrons, Eq. 2-19, may be represented in the form:

$$I(\theta) = a + b \sin^2 \theta . \quad (\text{E-1})$$

This equation is linear in a and b . Hence, a least squares procedure which calculates a and b may produce β values according to the relation:

$$\beta = \frac{4b}{3a + 2b} . \quad (\text{E-2})$$

We employ the method of weighted least squares¹ to calculate values of a and b . The functional over all data points, labelled i :

$$\sum_i g_i (y_i - bx_i - a)^2 \quad (\text{E-3})$$

is minimized, where:

$$x_i = \sin^2 \theta_i \quad (\text{E-4})$$

$$y_i = \frac{C_i \sin \theta_i P_0}{C_0 P_i} , \quad (\text{E-5})$$

and C_i and P_i are the counting rate and sample pressure and θ denotes $\theta = 90^\circ$. The weights, g_i , are inversely proportional to the variance in each y_i , namely the number of counts there (C_i).

Furthermore, we normalize the g_i to sum to N , the number of data

points. Thus:

$$g_i = \frac{N}{C_i \sum_j (C_j)^{-1}} \quad (\text{E-6})$$

The result of a small amount of algebra is:

$$a = \frac{SY \cdot DX - SX \cdot XY}{Q} \quad (\text{E-7})$$

$$b = \frac{N \cdot XY - SX \cdot SY}{Q} , \quad (\text{E-8})$$

where the following definitions are made:

$$SX = \sum_j g_j x_j \quad (\text{E-9})$$

$$SY = \sum_j g_j y_j \quad (\text{E-10})$$

$$DX = \sum_j g_j x_j^2 \quad (\text{E-11})$$

$$XY = \sum_j g_j x_j y_j \quad (\text{E-12})$$

$$Q = N \cdot DX - (SX)^2. \quad (\text{E-13})$$

E.2 Error analysis: goodness of fit

Error bars for β values are calculated by propagating errors associated with the coefficients a and b . The error bars reflect goodness of fit to Eq. 2-19 and include the variation of signal rates

because of counting (Poisson) statistics. The variance in β , σ_β^2 , is expressed as:²

$$\sigma_\beta^2 = \sigma_a^2 \left(\frac{\partial \beta}{\partial a} \right)^2 + \sigma_b^2 \left(\frac{\partial \beta}{\partial b} \right)^2, \quad (\text{E-14})$$

where:

$$\frac{\partial \beta}{\partial a} = \frac{-12b}{(3a + 2b)^2} \quad \text{and} \quad \frac{\partial \beta}{\partial b} = \frac{12a}{(3a + 2b)^2}. \quad (\text{E-15})$$

The variance of a and b , σ_a^2 and σ_b^2 , respectively, are taken from the diagonal elements of the matrix whose inverse is the variance-covariance matrix.¹ Thus:

$$\sigma_a^2 = \frac{DX}{Q(N-2)} \sum_i g_i (y_i - a - bx_i)^2 \quad (\text{E-16})$$

$$\sigma_b^2 = \frac{N}{Q(N-2)} \sum_i g_i (y_i - a - bx_i)^2. \quad (\text{E-17})$$

Clearly, large counting rates will reduce the proportion of statistical variation of counting rates in the total variance. Then, artifacts due to bad fits to Eq. 2-19 will be readily apparent. For diatomics and the inert gases, peak signal rates for many peaks in the 584 Å spectrum are high, so that σ_β^2 is a good index of experimental artifacts. In contrast, signal levels for organic compounds are typically low, 5-50 counts/second. Thus, even after long data acquisition periods and smoothing over many adjacent channels,³

the component of variance due to counting statistics may be non-negligible. In addition, error in the background subtraction procedure can influence σ_β^2 .

E.3 Error analysis: Poisson statistics

A second procedure can allow the isolation of the component of variance due to counting statistics alone. This permits isolation of the error in the background subtraction algorithm and error from lack of fit to Eq. 2-19.

When the experimentally fitted β value depends on a number of random variables, C_i , where each of these variables has a known variance of σ_i^2 , then the variance in β may be calculated by propagation:⁴

$$\sigma_\beta^2 = \sum_i \sigma_i^2 \left(\frac{\partial \beta}{\partial C_i} \right)^2. \quad (\text{E-18})$$

the form of $\frac{\partial \beta}{\partial C_i}$ is complex, but tractable:

$$\frac{\partial \beta}{\partial C_i} = \frac{12 g_i}{(3a + 2b)^2 Q^2 C_i} \left[(bx_i + a)Q(x_i \cdot SY - XY) + P \{ b(SY \cdot DX - XY \cdot SX) + a(SY \cdot SX - XY \cdot N) \} \right], \quad (\text{E-19})$$

where:

$$P = -DX - N \cdot x_i^2 + 2x_i \cdot SX. \quad (\text{E-20})$$

In general, the σ_β^2 from Eq. E-14 will be smaller than that of E-18, because the smoothing routine effectively improves the counting statistics. Counting rates fit to Eq. 2-19 are thus A times the printed counting rate, where A is the number of adjacent channels over which smoothing is performed.³ Thus, for comparison to σ_β^2 of Eq. E-14, the $\bar{\sigma}_\beta^2$ of Eq. 2-16 must be divided by A. The software package AUTOBETA prints σ_β and $\bar{\sigma}_\beta/\sqrt{A}$.

REFERENCES

1. N. R. Draper, H. Smith, Applied Regression Analysis (Wiley, New York, 1966) Chap. 2.
2. H. D. Young, Statistical Treatment of Experimental Data (McGraw-Hill, 1962) p. 96.
3. A. Savitzky, M. J. E. Golay, Anal. Chem. 36, 1627 (1964).
4. J. N. Franklin, private communication.

APPENDIX F - π Bands of Methyl-substituted Ethylenes

The following four figures support the results listed in Table V and plotted in Fig. 11 of Paper III. All four display an artifact for which we have not found means to compensate. With changing detector angle, peak positions shift slightly in energy. Because of the way PDP8/e software calculates the variation of β across bands, the result is an oscillatory variation of β across sharp structure. This effect is very pronounced for sharp structure (e.g., ethylene, argon) and less of a problem when counting rate varies slowly over a band (e.g., 2,3-dimethyl,2-butene). In any case, the intensities for which the error bars are the smallest are calculated by the peak finding software. We have calculated the variation of β across bands using these values of β , where possible.

Figure Captions

Figure F-1 Spectrum of the π region of ethylene, taken at a detector angle of 54.7° , over 150 channels, and with a dwell time of 24 sec/channel. Variation of β for features in the lower frame is given in the upper frame.

Figure F-2 Spectrum of the π region of isobutylene, taken at a detector angle of 54.7° , over 200 channels, and with a dwell time of 45 sec/channel. Upper frame has the same meaning as in Fig. F-1.

Figure F-3 Spectrum of the π region of 2-methyl,2-butene, taken at a detector angle of 54.7° , over 200 channels, and with a dwell time of 60 sec/channel. Upper frame has the same meaning as in Fig. F-1.

Figure F-4 Spectrum of the π region of 2,3-dimethyl,2-butene, taken at a detector angle of 54.7° , over 220 channels, and with a dwell time of 40 sec/channel. Upper frame has the same meaning as in Fig. F-1.

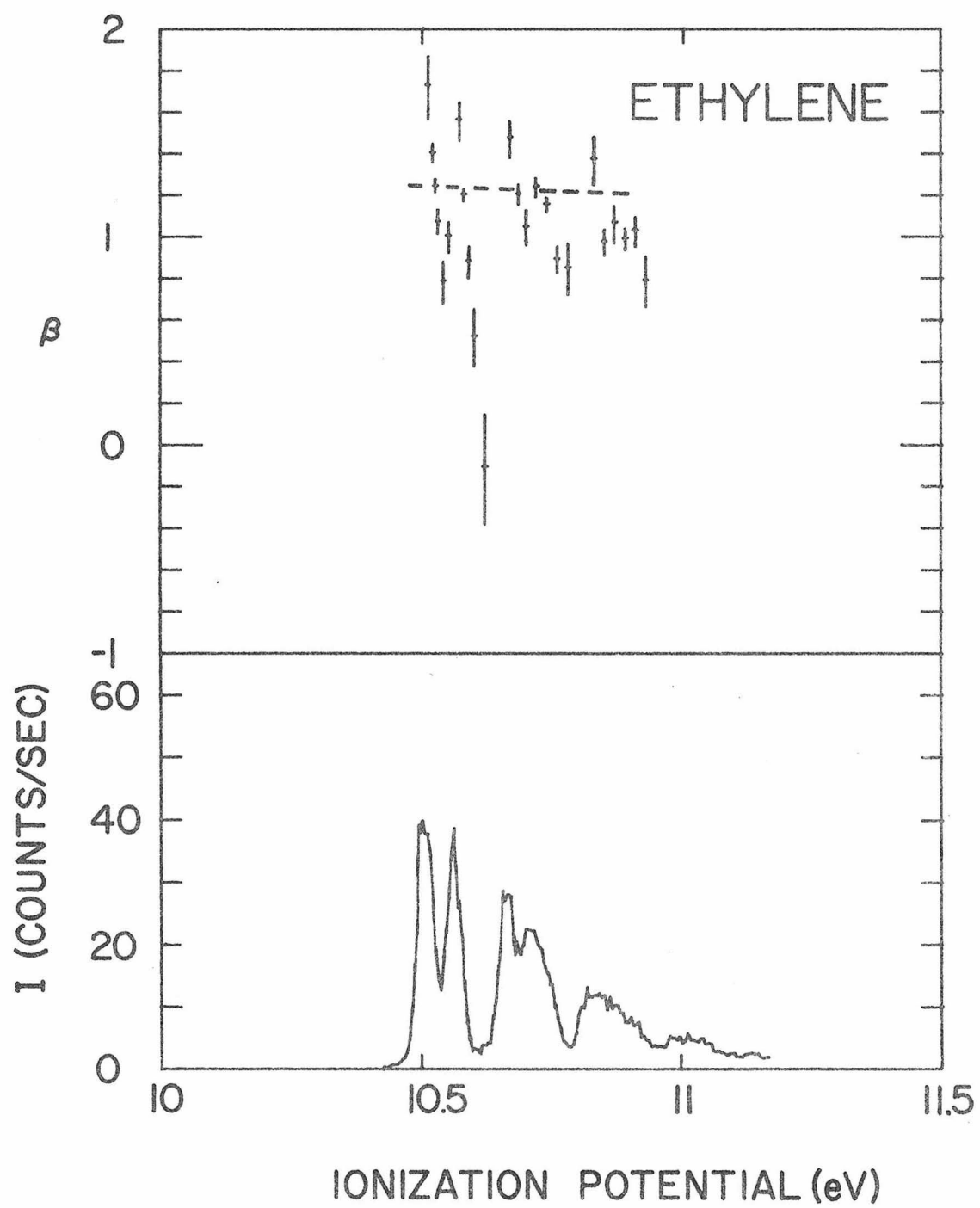


Figure F-1

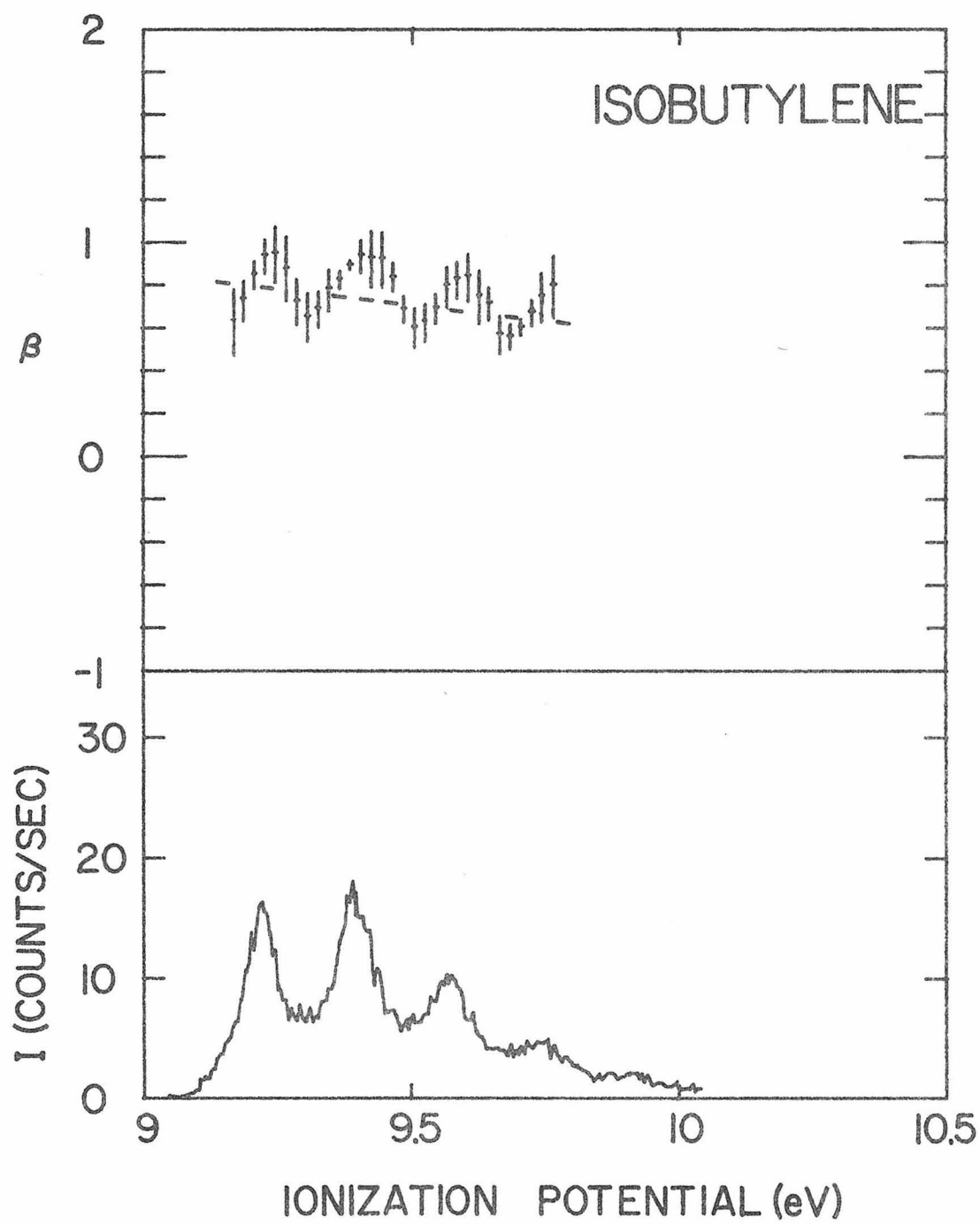


Figure F-2

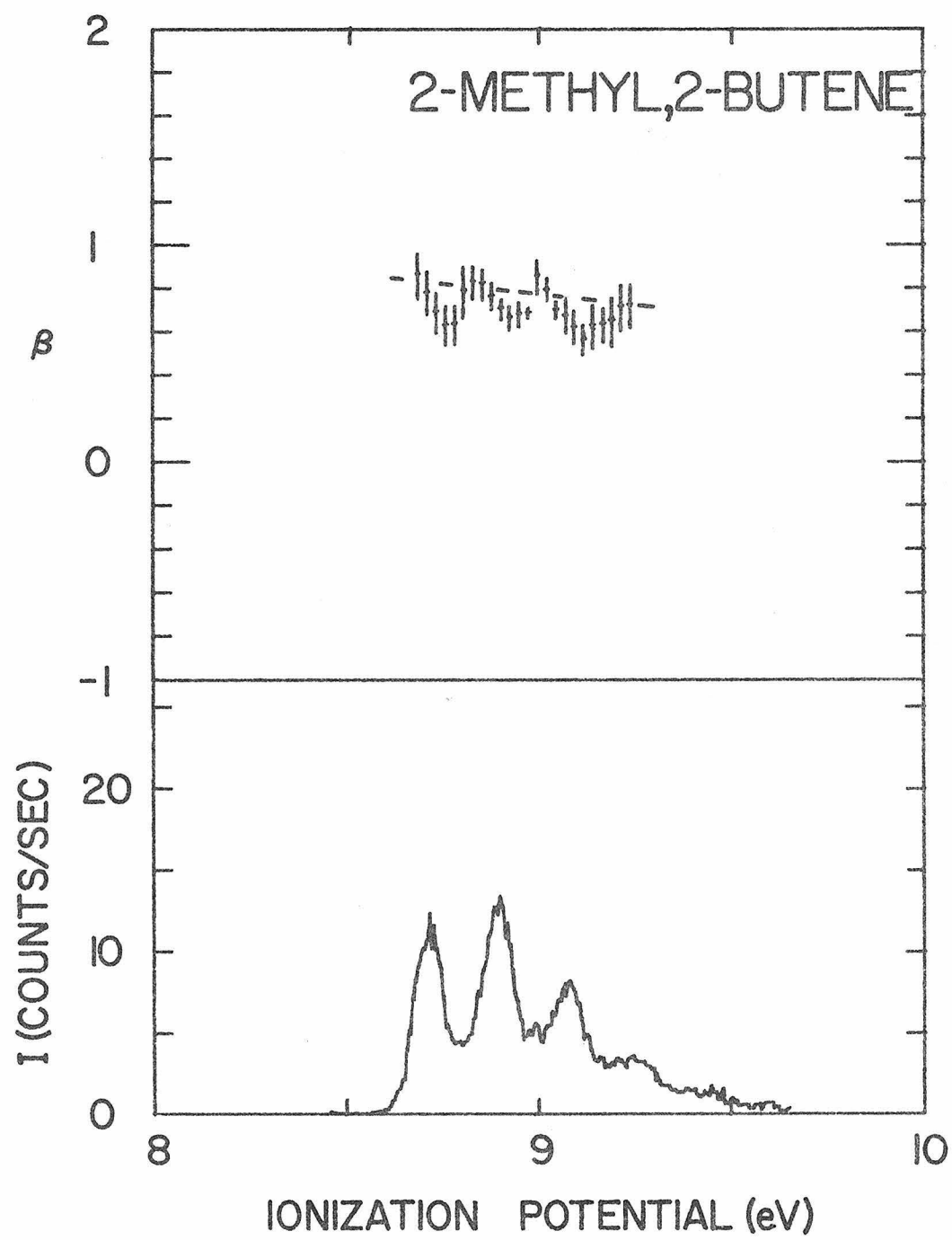


Figure F-3

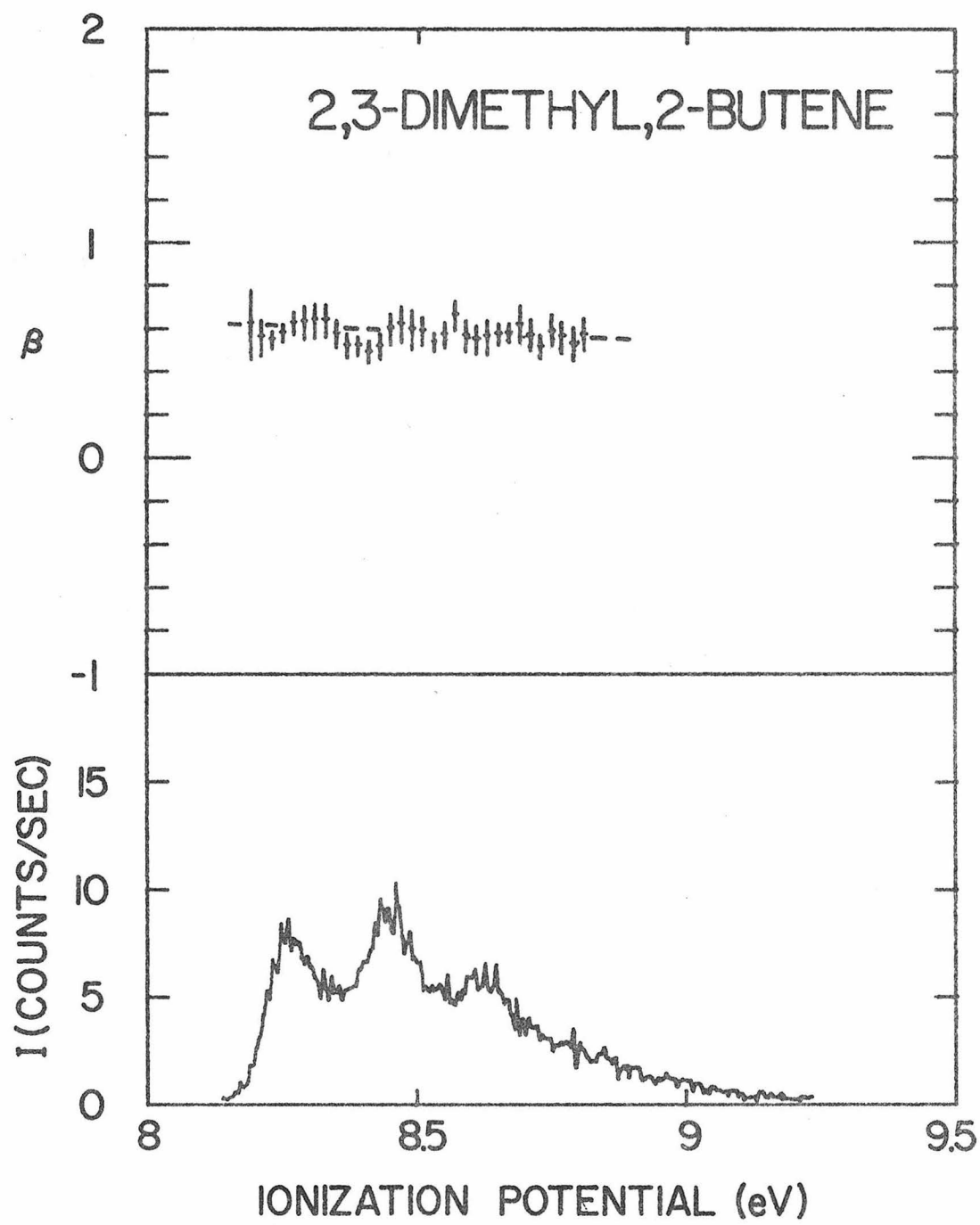


Figure F-4

APPENDIX G - List of Vendors

Advanced Techniques

3848 Colorado Blvd.

Pasadena, Ca. 91107

Redactron magnetic tape cassette transports

Calcomp Galaxies, Inc.

6955 Hayvenhurst Avenue

Van Nuys, Ca. 91406

PDP8/e semiconductor memory

Carborundum Co.

2240 S. Yates

Los Angeles, Ca.

Boron Nitride

Ceramaseal, Inc.

represented by:

Wadsworth-Pacific Mfg. Assoc., Inc.

15920 Temecula St.

Pacific Palisades, Ca. 90272

High vacuum feedthroughs

Cole Parmer Instrument Co.

7425 N. Oak Park Ave.

Chicago, Ill. 60648

Centrifugal pump for kerosene cooling

Costello-Little & Co.

8737 Venice Blvd.

Los Angeles, Ca. 90034

Decitek paper tape reader

CVC Products, Div. of Bendix

7120 Hayvenhurst

Van Nuys, Ca. 91406

Celvaseal leak spray, Convalex 10 pump oil, diffusion pumps

Digital Equipment Corp.

sales office:

871 S. Nash St., Suite 300

El Segundo, Ca. 90245

field service:

129 S. Myrtle St.

Monrovia, Ca.

PDP8/e minicomputer, interfaces, software

Dupont Co., Plastics Dept.

1800 N. Highland Ave.

Los Angeles, Ca. 90028

Vespel SP-1, SP-3 high vacuum plastic

Dynamics Associates

5190 W. Washington Blvd.

Los Angeles, Ca. 90016

Power Designs power supplies

Edwards High Vacuum, Inc.

343 Richmond St.

El Segundo, Ca. 90245

Electromechanical air admittance valves

Epic, Inc.

150 Nassau St.

New York, N.Y. 10038

Elima clip-on AC ammeter

Galileo Electro-Optics Corp.

represented by:

Griot Associates

504 Main St.

El Segundo, Ca. 90245

Channeltron and Spiraltron continuous dynode electron
multipliers

General Electric Co., Instrumentation Service

1138 164th Place

Hammond, Ind. 46320

Ionization gauge tubes

Granville-Phillips Co.

regional office:

1287 Lawrence Station Rd.

Sunnyvale, Ca. 94086

Vacuum traps, Schulz-Phelps ionization gauges and controllers,
variable leak valves

Hamilton Electrosales

10912 W. Washington

Culver City, Ca. 90230

Integrated circuits - Motorola, Signetics, National

discrete solid state components - Motorola, Westinghouse, G.E.

Carl Hermann Associates

1245 W. Walnut St.

Pasadena, Ca.

Bellows valves, molecular sieve traps

Hollywood Radio and Electronics

5250 Hollywood Blvd.

Hollywood, Ca. 90027

Lamps for counting interface display unit, RCA Numitron tubes

Kierulff Electronics

2585 Commerce Way

Los Angeles, Ca.

Magnecraft reed relays, Stancor transformers

Kramer Electronics

608 Sonora

Glendale, Ca.

Amphenol high density connectors

Matheson Gas Products

P.O. Box 608

Cucamonga, Ca. 91730

Sample gases, gas handling equipment (regulators)

McDanel Refractory Porcelain Co.

510 9th Ave.

P.O. Box 560

Beaver Falls, Pa. 15010

Ceramic rods

L. C. Miller Co.

717 Monterey Pass Road

Monterey Park, Ca. 91754

Electric discharge machine (EDM) machining of WC

Mil-Spec

15219 Stag St.

Van Nuys, Ca. 91405

Kynar insulated 30 AWG wire-wrappable wire

Minarik Electric Co.

224 E. Third St.

Los Angeles, Ca. 90013

Bodine fractional horsepower motors, Intermatic timers

Neely Sales and Service

6315 Arizona Place

Los Angeles, Ca. 90045

Sales and service of Hewlett Packard equipment

Perfection Mica Co.

Local distributor:

Mil-comm Distributors, Inc.

1609 Pontius

W. Los Angeles, Ca. 90025

Conetic AA alloy magnetic shielding

PI Instruments

12139 Chandler Blvd.

No. Hollywood, Ca. 91607

Disc shaft encoders

Porter Seal Co.

1833 Victory Blvd.

Glendale, Ca. 91201

Elastomeric o-rings

Shamrock Wire Sales

11811 E. Slauson Ave.

Santa Fe Springs, Ca. 90670

26 AWG magnet wire for Helmholtz coils

S. P. Marketing Co.

P.O. Box 745

Whittier, Ca. 90608

Utica wire wrapping tools

Terminal Systems, Inc.

11300 Hartland Ave.

No. Hollywood, Ca. 91605

Paper tape, paper tape punches, Teletype maintenance

Topaz Electronics

3855 Ruffin Road

San Diego, Ca. 92123

Uninterruptible power supply

Varian Corp. - NRC Vacuum Division

9907 S. Paramount Blvd.

Downey, Ca. 90240

Vacuum equipment: pumps, traps, gate valves, ionization
gauge controllers, flanges, feedthroughs, connectors, gaskets,
pump oil

Veeco Instruments, Inc.

13425 Wyandote St.

No. Hollywood, Ca. 91605

Thermocouple vacuum gauges

Victoreen Instrument Div.

10101 Woodland Ave.

Cleveland, Ohio

glass encapsulated high megohm resistors

VWR Scientific

S. Bonnie Beach Blvd.

Los Angeles, Ca. 90023

High frequency vacuum tester (Tesla coil), Briskear heating
tape

Willard Engineering

4378 W. 3rd St.

Los Angeles, Ca. 90020

Electromagnetic Products Co. large tool demagnetizers

W. D. Wilson Co.

1118 Mission St.

So. Pasadena, Ca.

Nupro and Whitey vacuum valves, Cajon and Swagelok vacuum fittings

Proposition IVariable Angle Photoelectron Spectroscopy of Para-hydrogen

To date no photoelectron angular distribution studies have centered on oriented molecules, where rotational quantum numbers are not in their thermal equilibrium distributions. Theory for the dependence of the photoelectron asymmetry parameter, β , on the various $j'' \rightarrow j'$ transitions for Hund's cases a and b has been developed by Buckingham, Orr, and Sichel.^{1,2}

Molecular hydrogen, exhibiting case b behavior, could allow direct comparison of theory and experiment. However, Carlson's experimental angular distribution study³ of H_2 ignored the rotational fine structure⁴ in the $X^2\Sigma_g^+$ band ($-\sigma_g$ 1s). A later study by Niehaus⁵ measured β values for the separate O ($\Delta J = -2$), Q ($\Delta J = 0$), and S ($\Delta J = +2$) branches, but not for the individual transitions. According to Asbrink's high resolution study of H_2 in thermal equilibrium,⁴ most of the photoelectron intensity can be attributed to $\Delta J = 0$ transitions. The Q-branch consists primarily of three principal peaks corresponding to (j'', j') transitions (0,0), (1,1), and (2,2). The S-branch consists of three transitions (0,2), (1,3), and (2,4). Only one O-branch transition could be isolated, (2,0).

We propose the measurement of β parameters for the individual rotational transitions in cooled para- H_2 .⁶ A study of para- H_2 would isolate only even J in initial and final states. Furthermore, the use of a sample beam source cooled to 77°K, instead of a sample chamber, would concentrate the H_2 principally in $j'' = 0$ initial

states. A sample chamber cooled to 77° K would present a serious difficulty. The surfaces would trap condensible vapors and energy resolution would then deteriorate. Energy resolution requirements are modest for studies of H₂. The only peaks present, those corresponding to the S-branch transition (0,2) and the Q-branch transition (0,0) are separated by 24 meV,⁴ easily within the capabilities of a high resolution spectrometer. An accompanying angular distribution study using a room temperature beam source of para-H₂ would allow for observation of the (2,0), (2,2), and (2,4) transitions. Only the S-branch peak (2,4) would overlap other structure in such an experiment. Other structure would be separated by at least 20 meV and would be directly observable.

A beam source could probably produce local gas densities equivalent to the pressure 10⁻⁴ torr.⁷ This pressure is rather low for such an experiment, but the experiment would still be possible. Since the sample would lie only in one j" state, all intensity would be concentrated in a few peaks. Interconversion of ortho-para in the supersonic expansion of a nozzle beam does not occur.⁸ Further, ortho-para conversion of H₂ must take place on surfaces and is slow, so that sample j-purity would be high.

So far, few accurate calculations of molecular photoelectron angular distributions have been performed. Close agreement with many of the experimental results presented in this thesis may not come for several years. The description of a slowly moving photoelectron in the non-central field of a molecular ion is a formidable

problem. The coupled integro-differential equations which result from imposing an antisymmetrized form on the electronic wavefunctions can be solved only for the simplest of molecules. Calculations for H_2 could benefit from the extensive work on electron- H_2 scattering.⁹ Results of an accurate close-coupled solution could be fed into the Buckingham-Orr-Sichel formalism^{1,2} for a direct comparison to the experimental results of the experiment we propose.

REFERENCES

1. A. D. Buckingham, B. J. Orr, J. M. Sichel, Phil. Trans. Roy. Soc. Lond. A268, 147 (1970).
2. J. M. Sichel, Mol. Phys. 18, 95 (1970).
3. T. A. Carlson, A. E. Jonas, J. Chem. Phys. 55, 4913 (1971).
4. L. Åsbrink, Chem. Phys. Lett. 7, 549 (1970).
5. A. Niehaus, M. W. Ruf, Chem. Phys. Lett. 11, 55 (1971).
6. H_2 at room temperature thermal equilibrium of ortho and para is $\frac{1}{4}$ para.
7. As measured for H_2 in the velocity selector chamber of the Kuppermann group molecular beam apparatus by M. Keil.
8. According to thermal conductivity measurements by R. H. Reiner, unpublished work.
9. As an example, A. Temkin, K. V. Vasavada, Phys. Rev. 160, 109 (1967).

Proposition II

An Atomic Fluorescence Study of the Photodissociation of Molecules of Astrophysical Interest

The study of photon-impact induced fluorescence of dissociation fragments is an important tool for the characterization of high-lying neutral states. The neutral states in the energy region 15-30 eV often predissociate to or directly dissociate to neutral excited fragments. An observation of the emission spectrum allows the identification of the fragments. A study of the variation of emission intensity with incident wavelength allows for sampling the range of dissociative states lying above the first ionization potential.

Until now, most studies of high energy electron-induced and photon-induced atomic fluorescence have examined atmospheric gases such as H_2 , ¹ O_2 , ¹ N_2 , ² CO_2 , ³ and N_2O . ⁴ Solar emission includes a considerable amount of vacuum-ultraviolet flux. ⁵ Thus, these studies have permitted inclusion of processes other than ionization by extreme ultraviolet radiation in models of upper atmospheric processes.

The emission accompanying dissociative excitation may be linked to diffuse structure in the HeII photoelectron spectrum attributed to 2-electron (doubly-excited) ionic states. Neutral Rydberg states surely lie in the energy region just below these ionic states and many of the ionic states in the energy region 15-30 eV are known to be dissociative. ⁶

Several molecules not included in the study of atmospheric processes have important astrophysical significance. Taking two

examples, HCN^7 and H_2CO^8 are known to exist in interstellar space. The inclusion of dissociative excitation in models of mass transport in interstellar space is probably important since other stars, like the sun, have substantial fluxes in the extreme ultraviolet.

We propose that the variation of the photon-impact atomic fluorescence of HCN and H_2CO be studied at variable incident photon energy. Each of the appropriate atomic fragments can be identified by its characteristic vacuum-ultraviolet emission, as seen in Table II-1. The experiment would be most easily performed in conjunction with one of the storage ring or synchrotron sources in this country.⁹

Instrumentation is relatively straightforward. Light from a storage ring or synchrotron port passes through an Sn or Al film, is monochromatized, and enters a sample chamber. Atomic fluorescence is observed perpendicular to the light axis using standard photon-counting techniques. The use of filters (LiF , CaF_2 , gaseous) allows for the determination of the emission wavelength to within a narrow range, adequate for the purposes of this study. The thresholds for atomic emissions can then be associated with any of the various dissociation limits of the molecule.

It is expected that this emission study might also aid in the understanding of the several features in the HeII photoelectron spectrum of HCN , CO , and N_2 attributed to double excitation.¹⁰ The states may be dissociative, since band envelopes are broad. Atomic multiplet appearance energies in the proposed experiment and an application of Wittmer-Wigner correlation rules¹¹ should shed light

TABLE II-1. Principal Vacuum Ultraviolet (Multiplet) Emission Lines

Source	Wavelength (Å)	Transition
HI	1216	$2p\ ^2P \rightarrow 1s\ ^2S$
CI	1329	$2s\ 2p^3\ ^3P \rightarrow 2s^2\ 2p^2\ ^3P$
	1561	$2s\ 2p^3\ ^3D \rightarrow 2s^2\ 2p^2\ ^3P$
	1657	$2p\ 3s\ ^3P \rightarrow 2p^2\ ^3P$
NI	1200	$2p^2\ 3s\ ^4P \rightarrow 2p^3\ ^4S$
	1494	$2p^3\ 3s\ ^2P \rightarrow 2p^3\ ^2D$
	1743	$2p^2\ 3s\ ^2P \rightarrow 2p^3\ ^2P$
OI	1304	$2p^3\ 3s\ ^3S \rightarrow 2p^4\ ^3P$

on the high-lying neutral dissociative states of HCN.

REFERENCES

1. e.g., M. J. Mumma, E. C. Zipf, J. Chem. Phys. 55, 1661 (1971).
2. e.g., L. C. Lee, R. W. Carlson, D. L. Judge, M. Ogawa, J. Chem. Phys. 61, 3261 (1974); Chem. Phys. Lett. 19, 183 (1973).
3. e.g., J. Ajello, J. Chem. Phys. 55, 3169 (1971).
4. L. C. Lee, R. W. Carlson, D. L. Judge, M. Ogawa, J. Phys. B. 8, 977 (1975).
5. R. Tousey, Space Sci. Rev. 2, 3 (1963).
6. e.g., for N₂, E. W. Thulstrup, A. Andersen, J. Phys. B 8, 965 (1975); D. C. Cartwright, T. H. Dunning, Jr., J. Phys. B 8, L100 (1975).
7. L. E. Snyder, D. Buhl, Ap. J. 163, L47 (1971).
8. P. Palmer, B. Zuckermann, D. Buhl, L. E. Snyder, Ap. J. 156, L147 (1969).
9. SURF-II, Gaithersburg, MD; SPEAR, Stanford, Ca; PSL-II, Stoughton, WI.
10. A. W. Potts, T. A. Williams, J. Electron Spectr. 3, 3 (1974) and references contained therein.
11. G. Herzberg, Molecular Spectra and Molecular Structure III Electronic Spectra and Electronic Structure of Polyatomic Molecules, (D. Van Nostrand, Princeton, 1967) p. 281.

Proposition III

Optoacoustic Spectroscopy in the Vacuum Ultraviolet

Most vacuum-ultraviolet (VUV) experimentation for $\lambda < 2000 \text{ \AA}$ has dealt with isolated molecules in the gas phase. In addition, solid state research in the VUV has become fruitful for studies¹ of collective and surface excitation. At the same time, the liquid phase has been largely ignored, although photoionization studies of liquids have been performed.^{2,3} Generally, if the sample is a liquid at room temperature, researchers choose to vaporize the sample by heating it. The interaction of light and liquid samples and the subsequent energy disposal steps can be more complicated and thus more interesting in the VUV than in the visible or infrared because of the potentially high density of excited states. Simultaneously, since most substances absorb strongly in the VUV, experimental problems can be formidable.

One experiment, in particular, could offer significant amounts of new information if extended into the VUV. After some early activity by A. G. Bell,⁴ opto-acoustic spectroscopy has been applied first in the infrared⁵ and then the visible/near UV⁶ spectral regions. When light falls intermittently on a sample material, the absorbed optical quanta can be degraded into heat pulses. Sound (pressure pulses) results at a frequency matching that of the light chopping. The use of a foil-electret microphone and lock-in detector⁶ allows for a high degree of apparatus sensitivity. If an electronically excited molecule cascades down through the various electronic-vibrational-rotational states rather than emitting or reacting, surrounding molecules are

heated. A comparison of the absorption spectrum with the opto-acoustic spectrum (sound level versus excitation energy) reveals which states are cascading and which are emitting or reacting. Changing the lock-in amplifier quadrature setting by 90° allows for measurement of de-excitation heat released slowly with respect to the chopping frequency.

It is proposed that the technique of opto-acoustic spectroscopy be applied in the vacuum-ultraviolet spectral region for studies of relaxation processes in bio-organic molecules. Standard commercial xenon continuum light sources and normal incidence monochromators provide adequate light for experiments in the VUV down to 1600 \AA . Because many bio-organic molecules absorb strongly in the vacuum ultraviolet, optical path lengths must be kept short. The high sensitivity⁶ of opto-acoustic spectroscopy (to almost 1 part in 10^9) can then allow for measurements of heat generated in solutions between transparent windows as closely spaced as $15\text{--}20 \text{ }\mu\text{m}$. In their study of amino acids dissolved in the solvent hexafluoroisopropanol, Snyder *et al.*⁷ were able to measure circular dichroism (CD) spectra in the VUV using a $15 \text{ }\mu\text{m}$ sample film formed between two polished CaF_2 windows. In a similar manner, the thin film of solutions of a variety of bio-organic substances could be coupled acoustically (via a gas phase, if necessary) to a microphone for opto-acoustic measurements. If warranted, digital signal averaging, as suggested by Cohen,⁸ could be employed to increase experimental sensitivity.

The use of aqueous solutions will allow for experiments to be

run as far into the VUV as 1600 Å. The onset of strong absorption of water lies at 1600 Å.⁹ Other solvents⁹ (alcohols, fluoroalcohols) might allow the spectral range to be extended even further. The principal relaxation mechanisms of lowest singlet states, other than singlet \rightarrow triplet conversion, is fluorescence. A weak (molar extinction coeff. $< 4 \times 10^2$) singlet absorption in the 1400-1600 Å region in the absorption spectra of fluoroalcohols should not be detected in the proposed experiment. Thus, in an aqueous solution, relaxation heat of solutes can be measured directly, without interference. Furthermore, the availability of window materials,¹⁰ rather than the transparency of solvents limits the spectral region covered.

A large variety of bio-organic substances is available for study using this technique. Recent CD studies of sugars,¹¹ polypeptides,¹² and DNA¹³ in aqueous solution were possible down to 1640 Å using a solution path length of 4 μm between quartz windows. In these studies, Johnson and coworkers sought to understand the conformation of the large molecules using the polarization of electronic transitions as a probe. The proposed experiment will probe the relaxation processes following electronic excitation in the spectral region below 2000 Å.

REFERENCES

1. Proceedings of the IV International Conference on Vacuum Ultraviolet Radiation Physics, Hamburg, 1974, E. E. Koch, R. Haensel, C. Kunz (Eds.) (Pergamon-Vieweg, Braunschweig, 1974) Chapters 4-6.
2. H. Siegbahn, K. Siegbahn, J. Electron Spectr. 2, 319 (1973).
3. P. Delahay, P. Chartier, L. Nemec, J. Chem. Phys. 53, 3126 (1970).
4. A. G. Bell, Proc. Amer. Ass. Advan. Sci. 29, 115 (1880).
5. L. B. Kreuzer, C. K. N. Patel, Science 173, 45 (1971).
6. W. R. Harshbarger, M. B. Robin, Accts. Chem. Res. 6, 329 (1973).
7. P. A. Snyder, P. M. Vipond, W. C. Johnson, Jr., Biopolymers 12, 975 (1973).
8. R. L. Cohen, Appl. Opt. 13, 2518 (1974).
9. M. B. Robin, Higher Excited States of Polyatomic Molecules (Academic Press, New York, 1974) p. 245.
10. UV grade suprasil-quartz transmits only to 1600 Å. Other window materials, such as CaF₂ or LiF, would be attacked by solvents. Thin films of Al or Sn are only partially transparent in the VUV, but are inert.
11. R. G. Nelson, W. C. Johnson, Jr., J. Amer. Chem. Soc. 94, 3343 (1972).
12. W. C. Johnson, Jr., I. Tinoco, Jr., J. Amer. Chem. Soc. 94,

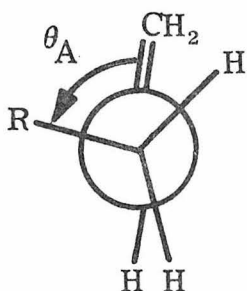
4389 (1972).

13. D. G. Lewis, W. C. Johnson, Jr., J. Mol. Biol. 86, 91 (1974).

Proposition IV

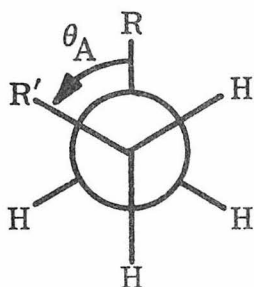
An Electron Diffraction Study of α, ω Di-olefins

The competitive through-space and through-bond interaction of two symmetry-equivalent semi-localized orbitals (as π) can lead to two possible orderings of the linear combinations,¹ depending on molecular geometry. The interactions of π moieties of α, ω di-olefins was discussed² earlier in this context. For these molecules, conformations can be thought of as combinations of:



$$\begin{aligned}
 \theta_A = 0^\circ & \quad \text{cis (C)} \\
 \theta_A = 120^\circ & \quad \text{skew (S)} \\
 \theta_A = 90^\circ & \quad \text{perpendicular (P)} \\
 \theta_A = 270^\circ & \quad \text{perpendicular (P')}
 \end{aligned}
 \tag{1}$$

orientations about single bonds between an sp^2 hybridized carbon atom and one hybridized sp^3 with:



$$\begin{aligned}
 \theta_B = 60^\circ & \quad \text{gauche (G)} \\
 \theta_B = 180^\circ & \quad \text{trans (T)}
 \end{aligned}
 \tag{2}$$

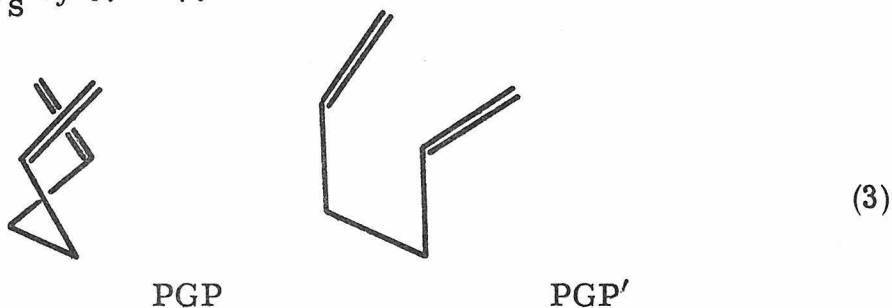
orientations about single bonds between two sp^3 hybridized carbons.

Several groups have discussed the conformations of the non-conjugated α, ω di-olefins but interpretations conflict for 1,5-hexadiene.

Shimanouchi *et al.*³ have conducted a study of the CH_2 -twisting bands in the infrared spectra of 1,5-hexadiene and a series of alkylated

ethylenes. From comparisons to the alkylated ethylenes, two bands in the liquid and glassy solid spectra near 650 and 560 cm^{-1} were assigned as skew and cis conformations, respectively, per Eq. 1. The only sharp feature (654 cm^{-1}) in the infrared spectrum of 1,5-hexadiene in the crystalline phase was attributed to the skew form exclusively. They concluded that many rotational isomers exist in the liquid and amorphous solid states and only one form, involving either a trans- or gauche- arrangement about the central single bond, remains in the crystal.

Bünzli *et al.*⁴ performed extended Hückel calculations on 7 conformations of 1,4-pentadiene and 2 conformations of 1,5-hexadiene. The conformation of 1,4-pentadiene which minimized the relative total energies were not cis- or skew- about the C(2)-C(3) and C(3)-C(4) bonds, but rather perpendicular for both. For 1,5-hexadiene, they give no conformational angles, but calculated that one conformation (possibly PGP) of symmetry C_2 is more stable than another (PGP') of symmetry C_s by 0.1 eV .



In the same extended Hückel treatment, Bünzli *et al.*⁴ calculated that the through-space interaction increases from 1,4-pentadiene to 1,5-hexadiene and that the through-bond interaction remains much

smaller in both cases. They presented photoelectron spectra which showed that the peak splitting in the π band increased from 1,4-pentadiene to 1,5-hexadiene, in agreement with the results of the calculation.

Several remarks relate to the two studies. First, as shown earlier,² the peak splitting in the π region decreases in going from 1,4-pentadiene to 1,5-hexadiene. Second, Bünzli *et al.*⁴ prefer one conformation of 1,5-hexadiene over another when the two have energies differing by a rather small energy on the basis of an extended Hückel (semi-empirical) calculation. A difference of 0.1 eV is too small to be significant for such a calculation. The calculations may be untrustworthy for determining the most stable conformation of 1,4-pentadiene as well.

Third, infrared spectroscopy is not as good a method of determining molecular conformations as other more direct techniques. Empirical correlations with related molecules are often valuable, but the complexity of the liquid and glassy solid spectra precludes any definitive vibrational assignments. Furthermore, Shimanouchi *et al.*³ did not consider the case where θ_A might be other than 0° or 120° . The extended Hückel calculation at least suggests that other conformations be considered.

It is proposed that the technique of gas-phase electron diffraction be applied to the series of non-conjugated α, ω di-olefins. By the sector-microphotometer method, electrons of energy 25-75 keV are focussed at a molecular beam and scattered electrons pass through a heart-shaped mask onto a photographic plate.⁵ A least-squares

analysis of the diffraction rings produced allows for the recovery of a nuclear radial distribution functions. The resulting internuclear distances are a thermal average over all possible conformations. The method is also capable of measuring torsional angles, as was done previously for the hydrocarbons 1,3,5-cis-hexatriene⁶ and 2,3-dimethyl,2-butene.⁷ The literature records electron diffraction studies of a range of n-alkanes,^{8,9} but no corresponding α,ω di-olefins except for 1,3-butadiene.¹⁰

If the energies of the various conformations of α,ω di-olefins are as widely spaced as was predicted by the study of 1,4-pentadiene, then one conformation should dominate. When the gas phase structure is determined, the interaction of the π moieties can be understood better and interpretations of the photoelectron spectra will have a firmer basis.

REFERENCES

1. E. Heilbronner, Israel J. Chem. 10, 143 (1972).
2. cf. Paper IV of Chapter 6, this work.
3. T. Shimanouchi, Y. Abe, Y. Alaki, Polymer J. 2, 199 (1971).
4. J. C. Bünzli, A. J. Burak, D. C. Frost, Tetrahedron 29, 3735 (1973).
5. S. H. Bauer in Physical Chemistry, An Advanced Treatise, Vol. IV D. Henderson (Ed.) (Academic Press, New York, 1970) p. 741.
6. M. Traetteberg, Acta Chem. Scand. 22, 2294 (1968).
7. J. L. Carlos, Jr., S. H. Bauer, J. Chem. Soc. Faraday II 70, 171 (1974).
8. R. A. Bonham, L. S. Bartell, D. A. Kohl, J. Amer. Chem. Soc. 81, 4765 (1959).
9. N. Norman, H. Mathisen, Acta Chem. Scand. 15, 1747 (1961); 18, 353 (1964).
10. K. Kuchitsu, T. Fukuyama, Y. Morino, J. Mol. Struct. 1, 463 (1968).

Proposition V

An Electron-photon Coincidence Study of Molecular Triplet States

To date electron impact coincidence studies of molecules have generally used high incident electron energies. Ejected electron spectra of NH_3 ¹ and CO ² have been measured in coincidence with keV energy projectile electrons having lost adjustable amounts of energy. Spectra resembling photoelectron spectra are so generated. The technique has even been applied for measuring photoelectron angular distributions.^{3,4} Fragmentation spectra of molecules have been measured^{5,6} in coincidence with keV energy projectile electrons, again having lost adjustable amounts of energy. Here, the spectra resemble those generated by photoionization mass spectrometry. High projectile energy electron-photon coincidence studies have been suggested,^{5,7} this time in order to simulate photofluorescence spectra. For photon-impact experiments related to the coincidence experiments above, the difficulties of working with continuum or multiple line light sources coupled with monochromators can be sizeable. Flexibility of the adjustable energy loss feature of electron-fragment coincidence experiments more than compensate for the low coincidence rates usually encountered.

The above high electron projectile energy studies necessarily are governed by optical selection rules. Taking the last example above, photofluorescence or keV energy electron-photon coincidence studies can only measure radiative decay of optically-allowed singlet excited states. Occasionally a dipole-forbidden singlet state is

encountered as a weak feature in an absorption spectrum. Generally, however, dipole-forbidden singlet states and molecular triplet states are inaccessible.

It is proposed that the technique of electron-photon coincidence be applied at low energies in order to study the radiative decay of excited molecular triplet states. Excited triplet states may decay by some of the same mechanisms available to excited singlet states.⁸ They may undergo intersystem crossing ($10^4 - 10^{12} \text{ sec}^{-1}$) to a manifold of states of different multiplicity. In condensed phases, the excited triplet states may undergo internal conversion to the lowest triplet on a time scale as fast as 10^{-12} sec . Alternatively, they may fluoresce to lower triplet states ($10^6 - 10^9 \text{ sec}^{-1}$) or phosphoresce to the ground singlet state ($10^{-2} - 10^4 \text{ sec}^{-1}$, i.e., rather improbable).

The apparatus proposed for the electron-photon coincidence study would be very similar to that used in the study of variable angle, low energy electron scattering.⁹ The apparatus would consist of a stationary electron gun, an internally silvered¹⁰ sample chamber, a stationary photon multiplier viewing the scattering region at right angles, and a rotatable electron energy analyzer. In order to maximize the detected photon signal, band-pass optical filters, rather than a monochromator, would isolate triplet state emissions from the possibly more intense emissions from the singlet state manifold. Electrons which inelastically scatter after producing dipole-allowed excited states are preferentially scattered in the forward direction. Outgoing electrons resulting from the electron exchange which must occur when

triplet states are produced are ejected more isotropically. Thus, in order to isolate triplet features to perform a coincidence study, the apparatus must have variable angle capability. To perform the coincidence study, a detected visible or ultraviolet photon arising in the scattering region would give rise to a single electrical pulse. The detected inelastically scattered electron would give rise to a second pulse which could be gated¹¹ with the first pulse in order to determine the number of true coincidences. A spectrum of coincidences versus electron energy loss, at the photon bandwidth of a single filter, could be taken at only a few detector angles in order to confirm the triplet nature of the two states.

It is suggested that the fluorescence of excited triplet states be monitored as a means of understanding the state ordering of the manifold of triplet states. Optical selection rules govern the fluorescence process, so that not all pairs of triplet states will be connected by emission. Thus, the low impact energy electron-photon coincidence spectrum can be used as a criterion for the reasonability of the various possible triplet state energy orderings.

Variable angle, low energy electron impact spectroscopy has been responsible for the identification of triplet states in a range of molecules.¹² It can detect only those triplet states which lie some distance from the maxima of (at closest, on the edge of) an allowed singlet feature. The proposed experiment will probably be able to isolate triplet states with the same energies as singlet states. Thus, it is envisioned that electron-photon coincidence will give the variable angle experiment additional sensitivity to triplet states.

REFERENCES

1. M. J. van der Wiel, C. E. Brion, J. Electron Spectr. 1, 443 (1972).
2. M. J. van der Wiel, C. E. Brion, J. Electron Spectr. 1, 309 (1972)
3. M. J. van der Wiel, C. E. Brion, J. Electron Spectr. 1, 439 (1972).
4. G. R. Branton, C. E. Brion, J. Electron Spectr. 3, 123 (1974).
5. C. Backx, M. J. van der Wiel in E. E. Koch, R. Haensel, C. Kunz (editors) Proc. of the IV International Conference on Vacuum Ultraviolet Radiation Physics, (Pergamon-Vieweg, Braunschweig, 1974) p. 137.
6. C. Backx, G. R. Wright, M. J. van der Wiel, in J. S. Risley, R. Geballe (editors) Electronic and Atomic Collisions (U. of Washington, Seattle, 1975) p. 812.
7. A number of experimental electron-photon coincidence studies have used lower electron energies and measured photon polarization in order to study the coherence and symmetry properties of the collision process, e.g., M. C. Standage, H. Kleinpoppen, ibid., p. 1140.
8. S. P. McGlynn, T. Azumi, M. Kinoshita, Molecular Spectroscopy of the Triplet State (Prentice-Hall, Englewood Cliffs, N.J., 1969) Chap. 1.
9. A. Kuppermann, J. K. Rice, S. Trajmar, J. Phys. Chem. 72, 3894 (1968).

10. M. Bloch, D. W. Turner, Chem. Phys. Lett. 30, 344 (1975).
11. M. J. van der Wiel, G. Wiebes, Physica 53, 225 (1971).
12. e.g., for 1,3-butadiene, O. A. Mosher, W. M. Flicker, A. Kuppermann, J. Chem. Phys. 59, 6502 (1973).